Nano-structured Materials Synthesized from Transition Metal Carbides / Nitrides for Electrocatalytic Applications

RAJINDER KUMAR

A thesis submitted for the partial fulfillment of

the degree of Doctor of Philosophy

Institute of Nano Science and Technology

Habitat Centre, Sector-64, Phase-10, Mohali, Punjab 160062, India

Indian Institute of Science Education and Research Mohali

Knowledge city, Sector 81, SAS Nagar, Manauli PO, Mohali 140306, Punjab, India.

March 2020

Dedicated to my Family

मेरी दुनिया में इतनी जो शौहरत हैं, मेरे माता पिता की बदौलत हैं।
जिस के होने से मैं खुदको मुक्कम्मल मानता हूँ, मेरे रब के बाद मैं बस अपने माँ-बाप को जानता हूँ।

To 'Maa and Daddy', it's impossible to thank you adequately for everything you've done, from loving me unconditionally to raising me in a stable household, where you instilled traditional values and taught your children to celebrate and embrace life. I could not have asked for better parents or role-models. I am dedicating this to you. What I achieved and what will be in future its all because of your efforts, compromises and hurdles you face for betterment of our life.

The important pillar of my life along with my parents is my wife "Ekta Grak". The encouragement, motivation and a emotional support that I got is the major reason that I could complete this work. I am really thankful to her dedication, compromises and the difficulties she faced during my PhD. The only reason behind the successful completion of this research work is her strength and determination of handling all the issues related to my family like a son. Having a life partner like her is totally a God's blessings.

The other strength of my life is my brother "Virender Kumar Grak". Living together to celebrating together, and encouraging each other is the strength of our relation. He helps me in all my Ups and Downs. I am really thankful to his support during completion of my research work. Recently he got married with "Ankita Grak" and I wish to my almighty that 'He' blesses him a happy and prosperous married life.

''माँ की ममता और पिता की क्षमता का अंदाजा लगाना संभव नही है...!''

Declaration

The work presented in this thesis has been carried out by me under the guidance of Dr. Vivek Bagchi and Dr. Ehesan Ali at the Institute of Nano Science and Technology Mohali. This work has not been submitted in part or in full for a degree, a diploma, or a fellowship to any other university or institute. Whenever contributions of others are involved, every effort is made to indicate this clearly, with due acknowledgement of collaborative research and discussions. This thesis is a bonafide record of original work done by me and all sources listed within have been detailed in the bibliography.

RAJINDER KUMAR

In my capacity as the supervisor of the candidate's thesis work, I certify that the above statements by the candidate are true to the best of my knowledge.

Dr. VIVEK BAGCHI

Dr. EHESAN ALI

Acknowledgements

Guru Brahmaa Guru Vishnu
Guru Devo Maheswara
Guru Saaksaat Param Brahma
Tasmai Shri Guruve Namaha

Guru Is Brahmaa (Who plants the qualities of goodness), Guru Is Vishnu (Who nurtures and fosters the qualities of goodness), Guru Is Maheswara (Who weeds out the bad quality), Guru Is Supreme Brahman Itself, offer thy adorations unto that peerless Guru.

First and foremost, I express my sincere and heartfelt gratitude to my Guru **Dr. Vivek Bagchi** for many insightful conversations, inspiring guidance and constant encouragement during the development of the ideas in this thesis as well as my stay in INST Mohali. His immense knowledge and passion for science always inspired me in understanding various aspects of material science. I thank **Mrs. Monika Singh Bagchi** for their affection and hospitality. I enjoyed being surrounded by such beautiful people.

I wish to express my heartful gratitude to the founding director of INST **Prof. A. K. Ganguli**, who gave me the opportunity to be a part of this prestigious institute and then for all the motivation, support and facilities he provided during my PhD time. I will always admire all the efforts he made from academic to hostel related issues for making my pleasant stay in INST and IISER and handles all these on his own. I also wish to express my gratitude to director **Prof. Amitava Patra** and **Prof. H. N. Ghosh** for their valuable contribution and support during my PhD work. Their kind words and the motivation during lab hour in Feynman Lab seating area inspire me for doing better in my research work. I also want to express thanks to our INST collaborators **Dr. Abir De Sarkar** and **Dr. Chandan Bera** who performed theoretical work and explored our work. I am thankful to Dr. Abir de Sarkar group and Dr. Chandan Bera group who helped me a lot while theoretically understanding the work we performed together. I also want to express my thanks to Dr. Seema Gautam in Dr. Abir De Sarkar Group and Ms. Harwinder Kaur in Dr. Chandan Bera group who theoretical explore our work and helped me in getting good publications. I also want to thank our outside collaborators **Dr. S Balasubramanium (JNCASR, Bengaluru), Dr. Dibyendu Bhattacharyya**

(BARC Mumbai, RRCAT Indore), Dr. Takahiro Maruyama (Meijo Uni., Japan) who helped me a lot in the material characterization. I also want to thank our collaborator **Dr. S. N. Jha** (BL-9, RRCAT) and his students Dr. Nidhi Tiwari and Dr. Ravi who helped me a lot in characterization and during the stay in RRCAT Indore.

I sincerely want to thank my **PhD Review Committee** for their valuable suggestion and guidance from time to time in my PhD.

I also want to express my heartful thank to **Dr. Sonalika Vaidya** and **Dr. Sangita Roy** for all their help, motivation and guidance since my first day in INST. I still remember the day I came in INST and met with them who told me about the lab rules and proper instrument uses in the labs and then visited me in IISER lab and helps me in getting the IISER hostels during initial days of my PhD. I also wants to thank Dr. Surajit Karmakar, Dr. Kamalakannan Kailasam, Dr. Ehesan Ali, Dr. Sharmistha Sinha, Dr. Suvankar Chakraverty, Dr. Kaushik Ghosh, Dr. Kiran Shankar Hazra, Dr. Rahul K. Verma, Dr. Tapasi Sen, Dr. Manish Singh, Dr. Menaka Jha, Dr. Sanyasinaidu Boddu and all other INST Faculty for helping me during my PhD and allowing me a easy access of facilities and teaching me the basics about the instruments during course work. I also want to thank IISER faculty who taught me about instrumentation and give me theoretical knowledge about the instruments and cleared my basics about the different instruments who helped me a lot during my PhD work.

I wish to express my gratitude to **Dr. C. R. Mariappan**, my teacher at NIT Kurukshetra, for his guidance and encouragements from my M. Tech. days. I also want to express my gratitude to the other faculty members of NIT Physics department, Prof. Ashavani Kumar, Prof. R.P. Chouhan, Prof. Neena Jaggi, Dr. Anurag Gaur and Dr. Ashok Kumar for their kind conversation and encouragement during my M. Tech. course in NIT Kurukshetra.

I also want to express my gratitude to Prof. Shyam Kumar, Prof. M.S. Yadav, Prof. R.K. Moudgil, Prof. Sanjeev Aggarwal, Prof. Fakir Chand, Prof. Rajesh Kharab Dr. Annu Sharma, Dr. Suman Mehandia, Dr. Manish Kumar at Kurukshetra University

Kurukshetra from my M.Sc. days who taught me physics and motivated me towards research.

I also express my sincere thanks to my lab mates Mrs. Ritu, Mr. Zubair, Mr. Ashish, Mrs. Shilpa, Mr. Deepak and Miss Ekta for helping me in my work during lab time. A special thank to Mrs. Ritu who helped me a lot in the beginning and together we sorted out the problem that we faced and learned the electrochemical study. I also want to thank Mr. Zubair who helped me a lot while finalizing the draft and gave his precious time for my work. I also want to thank our lab alumni Dr. Sushmita, Mr. Apurbo, Ms. Ashima, Mrs. Kanika and project trannie Ms. Shreya and Ms. Manali for helping me a lot.

I also want to thank my batch-mates Dr. Dimple, Mrs. Swati, Ms. Rashmi, Mr. Ashmeet, Mr. Ankur, Mr. Munish, Mr. Naimat, Mr. Soumen and Mr. Anup for helping me a lot in all my Ups and Downs during this PhD time. A special thanks to Swati who helped me a lot and especially her scooty saved my time and helped me in getting the work on time. A special thanks to Ms. Rashmi who helped me in finalizing the thesis. This contribution was most precious for me, Thank you, **Ms. Rashmi**. A special thanks to Ms. Deavsnshi, Mrs. Swati, Mrs. Ritu, Mr. Anup and Ms. Rashmi who generally forced me to go outside the lab for shopping, movies and tea. It was a pleasant time we all batch-mates visited different places during PhD time and helped each other in their difficult time. Thanks to all my those batch-mates also who left INST during my PhD, Mr. Sanjay, Mr. Arko and Ms. Devanshi for their valuable contribution and support.

I also want to thank the all Post-Doc who joined INST during my PhD. A special thank to Dr. Vinod Kumar, Dr. Sanjeev Kumar, Dr. Vijay Tomar, Dr. Bhagwati Sharma, Dr. Vishwajeet Gaikwad for their valuable guidance and support.

I also would like to thank my junior Ms. Ruchi, Ms. Renu, Mrs. Neha, Mr. Pulkit, Ms. Ankush, Mr. Phusphendra, Ms. Harsimran, Ms. Taru, Mr. Ravi, Mr. Krishna, Mr. Sushil, Ms. Pooja, Ms. Navneet, Ms. Supriya, Ms. Sunaina, Ms. Arti, Ms. Nidhi, Ms. Babita, Mrs. Aditi, Mrs. Deepika, Ms. Deepika, Mr. Rohit, Ms. Rimple, Mr. Ankush all the other juniors who helped me in different works during this time.

A special thanks to the “Chai group” and its healthy discussion during tea time. I thank this group and its spirit of asking everybody for the tea, lunch and dinner etc. Thank you

Dr. Sujit, Mr. Krishna, Ms. Supriya, Ms. Navneet, Ms. Sunaina, Mr. Kalpesh, Mr. Ankush and all others who involved time to time during tea time.

I express my warm feelings of gratitude to my M.sc. and M. Tech. friends who are my moral support and after so many years of separation from 'Kurukshetra', we still are bonded together and helping each other during their difficult time.

I express my intense feeling and gratitude towards my parents, wife, younger brother and all relatives for their love, affection and generous support which enabled me to successfully complete my work.

For infrastructural facility, I would like to thank the "Institute of Nanoscience and Technology" and "Indian Institute of Science Education and Research, Mohali and DST for financial support. I also want to thank XPS facility and it's incharge from IIT Kanpur for their help in characterizing the material. Special thanks to Mr. Vaibhav Vajpai (TEM operator) for his help in TEM analysis and characterization.

I also want to thank all Administrative staff, Technical, Non-teaching staff and Security staff of INST Mohali for their valuable contribution to the completion of my PhD. A special thank to **Late Shri P. K. Dutta,** Mrs. Gurveen, Mrs. Sweta, Mr. Dhanjeet and Mrs. Suman and others for their help in academic issues. A special thank to Vikram Bhaiya, Paramjeet Bhaiya, Ravinder Bhaiya (Bus driver), Vinod Bhaiya, Bharat Bhaiya who helped me a lot during lab work for transferring the lab instruments and other things from INST to IISER. Special thank to Butta Singh who serves tea in our cabins during the initial days of our PhD.

Above all, I thank the almighty for giving me this opportunity of writing this acknowledgement. Words are no measure to describe the forbearance and fortitude with which my parents and teachers inspired me. To them, I dedicate this work.

Rajinder Kumar

यदा यदा हि धर्मस्य ग्लानिर्भवति भारत। *अभ्युत्थानमधर्मस्य तदात्मानं सृजाम्यहम् ॥४-७॥* *परित्राणाय साधूनां विनाशाय च दुष्कृताम् ।* *धर्मसंस्थापनार्थाय सम्भवामि युगे युगे ॥४-८॥*	*yada yada hi dharmasya glanir bhavati bharata* *abhyutthanam adharmasya tadatmanam srjamy aham* *paritranaya sadhunam vinasaya ca duskritam* *dharma-samsthapanarthaya sambhavami yuge yuge*

"Srimad Bhagavad Gita"

Table of Contents

List of Figures

List of Tables

Abbreviations and Nomenclature

IAHE	International Association of Hydrogen Energy
XANES	X-ray absorption near-edge structures
EXAFS	Extended X-ray absorption fine structure
NEXAFS	Near Edge X-ray absorption fine structure
DCM	Double Crystal Monochromator
PCS	Photon Correlation Spectroscopy
HER	Hydrogen Evolution reaction
HMT	Hexamethylenetetramine
TEM	Transmission Electron Microscopy
HRTEM	High-resolution Transmission Electron Microscopy
XPS	X-ray Photoelectron Spectroscopy
RHE	Reversible Hydrogen Electrode
EIS	Electrochemical Impedance Spectroscopy
GCE	Glassy Carbon Electrode
LSV	Linear Sweep Voltammetry
PXRD	Powder X-ray Diffraction
SEM	Scanning Electron Microscopy
CPE	Constant Phase Element
Pt	Platinum
TEOS	Tetraethyl orthosilicate
g-C_3N_4	Graphitic carbon nitride
NH3	Ammonia
FT-EXAFS	Fourier Transform Extended X-ray absorption fine structure
VASP	Vienna ab-initio Simulation Package
GGA	Generalized Gradient Approximation

PAW	Projector Augmented Plane Wave
GO	Graphene Oxide
EDX	Energy Dispersive X-ray
CN	Coordination Number
DFT	Density Functional Theory
HCl	Hydrochloric
MOFs	Metal-Organic Framework
TMBs	Transition Metal Borides
TMSs	Transition Metal Sulphide
TMOs	Transition Metal Oxide
TMCs	Transition Metal Carbide
TMNs	Transition Metal Nitrides
TMSes	Transition Metal Selenides
TMPs	Transition Metal phosphides
mV	Milli Volt
Hz	Hertz
σ^2	Disorder (Debye-Waller) factors
η	Overpotential
mg	Milligram
mA	Milli Ampere
F	Faraday Constant
K_β	Boltzmann Constant
R	Gas Constant
λ	Wavelength
q	Charge
Å	Angstrom

μ	Absorbance Coefficient
ϕ	Work Function
μL	Micro litre
g	Gram
°C	Degree Centigrade

Abstract

Hydrogen is one of the cleanest forms of energy which can solve several issues, including global energy crisis, environmental pollution and depletion of fossils fuels. Hydrogen evolution reaction (HER), being a carbon-neutral process can reduce the carbon footprint in the earth's atmosphere. There is a variety of processes used for hydrogen production such as cracking of petroleum, hydrocarbon reforming, steam reforming of natural gases, coal gasification, etc. but these techniques are either costly or dependent on fossil fuels with the emission of hazardous by-products. Hence, the possibility of hydrogen production through electrocatalytic water splitting makes it a potential carbon-neutral process for fulfilling energy needs. To date, platinum supported materials are mostly found efficient and resourceful electrocatalysts towards hydrogen production. However, the large scale use of such catalysts is restricted by their scarcity and high cost of the material. In order to accomplish an industrial scale hydrogen production with minimum cost, extensive research has been devoted to discovering earth-abundant materials which have similar or better activity than platinum. Among non-noble metal catalysts, molybdenum based catalysts such as molybdenum carbide (Mo_2C), sulphide (MoS_2), nitride (Mo_2N), oxide (MoO_3), phosphide (MoP) etc. have been extensively explored for HER application. The present thesis focuses on the structural design and compositional modulation of molybdenum derivatives through an innovative *in-situ* synthesis route resulting in a biphasic system such as Mo_2C/Mo_2N, Mo_2C/MoO_2, $Mo_2C\backslash MoP$ etc. to enhance the catalytic activity. We have investigated the efficiency and durability of these composites for electrochemical hydrogen evolution in acidic medium. A detailed study of electrochemical hydrogen evolution revealed that the HER activity gets enhanced if Mo_2C and Mo_2N nanocomposite is used as electrocatalyst instead of Mo_2C, Mo_2N or a physical mixture of both. The catalyst exhibits an overpotential (η_{10}) of 96 mV with a Tafel slope of 37 $mVdec^{-1}$ and durability of 1000 cycles. For the first time, we proposed that molybdenum carbide and molybdenum nitride nanoparticles, if produced in situ, can lead to a synergistic effect on the HER activity. Theoretical studies are also in-alignment with the experimental findings, where an appreciable charge-transfer at the interface of these nanoparticles was revealed from the charge density plots. Such charge-transfer at the interface between Mo_2C and Mo_2N further facilitate the hydrogen evolution reaction. This is also supported by the free energy calculation which is very close to commercially available Pt/C catalyst. We have extended our investigation for other biphasic systems such as Mo_2C/MoO_2; $Mo_2C\backslash MoP$ and also explored the possibility of promoter elements for further enhancing the catalytic activity. Copper nanoparticles were found to improve the catalytic activity in one of the Mo_2C/Mo_2N composites by reducing the

overpotential at higher current density. The catalyst shows an enhancement in the stability (3000 cycles) and a drop in the overpotential (η_{30}) from 217 mV to 112 mV for the doped one under a current density of 30 mA/cm^2. Another potential composite of Mo_2C\MoP supported on mesoporous silica exhibits excellent durability of 5000 cycles and shows an overpotential of 88 mV with an onset potential of 31 mV and a Tafel slope of 37 mVdec^{-1}. The work embodied in this thesis represents a concerted effort to continue the development of biphasic nanostructures holding great possibilities for the generation of an efficient and cost-effective catalyst for large scale production of hydrogen.

Synopsis

This thesis entitled "Nano-structured Materials Synthesized from Transition Metal Carbides / Nitrides for Electrocatalytic Applications" explores the synthesis of earth-abundant molybdenum based electrocatalyst for HER applications.

A detailed literature survey on the relevant area benchmarking the status of our work is displayed in first chapter. Second chapter describes the materials and methods involved in the designing of several processes. Initially, a methodology was developed to synthesize molybdenum carbide and nitride nanoparticles *in-situ* in the same solid state reaction. Biomass based microfibrils were used as a carbon source and template for the synthesis and is described in third chapter. Nanostructuring and composition of the phases are extremely important for the enhancement of the HER activity and is exhibited in chapter 4 and chapter 5. The effect of promoter elements on the HER activity of the material have been explained in chapter 6. The HER activity of a composition consisting of molybdenum carbide and molybdenum phosphide was developed during an *in-situ* reaction was described in chapter 7.

The detailed outcomes of the various projects are briefly summarised chapter wise in the following content.

Chapter 1. Introduction

This chapter outlines the background, objectives, context of studies and the significance of the research program.

Chapter 2. Materials, Instrumentation and Experimental Procedures

In this chapter, the chemicals, reagents, and instrumentation used in this thesis will be described. The hydrothermal techniques and temperature-programmed annealing approach for the synthesis of catalyst material have been followed. The general overview of the experimental methods being employed in this research work is also given. The synthesis of nanostructured materials particularly for the HER has been extensively focused on and described in each relevant chapter.

Chapter 3. Uniformly Decorated Molybdenum Carbide/Nitride Nanostructures on Biomass Templates for Hydrogen Evolution Reaction Applications

The chapter consists of the natural biomass-based molybdenum carbide and molybdenum nitride has been *in-situ* synthesized. Natural fibrils derived from biomass used as a template to synthesize uniformly decorated nanoparticles (10−12 nm) of molybdenum carbide (Mo_2C) and molybdenum nitride (Mo_2N) supported on carbon. The nanoparticles have been synthesized through the carburization and nitridation of molybdenum on cotton fibrils, using a high-temperature solid-state reaction. The catalyst exhibits an onset potential of 110 mV and an overpotential of 167 mV to derive a cathodic current density of 10 mA cm^{-2}. The electrocatalyst also demonstrates excellent long term durability of more than 2500 cycles in acidic media with a Tafel slope value of 62 $mVdec^{-1}$. The catalyst specifically involves the use of carbon and nitrogen content present in the biomass.

Chapter 4. Nano-structured hybrid molybdenum carbides/nitrides generated *in-situ* for HER applications

A carbon-supported molybdenum carbide and molybdenum nitride nanohybrid have been synthesized. The material contained carbon-supported molybdenum carbide and nitride nanoparticles of size ranging from 8 to 12 nm exhibits excellent HER catalytic activity. This molybdenum based catalyst (MoCat) is designed as a highly efficient, low-cost (precious-metal-free), highly stable electrocatalyst for water electrolysis in acidic medium, synthesized using a simple methodology. These nanoparticles (β-Mo_2C and γ-Mo_2N) were produced *in-situ* using a metal precursor and C/N source in a controlled solid-state reaction. An overpotential of 96 mV for driving 10 mA/cm^2 of current density was measured for MoCat catalyst, which is very close to commercially available Pt/C catalysts (61mV). Herein, we could unambiguously provide an evidence for the existence of a synergistic effect existing between molybdenum carbide and molybdenum nitride nanoparticles yielding excellent HER activity, if synthesized *in-situ* in a controlled solid-state reaction. Thorough characterization and measurements of the MoCat catalyst revealed that it contains 53% of ß-Mo_2N and 47% of ɤ-Mo_2C. In a remarkable observation, it was noted that MoCat-m (Catalyst made from mixing individually synthesized ß-Mo_2N and ɤ-Mo_2C, pure phase nanoparticles in same or similar composition) fails to attain such high catalytic activity. It shows that the composition works only when the catalyst is synthesized *in-situ*. Theoretical studies are also in-alignment with the experimental findings, where an appreciable charge-transfer at the interface of these nanoparticles was revealed from the charge density plots. Such charge-transfer at the interface between Mo_2C and Mo_2N further facilitate the hydrogen evolution reaction. This is also supported by the free energy calculation which is very close to commercially available Pt/C catalyst. Most importantly, the synthesis of the MoCat

catalyst is simple and can be scaled up easily for large scale devices with ultra-low cost fulfilling its pre-requisites for an application.

Chapter 5. In-situ synthesized mesoporous Mo_2C/MoO_2 nanocomposite shows enhanced HER activity

This chapter describes the in-situ synthesis of MoO_2 and Mo_2C phase nanoparticles. A multiple solid-solid heteroatom interfaces when formed exhibits synergistic effect which not only decreases the overpotential for hydrogen evolution but also there is a significant enhancement in the stability of the material.[10] Herein a mesoporous composite of molybdenum carbide and molybdenum oxide on silica platform (SiMoCat) has been developed, which exhibits an overpotential of 71 mV for driving a current density of 10 mA/cm^2, very closed to the commercially available Pt/C (η_{10} = 60 mV) and a Tafel slope value of 35 mV/dec with an onset potential of 31 mV. The electrochemical stability of the catalyst after 3500 catalytic cycles does not show a significant change in the catalytic activity. The SiMoCat was obtained by a judicious variation in the catalyst precursor and the reaction conditions, resulting in a composition containing 51.3 % and 48.7 % of Mo_2C and MoO_2 respectively. Theoretical studies revealed that the integration of Mo_2C and MoO_2 interfaces within the material increases the number of states around the Fermi level due to the increase of charge transfer which enhances catalytic activity. The value of ΔG_{H^*} on C (-0.0019 eV) and O (-0.0017eV) site of Mo_2C/MoO_2 is much smaller than the individual Mo_2C (2.01 eV) and MoO_2 (7.14 eV) systems. Hence the H^* adsorption kinetics of the interface is better than the individual systems.

Chapter 6. Copper doped Mo_2C/Mo_2N hetero-structures showing enhanced hydrogen evolution in acidic medium

Chapter 6 illustrates the role of the promoter elements in the molybdenum derived composite to further enhance the HER catalytic activity.[11] The nanostructured electrocatalyst (CuMoCat) that consist of molybdenum carbide, molybdenum nitride and copper, forming a heterojunction within the composite. Copper doping in molybdenum carbide/nitride composite facilitates lowering of the overpotential at low current density. CuMoCat exhibits an overpotential of 84 mV with a Tafel slope value of 33 mV/dec and shows excellent stability of 3000 cycles in acidic media. The theoretical study reveals that Cu doping brings a change in the electronic properties of the catalyst, which improves the overall adsorption and desorption of hydrogen on the catalyst surface during the hydrogen evolution process. The Free Energy diagram for various adsorptions active

sites of CuMoCat displays a shift of free energy for Mo and N sites making these more favorable for HER with respect to Mo/N sites of the un-doped catalyst.

Chapter 7. Molybdenum carbide and molybdenum phosphide based hybrid materials for mutually enhanced hydrogen evolution reaction

Chapter 7 of this thesis describes the behaviour of the electrocatalyst (SiMoCP) consists of two HER active phases Mo_2C and MoP supported on mesoporous silica.[5] The study reveals that the combination of two HER active phases molybdenum carbide and molybdenum phosphide based composites have come out as competitive electrocatalyst for HER in past few years. Molybdenum carbide and molybdenum phosphide both shows high catalytic activity towards hydrogen evolution reaction. Herein, the catalyst exhibits a low overpotential of 88 mV at a current density of 10 mA cm^{-2} in the acidic medium. Furthermore, the long term durability of the SiMoCP upto 5000 cycles makes it catalytically more favourable towards stable electrocatalyst. The catalyst doesn't show any significant change in the overpotential even after 5000 catalytic cycles and have a Tafel slope value of 37 mV dec^{-1}. The chapter thoroughly describes the mutual enhancement in the catalytic activity and the stability of the material.

At the end of the thesis, other relevant information along with the future prospects of this work will be provided as an extension.

Chapter 1

Introduction

1. Introduction

1.1. Energy Crisis and Renewable Energy

Nature; essentially originate on closed material cycles in which the supplies endure through various chemical conversions. Then, ultimately at a certain phase, it trails off to the starting product so that a perspective of the energy supplies of the materials is ensured. Numerous paradigm of this belief can be found in nature like oxygen, carbon and nitrogen cycles etc.[1-2] Unfortunately, nowadays the humankind goes against this natural concept in many cases. Especially, since the starts of industrialization and urbanization scenario, greater than ever quantity of assets have been mined without being apologetic. Consequently, humankind needs to master several confronts. Energy and environment are two of the most alarming ever-increasing preoccupations of existing human society due to the significantly rising demand as well as the increasing deteriorative environment resulted from the exploitation of fossil fuels.[3] It's true that with the succession of this modern era the need and ignition of fossil fuels has steadily enhanced which significantly raise the overall temperature in addition to the intensification of carbon dioxide in the environment. The exponential increase in energy demand with the increase in the world economy and world population has newly been met by enhanced production of fossil-based fuels, including coal, oil, or gas and envisaged to be exhausted in fairly accurate 100 years. Fossil fuels like oil and coal have been the world's prime energy hoard since the commencement of the industrial age. Currently, 70% of energy fulfilment was obtained from these sources.[4-5] Fossil fuels have the advantage of being present as free energy in concentrated form. These complex molecules took millions of years to come into this form from natural routes. Furthermore, it also has an advantage that the energy extraction via the combustion of these fuels is moderately easy. But, due to the emission of greenhouse gases these non-renewable energy resources creates large environmental problems.[6-7] In 2012 the world's energy utilization was 5.79×10^{20} J, with potential energy demand estimated to reach 8.60×10^{20} J in 2040. The International Energy Agency also reported that the universal energy requirements will increase by 30% till 2040, and parallelly the greenhouse gases emission like CO_2 will reach nearly 35.7 Gt per year in 2040.[8-10] The drastic exploitation of the natural fuels add-on with the growing energy consumption and at the same time increases the green-house gas emission. In today's world assets are running low, greenhouse gasses are escalating and the ambience is changing. Besides that, due to the uneven circulation among countries, decreasing accessibility, and universal ecological issues are in the way of fossil fuels to be called as an ideal energy source. The "Intergovernmental Panel on Climate Change" had

already stated about the increase in average surface temperature and the average concentration of CO_2 in the atmosphere if the proper step not taken.[11-12] This decisive problem has become a universal challenge now, and the sustainable production of environmentally gracious carbon-neutral energy sources driving scientist to found a new alternative to fulfil the energy needs. Most of the countries put efforts towards the fulfilment of energy demands and lowering the carbon emission, yet the proposed target will not be met in a period as stipulated. These concerns urged the scientist and common man to move towards the other conversion technologies which must be environment friendly and can fulfill along with household needs.[8] At present time the largest fraction of the world's energy expenditure is based upon fossil fuels, but there is a vast tendency in substituting the fossil fuels with renewable assets like solar, wind and hydrothermal energy etc. The fossil fuels will get exhausted in the next few decades that's why the world is ardent to discover a substitute that will assure our acquire affluence and advance development permanently. Present expertise is already providing us with such unconventional energy sources like wind, turbines, photovoltaic cells, biomass plants and more.[9, 12] There has been a momentous investment in discovering and production of energy from renewable sources results in their increase in the share of total electricity production. The motive of enhancing the contribution of renewable energy towards daily households and industries is innumerable challenges that need to be cover. The renewable energy like solar energy, wind energy, tidal waves, hydro energy are some known natural energy sources but with their own limitations. The unconventional energy resources like sun and wind do not endow with a constant supply of energy, rather the natural constraints come ahead in solar and the wind energy production. Also, when we consider the use of renewable energy sources we must consider the factors like economy, the environment and human health too.[13] Hence, keeping in mind the already faced energy crisis and the prerequisite to store intermittent energy generation, eventually a non-polluting carbon-neutral fuel would be a better solution. One way of alleviating the energy demands is to use these diverse energy carriers whether there is a surplus or lack of renewable energy. However, these renewable energy sources are erratic, and energy would be wasted if it is not used sensibly. It's not always easy to utilize all the energy produced at peak hour production times.[5] If somehow, it possible to store the energy at its peak production hour and released on requirements when production reaches a minimum, it could be game-changer in the area of renewable energy. The task of either competently stock up of energy or coupling with energy storing system is the prime focus these days. The well-known storage technologies in present worlds belong to a system linked with mechanical storage,

thermally storage, batteries or as chemical bonds.[13-14] All individual storage technology has own positive and negative aspects. We will discuss all these technologies in the coming section.

1.2. Hydrogen; Clean Source of Energy

1.2.1. Hydrogen

The chemical fuels from renewable sources are one of the biggest achievement if succeed in the way of solving energy concerns. The hydrogen production from splitting water are among the similar type of key scientific challenges in 21st-century. Hydrogen, an easily available molecule that exists in gas and liquid form in our environment. Hydrogen having the lowest energy content by volume but highest by weight and due to its higher energy content is employed as a future energy carrier. Hydrogen provides three times more heating value compared to petroleum with zero harmful emission. Being manmade stimulate it goes through a sturdy production and expenses superior to the petroleum refining.[15]

1.2.2. Hydrogen Economy and Challenges

J. B. S. Haldane and Professor John Bockris first coin the term hydrogen economy. The economy essentially involved the concept of potential fuel which exists in the form of hydrogen, which basically terms as one of the safest and cleanest energy carrier among all the energy sources. But, regardless of these encouraging features molecular hydrogen is not generously available and has to generate from other hydrogen-combined sources through diverse approaches.[16-17] The economy is still grooming, perhaps it would be one of the massive infrastructures projects in the coming future. It generally related to hydrogen reservoirs, there transport and utilization in different ways. Hydrogen is an attractive energy carrier because of its carbon-free byproducts and which makes it potentially one of the clean energy sources. So, to explore a clean and safest carbon-free energy reservoir the development of what has become known as the hydrogen economy is necessary. There is no doubt that in the coming future the transformation of conventional energy-based technology into hydrogen-based technology will solve many of the energy and climate related universal problems. The hydrogen economy centred about the production, transportation and utilization of hydrogen instead of fossil fuels.[10, 18] As already discussed most of the energy-storing technology has been merely designed for electric energy purpose while hydrogen storage is totally a different concept. Since the hydrogen has no natural resources so it is widely dependent on the chemical industry. The 1973 oil crisis was one of the biggest factors to realize the importance of alternative energy sources.

This was the time when the concept of hydrogen energy was first introduced. In 1974, the first time a conference was organized focussed on hydrogen generation, utilization and its promotion were completed and an organization named as "International association from hydrogen energy" was founded. The main aim of the organization is to use and promote hydrogen as an energy carrier in the energy sector and energy-related industries. Hydrogen being a novel material for different fields, the scope of carbon-free energy source has increased its scalability. At present the optimization of the hydrogen-based industries has been advanced. The feasibility towards the industrialization with taking into accounts the limitation with the transformation of all types of energy sources into hydrogen-based techniques is really challenging.[15, 17, 19] There have been continues incessant worldwide to promote and establish such transformation which technically based on the hydrogen economy. The hydrogen extraction from fossil fuels has been highly influenced by the fuel reservoirs which going to diminishes in the coming future. So, the technology transformation from one to another while keen searching for hydrogen sources from non-fossil fuels is necessary. The transport, energy, industry sectors along with defence sector to the aviation sectors etc. it would have large possibilities. The budding energy demands for hydrogen generation from the inexhaustible sources are expected to fulfil in the near future. The typical scheme involved in the vast hydrogen economy is based on the hydrogen storage to the final stage distribution along with the concession and utilization.[18, 20] The universal availability of hydrogen along with its storage could be possible through integrating different power plants with hydrogen generation electrolyzers. However, the technical and economic challenges still exist in the hydrogen economy. A large number of issues are still related to hydrogen production like hydrogen storage, hydrogen transportation, hydrogen conversion and many other applications that belong to the hydrogen economy. The expansion of innovative comprehensive infrastructure is a stepwise itinerary and it requires unusual assessment tools. The assessment tools are such as cost-benefit estimation, sustainability assessments, optimization of supply chains, the superlative assignment of the edifice and practice utensils in an emergent souk, and, last but not least, safety threat evaluation and supervision. The hydrogen economy has been collectively projected as an advanced and eternal retort to the consistent problems tackled in today's world. It consists of inclusive ecological concern, running down of expected fuel assets, food scarcity and undernourishment and the intensifying expansion of the world inhabitants.[21-22] Hydrogen infrastructure is still in the way of development and in a decentralized manner, it would allow being used as fuel cell systems. It basically involves the system starting from hydrogen production to the accessibility to the last user. The hydrogen generation through diverse approaches, suitable storing system and the transport within the

safety measures to the last consumer is a very complicated task. Gas transportation and storage are a basic problem to be solved for providing faster industrialisation of hydrogen and fuel cell technology. Besides that, in terms of the transport industry, the establishments of hydrogen pipelines, creation of hydrogen-producing unit or storing unit along with hydrogen highways station to the ultimate addict is a decisive precondition before flourishing commercialization of automotive fuel cell technology.[22-23] In the concluding remarks, we can say that the major impediments about the expansion of the technology are high expenditure, lack of key technologies, and incompletion of hydrogen infrastructure that weakens the hydrogen economy. National and international legislation of the hydrogen production and its distribution also one of the major factors in standardizations of hydrogen use. Besides that, the configuration of the international approach that principally works on to lower the overall costs to put up an international hydrogen economy is necessary. The security standards and the ecology directive policies along with collaborative technology on hydrogen production worldwide are essential. The association establishment among all the industries and the research organization without harming their ethical privileges is the crucial task.[15, 21] The research publications and feasible study of the hydrogen projects in research centres and public education centre is the ground level concern to make the hydrogen-based economy. The major factor that can enhance the hydrogen production research is the government initiatives by promoting such ecologically valuable projects and providing funds to public and government-funded research institutes. The last thing that persuaded is if the hydrogen economy would really exist, it could alter the industry and energy sources scenario dramatically.

1.2.3. Infrastructure and Current Situation

In 2018, the World Hydrogen Energy Conference was organized between 17 to 22 June 2018 at Rio de Janeiro, in which Professor T. Nejat Veziroglud who is the founding president of the International Association Of Hydrogen Energy (IAHE). In his speech, he states and expects the complete transformation of the economy into hydrogen energy within the completion of this century. About 44 years ago, being a member of 'Hydrogen Romantics' with ten other members he also organised and chaired 'Hydrogen Economy Miami Energy (THEME) Conference'.[24-25] Besides that the people's concerns about future energy and the environment is it's urgency to focus on these issues. In the present situation, the essential concern is to recognize the foremost barricade to conquer energy crises and steps to take for the hydrogen operation. It is essential that all the non-economic difficulties must be trounced and the proper utilization of hydrogen must be incorporated in general decarbonization policy to attract awareness from research,

engineering, reserves and, last but not least, society.[17] Hydrogen has been considered as energy carrier two century ago but 1970s energy crisis motives researcher for technological advancement so that new energy sources can be explored in order to avoid future energy crisis. It is estimated that present reservoirs of fossil fuel can last long for a maximum of 40 years for petroleum which mainly is a source of the industrial and transport energy provider. Beside it, a maximum of 60 years for natural gas has been estimated that it will be exhausted within this time span if the current rate of consumption is continued, and 156 years for coal. Many scientists and engineers have agreed with the situation and consider that founding environmentally hygienic, economical and additionally sustainable energy is extremely imperative. It has been considered that this initiative for future energy requirement could substitute the accessible fossil fuel system and would be a supportive gesture in decoding present universal energy problems.[10, 26-28] The hydrogen economy in today's world is so fascinating that various agencies and nation stepping out towards hydrogen energy approach and investing immensely to establish a common hydrogen energy system of international standard. It is expected that hydrogen could fulfil approximately 18% of energy demands and can reduce around 6 Gt of greenhouse gases especially CO_2 annually. Besides that, hydrogen infrastructures could create about 3 million new jobs by 2050. In transportation, it is believed that hydrogen could run estimated 400 millions of cars which is the huge number and can be a large contributor in minimizing the greenhouse gases. An estimate of 15 to 20 million trucks that being is used in transports and around 5 million buses from private to government organizations in 2050 which seems to be approximately 20% to 25% of the transportation industry could run on hydrogen economy.[29-31] In present scenario hydrogen production globally reach to approximately 45–65 Mt per year as feedstock in different industries that's equivalent to 5.4–7.8 EJ. This amount is just ~1% of worldwide energy demand in today's date. Internationally, exponential growth in hydrogen-based manufacturing and rise in hydrogen stations functionality worldwide as of 2018 will be a good move toward carbon-free energy sources. In numerous countries, even hydrogen vehicles are commercially accessible, and it was estimated that till date 225000 fuel cell heating systems for domestic use have been used. This change represents a step taken just only five years ago which is the positive feedback towards the hydrogen economy.[30, 32-33] Hydrogen production and its distribution are a major concern and internationally, it requires a major boost to successfully construct a large hydrogen economy. Therefore to solve the technical difficulties and improvements in industries with expanding the multidisciplinary market various initiative and organization has been made worldwide. The public-private partnership among different government organization and private industries

already has been titled under a common agenda.[15, 22] A Hydrogen Council of thirteen international corporations recently formed with a theme concept of ‘‘to position hydrogen among the key solutions of the energy transition’’. The ‘Nationales Innovation program Wasserstoff-und Brennstoffzellentechnologie’, ‘Clean Energy Partnership’, ‘Japan Hydrogen & Fuel Cell Demonstration Project’, ‘Department of Energy’, ‘Fuel Cell and Hydrogen Joint Undertaking’, ‘California Fuel-Cell Partnership’, and ‘H2-Mobility’ are some worldwide projects and organization which fanatically working on to strengthen the hydrogen economy. The European Union, American agencies, Japan, China, Germany etc are major contributors to establish the hydrogen power plant in their country. Other than these countries, some countries like Australia, Taiwan, India, United Kingdom, Brazil etc are the recent initiator of the hydrogen economy.[30, 34] The European Commission High-Level group which works on the advancement and exploration of hydrogen and fuel cells technologies has already targeted to accomplish 35% for zero-carbon hydrogen-based vehicle till 2040 and a vast hydrogen economy till 2050. European H2Mobility programs have not only initiated the hydrogen generation but also it started construction of refuelling stations at prime locations. They suggested a system of 65 refuelling stations initially under hydrogen fuel cell programme in the United Kingdom by 2020 in order to start the market that expectedly will reach to 1150 stations as large number of the fuel cell by 2030 which almost cover the whole country.[32, 35-37] Alternatively, the U.S. Department of Energy set a target about the maximum of conventional energy-based office to convert into hydrogen-powered fuel cell vehicles till 2020. California could be considered as the world leader in hydrogen infrastructure development which had already established 39 open retail stations and approximately 6000 fuel cell vehicles are on the road.[36, 38] Japan as a major paradigm for the world and sturdily put down its supply from a foreign country, and its self-reliance proportion was about 6% in 2014 as compared to other countries. They have adopted the policy to reduce significantly the emitted greenhouse gases for 25.4% till 2030 as compared to 2005. In this context, "Japan Hydrogen Mobility” sets an objective to assemble a minimum of 80 stations by 2021, with taking the strategic initiative with vehicle companies and dealer. It is estimated that worldwide 330 hydrogen refilling stations are already installed as of 2018, in which majority near about half are only situated in Japan and the United State. United state has sold out 2750 fuel cell vehicles as of 2017, more than Japan and Europe collectively while China have a different strategy of fuel cell vehicle technology roadmap in which they has a reticent intention for installing 5000 FCEVs till the end of 2020 but an approximated scale of millions fuel cell vehicles before 2030.[30, 36, 39-40] Germany is efficient in solar panel construction but suffers from the apposite accessibility of solar energy

that hurdles the project and latterly drifts towards the hydrogen energy. In Germany, the "National Organization of Hydrogen and Fuel Cell Technology (NOW)" has attempted to ascertain 50 new stations program for the establishment of the hydrogen energy concept. They have also initiated many other strategic policies for the hydrogen economy establishment which mainly have a target to make hydrogen a suitable alternative instead of traditional energy sources. A hydrogen fuel-based train has been already trialled, but still, it needs very much improvement towards hydrogen fuel economy. Norway, Netherlands, Iceland and the United Kingdom like countries have already commenced and accelerated the funding for installing more hydrogen energy station in this initiative.[2, 32, 40] Other developed and undeveloped countries also had made the initiative to move their industries on a hybrid fuel system based on the hydrogen economy. Hydrogen energy system is expected to be highly efficient in the near future along with providing economic and environmental benefits. Since the suitable administration and transport infrastructure of hydrogen-based industries is still under process, it's not easy to resolve all issues related to the hydrogen economy.[18, 21] This is believed that the global hydrogen market will achieve a target of approx $33 billion increments over the next 4 years. The current market was about US$122 billion in 2018 and expected to reach a US $155 billion in 2022. Hydrogen being a synthetic fuel labelled under the immense production cost, significant research has been dedicated to hydrogen production especially for the use in the transport industry. Automobile industries like Honda, Toyota and Hyundai etc which are the leading manufacturer in two-wheelers have already on a track of the manufacturing hydrogen-based fuel cell vehicles. North America, Asia and Europe are the primary adopters for fuel cell vehicles. Since June 2018 California is leading in fuel cell vehicle market with delivering nearly 3000 vehicles with nearly 2000 vehicles have been sold out globally. The drift towards the fuel cell vehicles is still changing and one day it will be the largest market in the world.[17-18, 32, 41] Here, hydrogen production is mainly based on conventional sources and maximum comes from fossil fuels. Million of metric tons of hydrogen has been producing worldwide in which half of the contribution of about 48% is of steam reforming of natural gases then it second most contributor is partial oxidation of crude oil which has a contribution of 30%. The coal gasification/pyrolysis and water electrolysis have 18% and 4% respectively. All of these technologies have their own advantages but when comes to the clean and carbon-neutral process, water splitting considered as one of the best technique for hydrogen production.[21, 42]

The most common sources for industrial and merchant hydrogen, the coal gasification/pyrolysis and water electrolysis have covered approximately 95% and 4% contribution respectively of

current production. In view of the fact that over 95% of hydrogen has been generated by means of fossil fuels that could not be considered as a clean and green energy source. Other than this all process are extremely incompetent, pricey and energy-intensive. Water splitting strategy for hydrogen generation is a clean and safe process.[23, 43]

1.3. Water splitting and electrocatalysts

1.3.1. Water Splitting

The water-splitting process has a wide history of the generation of gases through electric discharge. It was the first documented electric discharge execution between two gold electrodes in the electrostatic machine by Jan Rudolph Deiman along with another scientist Adriaan Paets van Troostwijk in 1789 in Haarlem, The Netherlands. They used the Leyden jar which contained water to discharge the electric potential given between the two gold electrode. The gold electrode has the opposite charge and found that different kind of gas was evolved at both the electrode. Later the gas evolved was recognized as hydrogen and oxygen and a progressively prospective application was recognised. Later Alessandro Volta when contrived the voltaic column in 1800, William Nicholson and Anthony Carlisle were the people who used it for water electrolysis.[44-45] It is almost two centuries that water splitting considered as a sustainable solution for energy problems. The continuous efforts and modification in water electrolysis until 1869 makes it a cheap and smart innovation for hydrogen production in the scientific field. At the same time, Zénobe Gramme in 1869 invented the Gramme machine for hydrogen production. Later, Dmitry Lachinov in 1888 developed a method for industrial-scale hydrogen and oxygen production. Large numbers of electrolyzed and power plants of about 100 MW were built till 1930 which not only generating the hydrogen rather becomes a complete carbon-neutral source of energy.[46-47] But, the huge availability and the easy access of hydrocarbon and other energy sources like hydroelectricity from ammonia fertilizer industry close down this technique for some extent. It was the time of energy crisis in 1970s water electrolysis renewed its importance and built special coverage to solve the energy crisis and sustainable supply problems. It becomes the easiest hydrogen generation technique which seems to provide sustainable energy by decomposing water into hydrogen and oxygen. So, by improving the water electrolysis process could possibly replace the hydrogen as a primary fuel source. [17, 30]The water electrolysis with the evolution of hydrogen and oxygen gases along with a carbon-free byproduct is completely a carbon-neutral process. **Electrochemical water splitting**, **photoelectrochemical water splitting** and **photocatalytic water splitting** are three important ways for sustainable H_2 production. There are numerous growing hydrogen

production processes in advance period that includes **high-temperature steam electrolysis** in which steam as a water source change into the gases with experiencing the high-temperature heat, **solar thermo-chemical water splitting (artificial photosynthesis)** and **biological hydrogen production** etc are the other advanced process which mainly has an objective of hydrogen production through different concept. These terminologies named after the source involved in the biasing process to enhance the reaction kinetics by decreasing the activation energy.[19, 48-49]

1.3.2. Thermodynamics of electrocatalytic water splitting

Hydrogen and oxygen molecules are the basis of formation of water molecules. The decomposition of water by any means leads to the hydrogen and oxygen generation. Since we know hydrogen and oxygen are gases at room temperature and having very high gravimetric energy density thus combining them with suitable means gives a huge amount of energy and water as a by-product. In such a chemical reaction the energy component is so high that it could result in an explosion. But the reaction is not artlessly realistic and therefore does not leads to such adversity. Now, if we think about the reverse of this concept, means generating hydrogen and oxygen from water by providing the excess amount of energy could solve our energy problem to a large extent. The water-splitting basically engross the simulations production of hydrogen and oxygen at the different electrode of an electrolyzer.[20, 44, 46, 48] Water splitting without being a cost-competitive system as compared to other fuel energy systems, it explores the carbon-neutral method of hydrogen production by renewable and environment-friendly energy sources. Indeed, it offers a practical and ideal approach to hydrogen and oxygen production. The approach shows that a reaction occurs at the surface of the electrode in which reaction at cathode leads to the hydrogen generation while the anode evolves the oxygen.[45, 48] But the water splitting is not so straightforward process rather it requires energy input to initiate the decomposition process. The electrocatalytic water splitting occurs in a system called electrolyzer through an electrical charge transfer reaction. Thus, at the electrode-electrolyte interface, the water decomposition instigates by the electric supply which converts into chemical energy. In water electrolysis process, this energy input could be solar energy, electric energy, thermal or their combination and these catalysis process are terms as photocatalytic water splitting, electrocatalytic water splitting or photoelectrochemical water splitting etc.[50-51] Pure water does not have very much conductivity that's why a small amount of electrolytes such as salt or acid has been added into the water. The salt conduct electricity through electrically separated charged particles which on supplying additional electrical energy through metal or

any conductive material used as electrodes, gets accumulated on the oppositely charged electrode. The overall reaction that takes place in water splitting is as below:

Overall reaction $$2H_2O \rightarrow 2H_2 + O_2 \quad (1.1)$$

At Cathode (Reduction) $$2H_2O + 2e^- \rightarrow 2OH^- + H_2 \quad (1.2)$$

At Anode (Oxidation) $$2OH^- \rightarrow H_2O + {}^1/_2\, O_2 + 2e^- \quad (1.3)$$

The existing reversibility and absence of external supply between the two electrodes, there exist an open circuit voltage and termed as equilibrium potential.[52-53]

Overall electrode potential $$E^\circ = E_a^\circ - E_c^\circ \quad (1.4)$$

Wher E_a° and E_c° are the anodic and cathodic half cell electrode potential The energy is converted into the standard cell voltage with the following relation:

Gibbs free energy $$\Delta G^\circ = nFE^\circ \quad (1.5)$$

The total enthalpy for water splitting ΔH° = 286 kJ mol^{-1} while Gibbs free energy is ΔG° = 237 kJ mol^{-1}. Here n, F and E° are the number of electrons, F is Faraday constant and E° is the standard cell voltage respectively. From equation (1.5) including Gibbs free energy and the enthalpy, the total voltage that required in this process for overall water splitting is 1.23 eV and termed as reversible voltage. The reaction enthalpy basically is the term that defines the efficiency in water splitting and without considering this it is not practically possible to evaluate the total energy required for this process. The actual energy is measured by including enthalpy term ΔH° in equation (1.5). The overall voltage that used is the thermoneutral voltage which corresponds to a value of 1.48 eV. It is practically estimated that the maximum efficient water splitting has occurred when the process is evaluated between 1.22 and 1.48 eV. These theoretical and practically used energies or voltage corresponds to the low and high heating values for water splitting.[54-56] These two half cell reaction as in equation (1.2) and (1.3) are termed as hydrogen evolution reaction and oxygen evolution reaction respectively. Typically, these half cell reactions are oxidation and reduction reaction and can be sleek into a single term of equilibrium potential as below:

Nernst Equation $$E_{eq} = E^\circ + {}^{RT}/_{nF}\, ln\, {}^{a_0}/_{a_r} \quad (1.6)$$

at 25 °C and 1 atm under the standard condition where E_{eq} is the equilibrium potential, E° is the standard electrode potential and ${}^{a_0}/_{a_r}$ is the activity ratio that corresponds to the species in

the chemical reaction, R and T are the gas constant and absolute temperature, n and F have their usual meanings. On applying the Nernst equation on the reduction half-reaction it leads to equation 1.7 and similarly, on the oxidation half-reaction the equation 1.8 is obtained. Thus, the electrode potential for the half cell reaction w.r.t to the standard hydrogen electrode can be calculated as below:

HER $$E_{eq} = -0.591 * pH \quad (1.7)$$

OER $$E_{eq} = -0.591 * pH + 1.23 \quad (1.8)$$

From equation (1.7) and (1.8), it can be observed that the overall equilibrium potential for HER and OER varies with the *p*H of the solution and the same scale can be made independent on *p*H if the calculation is made based on hydronium ions in reversible hydrogen electrode. The potential value for HER and OER will be 0 and 1.23 V w.r.t reversible hydrogen electrode at any *p*H scale and such supporting ions alter the activity to some extent but thermodynamics of water splitting almost remains the same. From all the discussion above it clear that the overall potential requires to split the water is 1.23 V known as reversible electrode potential and while the Gibbs free energy change and enthalpy for the reaction need the energy of 237 kJ mol^{-1} and 286 kJ mol^{-1} respectively. This value of free energy is not obtainable at room temperature so the water-splitting reaction thermodynamically not feasible and can only occur if sufficient energy is provided.[57-58] The extra energy provided to overcome the activation barrier and to kick start the electrochemical reaction which is inherently slow is termed as overpotential. The charge migration, bubble formation, potential drop due to voltage supply further requires the higher potential. The influence of such barrier can't be ignored but the overall kinetic barriers can be minimized by thorough providing intermediate state to the reaction which requires less activation energy and could be completed at lower energy supply. These redox-active species by providing intermediates stages enhance the overall efficiency of the process. This could have happened only if the electrode material favours any particular side of reaction and lifts the overall reaction kinetics by minimizing the energy requirements. This intermediate platform for reactions any allows interconversion of electrical and chemical potential energy at lower potential and with a fast rate.[47, 59-60]

1.3.3. Electrocatalyst

The importance of catalysis was a well-known concept date back to the rising of civilization when the earlier epoch of mankind commences the production of alcohol through fermentation. This era of catalysis consists only of secluded interpretation that was intermittently acknowledged without any exertion made to elucidate these occurrences. Swedish chemist J. J. Berzelius for the Stockholm Academy in 1835 notice the enhancement in reaction kinetics on the involvement of some particular material. He describes and stated about the responsible forces for this enhancement named them catalytic forces and coined such materials as catalysis. This is perhaps the primary identification of catalysis as a wide-spreading natural phenomenon. Wilhelm Ostwald, later wrote that "there is probably no chemical reaction which can not be influenced catalytically". He described the working principle and explained that the catalyst presence accelerates the reaction kinetics without affecting the thermodynamic equilibrium of the chemical process.[61-62] This was the time when it was clear that implementing catalyst in the chemical process can lead to the industrial or financial gains along with solving time-consuming perspective. Such material not only decreases the activation energy for the reaction rather the more efficient and less time-consuming. In recent years the perception about such kind of materials has become of strategic importance and have been utilized in a broad area of research. The increased interests towards climate and environmental safety have encouraged the carbon-neutral process for energy transport and energy storage. A good catalyst should be highly active towards the reactant species and highly selective towards one of the products which direct the reaction process towards a specific product and avoids the side reactions. The selectivity and the stability of a catalyst are the main concern as the performance of the catalyst is much affected by the variation in *p*H, temperature and a strong oxidizing or reductive environment. These catalysts are divided into homogeneous and heterogeneous catalyst having important recognition in the field of electrocatalysis.[63-64] The homogeneous catalyst mainly subsists as alike phase as of reactant in the chemical reaction and that makes the separation process of each material time and energy-consuming process. However, the heterogeneous catalyst being a diverse phase as compared to the reactant exceptionally suitable for the catalytic process. The electrocatalyst and electrocatalysis focus on the catalytic activity of the material at the electrode surface in electrochemical processes. Bowden and Rideal in 1928, were the earliest pioneer who gives the concept of electrolysis and studied the electrode reaction. But, according to some scientist like Bockris and Khan, the term electrocatalysis has been introduced by T. Grubb in 1936, while his work on fuel cells. The process based upon the electron transport for oxidation

or reduction at the surface of the electrode material or at the electrode itself. It modifies the reaction kinetics and lowers the activation energy by providing an intermediate state in the reaction process. The electrocatalysis process investigates the material properties in a solution and establishes a relationship with reaction kinetics. The material used as an electrocatalyst in the chemical reaction having different activation energy and in turns having different bonding between the reactant, product and intermediates.[65-66] The surface catalytic reaction occurs through different reaction pathways because of modified thermodynamics by electrode material. Thus any modification or any change in the material or material property modifies the kinetic process. This describes the relative ability of a material to enhance the electrochemical process under the same condition. The reaction kinetics depends upon the strength of chemical bonds between electrode and electrolyte. An excellent selection of electrode material could enhance the efficiency of an electrolyzer many times. The search for such materials in order to improve the electrode stability and activity to reduce investment and operational expenses continues.[61-62, 65] The practical relevance of the catalyst entailed with a negotiation among different consideration of the material. The catalyst importance always based upon relative performance in terms of electrocatalytic activity, thermodynamic stability, durability along with the prime concern of its production cost. The activity of the material could be improved by improving the synthesis process and/or by the composite material having inherent synergy. Then, substituting the noble material with non-noble one may also achieve the desired target. The non-noble materials having a less tendency towards the electrocatalytic processes. Water splitting is one of the processes that purely based upon the electrode properties.[63, 67]

1.3.4. Selection approach for Electrocatalyst

The material selection and investigation to be a HER active catalyst is really an importat job for which different approaches have been introduced. The material selection is based upon the catalytic performance of the material in correlation with the conductivity, stability, work function and free energy adsorption etc. The adsorption of the hydrogen atom and binding strategy with the catalyst surface is the decisive factor for hydrogen evolution. Today, there are excellent computational research powers that it is now theoretically possible to evaluate the free energy that requires for adsorption of a hydrogen atom at the surface of an electrocatalyst.[68] The free energy gives an idea about the hydrogen bonding at the electrode surface. The free energy and the catalytic activity is a measure of catalysts performance of the catalyst and correlation could be understood with a simple graphic depiction called “Volcano plot”. The plot shaped like volcano predicts the comparative catalytic activity of materials based on the predicted hydrogen

binding energy of the intermediates. These plot consideration based upon the 'Sabtiar principle' which states that the binding energy for a good catalyst neither is too tight nor weak. The correlation legitimate sounds good only with adsorbant species that involves one intermediate species while for multi-electron system prophecy will become intricate.[69-70] Trasatti in 1972 describes the trends of an efficient catalyst with the help of Volcano plot based on hydride formation energy. The sequence and exact position in the plot for some metals are still under disputes but the inclusion of free energy value at one of the coordinate with catalytic activity on others coordinate in Volcano plot facilitates the easy prediction of a suitable catalyst. The plot displays two branches ($\Delta G > 0$ and $\Delta G < 0$) of the free energy with an intermediate $\Delta G = 0$ at the top of the Volcano as anticipated by Parson in 1958. The ascending branch which has positive free energy indicated that the adsorption process is slow while the negative branch signifies the strong adsorption process. Therefore, it scrutinizes that the plot designates the superlative recital material lies at the top of the plot. The activity trends are similar to the climbing an uphill and followed by the downhill on a Volcano, this similarity is the reason plot named as Volcano plot. It's interesting to see that the metal congener and their composite may lie on the opposite side of the Volcano plot.[45, 65, 69] The complex structure of the composites as compared to the to their congeners modify the adsorption sites and the property can alter completely in a different way. The modifies active sites could be active or hinder the hydrogen adsorption process, in turn, amends the catalytic activity of the material. Moreover, the heteroatom influence along with doping and the phase synergy remarkably affect the catalytic activity.

1.4. Hydrogen Evolution Reaction

At present hydrogen evolution is among the most important and demanding errands that require efficient strategy and exploration in present scenario especially in the field of the electrochemical reaction. The collective chemical kinetics is closely dependent upon the adsorption and desorption of hydrogen atom at the electrode surface. The adsorption and desorption involve the monoatomic sort of intermediated which moderates the hydrogen bonding at the electrode surface. The formation and breaking bond energies by clever selection of electrocatalysts make the hydrogen generation quit interesting through water splitting.[60, 70]

1.4.1. Fundamentals of HER

The overall water splitting is a *p*H-independent reaction in which *p*H terms of cathodic and anodic half cell reaction as mentioned in equation 1.2 and 1.3 nullify each other. But, individually in the half cell reaction *p*H will become one of the crucial factors and affects the hydrogen generation efficiency. The *p*H dependence in the system directly affects the potential required for each half cell reaction.[58] As already explained in the earlier sections the Nernst equation demonstrates the 59 mV decrease in potential with each unit increase in *p*H of the electrolyte. This equation shows that the potential required for the hydrogen evolution is not the same as the thermal equilibrium potential in acidic, alkaline or neutral media. However, there are various other factors responsible for the higher value of the overpotential which comes into consideration while hydrogen evolution. The inclusion of various environmental factors modifies the real-time required overpotential and the equation can be written as:

$$E = E_{RHE} + iR + \eta \qquad (1.9)$$

where *iR* is an ohmic potential drop and η is the overpotential.[60, 71]

The overpotential is the primary factor that defines the performance of electrodes and the electrolyzer and directly tells the efficiency of an electrolyzer. The value can be minimized by improving the catalytic activity of the electrocatalyst with proper selection of electrolyte. For example, a platinum electrocatalyst can reduce the overpotential value almost to zero voltage. The efficiency of an electrolyzer or in terms of the activity of electrocatalyst, the performance can be evaluated based on reaction rate and the hydrogen production.[66, 72-73] The hydrogen production mainly dependent on the pH of the solution either it's an acidic solution or an alkaline solution. The whole hydrogen generation kinetics proceeds through different mechanisms and depending upon this the whole mechanism has been categorised with different steps. The HER proceeds through the two-electron transfer process in which the role of electron and the step involved mainly decides the reaction rate, and the reaction rate is largely described by the ΔG_H. The value of ΔG_H describes binding strategy between the electrode and the hydrogen. A weak bonding of hydrogen with the electrode surface leads to the adsorption (Volmer) step, thus the overall reaction rate which will limit the Volmer step, while if there is a strong bonding between hydrogen and the electrode surface the reaction kinetics will limit by the desorption (Heyrovsky/Tafel) step. The hydrogen evolution reaction mainly occurs in two steps, the first one is Volmer step a universal step that followed by either Heyrosky step or Tafel

reaction. The proton in the electrolyte gets attached with the electrode surface followed by reduction and forms metal hydride bond. The hydrogen evolution then occurs through electrochemical step (Heyrovsky Step) or end by a chemical reaction between adsorbed hydrogen atoms on the surface of the electrode and the step named as Tafel step. In short, the HER reaction involves the conversion of proton or water into hydrogen depending upon the reaction medium and Volmer step followed by the Volmer-Heyvrosky or Volmer-Tafel mechanism to hydrogen generation. The hydronium acts as a hydrogen source in the acidic medium while the water itself acts as a hydrogen source in the alkaline medium due to the low concentration of the proton. The elementary reactions for the HER under acidic conditions are as follows:

Volmer Step	$M + H_3O^+ + e^- \rightarrow M - H_{ads} + H_2O$	(1.10)
Heyrovsky Step	$M - H_{ads} + H_3O^+ + e^- \rightarrow H_2 + H_2O$	(1.11)
Tafel Step	$2M - H_{ads} \rightarrow 2M + H_2$	(1.12)

Here, M represents the active sites of the catalyst, H_{ads} represents the adsorbed hydrogen on the active site, M-H represents the hydrogen-bond with metal active sites. Similarly, in alkaline media, the mechanism follows different Volmer-Heyrovsky and Vomer -Tafel step. The steps will be as follow:

Volmer Step	$M + H_2O + e^- \rightarrow M - H_{ads} + OH^-$	(1.13)
Heyrovsky Step	$M - H_{ads} + H_2O + e^- \rightarrow H_2 + M + OH^-$	(1.14)
Tafel Step	$2M - H_{ads} \rightarrow 2M + H_2$	(1.15)

The HER mechanism at active sites in an electrochemical process can be generalised through Tafel slope value derived from the polarization curve.[60, 71, 74-77] The Tafel slope value reflects the performance of the electrocatalysts and explains the various steps involved in the hydrogen evolution electrochemical reaction. However, the value of the Tafel slope could be affected by various other factors like applied potential and mass transport in the porous structure. The HER electrochemical kinetics can be expressed in terms of well known *Butler-Volmer equation* as below

$$i = i_\circ \exp\left[\left(\alpha_a n\eta F/RT\right) - \left(\alpha_c n\eta F/RT\right)\right] \quad (1.16)$$

The symbols used there have there usual meaning as mentioned earlier α_a and α_c, are the transfer coefficients, n and η are the number of electrons involved in the rate-determining step and the overpotential respectively. The constant terms like F the Faraday constant, R the gas constant and T the absolute temperature respectively have been used. The value $\eta = E^{\circ} - E_{eq}$ is essential potential for the overall water splitting and the equation (1.16) represent the total current involved in the reaction process. The expression consists of two different kinds of currents that following in electrolyzer, in which the first part contributes to the anodic current and the second represents the cathodic current. The applied potential critically decides the contribution of each term that involved in the reaction process, higher the applied potential contributions of one term will become more significant as compared to others. The equation (1.16) can be rewritten in anodic and cathodic contribution separately.

$$i_a = i_{\circ} \exp\left({}^{\alpha_a n \eta F}/_{RT}\right) \qquad (1.17)$$

$$i_c = i_{\circ} \exp\left({}^{\alpha_c n \eta F}/_{RT}\right) \qquad (1.18)$$

Or equation (1.17) $$i_a = i_{\circ} \exp\left({}^{\eta}/_{b}\right) \qquad (1.19)$$

Or equation (1.18) $$i_c = i_{\circ} \exp\left({}^{\eta}/_{b}\right) \qquad (1.20)$$

where $b = {}^{RT}/_{\alpha_a n \eta F}$ and $b = {}^{RT}/_{\alpha_c n \eta F}$ for anodic and cathodic branch respectively.

In terms of current density, the equation (1.16) can be rewritten as

$$j = j_{\circ} \exp\left[\left({}^{\alpha_a n \eta F}/_{RT}\right) - \left({}^{\alpha_c n \eta F}/_{RT}\right)\right] \qquad (1.21)$$

At higher potential, any one of the terms will be dominated and hence similar to equation (1.19) and (1.20) current density equation could be written as

$$j_a = j_{\circ} \exp\left({}^{\alpha_a n \eta F}/_{RT}\right) \qquad (1.22)$$

$$j_c = j_{\circ} \exp\left({}^{\alpha_c n \eta F}/_{RT}\right) \qquad (1.23)$$

Or equation (1.22) $$j_a = j_{\circ} \exp\left({}^{\eta}/_{b}\right) \qquad (1.24)$$

Or equation (1.23) $$j_c = j_{\circ} \exp\left({}^{\eta}/_{b}\right) \qquad (1.25)$$

Rearranging the terms and simplifying the equation the overpotential for half cell reaction can be measured as

$$\eta = 2.303\,(\,RT/\alpha_c nF\,)\log j_\circ + 2.303(\,RT/\alpha_c nF\,)\log j \qquad (1.26)$$

This equation can be compared with $\eta = a + b\log j$ and called a Tafel equation

Where $a = 2.303(\,RT/\alpha nF\,)\log j_\circ$ which is a constant quantity at the particular condition and the value $b = 2.303(\,RT/\alpha nF\,)$ is called a *Tafel slope* which can be obtained by plotting logarithmic of current density $j_{a/c}$ vs overpotential (η) where quantity $a = 2.303(\,RT/\alpha nF\,)\log j_\circ$ is intercept The *Tafel slope* value practically describes the profound insights in the mechanism or rate-determining step. It is usually expressed in $mVdec^{-1}$ and should have a small value as possible whereas $i_\circ$ is expressed in $mAcm^{-2}$ and should be as large as possible. From Tafel equation is easy to predict that overpotential can be minimized by using electrocatalysts which augments the kinetics of the electrode reaction either by providing higher values of the exchange current density $j_\circ$, without changing the reaction mechanism or by decreasing the slope of the equation, which means if there is an increase of charge transfer coefficient α, so a change of the reaction mechanism. Catalytic up-gradation or improving the efficiency of the HER process seems the finest accessible ways in water electrolysis process that can be accomplished by using electroactive materials. These materials could possibly work as suitably and efficient electrodes material for HER process in order to commercialise the hydrogen production at a large scale.[52, 66-67, 71, 75-76, 78]

1.4.2. Factors influencing the HER thermodynamics

The electrode materials significantly are the most important components for an electrochemical reaction. The catalytic activity modifies with the alteration of size, composition and structural features which can be tailored through nanostructuring, doping, interfacial structuring and enhancing the synergy between phases by *in-situ* grown of nanoparticles. Thus, rational design and frail regulation of interfacial structure can enhance the active sites means exposes the active sites on supports and intrinsic activity through regulation of electronic structure. The electrocatalytic reaction takes places at the surface of the catalyst, so the active site is the major factor that decides the catalytic activity of the material. The tailoring the geometry of the catalyst to improve and to expose the active phases assists remarkably assists the catalytic properties of the material. Besides, the catalyst support also facilitate the stability of the electrocatalyst material. The general consensus of increasing catalytic activity of the material belongs to the increase in the active site, providing synergy to the material, tailoring the

structural and electronic arrangements and assisting the electronic conduction through a conducting material etc.[53, 79-80] The various factors that enhance and modify these factors can arise from assembly of engineered surface and junction induced interfaces while the enhancement in reaction-diffusion can be established by a porous network. A brief discretion about the factors which we study and explores in the thesis work that involved in improving the catalytic activity is summarized below.

(i) Nanostructuring

The electrocatalysis process has endured remarkable progression in the last few decades, in part owing to enhancement in catalyst design at the nanoscale. These expansions have been essential for the recognition of and upgrading in alternative energy technologies based on electrochemical reactions. The catalytic reaction is generally kind of structure sensitive or structure insensitive reactions because the active species generally lies at the surface and edges of the material. The structure of sensitive active species plays a crucial role in catalytic activity. There interatomic spacing along with the crystal structure and crystallite size leads to the different catalytic activity of the material with variation in any one of the property. Nanostructuring manipulates and optimised the catalyst design and modifies the coordination and the bond relationship at the surface of the material. [81-82]The nanoparticle size could be the major factor to manage the extent of low-coordinated sites on the catalyst surface, which modifies and influence the reactant binding strength. These modifications of the active site and surface configuration provide the high surface to volume ratio that consequences in a higher density of surface active sites. The interfacial atoms on the surface of nanostructured materials lead to a high volume fraction of atoms which exceptionally prospect for scheming exterior chemistry and defects concentration. A perfect ability to control and synthesize such nanostructured material with a specific shape, size and morphology can be explored for such high activity of the material. Such catalysts can meet the terms directed as specific requirements in terms of selectivity. The surface property can be directed through crystallite size and crystallite phase modification. The selectivity towards a specific plane and specific structure could also be a factor for improving electrocatalytic activity. This chemistry between the surface and nanostructuring has provided many exciting developments and could revolutionize the chemical industrialisation. Still, the catalyst selectivity and the corresponding performance of materials necessitate many upgrading, understanding of structure properties, with well-defined size shape and composition.[83-84]

(ii) Doping heteroatoms

Heteroatom doping is an efficient method to further tune the electronic structure that further improves the catalytic activity of the host material. The charge redistribution of the host material caused by the introduction of foreign elements amends the electrical, catalytic and optical properties of the material. Such modification in the material results into the enhancement of active sites and optimises the energy related to the intermediate formation. The synergetic coupling of the host and doped metals highly induces the catalytic properties of the material. Boron, carbon, nitrogen, sulphur, phosphorous etc are such heteroatoms having different electronegativity than the host materials in a composite.[85] These heteroatoms doing does not changes the desired intrinsic features of the material with great potential of tuning electrocatalytic activity. The heteroatom atom on a metal surface can promote the intermediate steps that occur in water-splitting reactions. The inclusion of such elements generally decrease the activation energy barrier and facilitate the smooth happening of the reactions. There multiatom doping as compared to a single atom can precisely bring the desired structural and electronic changes for HER activity optimization. The dopant atom can directionally transfer the electron that leads to the changes in electronic structure and enhancement in the active sites which further assist the chemical process. The modulation and its extent depend upon the types of dopant elements and it's chemical state. Because particular heteroatoms with different size and the electronegativity could modify different Fermi levels and corresponding performance.[86-87]

(iii) Creating a porous structure

One of the esteemed chemicals confront in the trade of nanomaterials is to organize the placement of diverse chemistries in spatially distinct regions on a nanoscale object. Porous materials are pores containing solid phases composites in which mainly differentiated from the other solid material in this category because of the pores presents in them. This mainly leads to the basic difference between such porous materials and other solids. Therefore, the porous materials could be categorized in terms of different kind of pores that belongs to a different kind of porosity and pore size. The porous material having unique pore shape and corresponding specific surface area shows different catalytic activity in the electrocatalytic reaction. The collectively if we say porosity is the crucial parameters in such materials due to its noteworthy manipulation in chemical properties as well as physical and mechanical properties of the materials. The porosity is the other important aspects that assist the catalytic activity of the

materials. The catalyst design strategy engrosses the couture of structure of pores which endow with the unique product selectivity and belongs to the ultrahigh surface areas. According to the IUPAC definitions, the porous material has been broadly categorising in three categories depending upon the pore size of the material. Pores categories into the three main categories in which the first one is micropores that having a pore size less than 2 nm, the second category called as mesopores structured having a pore size between 2 and 50 nm and the third category are of macropores having pore size large than 50 nm respectively. The porous structure could be a composite of organic, inorganic and organic-inorganic combination.[88] The technology importance of porous structures lies in the ability of interaction of pore walls with the atoms, ions, molecules and supermolecules. The pore size and its distribution along with the shape size and the quantity have the ultimate tendency of convenient emancipation to capture liquid, gas molecules and solid particles. The tailoring of such porous materials with specific size and designed specifically to achieve desired results is highly recommendable in frontier research. Thus, it ultimate curios to design a pore of porous material behave as a functional phase within the material for optimized performance. A pore with restricted space and spatial captivity is one of the antique notions. The porous character significantly influences the mechanical, physical and chemical properties of the material. Nanostructuring porous structure has enthralled a lot of interest as possible materials for catalytic purposes due to synergy enhancement because of porosity and nanostructuring. Silica, carbon material, metal-organic frameworks, zeolites, aluminium-based composite etc are among few porous structured materials that could be a preferred choice for constructing metal-based or metal-free electrocatalyst for hydrogen generation purpose. In this thesis work, the silica and the carbon-based porous structure material has been used for the purpose of HER electrocatalyst.[83, 89]

(iv) Coupling conductive substrates or interfaces

Apart from the electrode material, the support material might also show has the capability of enhancing the activity and serves as the catalytic centre in the process of electrocatalysis. An approriate catalyst support generally provides the high surface area, enhanced conductivity and chemical stability etc. A catalyst adapts the chemical and physical properties of the supporting material that assist the chemical process. It performs an integral part of the catalyst in the electrochemical process and synergistically enhances the desired properties for hydrogen generation. The tunable properties of the substrate and the prime activity of the metal catalyst collectively can achieve the optimum performance for the catalyst. Especially, the selection of support materials is a challenging task, as the corrosive properties and structural variation while

the application in different solutions is the primary concern. Hybrid support material with tunable compositions has shown a remarkable piece of work towards the water-splitting. An optimised interaction not only supports the catalytic efficiency but also govern the new path to the hybrid nanostructure supported electrocatalyst. The supports consistently enhances the performance and satisfactorily enhances the durability of the catalyst. Thus, the choice of catalyst and the supports material is vital and highly influential aspects in the electrochemical industry.[71, 84, 90] Different morphology, composition, orientation and characteristics of the supporting material gives rise to special kind of catalytic activity. Briefly, its well studied that catalytic support by any means constitutes a very active area and develops a better electrocatalyst for HER applications. The interfacial contact between two contrast phases improves the catalytic activity of the material. The synergic effect introduced by the two or more different components can exhibit unique chemical and physical properties. The readjustment of electronic structure results in stabilizing active catalyst by facilitating diverse adsorption sites and accelerating charge transfer process. Some supported dispersing material prevents the agglomeration of the nanoparticles in the synthesis process and prevents the blockage of active sites. Sometimes its seen that the metal electrocatalyst gets leached out into the solution, a suitable supporting material could prevent this and stabilized the electrocatalytic activity. Though carbon and non-carbonaceous materials have been used for support materials, still the search is continuing for more better material. Carbon support like graphene oxide, graphene, carbon nanotubes, carbon nanobelts etc. are the well known conducting supports. Such nanostructures facilitate enhanced catalytic activity to the catalyst materials and improve the electrical and mechanical properties as well. For example, if taking the example of carbonaceous materials CNTs and CNFs possess superior electrical conductivity because of the high surface area lead to enhanced catalytic activity.[91-92] The non-carbonaceous material like silica, oxides and zeolites etc. also have picked up race as the supporting assistance. On the basis of a different kind of morphology and conductivity of the supporting material, the catalytic activity of the electrodes could be tuned to a specific purpose. These all are the well studied supporting material but graphene oxide, RGO, and silica are the widely used supporting material. In this work, the use of these supporting material as a carbon source or as supporting material along with the silica has been introduced and their electrocatalytic activity has been studied. Various oxides and their composites with other carbon compounds have been applied to the catalyst for better activity. Of course, SiO_2 is well known neutral material for catalyst support and the catalytic activity obtained by a combination of nanoparticle *in-situ* growth and such supports is interesting.[89, 93]

1.5. Molybdenum and Hydrogen production

In today's scenario, the electrochemical catalytic reaction is the promising method to produce renewable energy in which water, carbon dioxide and nitrogen are used to converts into high energy carrier such as hydrogen. Simultaneously or separately the same strategy has been also used to convert them into oxygen, hydrocarbons, ammonia etc. Electrocatalytic water splitting is among the best ways to produce a renewable source of energy. The electrocatalyst being an important part of the water-splitting reaction remarkably enhances the performance of the overall process. Electrocatalyst broadly has been categorized into noble metal electrocatalyst and non-noble electrocatalysts sections depending upon the abundance, cost, physical and chemical properties. A noble metal consists of Pt, the state of art HER electrocatalysts and Pt derived electrocatalyst materials which have excellent catalytic activity. The second category is of non-noble electrocatalyst which usually contained a transition metal like Mo, W, Ni, Cu, Co etc and their derivatives which could be the best alternative for the noble metal electrocatalysts. The third category of non-metal has also existed which includes the non-metal like boron, sulphur, carbon, nitrogen, phosphorus and selenium which serves as to construct metal-free electrocatalysts or can be used as heteroatom doping in the metal composites.[94-95] Although platinum is the best option for HER electrocatalyst, the cost and the dearth of such metals obstruct the commercial level hydrogen production. These factors make researchers to concern about the alternative of such material and use of non-noble metals. Non-noble electrocatalyst has been divide into two categories, one belongs to the organic liganded metals like Ni, Mo and Fe and inorganic compounds of metals. Interestingly hydrogenous is the best competitor to the platinum which functions even at thermodynamic equilibrium with high catalytic rate. Hydrogenous is the most efficient hydrogen-generating catalyst employing the first-row transition metals like Fe, Ni at the catalytic centre of their active sites. Another biocatalyst nitrogenase having Fe and Mo as catalytic active centres and assists in ammonia generation from nitrogen fixation and used for limited production of hydrogen. Hydrogen generation by mimicking the natural mechanism as in algal hydrogenases hydrogen production could be the sustainable alternative to industrial hydrogen production. The existence of Mo, Ni, Fe type metal in such biological process inspires the researcher to use such earth-abundant, catalytically favourable transition metals. In a distinctive the Volcano plot describes and pictorially represents the hydrogen adsorption energy of transition metal M = Nb, Mo, Ni, Pt, Au, Ag, etc. lies as Mo >Ni> Pt which signifies that the compared to Pt the other metals shows strong metal hydrogen bond (Mo, Ni) that could encumber the hydrogen discharge form active sites.[69, 96-99]

However, as mentioned in the previous section the inclusion of inorganic compounds can amend the bond between metal and hydrogen that could result into achieving a Gibbs free energy comparable to Pt for hydrogen generation in an acidic environment. The vast existence of Ni, Fe, Cu, Mo etc in earth crust that motivates the people to find out alternative form these transition metals could provide the economical and efficient electrocatalyst for water splitting reactions. Transition metal derivatives like metal carbide, metal oxide, metal sulphides, metal nitrides etc are among the known HER electrocatalyst. If the selection is made on the basis of economical and activity aspects among transition metal derivative, carbide could be the suitable candidate for HER electrocatalyst. Amongst the transition metal carbides, molybdenum derivatives especially molybdenum carbide could be the suitable candidate for HER electrocatalytic activity.[69-70, 90]

1.5.1. Molybdenum carbide as electrocatalyst

Molybdenum carbide has been getting attention since it was found that it could be a good catalyst for hydrogen evolution reaction. The pioneered work on carbide in transition metal was done by Lee *et al.* and Boudart's group in the eighties. They proposed that synthesis of molybdenum carbide through carburization process of bulk molybdenum oxides through a temperature programme reduction method in a gas atmosphere of 20% methane in hydrogen at 700 °C. Molybdenum carbide due to similar electron density of state of d-band to that of Pt shows excellent hydrogen adsorptive activity favourable to the HER electrocatalysis. Such activity originates from the metal-carbon bond formation as a result of the d-band modification in the structure of molybdenum carbide. However, in molybdenum carbide, the active sites are hampered by the poor processability and easy aggregation which leads to the activity degradation. The formation of the oxide materials in the surface of the molybdenum carbide is another factor that limits the corrosion of electroactive material in all pH range application. The problem generally minimized by using high surface area support material.[94, 100-101] Initially, molybdenum carbide has been used as supporting material for Pt electrocatalyst. In 2012 Vrubel et al when investigated the catalytic activity of Mo_2C in wide pH range with excellent activity it was assumed it could be the best alternative of Pt and WC based catalyst which has instability issues in wide pH range functioning.The optimisation and the activity upgrading has been continuing since then by nanostructuring and synergic enhancement.[100, 102] The stability and activity optimisation of the material has been performed and studied by nanostructuring, dopant, hybridization with supporting material. There has been a lot of theoretical and experimental studies on molybdenum carbide for improving the catalytic activity of the material. The

economical abundance and excellent sulfur toxicity resistance of molybdenum carbide categorised it a perfect substitute for noble metals. The comparable activity of molybdenum carbide not only in hydrogen generation but also has very good activity towards hydrocarbon dehydrogenation, hydrogenolysis and in isomerisation reaction. Such belongings of molybdenum carbide formulate the broad application prediction in the catalyst field together with the hydrogen generation process. The excellent catalytic activity was shown by molybdenum carbide in all pH range and the tunable properties regard it as the future electrocatalyst for hydrogen generation.[98, 101] From Vrubel to now a lot of improvement and studies have been performed to optimised the catalytic activity of molybdenum carbide which is still going on. Various optimization has been performed including nanostructuring process, heteroatom doping, conductive phases and synergic factors have been included in order to study the activity. MOFs supported MoCx nano-octahedron investigated by Xia et al. and ultrafine β-Mo_2C on graphene substrate produced by Chen et al. shows excellent catalytic activity. In recent times, Xu et al. developed the β-Mo_2C nanoparticles grown on N-doped carbon nanotubes have also been investigated and shows remarkable catalytic activity towards HER. However, there is still a large possibility for optimisation of material selection and catalyst designing, the struggle is till continue to obtain the best economical catalyst for HER applications. Other molybdenum derivatives like molybdenum oxide, sulphides, nitrides, phosphide and selenide etc. have also been investigated and their durability and scarcely aggregation tendency attract much attention towards HER applications.[85, 90, 100]

1.5.2. Molybdenum derived composites

Molybdenum carbide has been investigated through different synthesis and optimisation process. Similarly, other molybdenum derivatives like molybdenum nitride, molybdenum oxide, molybdenum phosphide, molybdenum sulphide and molybdenum selenide have been investigated. Because of there fascinating physicochemical properties, they also have accomplished significantly interest in hydrogen generation technology.[85, 103] However, the stability issues of Mo based derivatives under realistic catalytic condition got much concern in the field of catalytic study. The Mo based nanocrystals onto carbon or some other conductive substrates can efficiently enhance the structural as well as catalytic stability. The interesting properties of Mo/carbon-based nanostructure hybrid material have been tailored but the esteemed interaction between Mo-based composites and sustaining materials are still exigent. The dexterous tailoring of hybrid material assuages the agglomeration of metal species. These concerns have been challenged through using MOFs, polymers, polymer/organic substrates,

silica or other carbonaceous supports in order to improve the catalytic activity and stability of the Mo- based materials. The significant interaction between supports and metal efficiently manages the size and aggregation of the materials at high temperature.[100-101, 104]

1.5.3. Aim of the thesis

In recent years, the transition metal carbides (TMCs) have been highly explored and have been studied with outcomes of astonishing corrosion resistance with commendable catalytic activity. The high physical and chemical stability of the transition metals and is a low cost and potentially high catalytic activity it becomes a hotspot in the hydrogen generation technology. The TMCs have already been explored widely to be used as a catalyst in electrochemical reactions, especially for hydrogen production. The TMCs typical are interstitial alloys and by density functional theory (DFT) it can be elucidated that the electronic structures of the transition metals get modified on the inclusion of carbon atom on carbonisation. This modification approaches the similarity of these carbides to the Pt metals and hence transition metal carbides and their derivatives show exceptional catalytic activities towards HER. Especially the molybdenum carbide electronic structure has a very close resemblance to the platinum metal after incorporation of the carbon atom.[87, 94, 104] Molybdenum carbide has a tendency to works in the wide *p*H range. But, the lesser specific surface area of the materials leads to the lesser active sites, also the low electron conductivity hinders molybdenum carbide to works as efficiently HER catalyst. The general synthesis process for molybdenum carbide nanoparticles involves the use of carbonaceous gases in thermal reduction methods which involve the potential safety hazards. The high-temperature synthesis reaction and the carbonaceous gases lead to the sintering problem and the blockage of active sites by an excess amount of carbon in the synthesis process respectively. The activity of the catalyst hence can be increased through avoiding the sintering and by avoiding the loss of active sites. This whole process of increasing the efficiency of the electrode material could be done by different methods like by increasing the active surface area or active sites of the material, by increasing the conductivity of the material and by optimising the hydrogen adsorption energy of the material etc.[67, 94, 96, 101] The study reveals that the carbide requires an innovative synthesizing method to shrink its particles size. It also realized that the combination with the appropriate conducting substrate, such as graphene oxide, reduced graphene oxide, carbon nanotubes, carbon nanoribbons etc. enhances the catalytic activity. The combination of such conductive substrates not only improves the catalytic activity of the material it also provides the additional active sites for hydrogen adsorption process. The increasing of active sites and optimising the free energy

of hydrogen adsorption close to zero escorts with the fast kinetics for hydrogen evolution reaction. These all properties in a single synthesis are hard to obtain thus a combined process to achieve this target is formed. An *in-situ* synthesis approach is applied by providing all the initial precursor to the reaction module and the various properties of the material have been modified. In this thesis, the prime aim is to synthesis and study the catalytic activity and the factors involved in the catalytic activity enhancements of the molybdenum carbide-based electrocatalyst for hydrogen evolution reaction. The catalytic property of the molybdenum carbide-based catalysts motivates us to find out the best of molybdenum derived composites. The bulk structured carbide, nitrides, oxides and phosphide etc. having some stability or catalytic incompatibility towards the hydrogen evolution reactions, but the assistance of the conductive supports, heteroatoms and/or the synergy of the additional phase is a really interesting area for study. Based upon the catalytic activity of the different molybdenum based catalyst, here, in this thesis a strategy of the *in-situ* composite synthesis has been used, in which biphasic molybdenum based carbide/oxide, carbide/nitride, carbide/phosphide, doping of heteroatom in carbide/nitride along with the carbon or silica support materials has been investigated. The thesis involves the synthesis of molybdenum derives electrocatalyst, their characterization process and the theoretical outcomes towards the HER application. The investigation consists of different aspects of the material that describes thermodynamics involves in hydrogen generation, synergy achieved in the composites by the *in-situ* synthesis of binary phase molybdenum composites along with the adsorption properties and the electronic properties of the materials. There are interesting facts to know about the upshot of the supporting material like biomass, graphene oxide, reduced graphene oxide and silica on the molybdenum derives composites. The theoretical investigation of the active sites for hydrogen evolution and the corresponding experimental outcomes of the catalyst towards HER mechanism is commendable, in this context several factors influencing the adsorption properties have been investigated. In this work initially, we study the nanoparticles dispersed on the biomass template. The surface decorated dispersed nanoparticles are key factors that typically shows the activity towards the HER process. The dispersed nanoparticles usually obtained by the deposition techniques but here we have grown *in-situ* nanoparticles on biomass templates. After that, the conductive support like graphene oxide has been used and the hydrogen evolution properties have been studied. The idea epitomizes here may possibly provide design and enlargement of the nanoparticles synthesis with the use of other available biomass materials or conductive templates and biphasic composites. The expansion of customized efficient electrocatalyst materials is the existent need of today electrochemical water splitting processes.

Hence, the doping of heteroatoms has further studied the enhanced catalytic sites in the material and found that copper doping in the molybdenum carbide and molybdenum nitride provides long term stability with improved catalytic activity to the material.The nanostructuring contributes quantum effects to the catalyst nanoparticles and in turns the charge transport, adsorption process gets modified to the unique properties. However, the too-small nanoparticles have a large specific area and large specific surface energy and the use of such nanoparticles is sometimes getting incompatible to use as an electrode material. Thus, it becomes obligatory to integrate them into the other proper matrix. Such a matrix not only provides the extra active sites to the material but also optimised the distribution of nanoparticles and adsorption process on the catalyst material. The developments of such electrode materials on the porous structured material provides stability and improved catalytic activity to the nanoparticles. The aggregation of the nanoparticles which hinders the electrocatalytic activity limits by such porous structured supports. The limitation to aggregation and the enhanced stability to the nanoparticles protects their functionality and improves the processability of the composites. This kind of functionality has been achieved by synthesizing the *in-situ* molybdenum carbide and molybdenum oxide nanoparticles with the supports of silica structure. The molybdenum carbide is HER active materials while molybdenum oxide having a metallic structure with a small tendency towards being HER electrocatalysts in nanostructured form. The combination of both structures provides the enhanced electrocatalytic activity in acidic medium. Similar activity trends have been observed in the combination of two different HER active materials molybdenum carbide and molybdenum phosphide. The stability and the activity obtained in mutually contrast phases is highly remarkable. However, the inadequacy of active sites which could further be enhanced can be explored through different concept and strategy. The intrinsic activity and interlayer conductivity of the material could also be enhanced with some other synthesizing methods in coming future. Hence, a combined strategy to simultaneously increases these properties of the catalyst are mutually complementary. Indeed, we found nanocrystallites of molybdenum carbide with the existence of contrast phases like molybdenum nitride, molybdenum oxide and molybdenum phosphide along with assisted porous substrates and doped heteroatoms in biphasic composites. The heterojunctions such formed are most active centres in the molybdenum based electrocatalyst. Such synthesized molybdenum based materials could be extended further to the lab-scale water-splitting devices and applications.

References

1. Billatos, S., *Green technology and design for the environment*. CRC Press: **1997**.
2. Jaccard, M., *Sustainable fossil fuels: the unusual suspect in the quest for clean and enduring energy*. Cambridge University Press: **2006**.
3. Charter, M.; Tischner, U., *Sustainable solutions: developing products and services for the future*. Routledge: **2017**.
4. Popp, A.; Krause, M.; Dietrich, J. P.; Lotze-Campen, H.; Leimbach, M.; Beringer, T.; Bauer, N., Additional CO_2 emissions from land use change—forest conservation as a precondition for sustainable production of second generation bioenergy. *Ecological Economics* **2012,** *74*, 64-70.
5. Omer, A. M., Energy, environment and sustainable development. *Renewable and sustainable energy reviews* **2008,** *12* (9), 2265-2300.
6. Kneese, A., RU Ayres. *Economy & Ecology: Towards Sustainable Development* **2013,** *1*, 89.
7. Wuebbles, D. J.; Jain, A. K., Concerns about climate change and the role of fossil fuel use. *Fuel processing technology* **2001,** *71* (1-3), 99-119.
8. Chen, Z.; Chen, G., An overview of energy consumption of the globalized world economy. *Energy Policy* **2011,** *39* (10), 5920-5928.
9. Kadoshin, S.; Nishiyama, T.; Ito, T., The trend in current and near future energy consumption from a statistical perspective. *Applied Energy* **2000,** *67* (4), 407-417.
10. Moriarty, P.; Honnery, D., Global renewable energy resources and use in 2050. In *Managing Global Warming*, Elsevier: **2019**; pp 221-235.
11. Pachauri, R. K.; Allen, M. R.; Barros, V. R.; Broome, J.; Cramer, W.; Christ, R.; Church, J. A.; Clarke, L.; Dahe, Q.; Dasgupta, P., *Climate change 2014: synthesis report. Contribution of Working Groups I, II and III to the fifth assessment report of the Intergovernmental Panel on Climate Change*. Ipcc: **2014**.
12. Leichenko, R.; O'Brien, K., *Climate and society: transforming the future*. John Wiley & Sons: **2019**.
13. Owusu, P. A.; Asumadu-Sarkodie, S., A review of renewable energy sources, sustainability issues and climate change mitigation. *Cogent Engineering* **2016,** *3* (1), 1167990.
14. Purohit, I.; Sundaray, S.; Motiwala, S., Familiarization with Energy Storage Technologies and Their Relevance for Renewable Energy (RE) Based Power Generation. In *Low Carbon Energy Supply*, Springer: **2018**; pp 273-326.

15. Abdalla, A. M.; Hossain, S.; Nisfindy, O. B.; Azad, A. T.; Dawood, M.; Azad, A. K., Hydrogen production, storage, transportation and key challenges with applications: a review. *Energy conversion and management* **2018,** *165*, 602-627.

16. Zohuri, B., The Chemical Element Hydrogen. In *Hydrogen Energy*, Springer: **2019**; pp 1-35.

17. Zohuri, B., *Hydrogen energy: Challenges and solutions for a cleaner future*. Springer: **2018**.

18. Demirbas, A., Future hydrogen economy and policy. *Energy Sources, Part B: Economics, Planning, and Policy* **2017,** *12* (2), 172-181.

19. Cox, R., *Hydrogen: Its Technology and Implication: Production Technology*. CRC press: **2018**; Vol. 1.

20. Nikolaidis, P.; Poullikkas, A., A comparative overview of hydrogen production processes. *Renewable and sustainable energy reviews* **2017,** *67*, 597-611.

21. Scipioni, A.; Manzardo, A.; Ren, J., *Hydrogen economy: supply chain, life cycle analysis and energy transition for sustainability*. Academic Press: **2017**.

22. Dou, Y.; Sun, L.; Ren, J.; Dong, L., Opportunities and future challenges in hydrogen economy for sustainable development. In *Hydrogen Economy*, Elsevier: **2017**; pp 277-305.

23. Abe, J.; Ajenifuja, E.; Popoola, O., Hydrogen energy, economy and storage: review and recommendation. *International Journal of Hydrogen Energy* **2019**.

24. El-Emam, R. S.; Özcan, H., Comprehensive review on the techno-economics of sustainable large-scale clean hydrogen production. *Journal of Cleaner Production* **2019,** *220*, 593-609.

25. Sheffield, J. W., The Extraordinary Hydrogen Romantic-The Story of Dr. T. Nejat Veziroglu. *Международный научный журнал Альтернативная энергетика и экология* **2019,** (4-6), 12-13.

26. Team, G. E. A. W., Global Energy Assessment. *Cambridge Books* **2012**.

27. Brown, M. T.; Protano, G.; Ulgiati, S., Assessing geobiosphere work of generating global reserves of coal, crude oil, and natural gas. *Ecological Modelling* **2011,** *222* (3), 879-887.

28. Frumkin, H., Energy and Human Health. *Environmental Health: From Global to Local* **2016**, 345.

29. Garland, N. L.; Papageorgopoulos, D. C.; Stanford, J. M., Hydrogen and fuel cell technology: Progress, challenges, and future directions. *Energy Procedia* **2012,** *28*, 2-11.

30. Staffell, I.; Scamman, D.; Abad, A. V.; Balcombe, P.; Dodds, P. E.; Ekins, P.; Shah, N.; Ward, K. R., The role of hydrogen and fuel cells in the global energy system. *Energy & Environmental Science* **2019,** *12* (2), 463-491.

31. Romm, J. J., *The hype about hydrogen: fact and fiction in the race to save the climate*. Island Press: **2004**.

32. Apostolou, D.; Xydis, G., A literature review on hydrogen refuelling stations and infrastructure. Current status and future prospects. *Renewable and Sustainable Energy Reviews* **2019,** *113*, 109292.

33. Fikri, R. M.; Kim, B.; Hwang, M., Waiting Time Estimation of Hydrogen-Fuel Vehicles with YOLO Real-Time Object Detection. In *Information Science and Applications*, Springer: **2020**; pp 229-237.

34. Michaelowa, A.; Butzengeiger, S., Breakthrough of hydrogen technologies until 2030: chances and risks for Gulf countries, international policy implications. *EDA Insight. Research & Analysis* **2019**.

35. Bader, N.; Bleischwitz, R.; Madsen, A. N.; Andersen, P. D., EU policies and cluster development of hydrogen communities. *Bruges European Economic Research papers* **2008**.

36. Khalili, S.; Rantanen, E.; Bogdanov, D.; Breyer, C., Global Transportation Demand Development with Impacts on the Energy Demand and Greenhouse Gas Emissions in a Climate-Constrained World. *Energies* **2019,** *12* (20), 3870.

37. Hacking, N.; Pearson, P.; Eames, M., Mapping innovation and diffusion of hydrogen fuel cell technologies: Evidence from the UK's hydrogen fuel cell technological innovation system, 1954–2012. *International Journal of Hydrogen Energy* **2019,** *44* (57), 29805-29848.

38. Ehsani, M.; Gao, Y.; Longo, S.; Ebrahimi, K., *Modern electric, hybrid electric, and fuel cell vehicles*. CRC press: **2018**.

39. Iida, S.; Sakata, K., Hydrogen technologies and developments in Japan. *Clean Energy* **2019,** *3* (2), 105-113.

40. Tlili, O.; Mansilla, C.; Frimat, D.; Perez, Y., Hydrogen market penetration feasibility assessment: Mobility and natural gas markets in the US, Europe, China and Japan. *International Journal of Hydrogen Energy* **2019,** *44* (31), 16048-16068.

41. Bezdek, R. H., The hydrogen economy and jobs of the future. *Renew. Energy Environ. Sustain.* **2019,** *4*, 1.

42. Santhanam, K. S.; Press, R. J.; Miri, M. J.; Bailey, A. V.; Takacs, G. A., *Introduction to hydrogen technology*. John Wiley & Sons: **2017**.

43. Roberts, D., This company may have solved one of the hardest problems in clean energy. Feb: **2018**.

44. Diaz-Morales, O.; Calle-Vallejo, F.; de Munck, C.; Koper, M. T., Electrochemical water splitting by gold: evidence for an oxide decomposition mechanism. *Chemical Science* **2013,** *4* (6), 2334-2343.

45. Trasatti, S., Water electrolysis: who first? *Journal of Electroanalytical Chemistry* **1999,** *476* (1), 90-91.

46. Mostafaeipour, A.; Khayyami, M.; Sedaghat, A.; Mohammadi, K.; Shamshirband, S.; Sehati, M.-A.; Gorakifard, E., Evaluating the wind energy potential for hydrogen production: a case study. *International Journal of Hydrogen Energy* **2016,** *41* (15), 6200-6210.

47. Santos, D. M.; Sequeira, C. A.; Figueiredo, J. L., Hydrogen production by alkaline water electrolysis. *Química Nova* **2013,** *36* (8), 1176-1193.

48. Parkinson, B.; Turner, J.; Peter, L.; Lewis, N.; Sivula, K.; Domen, K.; Bard, A. J.; Fiechter, S.; Collazo, R.; Hannappel, T., *Photoelectrochemical water splitting: materials, processes and architectures*. Royal Society of Chemistry: **2013**.

49. Balthasar, W., Hydrogen production and technology: today, tomorrow and beyond. *International Journal of Hydrogen Energy* **1984,** *9* (8), 649-668.

50. Tee, S. Y.; Win, K. Y.; Teo, W. S.; Koh, L. D.; Liu, S.; Teng, C. P.; Han, M. Y., Recent progress in energy-driven water splitting. *Advanced Science* **2017,** *4* (5), 1600337.

51. Hilliard, S. Water splitting photoelectrocatalysis: the conception and construction of a photoelectrocatalytic water splitting cell. **2016**.

52. Godula-Jopek, A., *Hydrogen production: by electrolysis*. John Wiley & Sons: 2015.

53. Guo, Z.; Chen, Y.; Lu, N. L., *Multifunctional nanocomposites for energy and environmental applications*. John Wiley & Sons: **2018**.

54. Pascuzzi, S.; Anifantis, A. S.; Blanco, I.; Scarascia Mugnozza, G., Electrolyzer performance analysis of an integrated hydrogen power system for greenhouse heating. A case study. *Sustainability* **2016,** *8* (7), 629.

55. Penchini, D.; Cinti, G.; Discepoli, G.; Desideri, U., Theoretical study and performance evaluation of hydrogen production by 200 W solid oxide electrolyzer stack. *International journal of hydrogen energy* **2014,** *39* (17), 9457-9466.

56. Ulleberg, Ø., Modeling of advanced alkaline electrolyzers: a system simulation approach. *International journal of hydrogen energy* **2003,** *28* (1), 21-33.

57. Shinagawa, T.; Takanabe, K., Towards versatile and sustainable hydrogen production through electrocatalytic water splitting: electrolyte engineering. *ChemSusChem* **2017,** *10* (7), 1318-1336.

58. Giordano, L.; Han, B.; Risch, M.; Hong, W. T.; Rao, R. R.; Stoerzinger, K. A.; Shao-Horn, Y., pH dependence of OER activity of oxides: current and future perspectives. *Catalysis Today* **2016,** *262*, 2-10.

59. Zeng, K.; Eng, M., *Improvements and Optimisation of Water Electrolysis for Hydrogen Production*. University of Western Australia: **2012**.

60. Lasia, A., Mechanism and kinetics of the hydrogen evolution reaction. *international journal of hydrogen energy* **2019**.

61. Jorpes, J. E., *Jac. Berzelius: his life and work*. Univ of California Press: 1970; Vol. 7.

62. Lindström, B.; Pettersson, L. J., A brief history of catalysis. *Cattech* **2003,** *7* (4), 130-138.

63. Védrine, J. C., Heterogeneous catalysis on metal oxides. *Catalysts* **2017,** *7* (11), 341.

64. Singh, S. B.; Tandon, P. K., Catalysis: a brief review on nano-catalyst. *J Energy Chem Eng* **2014,** *2* (3), 106-115.

65. Trasatti, S., Electrocatalysis: understanding the success of DSA®. *Electrochimica Acta* **2000,** *45* (15-16), 2377-2385.

66. Angelo, A., Electrocatalysis of hydrogen evolution reaction on Pt electrode surface-modified by S-2 chemisorption. *International journal of hydrogen energy* **2007,** *32* (5), 542-547.

67. Wang, J.; Xu, F.; Jin, H.; Chen, Y.; Wang, Y., Non-noble metal-based carbon composites in hydrogen evolution reaction: fundamentals to applications. *Advanced materials* **2017,** *29* (14), 1605838.

68. Boudart, M.; Djéga-Mariadassou, G., *Kinetics of heterogeneous catalytic reactions*. Princeton University Press: **2014**.

69. Quaino, P.; Juarez, F.; Santos, E.; Schmickler, W., Volcano plots in hydrogen electrocatalysis–uses and abuses. *Beilstein journal of nanotechnology* **2014,** *5* (1), 846-854.

70. Laursen, A. B.; Varela, A. S.; Dionigi, F.; Fanchiu, H.; Miller, C.; Trinhammer, O. L.; Rossmeisl, J.; Dahl, S., Electrochemical hydrogen evolution: Sabatier's principle and the volcano plot. *Journal of Chemical Education* **2012,** *89* (12), 1595-1599.

71. Dubouis, N.; Grimaud, A., The hydrogen evolution reaction: from material to interfacial descriptors. *Chemical Science* **2019,** *10* (40), 9165-9181.

72. Millet, P.; Andolfatto, F.; Durand, R., Design and performance of a solid polymer electrolyte water electrolyzer. *International Journal of Hydrogen Energy* **1996,** *21* (2), 87-93.

73. Kumar, S. S.; Himabindu, V., Hydrogen production by PEM water electrolysis–A review. *Materials Science for Energy Technologies* **2019**.

74. Li, Y.; Wang, J.; Tian, X.; Ma, L.; Dai, C.; Yang, C.; Zhou, Z., Carbon doped molybdenum disulfide nanosheets stabilized on graphene for the hydrogen evolution reaction with high electrocatalytic ability. *Nanoscale* **2016,** *8* (3), 1676-1683.

75. Bockris, J. M.; Potter, E., The mechanism of the cathodic hydrogen evolution reaction. *Journal of The Electrochemical Society* **1952,** *99* (4), 169-186.

76. Bhardwaj, M.; Balasubramaniam, R., Uncoupled non-linear equations method for determining kinetic parameters in case of hydrogen evolution reaction following Volmer–Heyrovsky–Tafel mechanism and Volmer–Heyrovsky mechanism. *International journal of hydrogen energy* **2008,** *33* (9), 2178-2188.

77. Krstajić, N.; Popović, M.; Grgur, B.; Vojnović, M.; Šepa, D., On the kinetics of the hydrogen evolution reaction on nickel in alkaline solution: Part I. The mechanism. *Journal of Electroanalytical Chemistry* **2001,** *512* (1-2), 16-26.

78. Ni, M.; Leung, M. K.; Leung, D. Y., Parametric study of solid oxide steam electrolyzer for hydrogen production. *International Journal of Hydrogen Energy* **2007,** *32* (13), 2305-2313.

79. Arico, A. S.; Bruce, P.; Scrosati, B.; Tarascon, J.-M.; Van Schalkwijk, W., Nanostructured materials for advanced energy conversion and storage devices. In *Materials for sustainable energy: a collection of peer-reviewed research and review articles from Nature Publishing Group*, World Scientific: **2011**; pp 148-159.

80. Zhang, Z.-c.; Xu, B.; Wang, X., Engineering nanointerfaces for nanocatalysis. *Chemical Society Reviews* **2014,** *43* (22), 7870-7886.

81. Hensel, J.; Wang, G.; Li, Y.; Zhang, J. Z., Synergistic effect of CdSe quantum dot sensitization and nitrogen doping of TiO_2 nanostructures for photoelectrochemical solar hydrogen generation. *Nano letters* **2010,** *10* (2), 478-483.

82. Van Santen, R. A., Complementary structure sensitive and insensitive catalytic relationships. *Accounts of chemical research* **2009,** *42* (1), 57-66.

83. Garlyyev, B.; Fichtner, J.; Piqué, O.; Schneider, O.; Bandarenka, A. S.; Calle-Vallejo, F., Revealing the nature of active sites in electrocatalysis. *Chemical Science* **2019,** *10* (35), 8060-8075.

84. Fulekar, M., *Nanotechnology: importance and applications*. IK International Pvt Ltd: **2010**.

85. Jin, H.; Liu, X.; Chen, S.; Vasileff, A.; Li, L.; Jiao, Y.; Song, L.; Zheng, Y.; Qiao, S.-Z., Heteroatom-doped transition metal electrocatalysts for hydrogen evolution reaction. *ACS Energy Letters* **2019,** *4* (4), 805-810.

86. Yang, W.; Wang, Z.; Zhang, W.; Guo, S., Electronic-structure tuning of water-splitting nanocatalysts. *Trends in Chemistry* **2019**.

87. Ray, A.; Mukhopadhyay, I.; Pati, R. K., *Electrocatalysts for Fuel Cells and Hydrogen Evolution: Theory to Design*. BoD–Books on Demand: **2018**.

88. Cybulski, A.; Moulijn, J. A., *Structured catalysts and reactors*. CRC press: **2005**.

89. Rajagopalan, R.; Balakrishnan, A., *Innovations in engineered porous materials for energy generation and storage applications*. CRC Press: **2018**.

90. Zeng, M.; Li, Y., Recent advances in heterogeneous electrocatalysts for the hydrogen evolution reaction. *Journal of Materials Chemistry A* **2015,** *3* (29), 14942-14962.

91. Sun, S.; Sun, X.; Chen, Z.; Liu, Y.; Wilkinson, D. P.; Zhang, J., *Carbon Nanomaterials for Electrochemical Energy Technologies: Fundamentals and Applications*. CRC Press: **2017**.

92. Zhang, L.; Xiao, J.; Wang, H.; Shao, M., Carbon-based electrocatalysts for hydrogen and oxygen evolution reactions. *ACS Catalysis* **2017,** *7* (11), 7855-7865.

93. Yaldagard, M.; Jahanshahi, M.; Saghatoleslami, N., Non-carbonaceous nanostructured support materials for low temperature fuel cell electrocatalysts. *Nano Science and Nano Technology An Indian Journal* **2014,** *8*.

94. Kong, D.; Cha, J. J.; Wang, H.; Lee, H. R.; Cui, Y., First-row transition metal dichalcogenide catalysts for hydrogen evolution reaction. *Energy & Environmental Science* **2013,** *6* (12), 3553-3558.

95. Ghosh, S.; Basu, R. N., Multifunctional nanostructured electrocatalysts for energy conversion and storage: current status and perspectives. *Nanoscale* **2018,** *10* (24), 11241-11280.

96. Chen, Z.; Dodelet, J.-P.; Zhang, J., *Non-noble metal fuel cell catalysts*. John Wiley & Sons: **2014**.

97. Felton, G. A.; Glass, R. S.; Lichtenberger, D. L.; Evans, D. H., Iron-only hydrogenase mimics. Thermodynamic aspects of the use of electrochemistry to evaluate catalytic efficiency for hydrogen generation. *Inorganic chemistry* **2006,** *45* (23), 9181-9184.

98. Yan, Y.; Xia, B. Y.; Zhao, B.; Wang, X., A review on noble-metal-free bifunctional heterogeneous catalysts for overall electrochemical water splitting. *Journal of Materials Chemistry A* **2016,** *4* (45), 17587-17603.

99. Milton, R. D.; Abdellaoui, S.; Khadka, N.; Dean, D. R.; Leech, D.; Seefeldt, L. C.; Minteer, S. D., Nitrogenase bioelectrocatalysis: heterogeneous ammonia and hydrogen production by MoFe protein. *Energy & Environmental Science* **2016,** *9* (8), 2550-2554.

100. Toth, L., *Transition metal carbides and nitrides*. Elsevier: 2014.

101. Zhong, Y.; Xia, X.; Shi, F.; Zhan, J.; Tu, J.; Fan, H. J., Transition metal carbides and nitrides in energy storage and conversion. *Advanced science* **2016,** *3* (5), 1500286.

102. Pu, Z.; Wang, M.; Kou, Z.; Amiinu, I. S.; Mu, S., Mo_2C quantum dot embedded chitosan-derived nitrogen-doped carbon for efficient hydrogen evolution in a broad pH range. *Chemical Communications* **2016,** *52* (86), 12753-12756.

103. Morales-Guio, C. G.; Hu, X., Amorphous molybdenum sulfides as hydrogen evolution catalysts. *Accounts of chemical research* **2014,** *47* (8), 2671-2681.

104. Hu, Q.; Li, G.; Han, Z.; Wang, Z.; Huang, X.; Yang, H.; Zhang, Q.; Liu, J.; He, C., Recent progress in the hybrids of transition metals/carbon for electrochemical water splitting. *Journal of Materials Chemistry A* **2019,** *7* (24), 14380-14390.

Chapter 2

Materials, Instrumentation and Experimental Procedures

2. Materials and Methods

This chapter will outline the brief description of the material used and the synthesis methods followed in the catalyst formation. The complete details of the synthesis method and materials used for a particular catalyst are mentioned in the corresponding chapter 3 to chapter 7.

2.1. Materials

The precursors used in the thesis are all of the analytical grades and used without any further purification. The precursor-like ammonium molybdenum tetrahydrate ($(NH4)_6.Mo_7O_{24}.4H_2O$, Copper Nitrate trihydrate ($Cu(NO_3)_2.3H_2O$), Hexamethyltetramine ($C_6H_{12}N_4$), Tetraethyl orthosilicate ($(C_2H_5O)_4Si$); Melamine ($C_3H_6N_3$), Diammonium hydrogen phosphate ($(NH_4)_2HPO_4$); Ammonium Hydroxide ($NH_3.H_2O$), N, N Dimethylformamide ($HCON(CH_3)_2$, Glucose ($C_6H_{12}O_6$), Nafion perfluorinated resin solution, 5 wt % in lower aliphatic alcohols, sterilized cotton has been used in the catalyst synthesis. Acetic acid ($C_2H_4O_2$), Citric acid ($C_6H_8O_7$); Ammonium Hydroxide ($NH_3.H_2O$), Ethanol (C_2H_5OH), Hydrochloric Acid (HCl) and Graphite flakes are also used in the precursor synthesis. The respective company and the purity details have been described in the corresponding chapter. Deionised water is used in all the synthesis process.

The synthesis of graphene oxide is carried out with using sulphuric acid (H_2SO_4), phosphoric acid (H_3PO_4), potassium permanganate ($KMnO_4$), hydrogen peroxide (H_2O_2), and diethyl ether (CH_3OCH_3) along with the excess amount of deionized water.

2.2. Synthesis Methods

Initially, a metal precursor has been synthesised through a liquid phase solution method or hydrothermal method and the same metal precursor has been calcined with the desired non-metal precursor in an inert atmosphere. The process also involves the synthesis of conductive supports like graphene oxide and the reduced graphene oxide with the corresponding metal precursor before the catalyst synthesis.

2.2.1. Synthesis of Catalyst Precursors

The catalysts precursors have been synthesized by hydrothermal method and the liquid solution method. The complete description of the precursor synthesis has been described in the corresponding chapter from chapter 3 to chapter 7. Here, a brief description of the synthesis method and its principle has been explained.

2.2.1.1. Hydrothermal or Solvothermal Process

This method involves the synthesis of material via chemical reaction above the ambient temperature and pressure in a sealed container. The concept of the hydrothermal process instigates from some natural process occurs inside the earth crust under the effect of pressure and heat in the water as the solvent. In the non-natural hydrothermal synthesis, the material synthesis usually executes in the steel pressure vessel known as an autoclave. The hydrothermal process generally involves the water as a solvent but in an inorganic solvent, the process is termed as the solvothermal process.[1-2] The solvent occasionally acts as a catalyst and a medium for solubility of the metal precursor or salt at elevated temperature and pressure. The method has also been used for the creation of rough surface at a temperature above the ambient conditions and relatively high pressure. It provides single-step material synthesis relatively at mild conditions. The existence of synergistic effect under the combined effects of high temperature and pressure inside the autoclave produces a crystalline material which generally doesn't require any post-annealing treatments. The synthesis is completely environment-friendly and endows with superior dispersion in solution. Moreover, it is an inexpensive and easy method for crystal growth compared to other methods.[3-5]

2.2.1.2. Liquid Phase Method

In this method, the reaction proceeds through dissolving the reactant species under mild conditions in a certain solvent. The process either follows the dissolution of the material in water or forms a solution which could dry in the air, in vacuum or in the oven at mild temperature. The liquid phase method requires a very mild condition for the synthesis of material or precursors.[6-8]

2.2.1.3. Synthesis of graphene oxide and reduced graphene oxide

The substrates or support material like graphene oxide has been synthesized with well known improved Hummer method. The method involves the use of the desired amount of the graphite flakes (3 g) in the solution mixture of sulphuric acid (360 mL) and the phosphoric acid (40 mL) in 9:1 ratio. Then the solution mixture is stirred for ten minutes and 18 g of $KMnO_4$ is added which generally is an exothermic reaction. The mixture was stirred at a slightly high temperature of about 50 °C for 12 h followed by cooling at room temperature. The obtained solution was then poured into ice (400 mL) with the addition of 3 mol of hydrogen peroxide (H_2O_2). The mixture was filtered and the filtrate was centrifuged and washed with water (200 mL) followed by HCl (30%, 200 mL) and then with ethanol (200 mL). In each washing, the

solution was filtered and the filtrate was centrifuged. After the repetitive washing, the remaining material was coagulated with 200 mL ether and the resulting solution was filtered again. The remaining powder then was vacuum dried.[9-10] The obtained graphene oxide was further thermally reduced at 900 ℃ to obtain the reduced graphene oxide.

2.2.2. High-temperature calcination

The high-temperature treatments of the catalyst precursors synthesized through above-mentioned methods is a required process to finally obtained the carbide, nitride, oxides, phosphides and nitride etc. of transition metal. In this process, the obtained oxide precursor undergoes temperature-programmed calcination process either in an inert atmosphere or a gaseous source that contributes to the synthesis process of carbide, nitride, phosphide and sulphide etc. During the calcination process, the heating condition is controlled by the programmed temperature.[11-12] In temperature-controlled calcination method, the metal oxide reacts either with the gaseous source or with the solid present to yield the desired product. This method has been developed by Boudart et al. in order to synthesize the molybdenum carbide form molybdenum oxide in the presence of methane and hydrogen gas mixture. The yield of the final product highly influenced by the reactant ratio, gas rate and the calcination temperature which controls the specific surface area and the crystal structure of the material. The temperature-programmed method mostly has been used for the synthesis of metal carbides.[13-16]

2.3. Characterization Techniques

2.3.1. Powder X-ray diffraction

X-ray powder diffraction (XRD) is an analytical technique used for determining important properties of the crystal structure of a solid such as lattice constant, geometry, orientation, defects, and for identification of unknown materials. It was discovered by Max von Laue, in 1912. The principle of X-ray diffraction was explained by Lawrence Bragg presently termed as Bragg's Law (Equation 2.1). He proposed that when X-rays of a particular wavelength (usually ranging from 0.7 to 2θ) are shined on a crystalline sample, it gets scattered from the lattice planes separated by the interplanar distance d as shown in figure 2.1.[17-18]

When the scattered waves undergo constructive interference a Bragg's peak is observed. Constructive interference means the path lengths of the two waves is equal to an integer multiple of the wavelength of incident X-rays. The path difference between the two waves undergoing interference is given by $2d\sin\theta$, where θ is the glancing angle n is a positive integer and λ is the wavelength of the incident wave. The X-ray wavelength commonly

employed is the characteristic K_α radiation, λ = 1.5418 Å, emitted by Cu. XRD is a non-destructive technique that does not require elaborate sample preparation. Powder samples are finely grounded, homogenized, and then directly loaded on the XRD sample holder.[18-20]

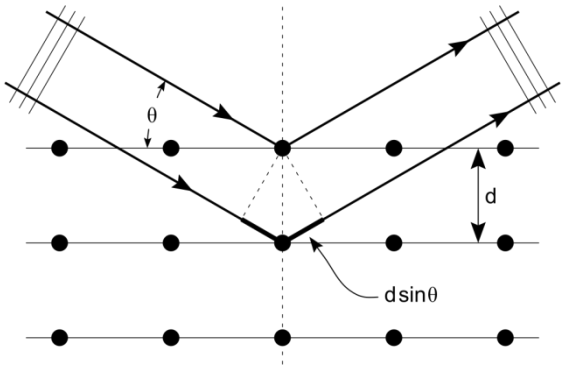

Figure 2.1. *The schematic showing the incident and the diffracted rays with path difference. (Image is taken from Wikipedia)*

Due to its easy handling, it is a widely used material characterization technique. Most of the materials have a unique diffraction pattern, a slight shift in the Bragg's peak indicates a change in the lattice constant of the structure which can be due to homogeneous strains. A theoretical structure can also be refined using a method known as Rietveld refinement. Further, the particle

$$2dsin\theta = n\lambda \qquad (2.1)$$

size of the powder can also be determined by using the Scherrer formula (Equation 2.2), which relates the particle size to the peak width.

$$D = \frac{K\lambda}{BCos\theta_B} \qquad (2.2)$$

Where λ is the wavelength of the X-rays, D is the size of the crystal, B is the full-width half maxima of the diffraction peak, Θ_B is the diffraction angle, and K is the Scherrer's constant of the order of unity for the usual crystal.[21-22] In this thesis, powder XRD measurements were performed to study the crystal structures of the materials. XRD patterns were recorded using a Bruker Eco D8 setup using Cu K_α radiation (λ = 0.154056 nm).

The compositional analysis of the catalyst phases is competed with Rietveld refinement using TOPAS 5 software Bruker and full proof measurements. The complete details of the respective measurements and the corresponding outcomes are given in the corresponding chapters of a particular catalyst.

2.3.2. Scanning electron microscope

A scanning electron microscope (SEM) is another type of electron microscope that uses a high energy electron beam for generating images of the sample. Unlike TEM, in SEM focused electron beam of spot size around 5 nm is made to raster scan over the sample surface with the help of deflection coils. The energy of the electron beam can be varied from a few hundred eV to 50 eV, depending on the nature of the sample. After striking the surface, the electrons penetrate the surface and different interactions take place that results in the emission of different types of electrons and photons from the sample. Secondary electrons are generated when incoming electron beam undergoes inelastic scattering with the atoms of the sample. A part of the energy is transferred to another electron which on gaining sufficient energy is emitted from the surface and is termed as a secondary electron.[23-24] A secondary electron is always emitted from the surface of the sample, as a result, it yields information about the surface and morphology of the material under analysis. Backscattered electrons, however, are produced due to elastic interactions between the beam and the sample. They have the same energy as that of the primary electron beam.

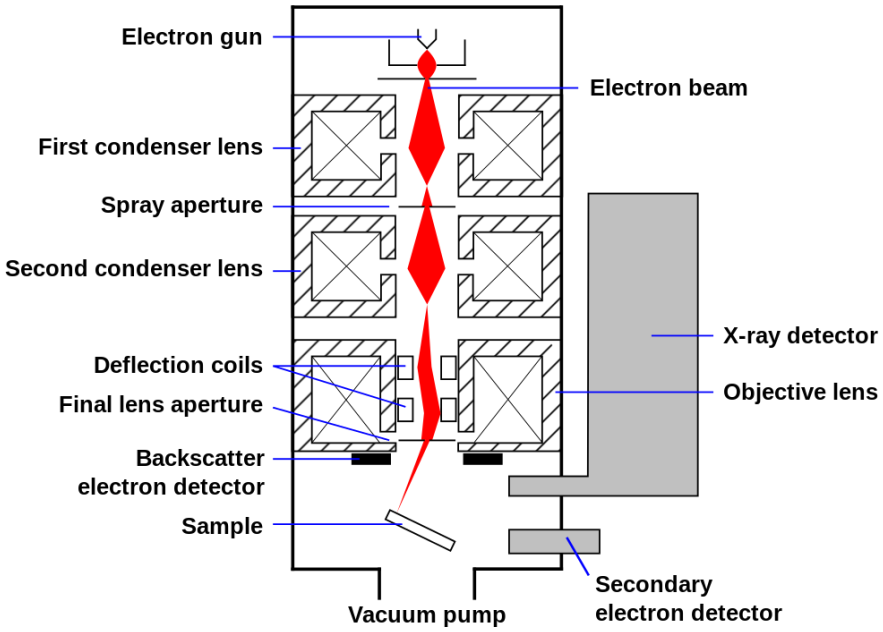

Figure 2.2. *Schematic showing components of SEM. (Image is taken from Wikipedia)*

The backscattering images are highly dependent on the atomic number of the material, higher the atomic number brighter the image and are used for determining the variation and distribution of an element in a material.[25-26] Another type of emitted electrons is termed as

Auger electrons or X-ray photons. When the interaction electrons of primary beam collide with the atom and eject a core electron, the excited atom emits characteristic X-ray photon or an Auger electron and comes to its ground state. These electrons are used for elemental and quantitative compositional analysis of a sample. In a typical SEM, normally backscattered and secondary electrons are detected. The emitted backscattered electrons are collected by a solid-state detector and an Everhart-Thornley detector for secondary electrons. A SEM (as shown in Figure 2.2) consists of an electron gun, high vacuum column through which electron beam travels, electron detector, sample chamber, and desktop for viewing and capturing the images of the samples.[27-29]

In the present thesis, the surface morphology and composition were examined by JEOL (JSM IT-300) scanning electron microscope equipped with the energy-dispersive X-ray spectroscopy (Bruker).

2.3.3. Transmission electron microscope

Transmission electron microscopy is a powerful structural characterization technique heavily used in material science, metallurgy, and biological sciences for determining the morphology, size, and crystal structure of the sample. A transmission electron microscope (TEM) works on the same principles as that of a light microscope but uses a high voltage electron beam instead of light as the source of illumination. The resolution of a light microscope is limited by the wavelength of light and is very well explained by Abbe's equation. In 1873, Ernst Abbe proposed that when the light of certain wavelength (λ) travels through a medium with 'n' refractive index making a half-angle Θ on the objective angular aperture then the minimum resolution that it can provide is given by equation 2.3.

$$d = \frac{\lambda}{2nsin\theta} \qquad (2.3)$$

Where $2nsin\theta$ is termed as the numerical aperture (NA) of the objective. If green light of wavelength 500 nm is used for illuminating a sample through an objective of NA '1', the Abbe's limit comes out to be 250 nm. This means if the distance between two molecules is equal to or less than 250 nm than the microscope will not able to resolve it. In a TEM, electrons are used as a source of illumination and their much lower wavelength makes it possible to get a resolution to the order of a few angstroms.[30-33]

A TEM instrument is composed of several components (shown in figure 2.3), which include an illumination system constituting an electron gun and the condenser system. In all the modern days TEM lanthanum hexaboride (LaB_6) crystal is used as the electron source. The electron gun generates an electron beam which falls on the sample. The condenser system focuses the generated electron beam onto the sample. Image producing system consists of objective, condenser, intermediate, and projector lenses and movable specimen stage. A condenser lens is responsible for primary beam formation, while the objective lens is used for initial magnification of the image, intermediate lenses magnify the image coming from the objective lens. At last, projector lens expands the beam onto a phosphor screen. Finally, the image recording system converts the electron image created on the fluorescent screen with the help of a CCD camera into a digital image.[34-36]

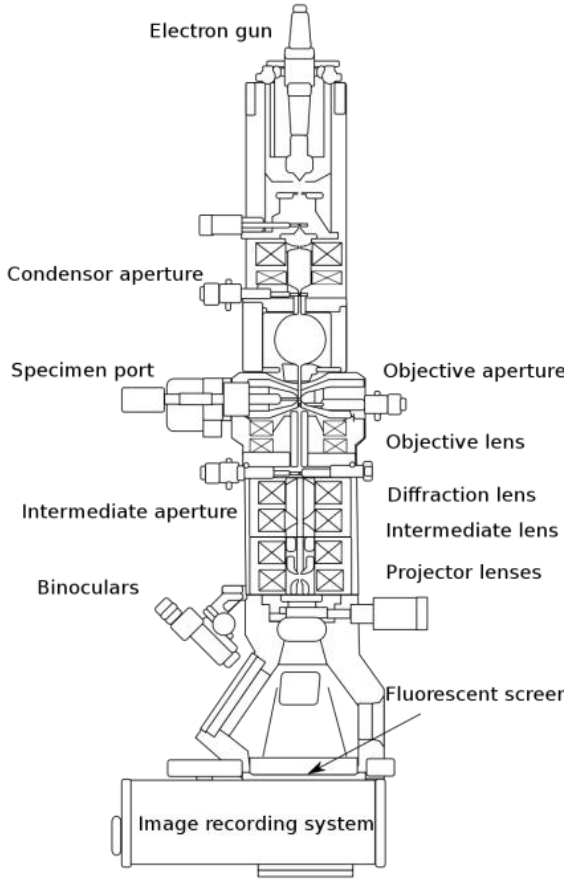

Figure 2.3. *Components of a transmission electron microscope. (Image is taken from Wikipedia)*

In the present thesis, TEM, high-resolution TEM (HRTEM), energy-dispersive X-ray analysis (EDX), scanning transmission electron microscope (STEM)-EDX, and selected area electron diffraction (SAED) measurements were carried out with a JEOL model 2100 instrument operated at an accelerating voltage of 200 kV.

2.3.4. BET Study

BET is the primary technique that has been in use for surface analysis of the materials. The surface properties like pore size, pore-volume, pore structure etc. are analyzed by the BET measurements. The BET analysis is based on the adsorption of the gas molecules on the surface of the material. The gas molecule adsorption basically acts as the basis of the BET technique for the measurements of different properties. Stephen Brunauer, Paul Hugh Emmett and Edward Teller were who describes the BET theory in 1938 and published an article about it. Brunauer et al extended the Langmuir theory of monolayer adsorption to multilayer adsorption and the interactions between gases and the solid material is described by the following equation

$$\frac{P/P_o}{V(1-P/P_o)} = \frac{1}{CV_m} + \frac{C-1}{CV_m} P/P_o \qquad (2.4)$$

where V is quantity adsorbed in cm^3 (STP)/g and V_m is the monolayer adsorbed gas quantity, P and P_o are the equilibrium and the saturation pressure while P/P_o corresponds to the relative pressure and C is a constant related to the heat of adsorption of the gas on the solid.[37-40]

The BET theory generally uses the multilayer adsorption of the gas molecules which are chemically inactive to the surface of the material. The carbon dioxide, argon, nitrogen and water are some adsorbate that generally has been in use for material analysis. The nitrogen is the prefered gaseous adsorbate that has been used for surface inquisitive in the BET method. The analysis is carried out at a nitrogen boiling point temperature (77 K). The surface area measurements by nitrogen multilayer adsorption are measured as a function of relative pressure. The same adsorbate is used for the measurements of the surface area at different temperature and measurement scale. The adsorbate molecule and its cross-section are the crucial factors that describe the surface area of the material because the surface area is generally known as a scale-dependent property. In this technique, the specific surface area of the material analysed on the basis of pore area and the external area which yields the important information about the surface porosity and the particles size of the materials. The BJH analysis further employed to specifically determine the pore area and specific pore volume using adsorption and desorption techniques. The BJH theory makes the pore size distribution independent on the external surface area of the material.[37, 41-43]

In the present thesis, the surface area and pore size distribution of the samples were done by Autosorb IQ Quantachrome instrument using the Brunauer-Emmett-Teller (BET) and the Barrett-Joyner-Halenda (BJH) equation for all the particle analysis.

2.3.5. X-ray photoelectron spectroscopy

X-ray photoelectron spectroscopy (XPS) is a surface characterization spectroscopic technique used for determining the elemental composition, empirical formula, oxidation state, and electronic state of elements present in the material to be analyzed. The basic components of the XPS system are shown in figure 2.4. XPS works on the principles of the photoelectric effect.

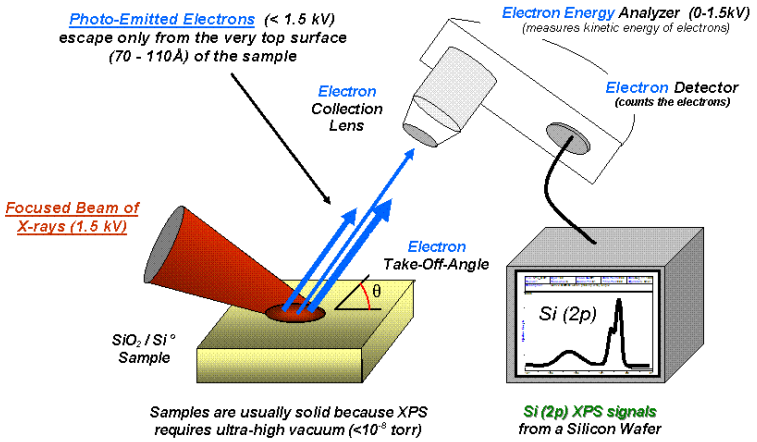

Figure 2.4. *Basic components of a monochromatic XPS system(Image is taken from Wikipedia)*

When X-ray beam of sufficient energy bombards on a sample i.e. if the photon energy is more than the binding energy of the core electron, the core electrons become excited and escape from the atom and emit out of the surface. The binding energy of solids is determined by equation 2.5.

$$BE = h\upsilon - KE - (\phi) \qquad (2.5)$$

Where BE is the binding energy of atom from where the electron has ejected, KE is the kinetic energy of the electron and Φ is the work function. The kind of radiation used decides the types of ejected electron and the techniques accordingly.[44-45] The UV rays can eject the valence electrons and provides the information about the bonding in molecules and the technique name as 'Ultraviolet Photoelectron Spectroscopy'. In order to eject the core electron, the sample is irradiated by the soft X-rays having energy range between 200-2000 eV, and the technique named as X-ray photoelectron spectroscopy. The most common sources are magnesium (Mg K_α

hν = 1.25 keV) and aluminium (Al Kα hν = 1.49 keV). The monochromatic beam penetrates the sample to few nanometers (3 – 10 nm for an Al K_α) and the emitted electrons directed to the analyzer through electrostatic or magnetic lenses. An XPS spectrum is obtained by plotting the number of electrons ejected with respect to their binding energy. A set of peaks emerge in an XPS spectrum that further helps in determining the chemical state and electronic state of the material under observation. A typical XPS system comprises of a source of X-rays, an ultra-high vacuum (UHV) stainless steel chamber with UHV pumps, an electron collection lens, an electron energy analyzer, Mu-metal magnetic field shielding, an electron detector system, a moderate vacuum sample introduction chamber, sample mounts, a sample stage, and a set of stage manipulators.[45-48]

In the present thesis, the X-ray photoelectron spectroscopy (XPS) analysis was carried out in PHI 5000 Versa Probe II, FEI Inc. scanning XPS microprobe and ESCALab: 220-IXL with Mg K_α non-monochromated X-ray beam having photon energy 1253.6 eV in order to know the chemical states of the materials.

2.3.6. Electrochemical Techniques

The electrocatalyst and the electrocatalysis terms have been widely accepted now in electrochemical reactions, although various controversy still exists about the emergence of the electrocatalysis process. The electrocatalysis deals with the electrode material and the electrode kinetics. The selectivity of the electrochemical reaction and the reaction kinetics are the basic terms that depend upon the electrode material. The reaction rate and electrocatalysis mechanism affected by the electrode material where such reaction occurs. The surface of such material having different active sites and these sites are regards as the centre for electrochemical reaction. The active sites adsorb the intermediates on the surface of the material which assists the reaction to proceed in a fast way. These sites generally involve the electron transfer and such material which adsorbs the intermediates are known as an electrocatalyst. The electrocatalyst has a fast electrochemical reaction rate as compared to other materials. The electrochemical techniques can be divided on the basis of control parameters like potential, current or charge. In this section, a brief description of the various techniques used in the electrochemical study and the terms involved throughout the thesis will be discussed particularly for the hydrogen evolution reaction.[49-52]

2.3.6.1. Electrochemical Process

Electrochemical techniques are the basis to understands the functionality of the electrode material at the surface of the material. The techniques involve a better understanding of the electrochemical processes occurs in the electrochemical cell. The electrochemical process generally is of two types, the Faradic in which electron and charge transfers through an electrode-electrolyte interface is in accordance with the Faraday law while other is the non-Faradic process. The charge transport through the interface is the reason for oxidation and reduction in the chemical reactions. This could be through any of the processes named as diffusion, convention or migration and completes the particular process. Thus, it's necessary to know the concentration of the reactant throughout the reaction and it's simply related to the time and distance from the electrode as expressed as the equations on the next page.[53-55]

$$I=dq/dt \tag{2.6}$$

$$i_c = -nFAk_{red}[O_{electrode}] \tag{2.7}$$

Where n, A, k_{red} and F have their usual meaning and $[O_{electrode}]$ is the concentration of the redox-active species near to the electrode surface. The diffusion-controlled processes are dependent on the strength of the movement species in accordance with time and distance from electrodes which are described by the Ficks laws;

Fick's first law $$J_o = -D_o \frac{\partial[O]}{\partial x} \tag{2.8}$$

Fick's second law $$\frac{\partial[O]}{\partial t} = D_0 \frac{\partial^2[O]}{\partial x^2} \tag{2.9}$$

and the change in Faradic current is given by the Cottrell equation and gives that much amount of current passes through the electrode surface according to Fick's second law;

$$|i| = nFA[O]\sqrt{D}/\sqrt{\pi}\sqrt{t} \tag{2.10}$$

The equation 2.10 gives the maximum output current that actually depends upon the current and voltage output conditions of the potentiostat.[55-59]

2.3.6.2. Electrode configuration: Two and three-electrode setup

The experiments were performed in a standard three-electrode setup electrochemical cell. The setup consists of the working electrode, reference electrode and counter electrode. The glassy

carbon electrode serves as a working electrode and Ag|AgCl (3M KCl) electrode has been used as a reference electrode. The platinum wire or carbon rod was used as a counter electrode in all the measurements. Although there is two-electrode configuration also available, the three-electrode setup has more authenticity and accuracy as compared to the two electrode setup. In the two-electrode set up the current and the voltage measurements senses between the same electrodes. The experiments generally have complex outcomes and consequent analysis. The two-electrode configuration generally used in electrochemical energy devices. The configuration also used in the systems in which a low current or a short time span of current is used. Such systems also have a well-poised counter electrode and have no significant drift over the course of the experiment.[60-62] In the three-electrode system, the reference electrode is different from the counter electrode and used as the third electrode in the system. This electrode is also connected to the working electrode in order to measure the voltage between the working and reference electrodes. In other words, here the counter and counter sense to counter electrode, working and working sense to the working electrode and the reference to the reference electrode is connected. The counter electrode's surface area needs to be higher than that of the working electrode, or otherwise, it will be a limiting factor in the kinetics of the reaction. In a two-electrode system, the measurements can be performed without reference electrodes but in a three-electrode configuration, we generally apply the difference in potential between the working and the counter electrode. The configuration measures only one half of the cell and allows the specific reaction to study with more accuracy. The setup analyze the whole electrochemical cell as compared to test a catalyst for half cell reaction.[53, 60, 62]

Here in this thesis, the measurements were conducted using CHI 660E and its updated version CHI 760E electrochemical potentiostat having three electrode configurations consist of Ag/AgCl, glassy carbon and carbon-based electrode as a reference, working and counter electrodes respectively.

2.3.6.3. Cyclic and Linear Sweep Voltammetry

The linear sweep voltammetry demonstrates the sweeping of potential with a constant rate within a potential window. If the same scan reverts, again and again, the technique is termed as the cyclic voltammetry and the recorded data as current vs potential represents the voltammogram. The activity of the material in HER study is evaluated with both of these techniques by comparing the data recorded in terms of the voltammogram and comparing with the other catalyst.[54, 63] The linear sweep voltammetry recorded at slow scan can be a useful

method to obtain the Tafel slope and can describe the mechanism through which the reaction proceeds. The cyclic voltammetry is used to evaluate the surface properties like oxide formation, mass loading and morphology of the catalyst through the electrode-electrolyte interface, the number of cycles along with scan rate and range of potential respectively. The activity of the material also affected if there is any change in structure or change in oxidation number of surface material that can be observed by the change in activity with respect to cycling. The repetitive cycles evaluate the stability of the catalyst which can be better demonstrates further with long term electrolysis at specific current density.[54, 64-65]

2.3.6.4. Electrode Kinetics

The electrode potential is the general terms that characterised the electrochemical reactions occurs at the surface of the electrode and the potential is termed as E_{rev} that has been evaluated from the Nernst Equation. From the electrochemical study of various materials and the expertise reveals that electrode potential sturdily affects the kinetics. This could be understood from the fact that some material rapidly evolves hydrogen at some potential while other requires higher potentials. All the Faradic process across the interface involves reduction and oxidation of the species by electron transfer. The electrode material and its structure, composition and nature along with the type of electrolyte also affect the electrochemical kinetics. In the equilibrium state, the **exchange current density (j_o)** describes the rate of electrochemical evet across the interface and measures the reversibility of the electrode reaction. The change in the value of potential from E_{rev} deviates the system from the equilibrium and a finite amount of current starts flowing through the electrochemical cell. Thus a finite potential necessitates that proceeds the electrochemical reaction and includes the thermodynamic and kinetic contribution that particularly describes the energy dissipation.[54, 61, 66-67] This potential or energy dissipated to surmount the reaction resistance is known as **overpotential**.

$$\eta = E - E_{rev} \qquad (2.11)$$

The **Butler-Volmer equation** relates the reaction rate with overpotential as follow (from equation 1.22 in chapter 1).

$$j = j_{\circ} \exp\left[\left(\alpha_a n\eta F/RT\right) - \left(\alpha_c n\eta F/RT\right)\right] \qquad (2.12)$$

This is the fundamental equation of electrode kinetic in the electrochemical process that depends upon the overpotential η and relates to the current density j_o. The equation demonstrates that with the change in the potential, the electrode reaction and its kinetics get

changed. α_a and α_c are the transfer coefficient related to the anodic and cathodic half cell reactions. The plot between η *vs* j is called the **polarization curve**. The whole process of energy dissipation or the potential applied is a combination of the potential require due to activation energy, a composition gradient near the interface and the ohmic resistance. The potential value described the behaviour of the electrochemical process and the Butler-Volmer equation describes the kinetics accordingly.[68-71] If the potential is very less ($|\eta| \leq 5$ mV), the Butler-Volmer equation describes a linear functionality between current density and the overpotential and it can be written as;

$$j = j_o\left(^{nF}/_{RT}\right)\eta \qquad (2.13)$$

The equation 2.13 establishes a linear relation to the current density and the overpotential within the slight potential range close to the equilibrium potential and corresponding slope of the equation describes the charge transfer resistance of the material. At the higher value of the potential the equation 2.12 describes the non-linear behaviour of the electrochemical reaction with potential and both the half cell anodic and cathodic reaction behaves independently and the equation seems to be followed the following equations;

From (2.12) anodic $$j_a = j_\circ \exp\left(^{\eta}/_{\mathrm{b}}\right) \qquad (2.14)$$

From (2.12) cathodic $$j_c = j_\circ \exp\left(^{\eta}/_{\mathrm{b}}\right) \qquad (2.15)$$

The equation could be expressed as $\eta = \mathrm{a} + \mathrm{b}\log j$, with a and b with their corresponding values. The semilogarithmic plot log j *vs*. η represents the **Tafel line** and evaluates the useful information about the kinetic parameters. The Tafel line generally represents both anodic and cathodic branch and extrapolation of the curve to $\eta = 0$, the value of current density j corresponds to the exchange current density j_o. The **Tafel slope** values describe the well-defined mechanism in the electrochemical system depending upon the Tafel slope values however its deals with the assumption that says Tafel slope is independent on the overpotential.[72-76] Hence, there is always an ambiguity about the mechanism and the assumption that says and depends upon the constant value of the Tafel slope. The current 'I' and current density '*j*' are the extensive quantities that depend upon the size and area of the electrode. The Tafel slope 'b' is an intensive quantity which basically rellies upon the reaction mechanism rather than the electrode size and becomes a significant factor in the electrochemical study. The comparative study of the material with their Tafel slope asses the activity of the corresponding material and facilitate in the pronouncement of a suitable catalyst for the hydrogen generation process. Thus

a low value of Tafel slope points towards the lower values of energy consumption and describes the suitable catalyst for a particular reaction with the same production rate.[53, 66, 73, 77]

2.3.6.5. Electrochemical impedance spectroscopy

The prime concern in an electrochemical study is to obtain the results with minimum errors. The potential requires to generates hydrogen in the electrochemical process based upon the conductivity or resistance of the material. Besides that, there are numbers of other resistive parameters also that affects the overall process of hydrogen evolution.[50, 78] The ohmic loss is the permanent loses that occurs in the measurements and need to be corrected. The factors involved in such loses could be resistance from electrolyte that or it could be from the circuit connection etc. Impedance spectroscopy is the technique used to measure such ohmic resistance that which responses to the applied potential at different AC frequencies. The corrected potential (V) was obtained by subtracting the ohmic and other resistance from the applied potential and considered as "*iR*-corrected" potential. The resistance has been calculated through the simulation process by applying resistance (R), capacitance (C) or a combination of resistance and capacitance (RC) along with considering the other diffusion process. The resistance R could be a normal resistance or a transfer resistance and Capacitance (C) could be considered as the double layer or capacitance due to surface properties of the electrode material.[73, 79-83]

$$E_{corrected} = E_{mesured} — iR \qquad (2.16)$$

Where iR is the term that consists of the overall resistive part of the circuit.

2.3.6.6. Stability

The selection of suitable material or the electrocatalysts for HER or any other electrochemical reaction entirely depends upon the two parameters in which one is the electrocatalytic effects and another one is the long term durability. The electrocatalytic activity is the prime factor that emphasis to study the electrochemical aspects of the material and entirely deals with the investigation of highly efficient HER electrocatalyst. The long term stability actually decides the catalyst efficiency of the material in a particular medium that also depends upon the working conditions.[51, 84-85] For a commercial electrocatalyst, the catalyst must have high electrocatalytic activity as the ohmic losses present in the system directly affects the current density of the material. The losses must be minimized and for that purpose concentrated electrolyte that predicted by *Kohlrausch's law* can be used. In other words, the charge species

like H^+ and OH^- generally used in the electrocatalytic system that provides the higher conductivity in the acidic and basic system respectively. Thus the catalyst must have been highly efficient to bear such harsh condition so that it can properly work for a long time span.[86-89] Such a crucial challenge is the biggest hurdle in finding a suitable catalyst for hydrogen generation system. Noble metal like platinum and platinum derivatives are the highly efficient and only naturally known catalyst which can fulfil such condition. Such a catalyst not only engaged owing to high efficiency but also have high corrosion resistance and stability in harsh mediums. Thus, the electrochemical engineering of the material towards the better choice of catalyst that efficiently generates the hydrogen is the crucial way to practically demonstrates the things. In the present thesis, the stability has been performed by the repetitive cycle in linear sweep voltammetry. The number of cycles and the corresponding time span during this process describes the better choice of the materials.[49, 83, 90]

2.3.7. EXAFS and XANES Study

The study of the internal structure and the local environment of the atom with absorption spectroscopy deals with the absorption coefficient (μ) and the energy of the incident and the excited electrons. The high energy electrons when exposed on the material the transmitted and the reflected component of the photoelectrons extracts the information about the internal structure of the material, molecules or a complex. The absorption coefficient gets modulated in accordance with the photoelectron scattering which basically is a function of photon energy. Such functionality of the absorption coefficient with the photon energy contains information about the atom and its local environment.[91-93]

X-ray absorption spectroscopy illustrates the internal structure of the material. The absorption spectra indicate the features of the condense matter on the basis of photoabsorption cross-section which describes the electronic transition that obtained between the atomic core level and the final state. The absorption spectra that obtained from the atomic core of the surface atom, on the basis of energy range could be divided into the two different energy region named as X-ray absorption near edge structures (XANES) and extended X-ray absorption fine structure (EXAFS). The XANES and EXAFS study for a particular material extract the information about symmetry, chemical bonding, interatomic distances and the coordination number. The study has an upper edge in determining the interatomic distance as compared to other techniques. XANES study deals within the few tens of eV of energy that ranges from the absorption edge to the threshold of EXAFS oscillation. In this energy range, the excited electrons have a continuum of

kinetic energy with a lager wavelength as compared to the interatomic distance between the central atom and the first neighbour. Here, the excited electron with low kinetic energy has a

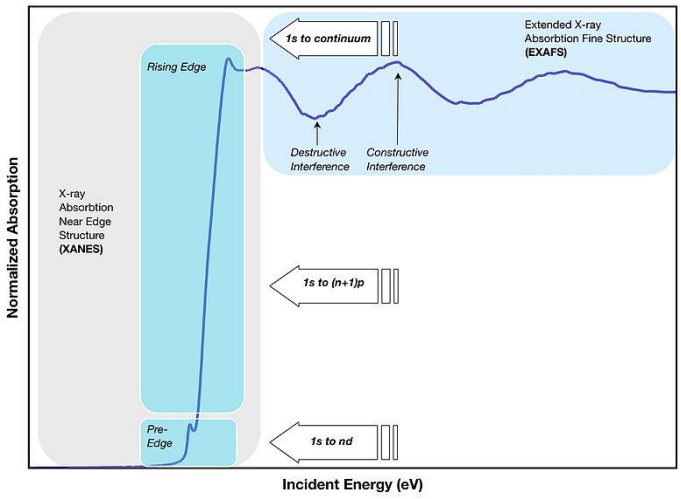

Figure 2.5. *Three regions of XAS (Image taken from Wikipedia)*

strong possibility of scattering by the neighbouring atoms. Consequently, the exciting photoelectron undergoes through multiple scattering within the cluster formed by the first coordination shell and ultimately the second and third.[91-92, 94] As the XANES study is independent on the crystal order and deals with the local site symmetry and thus the study could extract the information about the chemical bonding of unknown compounds and surface molecular complexes. The near-edge X-ray absorption fine structure ranges from the 5 eV above the absorption thresholds in which the photoelectron having very low kinetic energy (5-150 eV). This low energy of photoelectrons having very large backscattering amplitude from the atoms and the multiple scattering becomes predominant in this spectra. The XANES spectra near to the absorption edge also termed as the near edge X-ray absorption fine structure (NEXAFS) but due to the multiple scattering, the interpretation of the structure is not easy. The NEXAFS and EXAFS can be distinguished on the basis of the wavelength of the photoelectron and the interatomic distance of photo absorber-backscattering pair.[92, 95-96] The following equation 2.17 illustrates that at higher energy the wavelength is shorter than the interatomic distance which corresponds to the single scattering regime while at lower energy the higher wavelength associated with the multiple scattering regime. The high energy regime region having single scattering usually defines the near neighbour distance and coordination number.

$$E_{kinetic} = h\nu - E_{binding} = \hbar^2k^2/2m = \hbar^2(2\pi)^2/2m\lambda^2 \qquad (2.17)$$

The EXAFS spectra extended to the higher energy range from 40 eV to 800 eV above the absorption threshold and deal with the study of interatomic distance and the coordination number. This study gives information about the locality of absorbing atom and the local sensitivity is determined by the inelastic scattering to mean free path and the Debye-Wailer factor.[96-98]

Here, in this thesis, the X-ray absorption spectroscopy measurements of the Mo-based catalyst and other standard materials was carried out at Energy Scanning EXAFS beamline (BL-9) at INDUS-2 Synchrotron Source(2.5 GeV, 100 mA), 'Raja Ramanna Centre for Advanced Technology' (RRCAT), Indore, India. The beamline uses a double crystal monochromator (DCM) which works in the photon energy range of 4-25 KeV with a resolution of 104 at 10 KeV. A 1.5 m horizontal pre-mirror with meridional cylindrical curvature is used prior to the DCM for collimation of the beam and higher harmonic rejection. The second crystal of the DCM is a sagittal cylindrical crystal, which is used for horizontal focusing of the beam while another Rh/Pt coated bendable post mirror facing down is used for vertical focusing of the beam at the sample position. EXAFS measurements of these samples have been carried out in transmission mode at the Mo K-edge. For measurements in the transmission mode, the sample is placed between two ionization chamber detectors. The first ionization chamber measures the incident flux (I_o) and the second ionization chamber measures the transmitted intensity (I_t) and absorbance of the sample is obtained as $\mu = e^{-\frac{I_t}{I_0}}$. The EXAFS spectra of the samples at Mo K-edge were recorded in the energy range 19925- 20730 eV.[99-100]

2.3.8. Dynamic Light Scattering (DLS) measurements

The dynamic light scattering measurements provide the particle size of the sub-micron particle and macromolecules. This technique is also known as Quasi-Elastic Light Scattering (QELS) in some paces of the research while another name Photon Correlation Spectroscopy (PCS) which occasionally not termes as synonyms for DLS but use as for the similar purpose. DLS measurements based on the principle of time-resolved measurements of scattered light from the dispersion solution kept in the sample cell and measure the diffusion rate of the particles. The intensity of scattered light oscillates around an average value due to diffusion of particle and contains the information about the particle present in the solution. The frequency of such oscillation or fluctuation describes the diffusion coefficient of the particles that depends upon the size of particles. This fluctuation basically is because of the random motion of the particles and these motion could be modelled with Stokes-Einstein equation.[101-103]

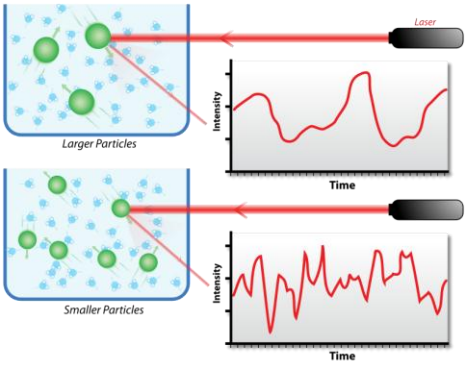

Figure 2.6. *A hypothetical dynamic light scattering of two samples: Larger particles on the top and smaller particles on the bottom (image taken from the Wikipedia)*

The equation 2.16 most often used as a determination of particle size in DLS measurements where D_h is termed as the hydrodynamic diameter of the particles.

$$D_h = K_\beta T / 3\pi\eta D_t \qquad (2.16)$$

The other terms like D_t are the translational diffusion coefficient that we could determine by dynamic light scattering, k_B Boltzmann's constant which generally we know and T is the absolute thermodynamic temperature which is the control parameters that we control while analysis and η is dynamic viscosity for a particular medium whose particle size need to determine. The size of particles simply given by the hydrodynamic radius that simply depends upon the mass and shape of the particle. In these measurements, the principle aspect of the study is the diffusion only while other effects like sedimentation, thermal disturbance of the particle and fluid flow are not in consideration. Such measurements decide the upper limit of detection of particle size in the system while the lower size based upon the time resolution of measurement device which generally lies within the few nanometers. Therefore, in laser diffraction techniques the dynamic light scattering for particle size analysis is an additional feature for sub-micrometre scale.[101, 104-106] The DLS can measure the particle size of the system that has a broad distribution of molecular masses and can detect the small quantity (< 0.01%) of higher mass species. In this measurement, there is no need of taking care of the particle agglomeration in the system but also it can't quantify the amount of aggregation. Another limitation is, it can not avoid interference caused by dust particles and other artefacts that influences the size of the nanoparticles. The DLS study is highly sensitive to the dictated

protocol for sample preparation, hence a small careless could result in the underestimation or overestimation of the results.[101, 103, 107]

In the present thesis, DLS measurements were performed on a Malvern zeta sizer Nano ZSP instrument.

References

1. Cambon, O.; Haines, J., Hydrothermal Crystal Growth of Piezoelectric α-Quartz Phase of AO_2 (A = Ge, Si) and MXO_4 (M = Al, Ga, Fe and X = P, As): A Historical Overview. *Crystals* **2017,** *7* (2).

2. Feng, S. H.; Li, G. H., Chapter 4 - Hydrothermal and Solvothermal Syntheses. In *Modern Inorganic Synthetic Chemistry (Second Edition)*, Xu, R.; Xu, Y., Eds. Elsevier: Amsterdam, **2017**; pp 73-104.

3. Alawad, O. A.; Alhozaimy, A.; Jaafar, M. S.; Aziz, F. N. A.; Al-Negheimish, A., Effect of Autoclave Curing on the Microstructure of Blended Cement Mixture Incorporating Ground Dune Sand and Ground Granulated Blast Furnace Slag. *International Journal of Concrete Structures and Materials* **2015,** *9* (3), 381-390.

4. Zhong, H.; Mirkovic, T.; Scholes, G. D., 5.06 - Nanocrystal Synthesis. In *Comprehensive Nanoscience and Technology*, Andrews, D. L.; Scholes, G. D.; Wiederrecht, G. P., Eds. Academic Press: Amsterdam, **2011**; pp 153-201.

5. Choi, J.-M.; Kim, S.-H.; Lee, S.-J.; Kim, S.-S., Effects of Pressure and Temperature in Hydrothermal Preparation of MoS_2 Catalyst for Methanation Reaction. *Catalysis Letters* **2018,** *148* (7), 1803-1814.

6. Aslanov, L. A.; Fetisov, G. V.; Paseshnichenko, K. A.; Dunaev, S. F., Liquid phase methods for design and engineering of two-dimensional nanocrystals. *Coordination Chemistry Reviews* **2017,** *352*, 220-248.

7. Karatutlu, A.; Barhoum, A.; Sapelkin, A., Chapter 1 - Liquid-phase synthesis of nanoparticles and nanostructured materials. In *Emerging Applications of Nanoparticles and Architecture Nanostructures*, Barhoum, A.; Makhlouf, A. S. H., Eds. Elsevier: **2018**; pp 1-28.

8. Xu, L.; Wang, M.; Li, L.; Yang, Z.; Li, J., One-step low-temperature liquid phase method for synthesis of three-dimensional porous graphene and applications in supercapacitor. *Materials Research Express* **2019,** *6* (5), 055603.

9. Marcano, D. C.; Kosynkin, D. V.; Berlin, J. M.; Sinitskii, A.; Sun, Z.; Slesarev, A.; Alemany, L. B.; Lu, W.; Tour, J. M., Improved Synthesis of Graphene Oxide. *ACS Nano* **2010,** *4* (8), 4806-4814.

10. Chen, J.; Yao, B.; Li, C.; Shi, G., An improved Hummers method for eco-friendly synthesis of graphene oxide. *Carbon* **2013,** *64*, 225-229.

11. Zhong, Y.; Xia, X.; Shi, F.; Zhan, J.; Tu, J.; Fan, H. J., Transition Metal Carbides and Nitrides in Energy Storage and Conversion. *Advanced science (Weinheim, Baden-Wurttemberg, Germany)* **2016,** *3* (5), 1500286-1500286.

12. Soares, S. F.; Fernandes, T.; Daniel-da-Silva, A. L.; Trindade, T., The controlled synthesis of complex hollow nanostructures and prospective applications†. *Proceedings of the Royal Society A: Mathematical, Physical and Engineering Sciences* **2019,** *475* (2224), 20180677.

13. Panda, R. N.; Dalavi, S. B.; Theerthagiri, J., Synthesis of High Surface Area W_2N and Co–W–N Nitrides by Chemical Routes. *Adsorption Science & Technology* **2012,** *30* (4), 345-354.

14. Araujo, C. P. B.; Souza, C. P. d.; Maia, L. M. D.; Souto, M. V. M.; Barbosa, C. M., On The Synthesis Of Molybdenum Carbide With Cobalt Addition Via Gas-Solid Reactions In A CH_4/H_2 Atmosphere. *Brazilian Journal of Chemical Engineering* **2016,** *33*, 577-588.

15. Volpe, L.; Boudart, M., Compounds of molybdenum and tungsten with high specific surface area: II. Carbides. *Journal of Solid State Chemistry* **1985,** *59* (3), 348-356.

16. Othman, M. R.; Helwani, Z.; Martunus; Fernando, W. J. N., Synthetic hydrotalcites from different routes and their application as catalysts and gas adsorbents: a review. *Applied Organometallic Chemistry* **2009,** *23* (9), 335-346.

17. Eckert, M., Max von Laue and the discovery of X-ray diffraction in 1912. *Annalen der Physik* **2012,** *524* (5), A83-A85.

18. Misture, S. T.; Snyder, R. L., X-ray Diffraction. In *Encyclopedia of Materials: Science and Technology*, Buschow, K. H. J.; Cahn, R. W.; Flemings, M. C.; Ilschner, B.; Kramer, E. J.; Mahajan, S.; Veyssière, P., Eds. Elsevier: Oxford, **2001**; pp 9799-9808.

19. Warren, B. E., *X-ray Diffraction*. Courier Corporation: 1990.

20. Suryanarayana, C.; Norton, M. G., *X-ray diffraction: a practical approach*. Springer Science & Business Media: **2013**.

21. Uvarov, V.; Popov, I., Metrological characterization of X-ray diffraction methods for determination of crystallite size in nano-scale materials. *Materials Characterization* **2007,** *58* (10), 883-891.

22. Holzwarth, U.; Gibson, N., The Scherrer equation versus the 'Debye-Scherrer equation'. *Nature Nanotechnology* **2011,** *6* (9), 534-534.

23. Khursheed, A., *Scanning electron microscope optics and spectrometers*. World scientific: **2011**.

24. Postek, M. T.; Howard, K.; Johnson, A.; McMichael, K., The scanning electron microscope. *Handbook of charged particle optics* **1997**, 363-399.

25. Richards, R.; Owen, G. R.; Ap Gwynn, I., Low voltage backscattered electron imaging (< 5 kV) using field emission scanning electron microscopy. *Scanning Microsc* **1999,** *13* (1), 55-60.

26. Joy, D. C., Beam interactions, contrast and resolution in the SEM. *Journal of Microscopy* **1984,** *136* (2), 241-258.

27. Vernon-Parry, K., Scanning electron microscopy: an introduction. *III-Vs Review* **2000,** *13* (4), 40-44.

28. Egerton, R.; Li, P.; Malac, M., Radiation damage in the TEM and SEM. *Micron* **2004,** *35* (6), 399-409.

29. MacDonald, N.; Waldrop, J., Auger electron spectroscopy in the scanning electron microscope: Auger electron images. *Applied Physics Letters* **1971,** *19* (9), 315-318.

30. Egerton, R. F., *Physical principles of electron microscopy*. Springer: 2005; Vol. 56.

31. Weisenburger, S.; Sandoghdar, V., Light microscopy: an ongoing contemporary revolution. *Contemporary Physics* **2015,** *56* (2), 123-143.

32. Krivanek, O. L.; Ursin, J. P.; Bacon, N. J.; Corbin, G. J.; Dellby, N.; Hrncirik, P.; Murfitt, M. F.; Own, C. S.; Szilagyi, Z. S., High-energy-resolution monochromator for aberration-corrected scanning transmission electron microscopy/electron energy-loss spectroscopy. *Philosophical Transactions of the Royal Society A: Mathematical, Physical and Engineering Sciences* **2009,** *367* (1903), 3683-3697.

33. Bozzola, J. J.; Russell, L. D., *Electron microscopy: principles and techniques for biologists*. Jones & Bartlett Learning: **1999**.

34. Reimer, L., *Transmission electron microscopy: physics of image formation and microanalysis*. Springer: **2013**; Vol. 36.

35. Edington, J. W.; Russell, K. T., *Practical electron microscopy in materials science*. Macmillan International Higher Education: **1977**.

36. Williams, D. B.; Carter, C. B., The transmission electron microscope. In *Transmission electron microscopy*, Springer: **1996**; pp 3-17.

37. Dent, R., A multilayer theory for gas sorption: Part I: sorption of a single gas. *Textile Research Journal* **1977,** *47* (2), 145-152.

38. Shunin, Y.; Bellucci, S.; Gruodis, A.; Lobanova-Shunina, T., Surface Nanophysics: Macro-, Meso-, Micro-and Nano-approaches. In *Nonregular Nanosystems*, Springer: **2018**; pp 115-146.

39. Davis, B. H., The BET Equation–Nominated for a Nobel Prize but Not Selected. In *The Posthumous Nobel Prize in Chemistry. Volume 1. Correcting the Errors and Oversights of the Nobel Prize Committee*, ACS Publications: **2017**; pp 165-206.

40. Dollimore, D.; Spooner, P.; Turner, A., The bet method of analysis of gas adsorption data and its relevance to the calculation of surface areas. *Surface Technology* **1976,** *4* (2), 121-160.

41. Hwang, N.; Barron, A. R., BET surface area analysis of nanoparticles. *The Connexions project* **2011**, 1-11.

42. Hayati-Ashtiani, M., Characterization of nano-porous bentonite (montmorillonite) particles using FTIR and BET-BJH analyses. *Particle & Particle Systems Characterization* **2011,** *28* (3-4), 71-76.

43. Coasne, B.; Gubbins, K. E.; Pellenq, R. J. M., A grand canonical Monte Carlo study of adsorption and capillary phenomena in nanopores of various morphologies and topologies: testing the BET and BJH characterization methods. *Particle & Particle Systems Characterization: Measurement and Description of Particle Properties and Behavior in Powders and Other Disperse Systems* **2004,** *21* (2), 149-160.

44. Proctor, A.; Sherwood, P. M., Data analysis techniques in x-ray photoelectron spectroscopy. *Analytical Chemistry* **1982,** *54* (1), 13-19.

45. Fadley, C. S., X-ray photoelectron spectroscopy: Progress and perspectives. *Journal of Electron Spectroscopy and Related Phenomena* **2010,** *178*, 2-32.

46. Barr, T. L., Advances in the Application of X-Ray Photoelectron Spectroscopy (ESCA) Part I. Foundation and Established Methods. *Critical Reviews in Analytical Chemistry* **1991,** *22* (1-2), 567-635.

47. Konno, H., Chapter 8 - X-ray Photoelectron Spectroscopy. In *Materials Science and Engineering of Carbon*, Inagaki, M.; Kang, F., Eds. Butterworth-Heinemann: **2016**; pp 153-171.

48. Petraki, F.; Papaefthimiou, V.; Kennou, S., The electronic structure of Ni-phthalocyanine/metal interfaces studied by X-ray and ultraviolet photoelectron spectroscopy. *Organic electronics* **2007,** *8* (5), 522-528.

49. Ashik, U. P. M.; Viswan, A.; Kudo, S.; Hayashi, J.-i., Chapter 3 - Nanomaterials as Catalysts. In *Applications of Nanomaterials*, Mohan Bhagyaraj, S.; Oluwafemi, O. S.; Kalarikkal, N.; Thomas, S., Eds. Woodhead Publishing: **2018**; pp 45-82.

50. Zheng, Y.; Jiao, Y.; Vasileff, A.; Qiao, S.-Z., The Hydrogen Evolution Reaction in Alkaline Solution: From Theory, Single Crystal Models, to Practical Electrocatalysts. *Angewandte Chemie International Edition* **2018,** *57* (26), 7568-7579.

51. Sapountzi, F. M.; Gracia, J. M.; Weststrate, C. J.; Fredriksson, H. O. A.; Niemantsverdriet, J. W., Electrocatalysts for the generation of hydrogen, oxygen and synthesis gas. *Progress in Energy and Combustion Science* **2017,** *58*, 1-35.

52. Bentley, C. L.; Kang, M.; Unwin, P. R., Nanoscale Surface Structure–Activity in Electrochemistry and Electrocatalysis. *Journal of the American Chemical Society* **2019,** *141* (6), 2179-2193.

53. Escobar Teran, F. D. A new approach towards understanding the ion transfer dynamics in nanostructured carbon-based thin films for energy storage applications. Université Pierre et Marie Curie - Paris VI, **2016**.

54. Elgrishi, N.; Rountree, K. J.; McCarthy, B. D.; Rountree, E. S.; Eisenhart, T. T.; Dempsey, J. L., A practical beginner's guide to cyclic voltammetry. *Journal of Chemical Education* **2018,** *95* (2), 197-206.

55. Dupont, M. F.; Donne, S. W., Faradaic and non-faradaic contributions to the power and energy characteristics of electrolytic manganese dioxide for electrochemical capacitors. *Journal of The Electrochemical Society* **2016,** *163* (6), A888-A897.

56. Seeber, R.; Zanardi, C.; Inzelt, G., Links between electrochemical thermodynamics and kinetics. *ChemTexts* **2015,** *1* (4), 18.

57. Biesheuvel, P.; Dykstra, J., The difference between Faradaic and Nonfaradaic processes in Electrochemistry. *arXiv preprint arXiv:1809.02930* **2018**.

58. Vayenas, C.; Bebelis, S.; Neophytides, S., Non-Faradaic electrochemical modification of catalytic activity. *The Journal of Physical Chemistry* **1988,** *92* (18), 5083-5085.

59. Oldham, K. B.; Spanier, J., The replacement of Fick's laws by a formulation involving semidifferentiation. *Journal of Electroanalytical Chemistry and Interfacial Electrochemistry* **1970,** *26* (2-3), 331-341.

60. Hernández-Cruz, M.; Galán-Vidal, C. A.; Álvarez-Romero, G. A.; Ramírez-Silva, M. T.; Páez-Hernández, M. E.; González-Vidal, J. L., Behavior of Two and Three Electrode Configuration and Different Mediators in Working Electrode on Development of Disposable Screen-Printing Biosensors for Determination of Free Cholesterol. *Journal of the Mexican Chemical Society* **2013,** *57*, 47-53.

61. Slesinski, A.; Frackowiak, E., Determination of accurate electrode contribution during voltammetry scan of electrochemical capacitors. *Journal of Solid State Electrochemistry* **2018,** *22* (7), 2135-2139.

62. Ianeselli, L.; Grenci, G.; Callegari, C.; Tormen, M.; Casalis, L., Development of stable and reproducible biosensors based on electrochemical impedance spectroscopy: Three-electrode versus two-electrode setup. *Biosensors and Bioelectronics* **2014,** *55*, 1-6.

63. Steimecke, M.; Rümmler, S.; Kühhirt, M.; Bron, M., A Linear Sweep Voltammetric Procedure Applied to Scanning Electrochemical Microscopy for the Characterization of Carbon Materials towards the Vanadium(IV)/(V) Redox System. *ChemElectroChem* **2016,** *3* (2), 318-322.

64. Davies, T. J.; Ward-Jones, S.; Banks, C. E.; del Campo, J.; Mas, R.; Muñoz, F. X.; Compton, R. G., The cyclic and linear sweep voltammetry of regular arrays of microdisc electrodes: fitting of experimental data. *Journal of Electroanalytical Chemistry* **2005,** *585* (1), 51-62.

65. Singh, T.; Dutt, J.; Kaur, S., Cyclic and linear sweep voltammetry at tubular electrodes: Part V. Kinetic processes. *Journal of electroanalytical chemistry and interfacial electrochemistry* **1991,** *304* (1-2), 17-30.

66. Kim, K.; Choi, S.; Kim, J.; Peak, S.; Goh, W., Electrochemical Investigation of Exchange Current Density of Uranium and Rare-earths Couples (M^{3+}/M^{0}) in LiCl-KCl Eutectic Electrolyte. **2015**.

67. Dubouis, N.; Grimaud, A., The hydrogen evolution reaction: from material to interfacial descriptors. *Chemical Science* **2019,** *10* (40), 9165-9181.

68. Mitra, S. K.; Chakraborty, S., *Microfluidics and nanofluidics handbook: fabrication, implementation, and applications*. CRC press: **2016**.

69. Seri, O.; Siree, B., The Differentiating Polarization Curve Technique for the Tafel Parameter Estimation. *Catalysts* **2017,** *7* (8), 239.

70. Rubi, J. M.; Kjelstrup, S., Mesoscopic Nonequilibrium Thermodynamics Gives the Same Thermodynamic Basis to Butler−Volmer and Nernst Equations. *The Journal of Physical Chemistry B* **2003,** *107* (48), 13471-13477.

71. Dreyer, W.; Guhlke, C.; Müller, R., A new perspective on the electron transfer: recovering the Butler–Volmer equation in non-equilibrium thermodynamics. *Physical Chemistry Chemical Physics* **2016,** *18* (36), 24966-24983.

72. Tilak, B.; Chen, C.-P., Generalized analytical expressions for Tafel slope, reaction order and ac impedance for the hydrogen evolution reaction (HER): mechanism of HER on platinum in alkaline media. *Journal of applied electrochemistry* **1993,** *23* (6), 631-640.

73. Ge, J.; Isgor, O., Effects of Tafel slope, exchange current density and electrode potential on the corrosion of steel in concrete. *Materials and Corrosion* **2007,** *58* (8), 573-582.

74. Kear, G.; Walsh, F. C., The characteristics of a true Tafel slope. *Corrosion and materials* **2005,** *30* (6), 51-55.

75. Lvov, S. N., *Introduction to Electrochemical Science and Engineering*. Crc Press: 2014.

76. Fletcher, S.; Varley, T. S., Beyond the Butler–Volmer equation. Curved Tafel slopes from steady-state current–voltage curves. *Physical Chemistry Chemical Physics* **2011,** *13* (12), 5359-5364.

77. Guerrini, E.; Trasatti, S., Recent developments in understanding factors of electrocatalysis. *Russian Journal of electrochemistry* **2006,** *42* (10), 1017-1025.

78. Koo, B.; Weiland, J. In *Experimental factors effecting stability of Electrochemical Impedance Spectroscopy Measurements*, 2018 40th Annual International Conference of the IEEE Engineering in Medicine and Biology Society (EMBC), 18-21 July 2018; **2018**; pp 2949-2952.

79. Battistel, A.; Fan, M.; Stojadinović, J.; La Mantia, F., Analysis and mitigation of the artefacts in electrochemical impedance spectroscopy due to three-electrode geometry. *Electrochimica Acta* **2014,** *135*, 133-138.

80. Macdonald, J. R.; Barsoukov, E., Impedance spectroscopy: theory, experiment, and applications. *History* **2005,** *1* (8), 1-13.

81. Macdonald, J. R.; Johnson, W. B., Fundamentals of impedance spectroscopy. *Impedance spectroscopy: theory, experiment, and applications* **2018**, 1-20.

82. Barsoukov, E.; Macdonald, J. R., Impedance Spectroscopy Theory, Experiment, and. *Applications, 2nd ed.(Hoboken, NJ: John Wiley & Sons, Inc., 2005)* **2005**.

83. Zhu, Y.; He, X.; Mo, Y., First principles study on electrochemical and chemical stability of solid electrolyte–electrode interfaces in all-solid-state Li-ion batteries. *Journal of Materials Chemistry A* **2016,** *4* (9), 3253-3266.

84. Liu, Y.; Yu, H.; Quan, X.; Chen, S.; Zhao, H.; Zhang, Y., Efficient and durable hydrogen evolution electrocatalyst based on nonmetallic nitrogen doped hexagonal carbon. *Scientific Reports* **2014,** *4* (1), 6843.

85. Geiger, S.; Kasian, O.; Mingers, A. M.; Nicley, S. S.; Haenen, K.; Mayrhofer, K. J. J.; Cherevko, S., Catalyst Stability Benchmarking for the Oxygen Evolution Reaction: The Importance of Backing Electrode Material and Dissolution in Accelerated Aging Studies. *ChemSusChem* **2017,** *10* (21), 4140-4143.

86. Robinson, R. A.; Stokes, R. H., *Electrolyte solutions*. Courier Corporation: **2002**.

87. Pletcher, D.; Walsh, F. C., *Industrial electrochemistry*. Springer Science & Business Media: **2012**.

88. May, P. M.; Rowland, D., Thermodynamic modeling of aqueous electrolyte systems: current status. *Journal of Chemical & Engineering Data* **2017,** *62* (9), 2481-2495.

89. Rice, S. A., *Diffusion-limited reactions*. Elsevier: **1985**.

90. Yan, Y.; Xia, B. Y.; Zhao, B.; Wang, X., A review on noble-metal-free bifunctional heterogeneous catalysts for overall electrochemical water splitting. *Journal of Materials Chemistry A* **2016,** *4* (45), 17587-17603.

91. Gaur, A.; Shrivastava, B. D.; Nigam, H., X-ray absorption fine structure (XAFS) spectroscopy–A review. *Proceedings of the Indian National Science Academy* **2013,** *79* (Part B), 921-966.

92. Norman, D., X-ray absorption spectroscopy (EXAFS and XANES) at surfaces. *Journal of Physics C: Solid State Physics* **1986,** *19* (18), 3273-3311.

93. Sólyom, J., *Fundamentals of the Physics of Solids: Volume 1: Structure and Dynamics*. Springer Science & Business Media: **2007**; Vol. 1.

94. Bunker, G., X-ray Absorption Spectrometers. In *Encyclopedia of Spectroscopy and Spectrometry*, Lindon, J. C., Ed. Elsevier: Oxford, **1999**; pp 2447-2453.

95. Degueldre, C. A., *The analysis of nuclear materials and their environments*. Springer: **2017**.

96. Koningsberger, D.; Prins, R., X-ray absorption: principles, applications, techniques of EXAFS, SEXAFS, and XANES. **1988**.

97. Bianconi, A.; Dell'Ariccia, M.; Durham, P. J.; Pendry, J. B., Multiple-scattering resonances and structural effects in the x-ray-absorption near-edge spectra of Fe II and Fe III hexacyanide complexes. *Physical Review B* **1982,** *26* (12), 6502-6508.

98. Mottana, A.; Marcelli, A., The historical development of X-ray Absorption Fine Spectroscopy and of its applications to Materials Science. In *A Bridge between Conceptual Frameworks*, Springer: **2015**; pp 275-301.

99. Bhattacharyya, D.; Poswal, A.; Jha, S.; Sabharwal, S., First results from a dispersive EXAFS beamline developed at INDUS-2 synchrotron source at RRCAT, Indore, India. *Nuclear Instruments and Methods in Physics Research Section A: Accelerators, Spectrometers, Detectors and Associated Equipment* **2009,** *609* (2-3), 286-293.

100. Deb, S.; Singh, G.; Gupta, P. In *Indus-2 Synchrotron Radiation Source: current status and utilization*, Journal of Physics: conference series, IOP Publishing: 2013; p 072009.

101. Berne, B. J.; Pecora, R., *Dynamic light scattering: with applications to chemistry, biology, and physics*. Courier Corporation: **2000**.

102. Sartor, M., Dynamic light scattering. *University of California: San Diego, CA, USA* **2003**, 2-21.

103. Pecora, R., Dynamic light scattering measurement of nanometer particles in liquids. *Journal of nanoparticle research* **2000,** *2* (2), 123-131.

104. Hassan, P. A.; Rana, S.; Verma, G., Making sense of Brownian motion: colloid characterization by dynamic light scattering. *Langmuir* **2015,** *31* (1), 3-12.

105. Khlebtsov, B.; Khlebtsov, N., On the measurement of gold nanoparticle sizes by the dynamic light scattering method. *Colloid Journal* **2011,** *73* (1), 118-127.

106. Hallett, F.; Watton, J.; Krygsman, P., Vesicle sizing: number distributions by dynamic light scattering. *Biophysical journal* **1991,** *59* (2), 357-362.

107. Lim, J.; Yeap, S. P.; Che, H. X.; Low, S. C., Characterization of magnetic nanoparticle by dynamic light scattering. *Nanoscale research letters* **2013,** *8* (1), 381.

Chapter 3

Uniformly Decorated Molybdenum Carbide/Nitride Nanostructures on Biomass Templates for Hydrogen Evolution Reaction Applications

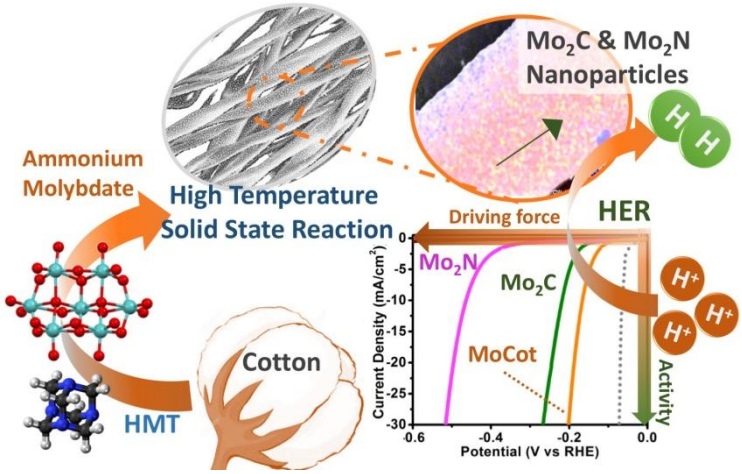

Abstract: *Natural fibrils derived from biomass were used as a template to synthesize uniformly decorated nanoparticles (10−12 nm) of molybdenum carbide (Mo_2C) and molybdenum nitride (Mo_2N) supported on carbon. The nanoparticles have been synthesized through the carburization and nitridation of molybdenum on cotton fibrils, using a high-temperature solid-state reaction. The catalyst exhibits an onset potential of 110 mV and an overpotential of 167 mV to derive a cathodic current density of 10 $mAcm^{-2}$. The electrocatalyst also demonstrates excellent long-term durability of more than 2500 cycles in acidic media with a Tafel slope value of 62 $mVdec^{-1}$.*

Brief Outcome: In this chapter, the catalyst named "SiMoCat" consist of nanoparticles of molybdenum carbide (Mo_2C) and molybdenum nitride (Mo_2N) with size 10-12 nm were grown uniformly on biomass (obtained from cotton) as a template by manipulating the reaction condition. The catalytic activity increases abruptly when both the nanoparticles were synthesized on the same carbon platform through the carburization and nitridation of molybdenum precursor by annealing at an appropriate temperature. The activation caused due to the synergistic effect of C-N present in the metal carbide/nitride nanoparticles through the carbon layers along the surface. The catalyst demonstrates low overpotential of 167 mV to derive a cathodic current density 10 $mAcm^{-2}$ with a low Tafel slope value of 62$mVdec^{-1}$. The catalyst also exhibits excellent stability of more than 2500 cycles in acidic media. This study will open up an area of exploration for developing inexpensive and highly stable electrocatalysts using several other biomass as templates for HER applications. Since the formation of uniform nanostructures was acquired from the inherent structure of the biomass templates. Hence the nature of the template used in the reaction is of tremendous importance. The morphology plays a crucial role in such kind of catalytic activity.

3.1. Introduction

The environmental concern regarding carbon-dioxide emission, global warming and increasing trend of energy requirements has augmented the urge to invent and use greener and renewable energy sources.[1] In this context, hydrogen could be one of the most feasible and promising energy carriers for future energy needs.[2] High energy density and sustainability of hydrogen as compared to other energy sources might provide carbon-neutral and clean energy for future needs.[3] The hydrogen production through electrochemical water splitting could be one of the most effective, economically sustainable and environment-friendly processes. In practice, Pt is still considered as one of the most effective, sustainable and universally accepted electrocatalysts for hydrogen generation.[4] However, the expense and availability of Pt make it limited for extensive use. Non-Nobel electrocatalysts having similar or better catalytic activity with respect to Pt can be one of the best alternatives for electrochemical hydrogen generation.[5-6] At present, the primary emphasis is being given in developing stable, low-cost and efficient electrocatalysts. Transition metals with well-known accessibility and remarkable tendency towards the electrochemical water splitting make it suitable for hydrogen generation.[7-8] Metal carbides have been used as supporting material to reduce the platinum loading as well as the overall cost of the HER catalyst. However, Vrubel et al.[9] have reported HER active molybdenum carbide for the first time in 2012. During 2012 – 2014, a transition took place in HER research, when people have started working on non-noble metal-based molybdenum catalysts. Later on, many reports were published on Mo-catalyst showing remarkably good activity towards hydrogen evolution reaction (HER).[9-12] Recently, binary phases of molybdenum based nanostructured materials have drawn remarkable attention because of high charge/mass-transfer ability on the electrode-electrolyte interface and to minimize interface resistance and enhance the catalytic performance of the electrocatalyst.[13-15] A report by Chen et al.[16] shows that a composite of molybdenum carbide and molybdenum nitride provides excellent synergic effects and improves the catalytic activity. A supporting template like holey carbon provides easy pathways to the charge transfer in heterojunction Mo_2C/Mo_2N/HGr nanostructure with outstanding catalytic activity and stability.[17] The d-band structure of the specific transition metals on heteroatoms doping gets modified which brings these composite into the category of near noble metals by improving the charge transfer process at interface.[11, 18-21] Besides this, a morphological variation using templates also plays a vital role in determining the catalytic activity.[22] Herein, we report an inexpensive synthesis of a nanostructured electrocatalyst

supported on carbon derived from cotton fibrils as templates. The use of templates not only provide carbon support for the nano-catalyst formed in the solid-state reaction but also enhances the charge transfer through the catalyst interface during the reaction.[23-24] The reaction condition was improvised in such a way, that both Mo_2C and Mo_2N nanoparticles were formed uniformly and simultaneously on the carbon support, which shows an overpotential of 167 mV in acidic media. This chapter provide an exciting insight towards a biphasic molybdenum derivative catalyst grown on natural biomass template and also introduce a new system for the fundamental study of nanohybrids with vast possibilities on the application on a realistic energy conversion system.

3.2. Experimental section

3.2.1. Materials

Chemicals used in the following reactions were purchased and used without further purification. Ammonium molybdate tetrahydrate ($(NH_4)_6.Mo_7O_{24}.4H_2O$), Sigma-Aldrich 99.0%; N, N-Dimethylformamide anhydrous, 99.8%, Sigma Aldrich; Nafion® perfluorinated resin solution, (5 wt. % in lower aliphatic alcohols); Hexamethylenetetramine ($C_6H_{12}N_4$) 95%, TCI; Ammonium Hydroxide $NH_3.H_2O$ (25%); Sterilized Cotton. Deionized water was used in all preparations.

3.2.2. Methodology

3.2.2.1. Synthesis of Catalyst

The synthesis of MoCot catalyst carried out in two steps. First, the preparation of the precursor and second, the calcination of the cotton soaked metal precursor by temperatures controlled annealing in ammonia and argon atmosphere at different time periods.

Synthesis of catalyst precursor (First Step). For the precursor, 0.01 mol of hexamethylenetetramine (HMT) and 0.001 mol of ammonium molybdate tetrahydrate ($(NH_4)_6Mo_7O_{24}.4H_2O$) were mixed into a solution of 2.5 mL of ammonia water (25%). The mixture was stirred until it becomes transparent. Then 1 g of finely chopped cotton was dipped and soaked into the solution mentioned above. The soaked cotton, along with the remaining solution, was transferred into a hydrothermal bomb and heated to 100 °C into an oven for 12 h.

The product obtained was then dried in a vacuum oven at 100 °C for 6 hours to yield a greenish-white mass.

Temperature programmed calcination of the precursor (Second step). This process is specifically designed for the synthesis of MoCot. The furnace was purged with argon initially for 20 minutes to make an inert environment for the sample before the reaction. The cotton soaked catalyst precursor (greenish-white mass) was heated to 650 °C with a ramp rate of 7 degrees/min in the tube furnace under argon with a flow of 30 mL/min. The reaction was held for one hour under ammonia at a flow rate of 20 mL/min and after that, the gas was switched to argon and the temperature raised to 750 °C and held for another 2.5 h. The MoCot catalyst was obtained by gradually cooling the product under argon. The simultaneous formation of the Mo_2C and Mo_2N nanoparticles is highly sensitive not only towards the initial stoichiometry of the catalyst precursor but also on the temperature manipulation with respect to the time and nature of the gases used.

All these parameters were judiciously optimized to obtain various compositions of Mo_2C and Mo_2N on carbon template.

Synthesis of MoCot1, MoCot2, Mo_2C and Mo_2N

The general synthesis procedure of all the catalyst consists of two major steps:

The first step involves the synthesis of the catalyst precursor which described below and complete detail is given in the above experimental section but the second step is different for corresponding catalysts which describe in detail in the following section:

First Step: The first step of these catalysts is the same as that of the MoCot catalyst in which initially slurry of cotton soaked molybdenum salt was formed at room temperature. This step is the same for all the catalysts which synthesized i.e., MoCot, MoCot1, MoCot2 Mo_2C and Mo_2N. Then the slurry is dried and after proper crushing, the obtained powder is calcined at a high temperature which is the second stage for the synthesis of molybdenum carbide and molybdenum nitride on carbon fibrils. The second step has been manoeuvred in such a way that that programmed temperature calcination gives the desired products.

Second step: In this step, the calcination of above-obtained catalyst-precursors for respective catalyst was carried out in such a way that it yields the desired products. The reaction parameters were manipulated in the following manner:

(a) MoCot1: For MoCot1 catalyst, the hold time in ammonia atmosphere was 30 minutes with a flow rate of 20 mL/min at temperature 650 °C and after that raised to 750 °C and held for 2.5 h in an argon atmosphere at a flow rate of 30 mL/min.

(b) MoCot2: For MoCot2, the hold time at 650 °C was 1.5 h in ammonia atmosphere with a flow rate of 20 mL/min followed by annealing at 750 °C for 2.5 h in an argon atmosphere at a flow rate of 30 mL/min.

(c) Mo_2C: The Mo_2C catalyst was synthesized simply by annealing the catalyst precursor at 750 °C for 2.5 h in an argon atmosphere at a flow rate of 30 mL/min throughout the synthesis process.

(d) Mo_2N: The Mo_2N catalyst obtained by annealing the catalyst precursor at 650 °C for two hours in the ammonia atmosphere with a flow rate of 20 mL/min.

Note: The heating rate in all the synthesis process was 7 °C /min, and the post-reaction cooling was done in an argon environment with a gas flow of 30 mL/min.

3.2.2.2. Physical characterization

X-ray diffraction (XRD) of the solid was done using a Bruker Eco D8 advance X Powder X-ray diffractometer using Ni filter employing Cu Kα radiation ((λ=1.54056 Å, 40 kV and 25 mA) in the 2θ range of 5º to 80º with an increment of .00190/Step. The surface area and pore size analysis of the samples were examined by nitrogen physisorption at 77 K in Autosorb IQ Quantachrome instrument using the Brunauer-Emmett-Teller (BET) and the Barrett-Joyner-Halenda (BJH) equation. Surface morphology was studied using Scanning electron microscope from JEOL (JSM IT-300) equipped with energy dispersive X-ray diffractometer (Bruker), and Transmission electron microscopy (TEM) images were acquired using a JEOL-2100 operated at 200 kV. The X-ray photoelectron spectroscopy (XPS) was performed on Esca Lab: 220-IXL with Mg-K_α non-monochromated X-ray beam having photon energy 1253.6 eV.

3.2.2.3. Electrochemical measurements

CHI 760E electrochemical workstation setup was used at room temperature for all the electrochemical measurements. Herein we have used conventional three-electrode cell system containing carbon-based electrode, Ag/AgCl electrode and glassy carbon electrode as a counter, reference and working electrode respectively. A dispersed ink of 5 µL was coated on to the surface of the working electrode employing drop-casting and dried under vacuum. The

overpotential and other electrochemical measurements were calculated with respect to Ag/AgCl electrode and further referenced with reversible hydrogen electrode (RHE) according to the equation E (RHE) = E (Ag/AgCl) + 0.059 pH + 0.197 V. For all the measurements, polarization curves were collected under argon at a scan rate of 5 mVs^{-1} containing 0.5 M H_2SO_4 solution unless otherwise mentioned. The overpotential was further corrected to eliminate the ohmic-drop according to the equation η corrected= η-iR_s whereas R_s is solution resistance. The EIS measurements were performed at particular values of the overpotential, i.e. η =50, 150 and 250 mV under a frequency range of 100000 Hz to 1 Hz.

3.2.2.4. The general methodology of electrode fabrication.

The catalyst ink was prepared by dispersing 5 mg of electrocatalyst powder into 500 µL of dimethylformamide containing 5 µL of 5 wt% Nafion and keeping it for 120 min under ultrasonication to form a homogeneous suspension. Initially, the glassy carbon electrode was polished with alumina powder (0.5-micron size) and used as a working electrode. A well-dispersed ink of 5 µL was coated onto the surface of a working electrode (GCE, 3 mm in diameters) by means of the drop-casting method and dried under vacuum. The electrochemical measurements were recorded in argon saturated 0.5 M H_2SO_4 solution at a scan rate of 5 mVs^{-1}. The commercially available Pt/C (20wt %) catalyst was also tested under similar conditions. Electrochemical stability tests were conducted up to 3000 LSV cycles in the same potential range as above but at a faster scan rate of 8 $mVsec^{-1}$.

3.3. Result and Discussion

The MoCot catalyst consisting of uniformly decorated molybdenum carbide/nitride nanostructures on biomass-template has shown good catalytic activity. Broadly, the reaction for the formation of Mo_2C/Mo_2N nanoparticles requires carbon, nitrogen and a metal source at moderately high temperature. It was observed that Mo_2C formed at a temperature as high as 750 ºC, whereas, Mo_2N can be synthesized at a relatively low temperature of 650 ºC. Continuing the reaction at 650 ºC would lead to the formation of only nitride and same reaction at 750 ºC would lead to the formation of the only carbide. The stoichiometry of the initial precursor mixture is also very crucial as it determines the final composition of the catalyst. The reaction condition is manoeuvred in such a way that; both the nanoparticles can be formed at different steps of the same reaction. The critical parameters are temperature, hold-time and gases, which are purged at an appropriate time. For example, ammonia was purged only during the formation temperature (650 ºC) of Mo_2N. The hexamethylenetetramine acts both as a reducing agent and a

carbon/nitrogen source during the annealing process.[25] Initially, Mo oxyanions decompose into MoO_3 and then in the presence of carbon/nitrogen source it reacts and forms Mo_2C and Mo_2N nanoparticles onto the fibril substrate at high temperatures. One exciting aspect of this reaction is that the fibril structure of the natural cotton remains intact, and only the growth of the nanoparticles was observed to form onto the surface of the fibre. Detailed reaction conditions were mentioned in the experimental section. The objective towards the formation of both the nanomaterials on the same carbon support lies in the fact that it would result in a synergistic effect between the Mo_2C and Mo_2N nanoparticles and thereby increase the overall catalytic activity.[15] Series of reactions were performed to produce several compositions of Mo_2C and Mo_2N out of which MoCot shows best catalytic activity.

Structural information of the catalyst was obtained from PXRD measurements as provided in figure 3.1a. PXRD pattern of catalyst after annealing, exhibit a series of characteristics peaks located at approximately 34.3°, 37.9°, 39.4°, 52.1°, 61.5°, 69.5°, 72.4, 74.5° and 75.4° which attributes to the diffractions of (100), (002), (101), (102), (110), (103), (200), (112) and (201) planes (PDF 35-0787) of Mo_2C hexagonal system. The peaks at 37.3°, 43.4°, 63.1° and 75.7°

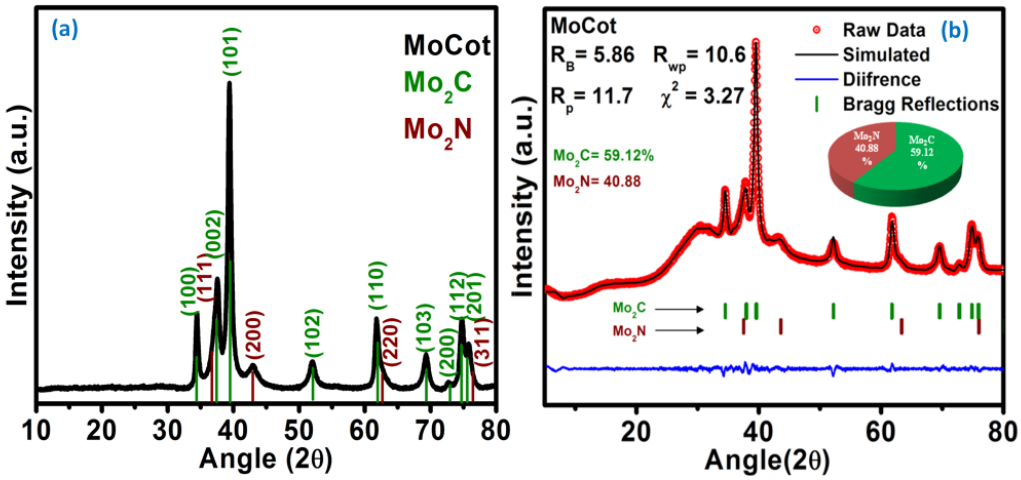

Figure 3.1. *Structural characterization (a) powder X-ray diffraction typically shows the formation of both Mo_2C-Mo_2N phases and (b) Compositional measurements: Rietveld analysis of catalyst shows a composition 59.12% and 40.88% of Mo_2C and Mo_2N respectively.*

are characteristics of γ-Mo_2N (PDF 25-1366) and correspond to (111), (200), (220) and (311) planes respectively. The XRD measurement confirmed that the Mo_2C-Mo_2N hybrid material (denoted as MoCot) was composed of hexagonal β-Mo_2C and cubic γ-Mo_2N respectively. Broad hump in the PXRD pattern at around 25º - 30º value, can be related to the mixed amorphous carbon phase which appears only in a slow scan. No other impurities or characteristic peaks of oxides etc. are observed. The XRD diffraction pattern indicates the co-existence of Mo_2C and Mo_2N in all the catalyst with variation in the composition of both. The catalyst was found to have 59.12% of Mo_2C and 40.88% Mo_2N nanoparticles respectively as calculated from Rietveld refinement (Figure 3.1b). Several other compositions were prepared out of which two compositions MoCot1 & MoCot2 which has a closer overpotential with respect to MoCot are mentioned in the experimental section. The Rietveld analysis and refinement parameters of MoCot1 and MoCot2 catalysts are given in figure 3.2 and figure 3.3 respectively.

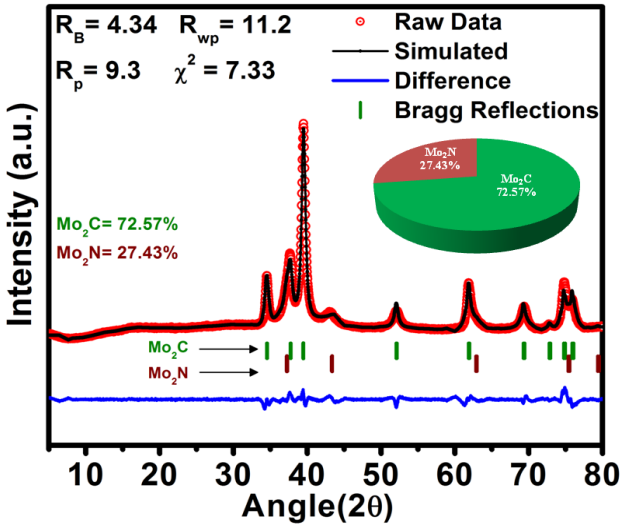

Figure 3.2. *Rietveld refinement of MoCot1 shows a composition of 72.57% and 27.43% of Mo_2C and Mo_2N respectively.*

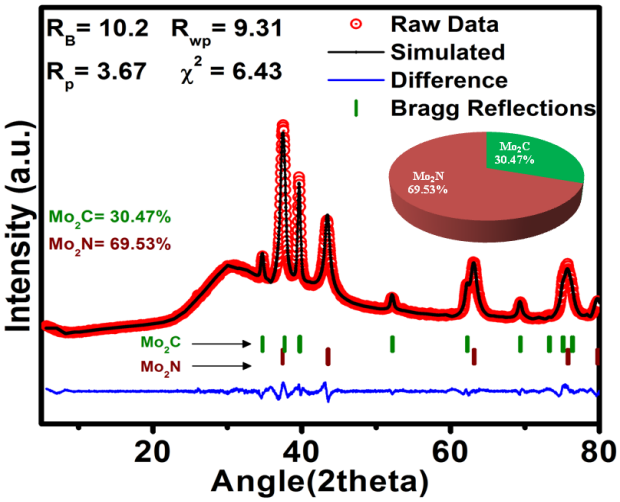

Figure 3.3. *Rietveld analysis of MoCot2 catalyst shows a composition of 30.47 % and 69.53 % of Mo_2C and Mo_2N respectively.*

A close look towards Scanning Electron Micrograph (Figure 3.4) along with elemental mapping gives detailed morphological information about the nanostructures and confirms the existence of two different phases. The image clearly shows that catalyst having well-decorated Mo_2C and Mo_2N nanoparticles developed on the fibril microstructure template, having different lengths.

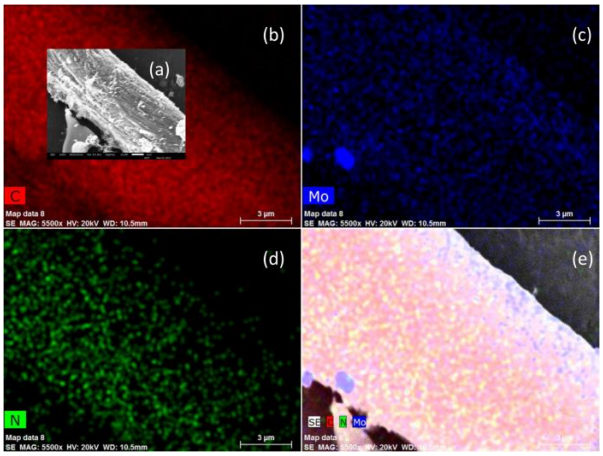

Figure 3.4. *Morphology characterization: Scanning Electron Microscopy (a) of as obtained MoCot catalyst and corresponding elemental mapping of the nanostructure showing the (b) Carbon, (c) Molybdenum and (d) Nitrogen elements that illustrate the uniform distribution of these on the fibril template. (e) SEM image shows the collective distribution of different elements (Mo, C and N) on the fibril structure.*

The carbon support inhibits the agglomeration of the metal carbide/nitride nanoparticles and thereby enhances the catalytic activity. TEM images (Figure 3.5 a, b & c) clearly showing the nanoparticles of the order of 10–12 nm, at two different scales. High-resolution (HR) TEM image (Figure 3.5c inset) shows the two adjoining phases of nanoparticles with an interface. The visible crystal fringe-width of 0.26 nm corresponds to (100) plane and 0.24 nm to (111) planes of Mo_2C and Mo_2N respectively.[19, 26]

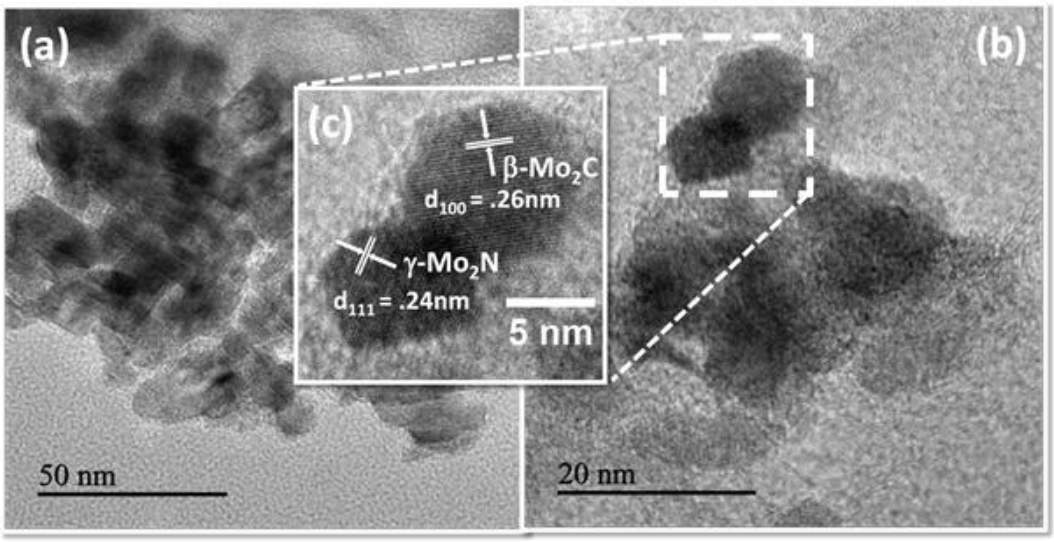

Figure 3.5. *Microscopic characterization of MoCot catalyst: A transmission electron microscopic images of MoCot at (a) medium (b) low and inset-(c) high magnification: showing the fringe width 0.26 nm and 0.24 nm consistent with the (100) and (111) planes of Mo_2C and Mo_2N nanocrystals.*

The surface area, pore size and its distribution and porosity of the nanohybrid material was investigated by N_2 adsorption/desorption measurements (Figure 3.6). The figure typically demonstrates the type-IV curve shape of BET isotherm. As evident from the BET measurements, nanohybrid material is having a surface area of 63 $m^2 g^{-1}$ in which mesopores are predominantly distributed over a range of 30 nm (Figure 3.6, inset).

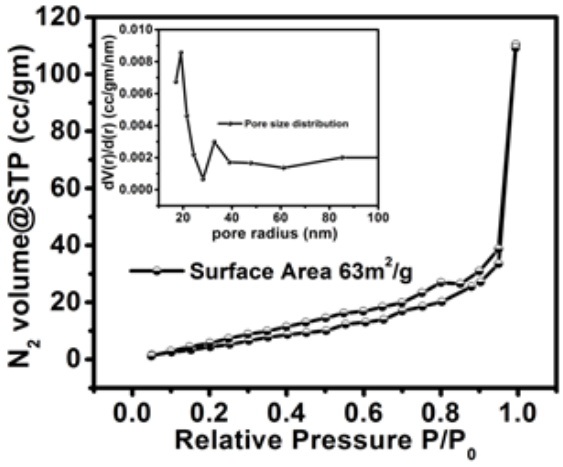

Figure 3.6. *Nitrogen adsorption BET isotherms and inset showing BJH pore distribution of the catalyst.*

This distribution indicates the material to be of mesoporous, which favours mass transport and adsorption. Formation of uniform nanostructures is essentially acquired from the inherent morphology of the biomass templates. Hence the template used in the reaction is of extreme importance. The N_2 adsorption isotherm os the catalyst MoCot1 and MoCot2 are shown in figure 3.7a and figure 3.7b which shows a surface area of 52.27 m^2/gm and 15.19 m^2/gm respectively.

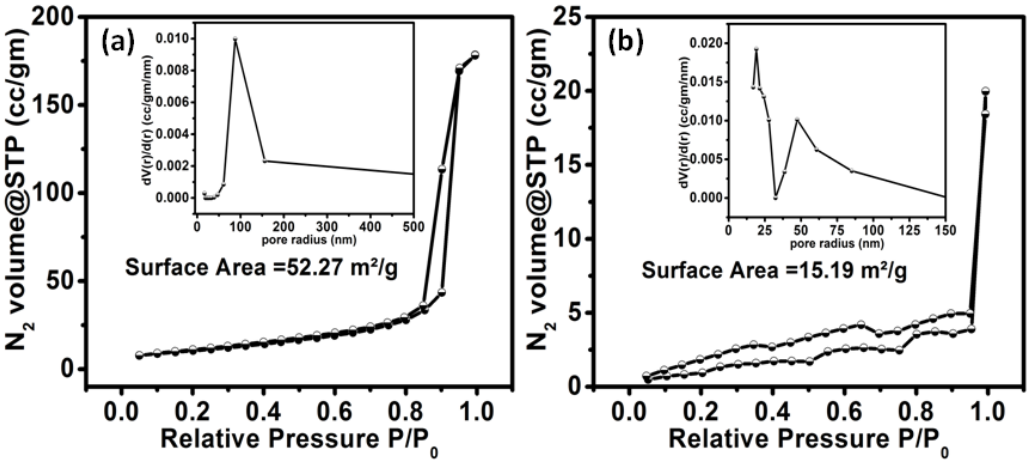

Figure 3.7. *Nitrogen adsorption BET isotherms and inset showing BJH pore distribution of the catalyst (a) MoCot1 and (b) MoCot2 respectively.*

X-ray photoelectron spectroscopy (XPS) further affirmed the chemical state of the catalyst. The wide range energy survey scan (Figure 3.8a) indicates the presence of C, Mo and N elements in the hybrid structure. The survey XPS spectrum shows five characteristic signals which are located at 233.6, 285.8, 398.1, 416.5, 532.2 eV, consistent with Mo 3d, C 1s, N 1s (Mo $3p_{3/2}$), Mo $3p_{1/2}$ and O 1s, respectively. The high-resolution spectrum of Mo 3d (Figure 3.8b) shows splitting in the core level due to spin-orbit coupling into $3d_{5/2}$ and $3d_{3/2}$ peaks. These peaks with binding energies values at 228.4 eV and 231.5 eV describe as Mo $3d_{5/2}$ and Mo $3d_{3/2}$ of Mo^{2+} spectral lines, respectively and confirms the presence of Mo_2C[27-28]. Other peaks at 235.1 eV and 235.9 eV are indicating the presence of Mo_4O_{11} and MoO_3 [29-31] while 232.4 eV and 229.2 eV may be assigned to MoO_2.[32] Surface oxidation of Mo_2C (during the XPS measurements) is the reason for the indication of the presence of a high concentration of molybdenum oxides. The Mo $3d_{5/2}$ peak of Mo_2N appears at around 228.7 eV which is overshadowed due to the adjacent

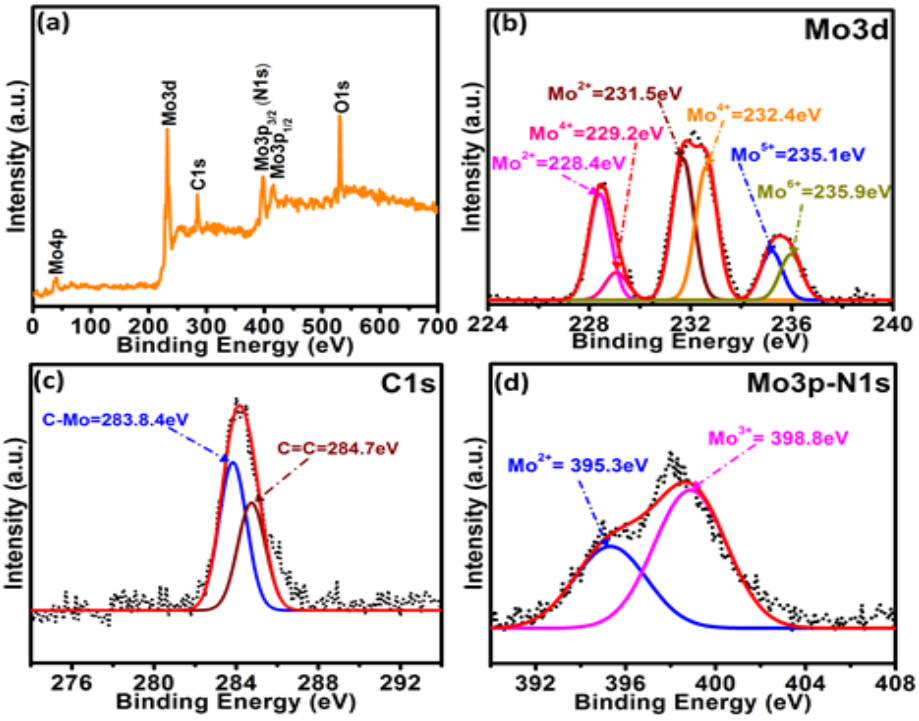

Figure 3.8. *X-ray photoelectron spectroscopy (XPS) of MoCot catalyst: Wide-scan survey spectra (a) and High-resolution spectra of Mo 3d (b), C1s (c) and N 1s (d) electron: Experimental data (dotted curve) and fitting results (solid curve). The peaks are assigned by oxidation states of different elements with their corresponding binding energy.*

peak.[33] In C1s energy spectra (Figure 3.8c) were deconvoluted into two peaks centred at 283.8 eV and 284.7 eV shows the binding energy of Mo-C and C=C species respectively.[27, 34] Deconvolution of the N 1s and Mo $3p_{3/2}$ peaks depict two different Mo $3p_{3/2}$ peaks having binding energies 398.8 eV and 395.3 eV respectively (Figure 3.8d). The binding energy of 395.3 eV may be attributed to Mo $3p_{3/2}$ of Mo_2N[35] and the binding energy of 398.8 eV is due to Mo $3p_{3/2}$ of MoO_3. The overlap of N 1s peaks of Mo_2N and pyridinic-N respectively with Mo 3p peaks might significantly enhance the electrochemical activation of graphitic carbon.[35] Use of extrinsic nitrogen during the pyrolysis of biomass or performing the reaction under nitrogen-rich conditions, species may be generated with an abundance of pyridinic-N, pyrrolic-N, quaternary-N, and pyridone-N oxides.[36-37] Among the nitrogen species, the formation of pyridinic N dominates over the other species which is favourable to HER performance. The HER activity of all the catalysts was primarily measured by linear sweep voltammetry in 0.5 M H_2SO_4 saturated with argon at 25 degree centigrade using three-electrode cells. In order to perform a systematic study, Mo_2C and Mo_2N have also been synthesized with the same method as was done for MoCot, but varying the parameters and gases used in the reaction. The commercially available Pt/C (20 wt%) catalysts were also tested under similar conditions. As depicted from figure 3.9, MoCot has an onset potential of nearly 110 mV. The polarization curves at rate 5 mV/sec were calculated with considering the iR-compensation. From the polarization curve (Figure 3.9a), it can be concluded that MoCot is HER active and having overpotential of 167 mV to derive the current density of 10 mA/cm^2. The comparison of MoCot catalyst with that of Mo_2C (218 mV) and Mo_2N (465 mV) catalyst undoubtedly confirms that the catalytic activity MoCot is way too better than the other two. Tafel slope value has a high significance not only in determining the possible reaction pathway but also in predicting the adsorption behaviour of the catalyst for a quantitative determination of HER kinetics.[38] A description of the procedure for electrode fabrication is described in the experimental section. Theoretically, for Tafel slope, the linear portions must fit with equation $\eta = b\log(j) + a$, where a is the Tafel constant, b is the Tafel slope, j is the current density, and η is the overpotential.[39] Here we have calculated Tafel plots for MoCot and of pure Mo_2C, Mo_2N and PtC (20%) as shown in figure 3.9b. The Tafel slope values of 62, 85, 196 mV/dec were measured for MoCot, Mo_2C, and Mo_2N respectively. The same for commercially available Pt/C catalyst was found to be ~35 mV/dec. However, with respect to Mo_2C, and Mo_2N, MoCot have a lower value suggesting that the reaction proceeds through a mixed Volmer-Heyrovsky process and thus recombination step is the rate-determining step.

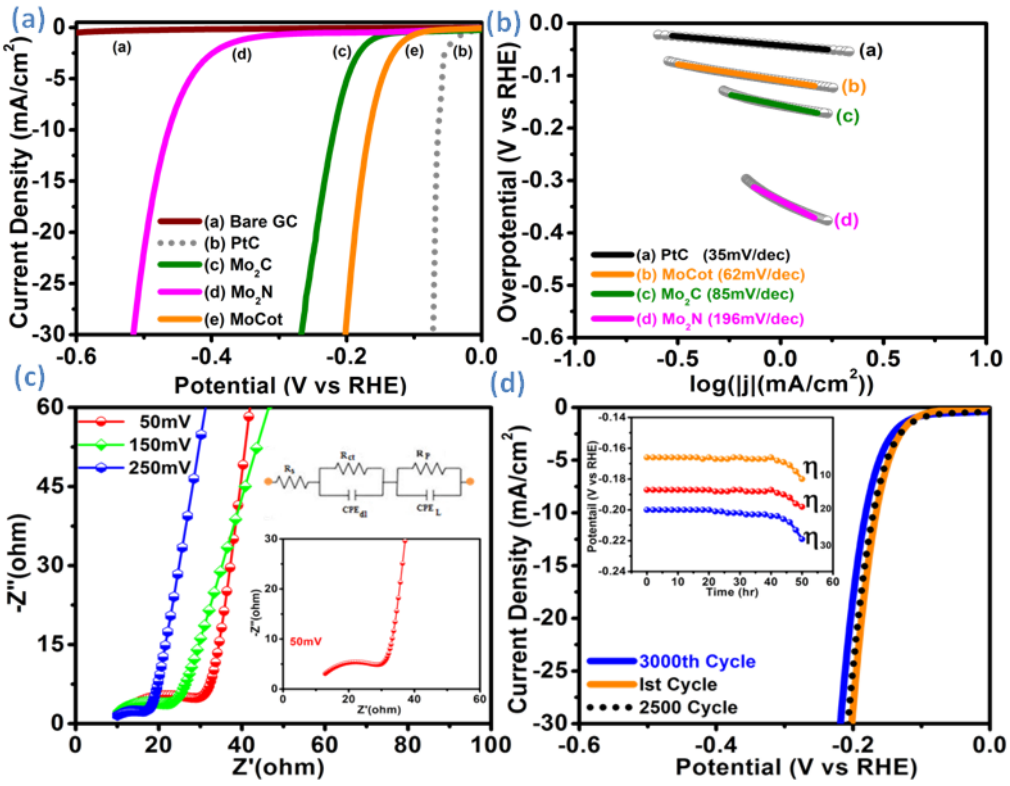

Figure 3.9. *Electrochemical measurements of specific electrocatalysts for hydrogen evolution in 0.5 M H_2SO_4 acidic medium. (a) Polarization curves (iR-corrected) of MoCot compared with other electrode (b) the corresponding Tafel plots derived from the curve (c) EIS Nyquist Plot (with corresponding equivalent circuit) of the electrode @50 mV, @150 mV and @250 mV (inset shows zoomed Nyquist plot of electrode @50 mV) (d) Figure shows the LSV stability curve at 1st, 2500th and 3000th cycle (inset shows the potential testing at constant current density 10 mAcm^{-2}, 20 mAcm^{-2} and 30 mAcm^{-2}.*

Transport properties and interfacial interactions of the concerned catalyst were investigated by electrochemical impedance spectroscopy (EIS) with an overpotential of 50, 150 and 250 mV in 0.5 M H_2SO_4 aqueous solution (Figure 3.9c). The Nyquist plot reveals the effective resistance shown by the electrocatalyst resulting from the combined effects of ohmic resistance and reactance. Simulating and simultaneous fitting of the experimental curve with the equivalent circuit provides information regarding the contribution of each component. Here, the fitting of the plot with the equivalent circuit shows two time-constant components R_{ct}-CPE_{dL} and R_p-CPE_L along with an uncompensated solution resistance R_s (in series) describing the response of

HER on the catalyst modified electrode. CPE is the constant phase angle element, which represents the double-layer capacitance of the solid electrode. The R_{ct}-CPE_{dL} is related to the charge-transfer process, and R_p-CPE_L can be correlated with the surface porosity.[26, 40] The charge transfer resistance varies inversely with respect to the potential applied. A charge transfer resistance (R_{ct}) of 20 ohms is obtained in the low-frequency region when a potential of 50 mV is applied. The smaller value of R_{ct} implies a larger number of active sites present in the catalyst, and hence, the charge transfer between the electrode and electrolyte would be high, which favours the HER process**.** The durability measurement (Figure 3.9d) indicates a high stability performance of the catalyst and shows no significant change in the overpotential of the catalyst even after 2500 LSV cycles. The stability trend (inset Figure 3.9d) measured at higher current densities, i.e., 20 and 30 mA/cm^2 are similar to that of 10 mA/cm^2 suggesting that the

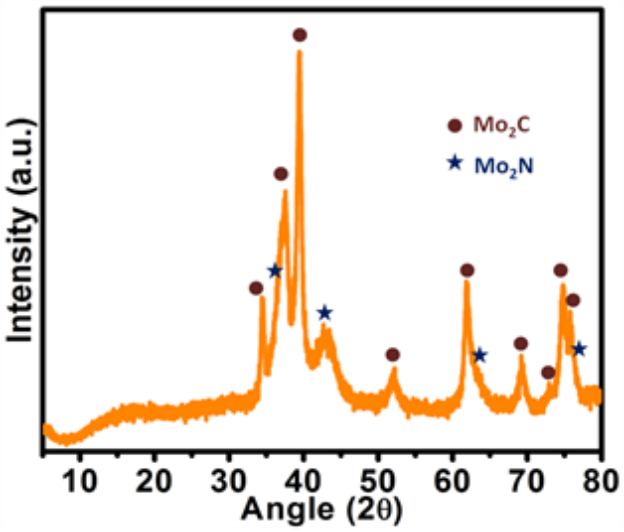

Figure 3.10. *PXRD patterns of isolated electrocatalyst after a durability test of 2500 cycle.*

electrocatalytic activity profile does not change at high current density. The stability of the MoCot composite was further verified by X-ray analysis of the catalyst after 2500 cycles (Figure 3.10). The composition was found to be consistent with the one recorded before the reaction. Thus the catalyst demonstrates good stability towards HER process. A comparative electrochemical study of the other two extreme compositions has also been performed and the corresponding LSV plot of the MoCot1 & MoCot2 composites along with the physical mixture of Mo_2C and Mo_2N catalyst (MoCot-m) is shown in Figure 3.11.

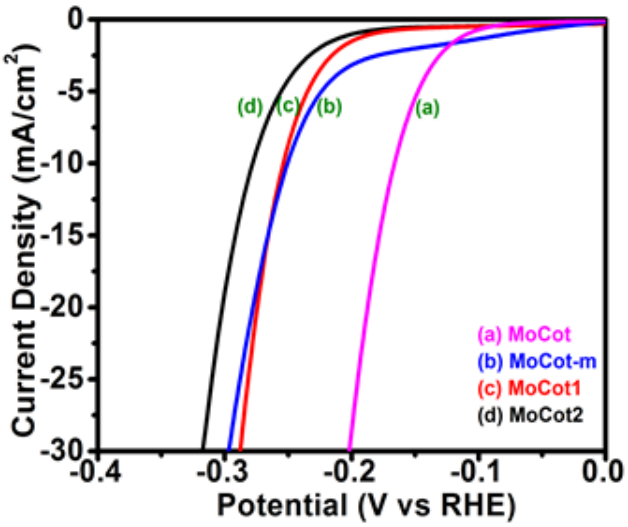

Figure 3.11. *Electrocatalytic measurements of electrodes for hydrogen evolution in 0.5 M H_2SO_4 solution.*

The overall electrochemical study ends with the result that the catalyst MoCot have better electrocatalytic activity as compared to the individual Mo_2C, Mo_2N and physical mixture of the Mo_2C and Mo_2N.

3.4. Conclusion

In this work, nanoparticles of molybdenum carbide (Mo_2C) and molybdenum nitride (Mo_2N) with size 10–12 nm were grown uniformly on biomass (used as a template obtained from cotton) by manipulating the reaction conditions. Formation of uniform nanostructures was acquired from the inherent structure of the biomass templates. Hence the nature of the template used in the reaction is of tremendous importance. The catalytic activity increased abruptly when both the nanoparticles were grown on the same carbon platform through the carburization and nitridation of molybdenum precursor by annealing at an appropriate temperature. The activation caused possibly due to the synergistic effect of C-N present in the metal carbide/nitride nanoparticles through the carbon layers along the surface. The catalyst demonstrates long-term stability and high conductivity in acidic media and exhibits an onset potential of 110 mV and an overpotential of 167 mV to derive a cathodic current density 10 $mAcm^{-2}$. The electrocatalyst also exhibits high stability of withstanding more than 2500 cycles in acidic media with a Tafel slope value of 62 $mVdec^{-1}$. This study will open up an area of exploration for developing nanostructured binary composites on biomass as templates for HER application. The process is inexpensive and produces highly stable electrocatalysts. The methodology can be applied to

numerous kind of biomass having different morphologies as the later plays a crucial role in catalytic activity.

Note:

- The permission has been granted by the authors and corresponding author of the published paper prior to adopting in the present thesis. The associated relevant publication is:

Rajinder Kumar, Zubair Ahmed, Ritu Rai, Ashish Gaur, Shilpa Kumari, Takahiro Maruyama and Vivek Bagchi "Uniformly decorated molybdenum carbide/nitride nanostructures on biomass template for HER application" ***ACS Omega***, 2019, 4, 9, 14155-14161.

References

1. Fankhauser, S.; Jotzo, F., Economic growth and development with low-carbon energy. *Wiley Interdisciplinary Reviews: Climate Change* **2018,** *9* (1), e495.

2. H. P. T. Team, e., Hydrogen production road map: Technology pathways to the future FreedomCAR & Fuel partnership. **2009**.

3. Hosseini, S. E.; Wahid, M. A., Hydrogen production from renewable and sustainable energy resources: Promising green energy carrier for clean development. *Renewable and Sustainable Energy Reviews* **2016,** *57*, 850-866.

4. Cheng, N.; Stambula, S.; Wang, D.; Banis, M. N.; Liu, J.; Riese, A.; Xiao, B.; Li, R.; Sham, T. K.; Liu, L. M.; Botton, G. A.; Sun, X., Platinum Single-Atom and Cluster Catalysis of the Hydrogen Evolution Reaction. *Nat. Commun.* **2016,** *7*, 13638.

5. Kou, Z.; Wang, T.; Cai, Y.; Guan, C.; Pu, Z.; Zhu, C.; Hu, Y.; Elshahawy, A. M.; Wang, J.; Mu, S., Ultrafine Molybdenum Carbide Nanocrystals Confined in Carbon Foams via a Colloid-Confinement Route for Efficient Hydrogen Production. *Small Methods* **2018,** *2* (4), 1700396.

6. Amiinu, I. S.; Pu, Z.; Liu, X.; Owusu, K. A.; Monestel, H. G. R.; Boakye, F. O.; Zhang, H.; Mu, S., Multifunctional Mo–N/C@MoS_2 Electrocatalysts for HER, OER, ORR, and Zn–Air Batteries. *Advanced Functional Materials* **2017,** *27* (44), 1702300.

7. Zhong, Y.; Xia, X.; Shi, F.; Zhan, J.; Tu, J.; Fan, H. J., Transition Metal Carbides and Nitrides in Energy Storage and Conversion. *Advanced science (Weinheim, Baden-Wurttemberg, Germany)* **2016,** *3* (5), 1500286-1500286.

8. Kitchin, J. R.; Norskov, J. K.; Barteau, M. A.; Chen, J. G. G., Trends in the Chemical Properties of Early Transition Metal Carbide Surfaces: A Density Functional Study. *Catal. Today* **2005,** *105*, 66.

9. Vrubel, H.; Hu, X., Molybdenum Boride and Carbide Catalyze Hydrogen Evolution in Both Acidic and Basic Solutions. *Angew. Chem., Int. Ed.* **2012,** *51*, 12703.

10. Liu, Y.; Yu, G.; Li, G. D.; Sun, Y.; Asefa, T.; Chen, W.; Zou, X., Coupling Mo_2C with Nitrogen-Rich Nanocarbon Leads to Efficient Hydrogen-Evolution Electrocatalytic Sites. *Angew. Chem., Int. Ed.* **2015,** *54*, 10752.

11. Shi, Z. P.; Gao, B. X.; Mo, Q. J.; Shao, Z. J.; Nie, K. Q.; Liu, B. L.; Zhang, H. B.; Wang, Y. X.; Zhang, Y. H.; Gao, Q. S.; Sun, X. H.; Cao, X. M.; Hu, P.; Tang, Y., Organic-Inorganic-Hybrid-Derived Molybdenum Carbide Nanoladders: Impacts of Surface Oxidation for Hydrogen Evolution Reaction. *Chemnanomat* **2018,** *4* (2), 194-202.

12. Zhang, Q.; Jiang, Z.; Tackett, B. M.; Denny, S. R.; Tian, B.; Chen, X.; Wang, B.; Chen, J. G., Trends and descriptors of metal-modified transition metal carbides for hydrogen evolution in alkaline electrolyte. *ACS Catalysis* **2019**.

13. Chen, J.; Yang, Y.; Su, J.; Jiang, P.; Xia, G.; Chen, Q., Enhanced Activity for Hydrogen Evolution Reaction over CoFe Catalysts by Alloying with Small Amount of Pt. *ACS Applied Materials & Interfaces* **2017,** *9* (4), 3596-3601.

14. Chen, Y. Y.; Zhang, Y.; Jiang, W. J.; Zhang, X.; Dai, Z.; Wan, L. J.; Hu, J. S., Pomegranate-Like N, P-Doped Mo_2C@C Nanospheres as Highly Active Electrocatalysts for Alkaline Hydrogen Evolution. *ACS Nano* **2016,** *10*, 8851.

15. Kumar, R.; Rai, R.; Gautam, S.; De Sarkar, A.; Tiwari, N.; Jha, S. N.; Bhattacharyya, D.; Ganguli, A. K.; Bagchi, V., Nano-structured hybrid molybdenum carbides/nitrides generated in situ for HER applications. *Journal of Materials Chemistry A* **2017,** *5* (17), 7764-7768.

16. Chen, W.-F.; Iyer, S.; Iyer, S.; Sasaki, K.; Wang, C.-H.; Zhu, Y.; Muckerman, J. T.; Fujita, E., Biomass-derived electrocatalytic composites for hydrogen evolution. *Energy & Environmental Science* **2013,** *6* (6), 1818-1826.

17. Yan, H.; Xie, Y.; Jiao, Y.; Wu, A.; Tian, C.; Zhang, X.; Wang, L.; Fu, H., Holey Reduced Graphene Oxide Coupled with an Mo_2N–Mo_2C Heterojunction for Efficient Hydrogen Evolution. *Advanced Materials* **2018,** *30* (2), 1704156.

18. Wan, C.; Regmi, Y. N.; Leonard, B. M., Multiple Phases of Molybdenum Carbide as Electrocatalysts for the Hydrogen Evolution Reaction. *Angew Chem Int Edit* **2014,** *53* (25), 6407-6410.

19. Liang, P.; Gao, H.; Yao, Z.; Jia, R.; Shi, Y.; Sun, Y.; Fan, Q.; Wang, H., Simple synthesis of ultrasmall β-Mo_2C and α-MoC_{1-x} nanoparticles and new insights into their catalytic mechanisms for dry reforming of methane. *Catalysis Science & Technology* **2017,** *7* (15), 3312-3324.

20. Levy, R. B.; Boudart, M., Platinum-Like Behavior of Tungsten Carbide in Surface Catalysis. *Science* **1973,** *181* (4099), 547-549.

21. Cheng, R.; He, H.; Pu, Z.; Amiinu, I. S.; Chen, L.; Wang, Z.; Li, G.; Mu, S., Shrunken hollow Mo-N/Mo-C nanosphere structure for efficient hydrogen evolution in a broad pH range. *Electrochimica Acta* **2019,** *298*, 799-805.

22. Zhang, H.; Nai, J.; Yu, L.; Lou, X. W., Metal-Organic-Framework-Based Materials as Platforms for Renewable Energy and Environmental Applications. *Joule* **2017,** *1* (1), 77-107.

23. Xiao, J.; Zhang, Y.; Zhang, Z.; Lv, Q.; Jing, F.; Chi, K.; Wang, S., Self-Supported Biocarbon-Fiber Electrode Decorated with Molybdenum Carbide Nanoparticles for Highly Active Hydrogen-Evolution Reaction. *ACS Applied Materials & Interfaces* **2017,** *9* (27), 22604-22611.

24. Zeng, L.; Zhao, S.; He, M., Macroscale porous carbonized polydopamine-modified cotton textile for application as electrode in microbial fuel cells. *Journal of Power Sources* **2018,** *376*, 33-40.

25. Wang, Z.-Q.; Zhang, Z.-B.; Zhang, M.-H., The efficient synthesis of a molybdenum carbide catalystvia H_2-thermal treatment of a Mo(vi)–hexamethylenetetramine complex. *Dalton Transactions* **2011,** *40* (5), 1098-1104.

26. Song, Y.-J.; Yuan, Z.-Y., One-pot Synthesis of Mo2N/NC Catalysts with Enhanced Electrocatalytic Activity for Hydrogen Evolution Reaction. *Electrochimica Acta* **2017,** *246*, 536-543.

27. Guo, J.; Wang, J.; Xuan, C.; Wu, Z.; Lei, W.; Zhu, J.; Xiao, W.; Wang, D., Molybdenum carbides embedded on carbon nanotubes for efficient hydrogen evolution reaction. *Journal of Electroanalytical Chemistry* **2017,** *801*, 7-13.

28. Yang, X.; Feng, X.; Tan, H.; Zang, H.; Wang, X.; Wang, Y.; Wang, E.; Li, Y., N-Doped graphene-coated molybdenum carbide nanoparticles as highly efficient electrocatalysts for the hydrogen evolution reaction. *Journal of Materials Chemistry A* **2016,** *4* (10), 3947-3954.

29. Barkat, L.; Hssein, M.; El Jouad, Z.; Cattin, L.; Louarn, G.; Stephant, N.; Khelil, A.; Ghamnia, M.; Addou, M.; Morsli, M.; Bernède, J. C., Efficient hole-transporting layer MoO_3:CuI deposited by co-evaporation in organic photovoltaic cells. *physica status solidi (a)* **2017,** *214* (1), 1600433.

30. Qin, P.; Fang, G.; Ke, W.; Cheng, F.; Zheng, Q.; Wan, J.; Lei, H.; Zhao, X., In situ growth of double-layer MoO_3/MoS_2 film from MoS_2 for hole-transport layers in organic solar cell. *Journal of Materials Chemistry A* **2014,** *2* (8), 2742-2756.

31. Pan, Y.-X.; Peng, J.-B.; Xin, S.; You, Y.; Men, Y.-L.; Zhang, F.; Duan, M.-Y.; Cui, Y.; Sun, Z.-Q.; Song, J., Enhanced Visible-Light-Driven Photocatalytic H2 Evolution from Water on Noble-Metal-Free CdS-Nanoparticle-Dispersed Mo_2C@C Nanospheres. *ACS Sustainable Chemistry & Engineering* **2017,** *5* (6), 5449-5456.

32. Wang, D.; Wang, J.; Luo, X.; Wu, Z.; Ye, L., In Situ Preparation of Mo_2C Nanoparticles Embedded in Ketjenblack Carbon as Highly Efficient Electrocatalysts for Hydrogen Evolution. *ACS Sustainable Chemistry & Engineering* **2018,** *6* (1), 983-990.

33. Liu, J.; Tang, S.; Lu, Y.; Cai, G.; Liang, S.; Wang, W.; Chen, X., Synthesis of Mo_2N nanolayer coated MoO_2 hollow nanostructures as high-performance anode materials for lithium-ion batteries. *Energy & Environmental Science* **2013,** *6* (9), 2691-2697.

34. Chen, I. W. P.; Huang, C.-Y.; Jhou, S.-H. S.; Zhang, Y.-W., Exfoliation and Performance Properties of Non-Oxidized Graphene in Water. *Scientific Reports* **2014,** *4*, 3928.

35. Ojha, K.; Saha, S.; Banerjee, S.; Ganguli, A. K., Efficient Electrocatalytic Hydrogen Evolution from MoS_2-Functionalized Mo_2N Nanostructures. *ACS Applied Materials & Interfaces* **2017,** *9* (23), 19455-19461.

36. Xu, L.; Yao, Q.; Deng, J.; Han, Z.; Zhang, Y.; Fu, Y.; Huber, G. W.; Guo, Q., Renewable N-Heterocycles Production by Thermocatalytic Conversion and Ammonization of Biomass over ZSM-5. *ACS Sustainable Chemistry & Engineering* **2015,** *3* (11), 2890-2899.

37. Zheng, Y.; Wang, Z.; Liu, C.; Tao, L.; Huang, Y.; Zheng, Z., Integrated production of aromatic amines, aromatic hydrocarbon and N-heterocyclic bio-char from catalytic pyrolysis of biomass impregnated with ammonia sources over Zn/HZSM-5 catalyst. *Journal of the Energy Institute* **2019**.

38. Li, Y.; Wang, H.; Xie, L.; Liang, Y.; Hong, G.; Dai, H., MoS_2 Nanoparticles Grown on Graphene: An Advanced Catalyst for the Hydrogen Evolution Reaction. *Journal of the American Chemical Society* **2011,** *133* (19), 7296-7299.

39. Firmiano, E. G. S.; Cordeiro, M. A. L.; Rabelo, A. C.; Dalmaschio, C. J.; Pinheiro, A. N.; Pereira, E. C.; Leite, E. R., Graphene oxide as a highly selective substrate to synthesize a layered MoS2 hybrid electrocatalyst. *Chemical Communications* **2012,** *48* (62), 7687-7689.

40. Wu, Z.; Wang, J.; Liu, R.; Xia, K.; Xuan, C.; Guo, J.; Lei, W.; Wang, D., Facile preparation of carbon sphere supported molybdenum compounds (P, C and S) as hydrogen evolution electrocatalysts in acid and alkaline electrolytes. *Nano Energy* **2017,** *32*, 511-519.

Chapter 4

Nano-structured hybrid molybdenum carbides/nitrides generated in-situ for HER applications

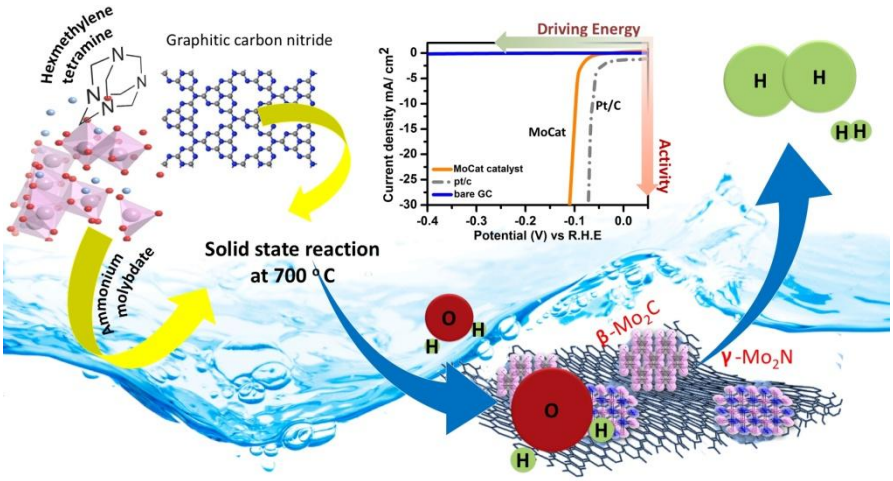

Abstract: *Nanohybrid material containing carbon-supported molybdenum carbide and nitride nanoparticles of size ranging from 8 to 12 nm, exhibits excellent HER catalytic activity. This molybdenum based catalyst (MoCat) is designed as a highly efficient, low-cost (precious-metal free), highly stable electrocatalyst for water electrolysis in acidic medium, synthesized using a simple methodology. These nanoparticles (β-Mo_2C and γ-Mo_2N) were produced in-situ using a metal precursor and C/N source in a controlled solid-state reaction. An overpotential of 96 mV for driving 10 mA/cm^2 of current density was measured for MoCat catalyst, which is very close to commercially available Pt/C catalysts (61mv).*

Brief Outcome: In this chapter, we report an HER catalyst having carbon-supported nanostructured molybdenum nitrides and carbides, showing unprecedented high electrocatalytic activity in acidic conditions. This work has opened up an area of huge potential, highlighting immense possibilities for the improvement of the HER performance in these materials. Several reports were made where Mo_2C or Mo_2N have appeared to be a potential candidate for the HER reaction, however to the best of our knowledge, before this, no one has studied the interface of the Mo_2C and Mo_2N to show the synergistic augmentation of HER activities. Most importantly, the synthesis of the MoCat catalyst is simple and can be scaled up easily for large scale devices with ultra-low-cost fulfilling its pre-requisites for an application. This kind of in-situ synthesis can be extended to other metals such as W, Nb, Ta and Ti to produce efficient electrocatalyst. Numerous possibilities of making composites with promoter elements such as Fe, Co, Ni, and Cu are there to be explored for the enhancement of the catalytic activity.

4.1. Introduction

Hydrogen is an attractive alternative to fossil fuels and can be used as a primary source in a wide range of transportation and power generation applications. Huge global energy demands along with diminishing fossil fuels and climatic change have urged intense interest in developing alternative carbon-free energy technologies.[1-2] An attractive approach to this ultimate goal is to achieve an efficient splitting of water to hydrogen and oxygen using solar energy input since the generation and combustion of hydrogen from water is carbon neutral and the sunlight is a sustainable energy source.[3-4] Water splitting using solar energy is one of the most appealing methods for solar energy conversion and storage. For efficient water splitting, active catalysts for hydrogen evolution reaction (HER) are required. Hydrogen generation has been attempted for decades using precious metals like platinum, palladium and their composites, but their high cost and low abundance are severe hurdles for large scale applications.[5] These constrain lead to the quest and development of low-cost HER catalyst. Substantial exploration has been done in this area to develop catalysts based on transition metal complexes, alloys, and their composites,[6-9] molybdenum sulphides(MoS_2),[10-14] Mo_2C and Mo_2N,[15-21] Metal phosphides[22-25] and others[26-28] for substituting the Pt-group metals. Molybdenum sulfide featuring exceptional electronic and optical properties is found to be an attractive non-metallic HER catalyst, which is potentially useful for acidic HER condition.[24-28] Hinnemann *et al*. reported that the free energy necessary for optimal binding of atomic hydrogen to the catalyst should be close to zero.[29] While composites of nitrogen rich 2-D materials with Mo_2C have also shown remarkable HER catalytic activities.[30-31]

This chapter demonstrates an innovative yet simple *in-situ* synthesis of "carbon-supported nanostructured molybdenum nitrides and carbides" showing unprecedented high electrocatalytic activity in acidic conditions. A synergistic effect in these nanoparticles was observed only when the composite is synthesized *in-situ*. Hence, the main emphasis was given to understand the synergy of these nanostructured materials and to explore the possibilities in terms of HER applications. A detailed theoretical (DFT) calculation shows an appreciable charge transfer at the interface of these nanoparticles. Several reports were made where Mo_2C or Mo_2N have appeared to be a potential candidate for the HER reaction, however, no one has studied the interface of the Mo_2C and Mo_2N to show the synergistic enhancement of HER activities. To the best of our knowledge, an in-depth study to correlate the synergistic effect with the catalytic activity of Mo_2C-Mo_2N interface in these materials has not been reported so far.

4.2. Experimental section

4.2.1. Materials

Chemicals used in the synthesis are ammonium molybdate tetrahydrate ($(NH_4)_6.Mo_7O_{24}.4H_2O$) 99.0%; Hexamethyltetramine ($C_6H_6N_4$) 99%, Nafion® perfluorinated resin solution (5 wt. %); N, N-Dimethylformamide anhydrous (99.8%), Urea (NH_2CONH_2) 99.8%, purchased from Sigma Aldrich chemicals Pvt. Ltd. Other chemicals like Ammonium Hydroxide ($NH_3.H_2O$) 25% were procured from Merck chemicals. The entire chemicals were used as obtained. Deionized water was used in all preparations.

4.2.2. Methodology

4.2.2.1. Synthesis of g-C_3N_4

Graphitic nitride was synthesized from the reported method with a slight change in the temperature.[32] The urea was heated at 400 °C for one hour and further heated at 550 °C for 1.5 h in the inert atmosphere with a ramp rate of 400 °C/h.

4.2.2.2. Synthesis of Mo_2C and Mo_2N.

Carbon supported Mo_2C was synthesized by annealing the mixture of the metal precursor and graphitic carbon nitride in argon purged tubular furnace at 700 ^oC for two hours and similarly carbon-supported Mo_2N was synthesized by annealing at 600 ^oC for 2 h in NH_3 gas flow**.**

4.2.2.3. Synthesis of MoCat Catalyst

The MoCat catalyst was synthesized by temperature-programmed carburization of metal precursor in the presence of graphitic carbon nitride (g-C_3N_4) and hexamethylenetetramine (HMT). The overall synthesis involves two major steps:

First is the preparation of metal precursor and the second step is high-temperature carburization of metal and C/N source. Briefly, for the synthesis of metal precursor, 1.40 g (0.01 mol) of HMT (hexamethyl tetraamine), 1.235 g (0.001 mol) of ammonium molybdate tetrahydrate ($(NH_4)_6Mo_7O_{24}.4H_2O$), 2 ml of ammonium hydroxide (25%) and water (0.5 ml) were mixed to make a slurry which was dried at 80°C for 12 hours to obtain the metal precursor. Graphitic carbon nitride (g-C_3N_4) was synthesized from reported method[32] with little modification. In the second step, the metal precursor and g-C_3N_4 were weighed in the ratio 1: 0.025 (g/g), mixed thoroughly using a mortar pestle and annealed in a quartz tube furnace in NH_3 with a flow of 40

mL/min at a ramp of 400 °C/hr from ambient to 600 °C. NH_3 was switched with Argon gas at 700 °C and purged for 2 hours with a flow of 40 mL/min. The argon gas was kept on purging throughout the reactor until the end of the reaction.

4.2.2.4. Physical Characterization

All the material was characterised by using Bruker Eco D8 advance X Powder X-ray diffractometer between 2θ angle 5º to 80º. The sample was exposed by Cu-Kα radiation with wavelength (λ) 1.54056 Å through Ni filter operated at 40 kV and 25 mA current with an incremental step 0.00190º/step and obtained diffraction pattern was studied for sample analysis. The surface characterizations of all the materials were completed by using Autosorb IQ Quantachrome instrument by conducting nitrogen adsorption-desorption isotherm at 77 K. Initially, the samples were outgassed before measurements at 200 °C for 6 h under vacuum in the degassing port of the adsorption analyzer. The pore analysis and surface area were calculated by Barrett-Joyner-Halenda (BJH) and Brunauer-Emmett-Teller (BET) equations respectively. The surface morphology and composition were examined by JEOL (JSM IT-300) scanning electron microscope equipped with the energy-dispersive X-ray spectroscopy (Bruker). The transmission electron microscopy and STEM images were recorded at an accelerated voltage of 200 kV with JEOL-2100. The copper grids with carbon coating were used as sample holders for TEM analysis. The XANES and EXAFS measurements of the Mo based catalysts along with the Mo standards have been carried out at the Indus-2 Synchrotron Source (2.5 GeV, 100 mA), beamline (BL-9) at RRCAT, Indore, India.

4.2.2.5. Electrochemical measurements

The working electrode was prepared as follows: 4 mg of carbon-supported catalyst was dispersed in 495 µl of dimethylformamide and 5 µl of Nafion using Labsonic LBS2-10 BATH Sonicator for 60 min. 10 µl of dispersed ink was drop cast on the clean and polished glassy carbon electrode. The electrode was dried under vacuum. Catalytic activity was measured using electrochemical workstation CHI660E. Calomel electrode was used as a reference electrode. Platinum wire and glassy carbon electrode were used as counter and working electrode respectively. Polarization curves were collected in an Ar purged 1 M H_2SO_4 solution at a scan rate of 2 mVs^{-1}. The long-term durability tests were performed in an Ar-purged 1 M H_2SO_4 solution by recording the overpotential needed to drive 10 mA cm^{-2} of current density. The overpotential of all catalytic material was quoted w.r.t. R.H.E electrode and further corrected by ohmic drop according to the equation $\eta_{corrected} = \eta - iR_s$ whereas R_s is solution resistance. The EIS

measurements were carried out from 100 000 Hz to 1 Hz at selected values of the overpotential i.e. (η =100, 250 and 400 mV).

4.2.2.6. X-ray Absorption Spectroscopy

Mo based catalysts were characterized using X-ray absorption spectroscopy. The X-ray Absorption Spectroscopy measurements of the Mo based catalysts along with the Mo standards were carried out at the Energy Scanning EXAFS beamline (BL-9) at the INDUS-2 Synchrotron Source (2.5 GeV, 100 mA), Raja Ramanna Centre for Advanced Technology (RRCAT), Indore, India.[33-34] The beamline uses a double crystal monochromator (DCM) which works in the photon energy range of 4-25 KeV with a resolution of 10^4 at 10 KeV. A 1.5 m horizontal pre-mirror with meridional cylindrical curvature is used prior to the DCM for collimation of the beam and higher harmonic rejection. The second crystal of the DCM is a sagittal cylindrical crystal, which is used for horizontal focusing of the beam while another Rh/Pt coated bendable post mirror facing down is used for vertical focusing of the beam at the sample position. EXAFS measurements of these samples have been carried out in transmission mode at the Mo K-edge. For measurements in the transmission mode, the sample is placed between two ionization chamber detectors. The first ionization chamber measures the incident flux (I_o) and the second ionization chamber measures the transmitted intensity (I_t). From these intensities, the absorbance of the sample is found as a function of energy. For measurements in the transmission mode, the sample is placed between two ionization chamber detectors. The first ionization chamber measures the incident flux (I_o) and the second ionization chamber measures the transmitted intensity (I_t) and the absorbance of the sample is obtained as $\mu = \exp - {I_t}/{I_o}$. The EXAFS spectra of the samples at Mo K-edge were recorded in the energy range 19925-20730 eV.

EXAFS: The EXAFS analysis performed and with a relation ($\mu(E)$ versus E) spectra of Mo based catalysts samples along with Mo standards at Mo K-edge is observed. To take care of the oscillations in the absorption spectra, the energy-dependent absorption coefficient $\mu(E)$ has been converted to absorption function $\chi(E)$ defined as follows.[35-36]

$$\chi(E) = (\mu(E) - \mu_\circ(E))/\Delta\mu_\circ(E_\circ) \qquad (4.1)$$

Where $E_\circ$ is the absorption edge energy, $\mu_\circ(E_\circ)$ is the bare atom background and $\Delta\mu_\circ(E_\circ)$ is the step in the $\mu(E)$ value at the absorption edge. After converting the energy scale to the photoelectron wave number scale (k) as defined by,

$$k = \sqrt{2m(E - E_\circ)/h^2} \qquad (4.2)$$

the energy-dependent absorption coefficient $\chi(E)$ has been converted to the wavenumber dependent absorption coefficient $\chi(E)$, where m is the electron mass. Finally, $\chi(k)$is weighted by k to amplify the oscillations at high k and the $\chi(k)k$ functions are Fourier transformed in R space to generate the $\chi(R)$versus R (or FT-EXAFS) spectra in terms of the real distances from the centre of the absorbing atom. It should be mentioned here that a set of EXAFS data analysis program available within the IFEFFIT software package has been used for reduction and fitting of the experimental EXAFS data[37]. This includes data reduction and Fourier transform to derive the $\chi(R)$ versus R spectra from the absorption spectra (using ATHENA software), generation of the theoretical EXAFS spectra starting from an assumed crystallographic structure and finally fitting of the experimental data with the theoretical spectra using the FEFF 6.0 code(using ARTEMIS software). The bond distances (R), co-ordination numbers (including scattering amplitudes) (CN) and disorder (Debye-Waller) factors (σ^2), which give the mean-square fluctuations in the distances, have been used as fitting parameters. The goodness of the fit in the above process is generally expressed by the R_{factor} which is defined as:

$$R_{factor} = \sum \frac{[\mathrm{Im}(\chi_{dat}(r_i) - \chi_{th}(r_i)]^2 + [\mathrm{Re}(\chi_{dat}(r_i) - \chi_{th}(r_i)]^2}{[\mathrm{Im}(\chi_{dat}(r_i)]^2 + [\mathrm{Re}(\chi_{dat}(r_i)]^2} \qquad (4.3)$$

where, χ_{dat} and χ_{th} refer to the experimental and theoretical values $\chi(r)$ respectively and Im and Re refer to the imaginary and real parts of the respective quantities. A Fourier transformed EXAFS (FT-EXAFS) $'\chi(R)$' versus 'R' spectra of all the Mo based catalyst samples at the Mo K-edge along with the best fit theoretical spectra is obtained. The data have been fitted in the k range of 3-10 $Å^{-1}$ and up to 3.6 Å in 'R' space.

4.2.2.7. Computational details

All the calculation has been performed using density functional theory within the frame of Vienna ab-initio simulation package (VASP).[35-38] All the energies have been calculated self-consistently with generalized gradient approximation (GGA) using Perdew-Burke-Ernzerhof exchange-correlation functional.[39-40] The electron-ion interaction is described by projector-augmented plane wave (PAW).[41-42] Convergence threshold for energy and force are set at 10^{-4} eV and 0.03 eV/Å.

4.3. Results and discussion

The MoCat catalyst was synthesized by temperature-programmed carburization of metal precursor in presence of graphitic carbon nitride (g-C_3N_4) and hexamethylenetetramine (HMT). The overall synthesis is a two steps synthesis in which the first step involves the synthesis of metal precursor involving hexamethylenetetramine with ammonium molybdate. The second step is the high-temperature calcination of the obtained metal precursor with g-C_3N_4. The complete description of the synthesis has been given in the experimental section. A certain variation in the reaction condition was done to obtain pure β-Mo_2C or γ-Mo_2N phases (as described in the experimental part). The electrocatalytic HER performance of the MoCat catalyst was evaluated in a conventional three-electrode system. For comparison, the catalytic activity of commercial Pt/C (20 wt%) of Pt on carbon black from Sigma Aldrich), β-Mo_2C, γ-Mo_2N and MoCat-m, a physical mixture of Mo_2C (47%) & Mo_2N (53%), were studied. All the experiments were conducted in Ar purged 1M H_2SO_4 further corrected for iR correction and the potentials were quoted w.r.t to R.H.E. It is evident from the polarization curves that MoCat catalyst shows a much better catalytic activity over the other molybdenum catalysts with onset potential of 44 mV, which is very close to the commercially available Pt/C catalyst (having onset potential close to zero). The Pt/C catalyst exhibited high HER catalytic activity with a low overpotential, η_{10} (defined as the potential at 10 mA/cm^2 of cathodic current density) of 61 mV. From 1 Sun of AM 1.5 illumination, the solar photon produces a charge-carrier flux of 10–20 mA/cm^2 to a planar electrode surface. Hence, we have chosen 10 mA/cm^2 as the reference current density for measuring the overpotential.[43] The overpotential η_{10} for MoCat catalyst was found to be 96 mV whereas β-Mo_2C, γ- Mo_2N shows a higher value of 240 mV and 350 mV respectively as shown in figure 4.1a and 4.1b respectively. Furthermore, a comparison of the MoCat-m catalyst (which is merely a physical mixture of 47% of β-Mo_2C and 53% γ-Mo_2N, independently synthesized pure phased nanoparticles) with respect to MoCat, shows relatively poor catalytic activity (η_{10} = 310 mV) shown in figure 4.2a.

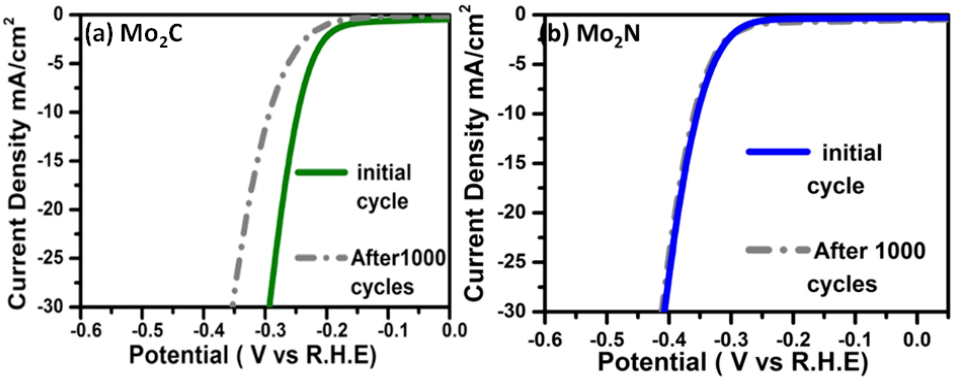

Figure 4.1. *Polarization Curve of (a) Mo_2C (b) Mo_2N before and after 1000 cycle recorded in 1 M H_2SO_4 at a scan rate of 7 mV/sec.*

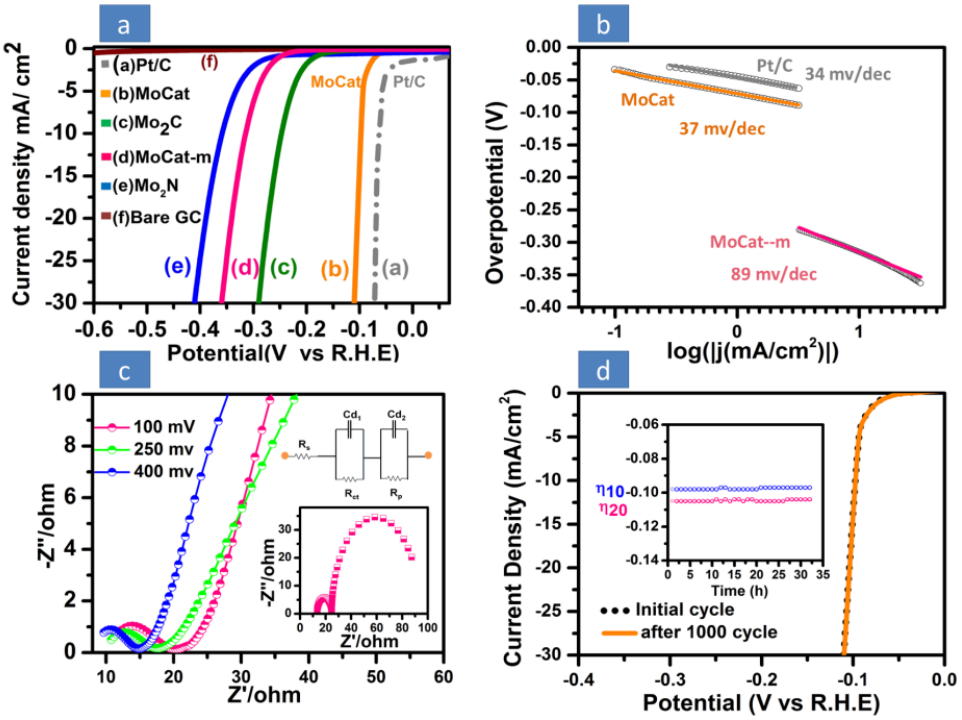

Figure 4.2. *(a) Polarization curves of MoCat and a comparison with other catalysts in 1 M H_2SO_4 at a scan rate of 2 mV/sec (b) Tafel plots of commercially available Pt/C and MoCat catalyst. (c) Nyquist plots of the MoCat catalyst recorded at selected over-potentials in an Ar purged 1 M H_2SO_4 solution (c) Nyquist plot at 0.1 V fitted using RC circuit shown in inset (d) stability curve of MoCat catalyst (inset: stability plot at two different current densities with respect to time.)*

The linear portion of the Tafel plots of MoCat catalyst shows a much smaller slope when fitted to Tafel equation ($\eta = b\ log\ j + a$, where j is the current density and b is the Tafel slope, figure 4.2b), indicating a fast electron transfer through the electrode interface. For the HER in acidic media, three possible reaction steps have been suggested.[44]
First step: Volmer reaction (Primary discharge step):

$$H_3O^+ + e^- \rightarrow H_{ads} + H_2O \qquad b = 2.3RT/\alpha F \approx 120mV/dec \qquad (4.4)$$

where R is the ideal gas constant, T is the absolute temperature, $a \approx 0.5$ is the symmetry coefficient, and F is the Faraday constant. This step is followed by either Heyrovsky reaction (an electrochemical desorption step),

$$H_{ads} + H_3O^+ + e^- \rightarrow H_2 + H_2O \qquad b = 2.3RT/(1+\alpha F) \approx 40mV \qquad (4.5)$$

Or Tafel reaction (a recombination step),

$$H_{ads} + H_{ads} \rightarrow H_2 \qquad b = 2.3RT/2F \approx 30mV \qquad (4.6)$$

The Tafel slope is a characteristic property of the catalyst that is determined by the rate-determining step of the HER. The determination of the Tafel slope is extremely important for the interpretation of the elementary steps involved. A very high H_{ads} coverage ($\theta_H \approx 1$), on a Pt surface, is known to proceed through the mechanism followed by equations 4.4 and 4.6 i.e., Volmer-Tafel steps, and the recombination step is the rate-determining step at low overpotentials, as evident from the Tafel slope of 30 mV/dec. For MoCat, the observed Tafel slope of ~37 mV/decade, suggesting that electrochemical desorption is the rate-limiting step and thus that the Volmer Heyrovsky HER mechanism (equations 4.4 and 4.5) is operative in the HER. For a further understanding of the catalytic behaviour, electron impedance spectroscopy (EIS) was carried out at different applied potentials. The Nyquist plots of EIS responses at different overpotentials are shown in figure 4.2c. The inset represents the simulated version of a plot measured at 100 mV and their equivalent circuit used for fitting. The semicircle at low-frequency region typically indicates the charge transfer resistance which is around 12 ohms for MoCat catalyst indicating the occurrence of faster electrode kinetics. However, MoCat-m manifests a very high impedance of around 200 ohms as shown in figure 4.3a and 4.3b.

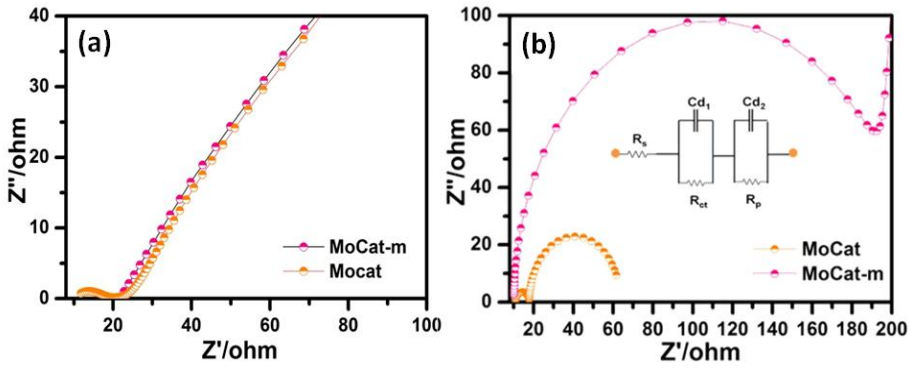

Figure 4.3. *(a) Nyquist plot of MoCat and MoCat-m (b) Nyquist plot of MoCat and MoCat-m at 100 mV fitted using RC circuit shown in the inset.*

To ensure the long-term durability of the catalyst, polarization curves were recorded at a scan rate of 7 mV s^{-1} for 1000 cycles as shown in figure 4.2d. As evident from the above stability plot, no significant difference was observed in the polarization curves, before and after 1000 cycles, which ensures high stability of the catalyst. A plot of overpotential vs time is shown at η_{10} and η_{20} respectively further supporting the above stability measurements (inset Figure 4.2d). The structure and composition of the MoCat catalyst were studied using powder X-ray diffraction (PXRD), XANES, EXAFS, FESEM, TEM, EDAX, and HRTEM. Primarily, PXRD analysis showed the presence of both β-Mo_2C and γ-Mo_2N phases in the catalyst. Rietveld refinement further confirmed the ratio of β-Mo_2C/γ-Mo_2N phases to be 47:53 (Figure 4.4a and 4.4b). Mo K-edge XANES spectra of Mo_2C, Mo_2N, Mo-foil, ammonium molybdate and MoCat respectively (Figure 4.4c), reveals that MoCat catalyst has a similar oxidation state as that of Mo-Foil and the spectrum holds a similar position with respect to Mo_2C and Mo_2N. Owing to the higher oxidation state of molybdenum in ammonium molybdate shows a right shift of the spectrum (see the solid grey line). The first major peak in the radial distribution function (Figure 4.4d) of the EXAFS spectrum of γ-Mo_2N, corresponds to the nearest nitrogen shell, while the second and third peaks correspond to Mo and N atoms respectively from the central Mo atom.

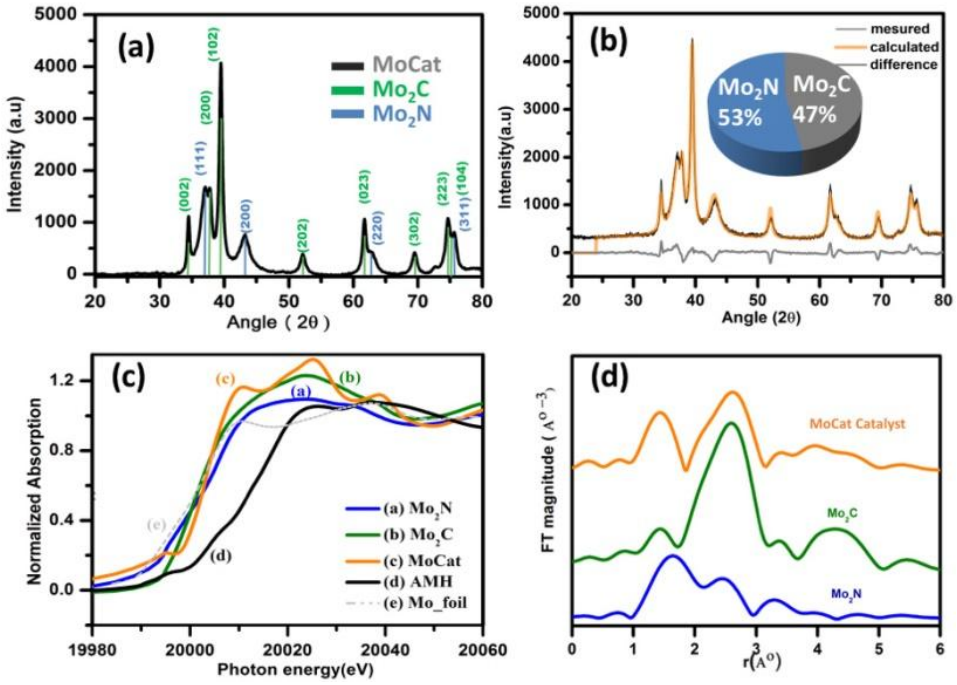

Figure 4.4. *(a) PXRD spectra of MoCat catalyst (b) Rietveld refinement analysis showing the percentage of composition of MoCat catalyst (c) Normalized experimental XANES spectra of Mo foil, Ammonium molybdate (AMH), Mo_2C, Mo_2N and MoCat catalyst measured at Mo K-edge (d) EXAFS spectra of Mo_2C, Mo_2N and MoCat catalyst.*

Table 4.1. *EXAFS fitted as calculated parameters for Mo_2C, Mo_2N and MoCat catalyst.*

(Mo_2N structure)		Mo_2N
Mo-N	CN(6)	4.72±0.96
	R	2.08±0.02
	σ^2	0.016±0.002
Mo-Mo	CN(12)	10.82±2.04
	R	2.86±0.02
	σ^2	0.018±0.001
Mo-N	CN(8)	8.96±1.36
	R	3.62±0.02
	σ^2	0.002±0.001
R_{factor}		0.004

		Mo_2C	MoCat
Mo-C	CN(6)	5.53±1.26	5.53±1.26
	R	2.14±0.04	2.17±0.02
	σ^2	0.024±0.009	0.014±0.003
Mo-Mo	CN(12)	11.46±1.68	10.8±2.28
	R	2.93±0.01	2.94±0.01
	σ^2	0.011±0.001	0.014±0.001
		0.001	0.005

The theoretical FT-EXAFS spectra have been generated assuming the model γ-Mo_2N namely the first nitrogen shell (Mo-N1) with coordination number (CN) of 6, second Mo shell (Mo-Mo) having CN of 12 and third nitrogen shell (Mo-N) with CN of 8. In β-Mo_2C, the first peak corresponds to the nearest carbon (Mo-C) shell with the CN of 6 and the second major peak corresponds to (Mo-Mo) shell with the CN of 12. The best fit results of the radial distribution of MoCat catalysts (Figure 4.4d) further confirms the composition obtained from Rietveld refinement. The fitted parameters and as obtained values for coordination numbers, R and σ mentioned in table 4.1. Transmission electron microscopy (TEM) and Scanning electron microscopy (SEM) are also in-line with the previous observations. FESEM image (Figure 4.5a) exposes the porous morphology of the catalyst.

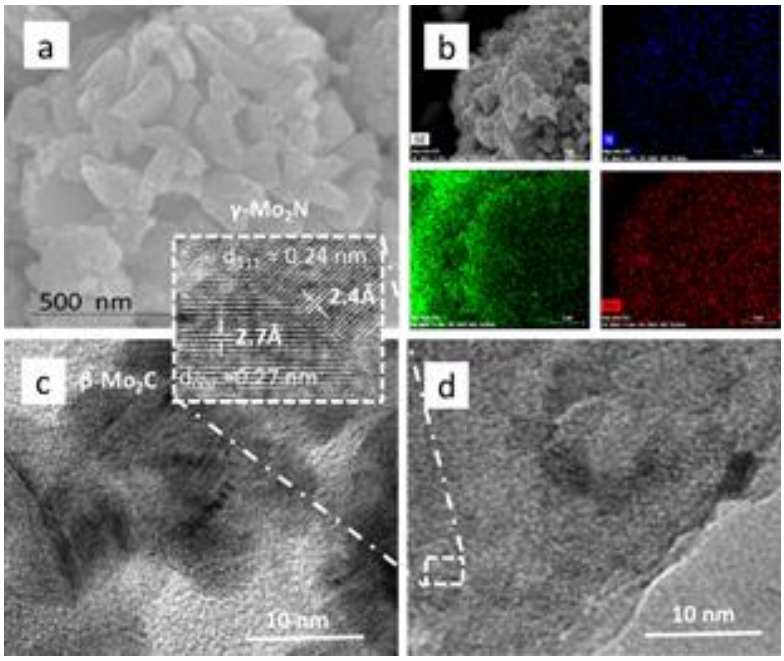

Figure 4.5. *(a) FESEM micrograph of the MoCat -catalyst. (b) FESEM images at low resolution and the corresponding elemental mapping (C) HRTEM showing the lattice fringes (d) HRTEM showing the formation of several interfaces of both having γ-Mo_2N and β-Mo_2C nanocrystals(See the zoomed-in section).*

Elemental mapping of MoCat (Figure 4.5b) revealed that the Mo, N, and C atoms were homogeneously distributed over the entire material, suggesting that the Mo_2C/Mo_2N nanocrystals were uniformly distributed within the carbon matrices. TEM images showing a uniform formation of Mo_2C/Mo_2N nano-crystallites of sizes ranging from 8 to

12 nm. The high-resolution TEM micrograph shows the cubic structure of the γ-Mo_2N nanoparticles with a 2.4 Å spacing of lattice fringes of the (111) planes and 2.7 Å, corresponding to the crystal (002) planes of the orthorhombic β-Mo_2C (Figure 4.5c). A solid solution in nano-dimensions with interfaces was observed (See the zoomed version of Figure 4.5d) in all micrograph. The porous morphology of the catalyst as observed in the FESEM analysis was further confirmed by BET surface area analysis, which gives a surface area of 254 m^2/g (Figure 4.6).

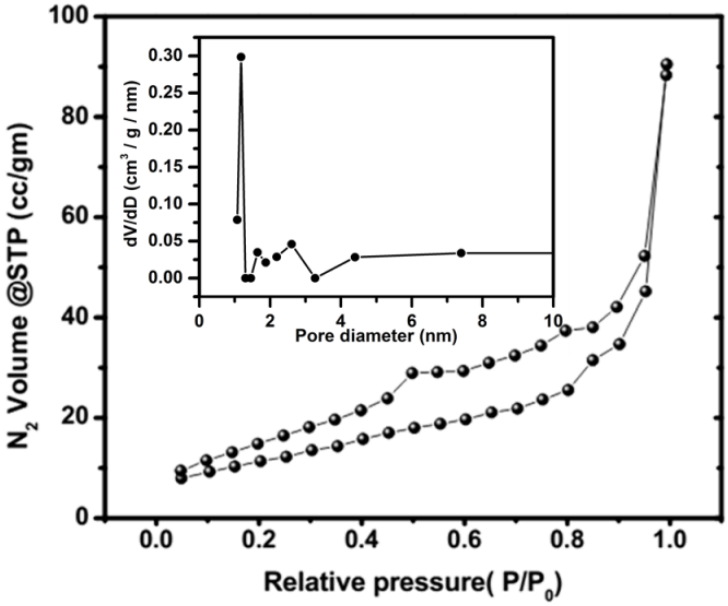

Figure 4.6. *BET isotherm of MoCat catalyst with BJH pore size distribution shown in the inset*

The HRTEM observation reveals the creation of interfaces between the nanoparticles in different crystallites. This inspired us to do a theoretical investigation to understand the origin of enhanced HER activity with respect to individual Mo_2C, Mo_2N, and MoCat-m. Theoretical calculations show that the Mo_2C acts as an electron donor for the adjacent C atoms in the carbon layers, whereas the Mo_2N functions as an electron acceptor; this synergy between Mo_2C and Mo_2N dopants is found to yield unprecedented, highly active catalytic sites on the carbon layers that are more active than those in Mo_2C or Mo_2N. The DFT study of β-Mo_2C, γ-Mo_2N, and Mo_2C-Mo_2N were performed by utilizing VASP code within DFT formalism. The generalized gradient approximation (GGA) in the Perdew−Burke−Ernzerh (PBE) format is used in all calculations.[35-37] Relativistic effects were included in the pseudopotential of Molybdenum. The structural relaxations were examined until the Hellmann−Feynman force on each atom is less than 0.01 eV/Å, and

the energy convergence criterion was set to 10^{-5} eV. A supercell of 3×3 and the 3×3×1 k sampling in Brillouin zone was employed in all calculations. Here it is observed that there is a significant charge transfer at the interface of these nanoparticles. It can be perceived from the charge density plots (Figure 4.7). Appreciable charge transfers at the interface between Mo_2C and Mo_2N further facilitate the binding and removal of hydrogen on and from the surface. Bader charge analysis has also been computed to verify the actual transfer of charge at the interface.

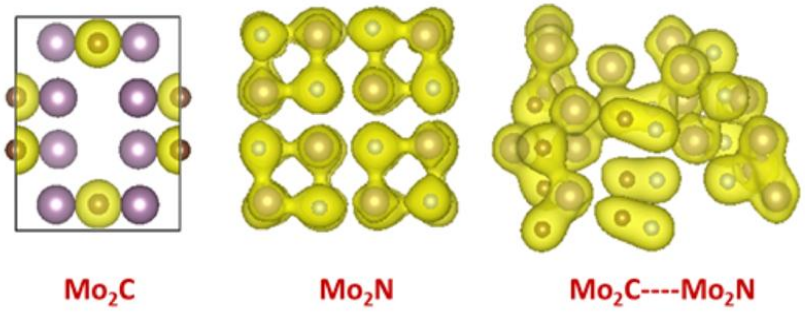

Figure 4.7. *Charge density plots Mo_2C, Mo_2N and Mo_2C-Mo_2N nano-particles*

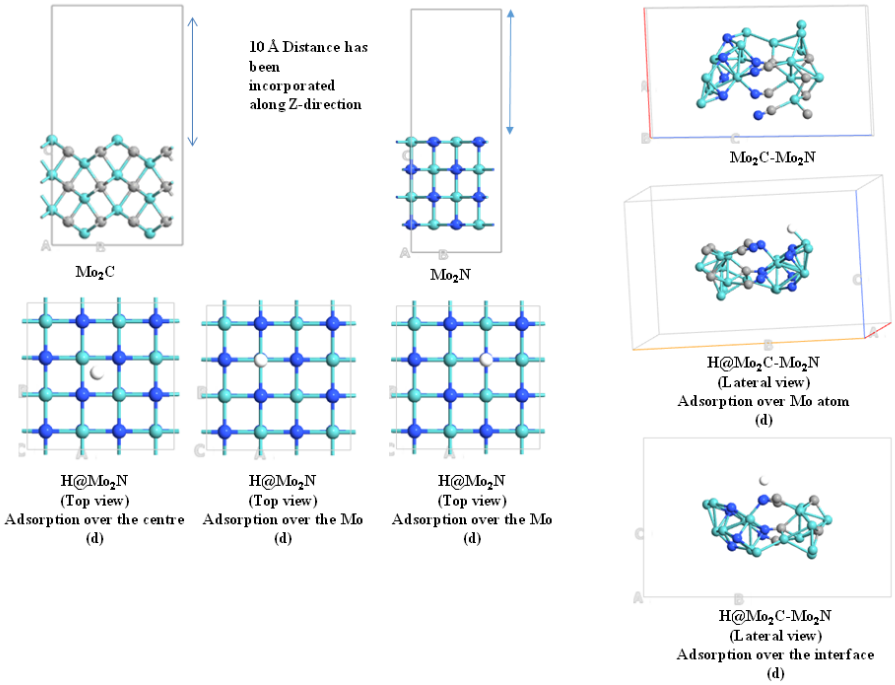

Figure 4.8. *Initial geometries of pristine and adsorbed system of Mo_2C, Mo_2N and Mo_2C-Mo_2N*

For the comparative, we have constructed the theoretical model of slabs of Mo_2C, Mo_2N, and interface of Mo_2C-Mo_2N, H@Mo_2C, H@Mo_2N and H@Mo_2C-Mo_2N. Particularly we have considered 001 facets with Mo-terminated surface as an active surface of β-phase of Mo_2C and γ-phase of Mo_2N. Nanoparticles of Mo_2C and Mo_2N are constructed by modelling the slab with six layers of Mo-C and four layers of Mo-N. All the geometries are relaxed using selective dynamics implemented within VASP by keeping the first three layers translate and rest layers fix. Different adsorption sites have been considered for the H atoms over Mo_2C, Mo_2N and Mo_2C-Mo_2N (Figure 4.8). In the case of Mo_2C, hydrogen is adsorbed over the centre. In Mo_2N, H is adsorbed over the centre, over the Mo atom and the N atom. In case of interface Mo_2C and Mo_2N, two adsorption sites have been considered: one is over the Mo side and another is over the N-atom near the interface. Initial geometries of Mo_2C, Mo_2N and Mo_2C-Mo_2N are depicted in figure 4.8. and relaxed geometry is depicted in figure 4.9.

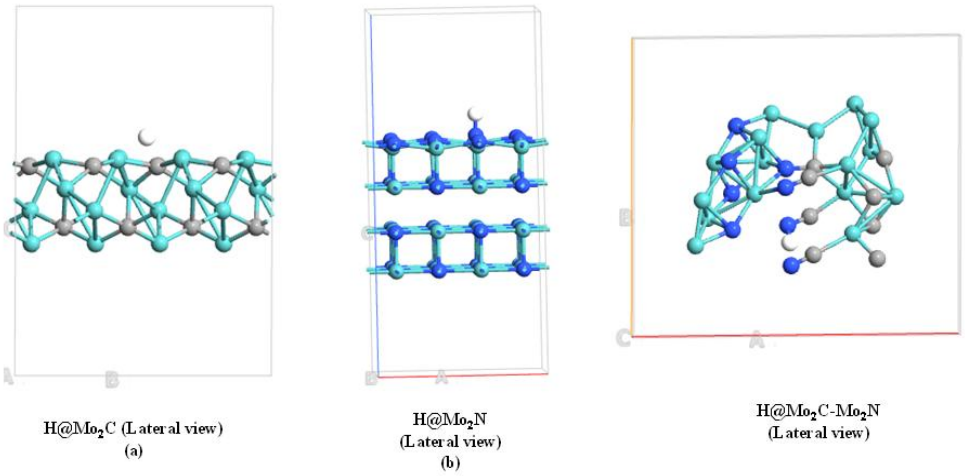

Figure 4.9. *Relaxed geometries of pristine and hydrogen adsorbed over the nanoparticles Mo_2C, Mo_2N, and Mo_2C-Mo_2N*

To understand electrocatalytic properties of MoCat, we have used DFT calculations, where the thermochemistry of hydrogen evolution reaction (HER) can be explained.[29] Gibbs free energy is an important parameter used to assess the catalytic activity of material for hydrogen evolution. In a different perspective, recollecting the mechanism, HER can also be represented as $H^+ + e^- + * \rightarrow H^*$, showing the bonding of H^+ to the catalyst surface, where "*" represents the suitable binding sites on the catalytic surfaces followed by reduction; Desorption of H_2 molecule from the surface through one of these

processes: $2H^* \rightarrow H_2 + 2^*$ or $H^+ + e^- \rightarrow H_2 + *$. Particularly, DFT calculations of thermochemistry are independent of the precise mechanism of the 2nd step. However, it is a necessary, (but not sufficient) condition for a material to be an ideal catalyst is that the free energy of adsorbed hydrogen should be close to that of the reactant or product (i.e., $\Delta G_H \approx 0$). Our calculations of Gibbs free energy (ΔG_H) for all the relevant catalysts (namely β-Mo_2C, γ-Mo_2N, and MoCat (β-Mo_2C/γ–Mo_2N)) are described in figure 4.10. MoCat is found to be very close to Pt/C (commercially available) catalyst in the calculated free-energy diagram of HER at equilibrium potential. Apparently, a positive value of ΔG_H of the catalyst may be confusing to the readers. However, the most intriguing part here is that a slight positive ΔG_H value optimizes the catalytic activity by percolating the effect towards high negative values of β-Mo_2C and γ-Mo_2N nanoparticles through carbon layers present in MoCat.

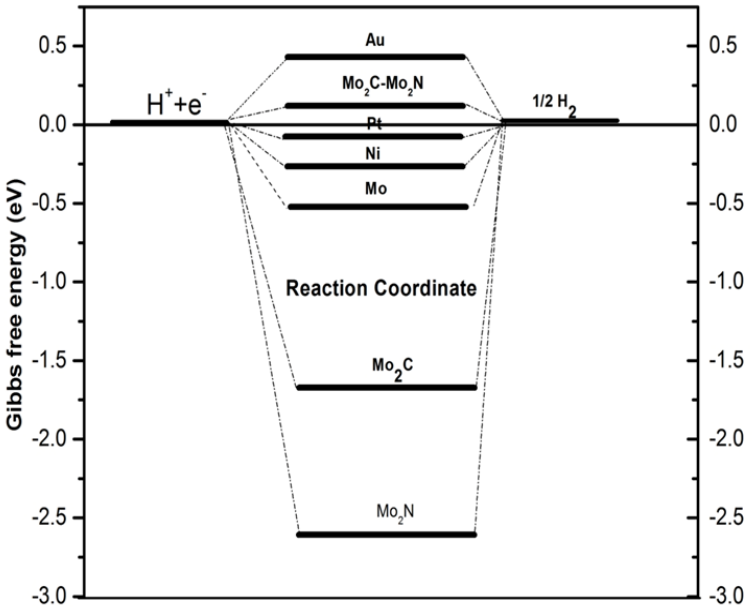

Figure 4.10. *The calculated free-energy diagram of HER at equilibrium potential for three possible structures, namely Mo_2C, Mo_2N and MoCat (Mo_2C-Mo_2N) catalyst.*

Further, the adsorption energy of the hydrogen on different slabs has been calculated as follow

$$\Delta E_H = E(system + H) - E(system) - E(H) \qquad (4.7)$$

Where E(system+H) is the total energy of the system with H atom adsorbed on the surface, E(system) is the total energy of system and E (H) is the total energy of H atom. The calculated adsorption and Gibbs free energy of the system have been given in table 4.2.

Table 4.2. *Adsorption energy and Gibbs free for all the systems*

System	*Adsorption energy (E_d) (in eV)*	*Gibbs free energy (ΔG_H) (in eV)*
H@Mo_2C	*-1.89*	*-1.65*
H@Mo_2N	*-2.84*	*-2.60*
H@Mo_2C-Mo_2N	*-0.23*	*0.12*

The corresponding lattice parameters are as calculated in table 4.3.

Table 4.3. *The lattice parameters (Å) of the supercells for all the systems*

Table	*a*	*b*	*c*
Mo_2C	*9.472*	*12.116*	*20*
Mo_2N	*6.642*	*6.642*	*20*
Mo_2C-Mo_2N	*9.044*	*15.400*	*17.77*
H@Mo_2C	*9.681*	*11.671*	*16.571*
H@Mo_2N	*8.366*	*8.399*	*19.106*
H@Mo_2C-Mo_2N	*15.743*	*19.915*	*12.634*

4.4. Conclusion

This chapter provides evidence for the existence of a synergistic effect existing between molybdenum carbide and molybdenum nitride nanoparticles yielding excellent HER activity if synthesized *in-situ* in a controlled solid-state reaction. Thorough characterization and measurements of the MoCat catalyst revealed that it contains 53% of γ-Mo_2N and 47% of β-Mo_2C. In a remarkable observation, it was noted that MoCat-m (Catalyst made from mixing individually synthesized γ-Mo_2N and β-Mo_2C, pure phase nanoparticles in same or similar composition) fails to attain such high catalytic activity.

It shows that the composition works only when the catalyst is synthesized *in-situ*. Theoretical studies are also *in-alignment* with the experimental findings, where an appreciable charge-transfer at the interface of these nanoparticles was revealed from the charge density plots. Such charge-transfer at the interface between Mo_2C and Mo_2N further facilitate the hydrogen evolution reaction. This is also supported by the free energy calculation which is very close to commercially available Pt/C catalyst. Most importantly, the synthesis of the MoCat catalyst is simple and can be scaled up easily for large scale devices with ultra-low-cost fulfilling its pre-requisites for an application. These findings would open up a huge area of research in the relevant areas as this kind of *in-situ* synthesis can be extended to other metals such as W, Nb, Ta and Ti to produce efficient electrocatalyst. Numerous possibilities of making composites with promoter elements such as Fe, Co, Ni, and Cu are also there to be explored for the enhancement of the catalytic activity.

Note:

- The permission has been granted by the author and corresponding author of the published paper prior to adopting in the present thesis. The associated relevant publication is:

Rajinder Kumar‡, Ritu Rai‡, Seema Gautam, Abir De Sarkar, Nidhi Tiwari, Shambhu Nath Jha, Dibyendu Bhattacharyya, Ashok K. Ganguli and Vivek Bagchi "Nano-structured hybrid molybdenum carbides/nitrides generated *in situ* for HER applications" ***Journal of Material Chemistry A***, 2017,**5**, 7764-7768 ***(*** ‡***Equal Contribution***)

References

1. Team, H., Hydrogen Production Road Map: Technology Pathways to the Future. *FreedomCAR & Fuel partnership* **2009**, 1-76.

2. Turner, J. A., Sustainable hydrogen production. *Science* **2004,** *305* (5686), 972-974.

3. Stamenkovic, V. R.; Mun, B. S.; Arenz, M.; Mayrhofer, K. J.; Lucas, C. A.; Wang, G.; Ross, P. N.; Markovic, N. M., Trends in electrocatalysis on extended and nanoscale Pt-bimetallic alloy surfaces. *Nature materials* **2007,** *6* (3), 241-247.

4. Wang, J.; Cui, W.; Liu, Q.; Xing, Z.; Asiri, A. M.; Sun, X., Recent progress in cobalt-based heterogeneous catalysts for electrochemical water splitting. *Advanced materials* **2016,** *28* (2), 215-230.

5. Esposito, D. V.; Hunt, S. T.; Kimmel, Y. C.; Chen, J. G., A new class of electrocatalysts for hydrogen production from water electrolysis: metal monolayers supported on low-cost transition metal carbides. *Journal of the American Chemical Society* **2012,** *134* (6), 3025-3033.

6. Vineesh, T. V.; Mubarak, S.; Hahm, M. G.; Prabu, V.; Alwarappan, S.; Narayanan, T. N., Controllably Alloyed, Low Density, Free-standing Ni-Co and Ni-Graphene Sponges for Electrocatalytic Water Splitting. *Sci Rep* **2016,** *6*, 31202.

7. Ma, Y.; Dai, X.; Liu, M.; Yong, J.; Qiao, H.; Jin, A.; Li, Z.; Huang, X.; Wang, H.; Zhang, X., Strongly Coupled FeNi Alloys/$NiFe_2O_4$@Carbonitride Layers-Assembled Microboxes for Enhanced Oxygen Evolution Reaction. *ACS applied materials & interfaces* **2016,** *8* (50), 34396-34404.

8. Bates, M. K.; Jia, Q.; Ramaswamy, N.; Allen, R. J.; Mukerjee, S., Composite Ni/NiO-Cr_2O_3 Catalyst for Alkaline Hydrogen Evolution Reaction. *The journal of physical chemistry. C, Nanomaterials and interfaces* **2015,** *119* (10), 5467-5477.

9. Miseki, Y.; Kudo, A., Water splitting over new niobate photocatalysts with tungsten-bronze-type structure and effect of transition metal-doping. *ChemSusChem* **2011,** *4* (2), 245-51.

10. Gao, M. R.; Liang, J. X.; Zheng, Y. R.; Xu, Y. F.; Jiang, J.; Gao, Q.; Li, J.; Yu, S. H., An efficient molybdenum disulfide/cobalt diselenide hybrid catalyst for electrochemical hydrogen generation. *Nature communications* **2015,** *6*, 5982.

11. Jaramillo, T. F.; Jorgensen, K. P.; Bonde, J.; Nielsen, J. H.; Horch, S.; Chorkendorff, I., Identification of active edge sites for electrochemical H_2 evolution from MoS_2 nanocatalysts. *Science* **2007,** *317* (5834), 100-2.

12. Merki, D.; Hu, X., Recent developments of molybdenum and tungsten sulfides as hydrogen evolution catalysts. *Energy & Environmental Science* **2011,** *4* (10), 3878-3888.

13. Seger, B.; Laursen, A. B.; Vesborg, P. C. K.; Pedersen, T.; Hansen, O.; Dahl, S.; Chorkendorff, I., Hydrogen Production Using a Molybdenum Sulfide Catalyst on a Titanium-Protected n plus p-Silicon Photocathode. *Angew Chem Int Edit* **2012,** *51* (36), 9128-9131.

14. Benck, J. D.; Chen, Z.; Kuritzky, L. Y.; Forman, A. J.; Jaramillo, T. F., Amorphous Molybdenum Sulfide Catalysts for Electrochemical Hydrogen Production: Insights into the Origin of their Catalytic Activity. *Acs Catal* **2012,** *2* (9), 1916-1923.

15. Wu, H. B.; Xia, B. Y.; Yu, L.; Yu, X.-Y.; Lou, X. W. D., Porous molybdenum carbide nano-octahedrons synthesized via confined carburization in metal-organic frameworks for efficient hydrogen production. *Nature communications* **2015,** *6*.

16. Ma, F. X.; Wu, H. B.; Xia, B. Y.; Xu, C. Y.; Lou, X. W., Hierarchical beta-Mo_2C Nanotubes Organized by Ultrathin Nanosheets as a Highly Efficient Electrocatalyst for Hydrogen Production. *Angew Chem Int Edit* **2015,** *54* (51), 15395-15399.

17. Liao, L.; Wang, S.; Xiao, J.; Bian, X.; Zhang, Y.; Scanlon, M. D.; Hu, X.; Tang, Y.; Liu, B.; Girault, H. H., A nanoporous molybdenum carbide nanowire as an electrocatalyst for hydrogen evolution reaction. *Energy & Environmental Science* **2014,** *7* (1), 387-392.

18. Youn, D. H.; Han, S.; Kim, J. Y.; Kim, J. Y.; Park, H.; Choi, S. H.; Lee, J. S., Highly Active and Stable Hydrogen Evolution Electrocatalysts Based on Molybdenum Compounds on Carbon Nanotube-Graphene Hybrid Support. *ACS nano* **2014,** *8* (5), 5164-5173.

19. Ma, L.; Ting, L. R. L.; Molinari, V.; Giordano, C.; Yeo, B. S., Efficient hydrogen evolution reaction catalyzed by molybdenum carbide and molybdenum nitride nanocatalysts synthesized via the urea glass route. *J Mater Chem A* **2015,** *3* (16), 8361-8368.

20. Chen, W. F.; Wang, C. H.; Sasaki, K.; Marinkovic, N.; Xu, W.; Muckerman, J. T.; Zhu, Y.; Adzic, R. R., Highly active and durable nanostructured molybdenum carbide electrocatalysts for hydrogen production. *Energy & Environmental Science* **2013,** *6* (3), 943-951.

21. Zhao, Y.; Kamiya, K.; Hashimoto, K.; Nakanishi, S., In Situ CO_2-Emission Assisted Synthesis of Molybdenum Carbonitride Nanomaterial as Hydrogen Evolution Electrocatalyst. *Journal of the American Chemical Society* **2015,** *137* (1), 110-113.

22. Yan, H. J.; Tian, C. G.; Wang, L.; Wu, A. P.; Meng, M. C.; Zhao, L.; Fu, H. G., Phosphorus-Modified Tungsten Nitride/Reduced Graphene Oxide as a High-Performance, Non-Noble-Metal Electrocatalyst for the Hydrogen Evolution Reaction. *Angew Chem Int Edit* **2015,** *54* (21), 6325-6329.

23. Popczun, E. J.; McKone, J. R.; Read, C. G.; Biacchi, A. J.; Wiltrout, A. M.; Lewis, N. S.; Schaak, R. E., Nanostructured Nickel Phosphide as an Electrocatalyst for the Hydrogen Evolution Reaction. *Journal of the American Chemical Society* **2013,** *135* (25), 9267-9270.

24. Xiao, P.; Sk, M. A.; Thia, L.; Ge, X. M.; Lim, R. J.; Wang, J. Y.; Lim, K. H.; Wang, X., Molybdenum phosphide as an efficient electrocatalyst for the hydrogen evolution reaction. *Energy & Environmental Science* **2014,** *7* (8), 2624-2629.

25. Jiang, N.; You, B.; Sheng, M. L.; Sun, Y. J., Electrodeposited Cobalt-Phosphorous-Derived Films as Competent Bifunctional Catalysts for Overall Water Splitting. *Angew Chem Int Edit* **2015,** *54* (21), 6251-6254.

26. Faber, M. S.; Jin, S., Earth-abundant inorganic electrocatalysts and their nanostructures for energy conversion applications. *Energy & Environmental Science* **2014,** *7* (11), 3519-3542.

27. Vrubel, H.; Hu, X. L., Molybdenum Boride and Carbide Catalyze Hydrogen Evolution in both Acidic and Basic Solutions. *Angew Chem Int Edit* **2012,** *51* (51), 12703-12706.

28. Morales-Guio, C. G.; Stern, L. A.; Hu, X., Nanostructured hydrotreating catalysts for electrochemical hydrogen evolution. *Chem Soc Rev* **2014,** *43* (18), 6555-69.

29. Hinnemann, B.; Moses, P. G.; Bonde, J.; Jørgensen, K. P.; Nielsen, J. H.; Horch, S.; Chorkendorff, I.; Nørskov, J. K., Biomimetic Hydrogen Evolution: MoS_2 Nanoparticles as Catalyst for Hydrogen Evolution. *Journal of the American Chemical Society* **2005,** *127* (15), 5308-5309.

30. Liu, Y.; Yu, G.; Li, G. D.; Sun, Y.; Asefa, T.; Chen, W.; Zou, X., Coupling Mo_2C with Nitrogen-Rich Nanocarbon Leads to Efficient Hydrogen-Evolution Electrocatalytic Sites. *Angewandte Chemie* **2015,** *54* (37), 10752-7.

31. Li, J. S.; Wang, Y.; Liu, C. H.; Li, S. L.; Wang, Y. G.; Dong, L. Z.; Dai, Z. H.; Li, Y. F.; Lan, Y. Q., Coupled molybdenum carbide and reduced graphene oxide electrocatalysts for efficient hydrogen evolution. *Nature communications* **2016,** *7*, 11204.

32. Liu, J.; Zhang, T.; Wang, Z.; Dawson, G.; Chen, W., Simple pyrolysis of urea into graphitic carbon nitride with recyclable adsorption and photocatalytic activity. *Journal of Materials Chemistry* **2011,** *21* (38), 14398-14401.

33. Basu, S.; Nayak, C.; Yadav, A.; Agrawal, A.; Poswal, A.; Bhattacharyya, D.; Jha, S.; Sahoo, N. In *A comprehensive facility for EXAFS measurements at the INDUS-2 synchrotron source at RRCAT, Indore, India*, Journal of Physics: Conference Series, IOP Publishing: 2014; p 012032.

34. Poswal, A.; Agrawal, A.; Yadav, A.; Nayak, C.; Basu, S.; Kane, S.; Garg, C.; Bhattachryya, D.; Jha, S.; Sahoo, N. In *Commissioning and first results of scanning type EXAFS*

beamline (BL-09) at INDUS-2 synchrotron source, AIP Conference Proceedings, AIP: 2014; pp 649-651.

35. Kresse, G.; Hafner, J., Ab initio molecular-dynamics simulation of the liquid-metal–amorphous-semiconductor transition in germanium. *Physical Review B* **1994,** *49* (20), 14251.

36. Kresse, G.; Furthmüller, J., Efficiency of ab-initio total energy calculations for metals and semiconductors using a plane-wave basis set. *Computational Materials Science* **1996,** *6* (1), 15-50.

37. Kresse, G.; Hafner, J., Ab initio molecular dynamics for liquid metals. *Physical Review B* **1993,** *47* (1), 558.

38. Kresse, G.; Furthmüller, J., Efficient iterative schemes for ab initio total-energy calculations using a plane-wave basis set. *Physical review B* **1996,** *54* (16), 11169.

39. Perdew, J. P.; Burke, K.; Ernzerhof, M., Generalized gradient approximation made simple. *Physical review letters* **1996,** *77* (18), 3865.

40. Burke, K.; Perdew, J. P.; Ernzerhof, M., Generalized Gradient Approximation Made Simple [Phys. Rev. Lett. 77, 3865 (1996)]. *Phys. Rev. Lett* **1997,** *78*, 1396.

41. Blöuml, P. E., Projector augmented-wave method [J]. *Phys Rev B* **1994,** *50* (24), 17953-17979.

42. Kresse, G.; Joubert, D., From ultrasoft pseudopotentials to the projector augmented-wave method. *Physical Review B* **1999,** *59* (3), 1758.

43. Walter, M. G.; Warren, E. L.; McKone, J. R.; Boettcher, S. W.; Mi, Q.; Santori, E. A.; Lewis, N. S., Solar water splitting cells. *Chem Rev* **2010,** *110* (11), 6446-73.

44. Conway, B. E.; Tilak, B. V., Interfacial processes involving electrocatalytic evolution and oxidation of H_2, and the role of chemisorbed H. *Electrochim Acta* **2002,** *47* (22–23), 3571-3594.

Chapter 5

In-situ synthesized mesoporous Mo_2C/MoO_2 nanocomposite shows enhanced HER activity

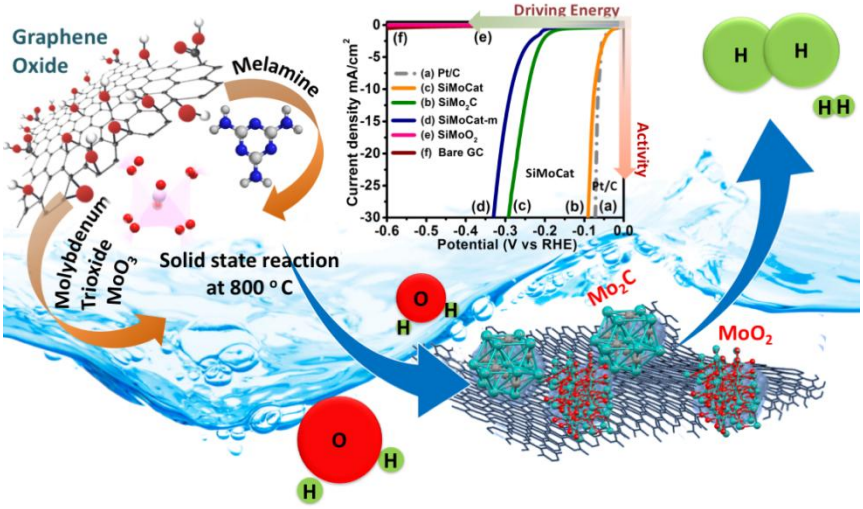

Abstract: *Hydrogen being a promising source of clean energy alternative, the production of hydrogen using electrocatalysis and development of such carbon-neutral energy conversion technologies are very crucial. Lately electrocatalysts with multiple solid-solid heteroatom interfaces gaining importance due to their improved HER activity. Herein, a mesoporous composite of molybdenum carbide and molybdenum oxide on silica platform (SiMoCat) has been developed, which exhibits an overpotential of 71 mV for driving a current density of 10 mA/cm^2, very closed to the commercially available Pt/C (η_{10} = 60 mV) and a Tafel slope value of 35 mV/dec with an onset potential of 31 mV. The electrochemical stability of the catalyst after 3500 catalytic cycles do not show a significant change in the catalytic activity. The SiMoCat was obtained by a judicious variation in the catalyst precursor and the reaction conditions, resulting in a composition containing 51.3 % and 48.7 % of Mo_2C and MoO_2 respectively.*

Brief Outcome: In this chapter, a new composite, was developed by the in-situ synthesis of molybdenum carbide and oxide nanoparticles into a porous silica platform, as a highly active and durable nonprecious metal electrocatalyst for Hydrogen Evolution Reaction (HER). We are maned it "SiMoCat", which exhibits an overpotential of 71 mV for driving a current density of 10 mA/cm^2, very close to the commercially available Pt/C (η_{10} = 60 mV) and a Tafel slope value of 35 mV/dec with an onset potential of 31 mV. The electrochemical stability of the catalyst after 3500 catalytic cycles do not show a significant change in the catalytic activity. The SiMoCat was obtained by a judicious variation in the catalyst precursor and the reaction conditions, resulting in a composition containing 51.3 % and 48.7 % of Mo_2C and MoO_2 respectively. Lately, electrocatalysts with multiple solid-solid heteroatom interfaces gaining importance due to their improved HER activity. In a solid-solid interface, heteroatoms play a significant role in determining the catalytic activity of the material. By using state-of-the-art density functional calculations, Gao et al., have demonstrated that 2D-MXenes (new family of two-dimensional (2D) transition metal carbides), which are terminated by a mixture of oxygen atoms and hydroxyl moieties, should exhibit high HER activity. Similar interaction might exist in SiMoCat catalyst which contains two phases, Mo_2C and MoO_2, creating several interfaces on Silica platform.

5.1. Introduction

The energy crisis associated with extensive dependence on fossil fuels and apprehension of global warming has prompted us to explore the clean and regenerative energy sources.[1] In this regard, the safe production of eco-friendly fuels using sustainable energy resources has become a highly exigent task.[2-3] However, a dynamic seasonal and regional inconsistency along with the daily intermittent are crucial factors that limit the use of these immensely accessible renewable energy sources.[4] This volatility of energy possibly will be solved if this could be accumulated and bring into use after being translated into a secure form of energy carrier like hydrogen. As a promising alternative, hydrogen having the highest gravimetric energy density could be considered as a sustainable solution for minimizing greenhouse effect and depletion of petroleum products.[5] In this context, electrocatalytic water splitting is an inspiring way to step towards carbon-neutral, renewable and green energy technologies.[6] Usually, noble metals and their derivatives are known to be the most efficient electrocatalysts for HER applications. These catalysts effectively facilitate the hydrogen evolution reaction by generating large cathodic current at a very low overpotential; however, scarcity, storage and high cost are among the major limitations involved using noble-metal based catalyst, which consequently confines the industrial production of hydrogen.[7-8] Thus the enviable approach of probing earth-abundant metal-based electrocatalysts could formulate the hydrogen evolution process on commercial-scale.[9-10] Therefore enormous efforts have been made in searching an abundant metal catalyst including transition metal carbides, nitrides, oxides, sulphides, bromides, phosphides and their composites, for HER in acidic conditions. Their significant properties including, electrical conductivity and chemical stability, features them as an economically viable, non-noble metal alternative for hydrogen generation. In this connection, molybdenum based catalysts such as Molybdenum carbide (Mo_2C), sulphide (MoS_2), nitride (Mo_2N), oxide (MoO_3), phosphide (MoP) and their composites are well-known electrocatalysts in molybdenum family which have been extensively explored.[11] The composites like Mo_2C/Mo_2N,[12] Mo_2C/MoS_2[13] Mo_2C/Mo_2N/HrGO,[14] Mo_2C/NRGO, Mo_2C/CNT, Mo_2C/RGO/CNT [15-17] Mo_2C/RGO,[18] etc., are also reported in the recent literature, which performs HER excellently in acid or alkaline media. All these reports indicate the existence of mutual interaction between the interfaces of unlike phases which resulted in an enhancement in the electrocatalytic activity, can be termed as "Synergistic effect". In the present chapter, we demonstrate that the Mo_2C/MoO_2 binary phase also shows such an effect only when the composite is synthesized *in-situ*.[15, 19] Here, we synthesised the silica-based Mo_2C/MoO_2 composite by temperature-programmed reduction

method to yield "SiMoCat". The synthesis particularly involves the partial carburization of mesoporous silica-containing MoO_3 oxide precursor at high temperature, resulting in two phases, namely Mo_2C and MoO_2 supported on amorphous silica. The onset potential (31 mV), overpotential (71 mV), and the Tafel slope (35 mV/dec) value, are very close to the commercially available Pt/C with long term stability of more than 3500 cycles. Such binary phases contain intermingled boundaries of Mo_2C and MoO_2 nanostructures results in curtailing the charge resistance and hence favouring the catalytic activity. The theoretical exploration of silica assisted molybdenum carbide, and molybdenum oxide also indicates and supports the superior activity compared to the single phases.

5.2. Experimental section

5.2.1. Materials

All the chemicals used in the synthesis of catalysts were purchased from the undermentioned brand and was used as obtained. Nafion® perfluorinated resin solution; Ammonium molybdate tetrahydrate ($(NH_4)_6.Mo_7O_{24}.4H_2O$); Citric Acid; N, N-Dimethylformamide anhydrous, 99.8%; Ammonium Hydroxide $NH_3.H_2O$ (25%); Melamine; Graphite flakes and Tetraethyl Orthosilicate (TEOS); were purchased from Sigma Aldrich. Deionised water was used in all preparations.

5.2.2. Methodology

5.2.2.1. Synthesis of Catalyst

The catalyst synthesis involves two major steps in which the first step is the synthesis of the metal precursor and then followed by the partial carburisation of the oxide metal precursor at high temperature in an inert environment.

Step 1: Synthesis of catalyst precursors:

a. Hydrolysed TEOS: A hydrolysed suspension of TEOS was prepared by Stöber-Fink-Bohn method with little modification.[20] Typically, two mother solutions were made in which the first solution contained 0.022 moles of TEOS in 25 mL of ethanol and the second solution contained 15 mL of ammonium hydroxide (12%). Both the solutions were mixed and stirred overnight until a turbid suspension was obtained, which was further used for the synthesis of silica-supported molybdenum oxide nanoparticles.

b. Synthesis of Silica supported MoO_3 nanoparticles (Si-MoO_3). A hydrothermal method was followed, where 0.001 mole (1.2358 g) of ammonium molybdate tetrahydrate $(NH_4)_6Mo_7.O_{24}.4H_2O$ and 0.03 mole (5.8 g) of citric acid were dissolved into 20 mL of distilled water in a 50 mL glass beaker and kept for 60 minutes stirring at room temperature until the solution becomes transparent. The *p*H of the solution was maintained between 1-2, by adding a few drops of 12 M HCl, which resulted in a blue coloured solution indicating a partial reduction of Mo^{+6} to Mo^{+5}. The hydrolysed TEOS turbid suspension (which was prepared in the first step), was added to the blue coloured solution and heated into an autoclave at 180 °C for 24 h. The obtained hydrothermal product was dried and annealed at 500 °C for 2 hours with a ramp rate of 400 °C /h under argon atmosphere.

c. Synthesis of MoO_3 nanoparticles. The synthesis of MoO_3 nanoparticles involves the same procedure as in the above section 'b'. The only difference is that in these nanoparticles synthesis there is no use of hydrolysed TEOS and the obtained product is used for the Mo_2C and MoO_2 synthesis.

d. Synthesis of GO-based carbon source. GO was synthesised by the well-known Hummer's method from graphite flakes. Initially, 500 mg of GO with 1 g of melamine was sonicated in 10 mL of distilled water for two hours. The resulting suspension was dried and heated at 450 °C for one hour and at 550 °C for two hours with a ramp rate 400 °C/h into a covered crucible in a tube furnace under argon. The greyish mass evolved in the reaction was further used for the catalyst synthesis.

Step 2: High-temperature calcination of the oxide precursor

e. Synthesis of SiMoCat. In a reaction, 25 mg silica-supported MoO_3 (Si-MoO_3) nanoparticles were mixed with 200 mg of GO-based carbon source, and placed in a tube-furnace. In the beginning, the tube furnace was purged with argon gas for half-an-hour to remove the unwanted gases. The mass was heated to 800 °C with a ramp rate of 400 °C/h with a flow rate of 30 mL/min and was held for three hours. The SiMoCat catalyst was obtained by steady cooling of the product under argon. A composite of Mo_2C and MoO_2 nanoparticles was formed *in-situ* during the solid-state reaction which is highly susceptible to the temperature manipulation and initial quantity of the precursors used in the reaction. All these factors were optimised appropriately to obtain a variety of compositions (Si-Mo_2C, Si-MoO_2, SiMoCat1, SiMoCat2,) of Mo_2C and MoO_2 as discussed below.

f. Synthesis of MoO_2. MoO_2 catalyst was synthesized by annealing 15 mg of MoO_3 with 100 mg of GO-based carbon source (preparation described in the experimental section of the manuscript) at 800^0 C for 1 h in an argon atmosphere at a flow rate of 30 mL/min.

g. Synthesis of Mo_2C. For Mo_2C catalyst has been synthesized with 15 mg MoO_3 nanoparticles and 250 mg GO-based carbon source, mixed in a mortar pestle. The mixture was heated at 800 ^{0}C for 3 h in an argon atmosphere with a flow rate of 30 mL/min.

h. Synthesis of silica-based MoO_2 (Si-MoO_2). Si-MoO_2 was synthesized by annealing 25 mg of Si-MoO_3 (as described in section 'b') with 100 mg of GO-based carbon source annealed at 800^0 C for 1 h in an argon atmosphere at a flow rate of 30 mL/min.

i. Synthesis of silica-based Mo_2C (Si-Mo_2C). Si-Mo_2C catalyst was synthesized annealing 25 mg Si-MoO_3 nanoparticles (as described in section 'b') and 250 mg GO based carbon source was mixed in a mortar pestle. The mixture was heated at 800 ^{0}C for 3 h in an argon atmosphere with a flow rate of 30 mL/min.

j. Synthesis of SiMoCat1. SiMoCat1 was synthesized by annealing a mixture of 25 mg Si-MoO_3 precursor (as described in section 'b') and 225 mg of GO-based carbon source for 3.5 h at 800 ^{0}C in an argon atmosphere.

k. Synthesis of SiMoCat2. SiMoCat2 was synthesized by annealing a mixture of 25 mg Si-MoO_3 precursor (as described in section 'b') and 100 mg of GO-based carbon source for 2.5 h at 800 ^{0}C in an argon atmosphere.

Note: The heating rate in all the synthesis process was 400 ^{0}C/min, and the post-reaction cooling was done in an argon environment with a gas flow of 30 mL/min.

5.2.2.2. Physical characterisation.

The SiMoCat was characterised using several techniques, which are described as follows. Preliminary analysis was done by Powder X-Ray diffraction (Bruker Eco D8 advance diffractometer, by using Ni filter employing Cu Kα radiation, λ=1.54056 Å, 40 kV and 25 mA, in the 2θ range of 5 to 80 with an increment of 0.00190/Step). The surface area and pore size distribution of the samples were done by Autosorb IQ Quantachrome instrument using the Brunauer-Emmett-Teller (BET) and the Barrett-Joyner-Halenda (BJH) equation. The SEM micrographs of the sample were generated using JEOL, JSM IT-300 equipped with energy dispersive X-ray diffractometer (Bruker) to study the surface morphology and elemental

composition. Transmission electron microscopy (TEM) images were acquired using a JEOL-2100 operated at 200 kV. The XANES and EXAFS measurements of the Mo based catalysts along with the Mo standards have been carried out at the Indus-2 Synchrotron Source (2.5 GeV, 100 mA), beamline (BL-9) at RRCAT, Indore, India.

5.2.2.3. Electrochemical measurements

The electrochemical measurements were conducted using CHI 760E electrochemical potentiostat having three electrode configurations consist of Ag/AgCl, glassy carbon and carbon-based electrode as a reference, working and counter electrodes respectively. Initially, a homogeneous suspension of each catalyst was prepared using 5 mg of catalyst in 495 µL of DMF and 5 µL (5 wt %) of Nafion as a binder. The suspension so formed sonicated for 2 hours using Labsonic LBS2-10 Bath Sonicator, before drop-casting, on the surface of the electrode. The glassy carbon electrode has been polished with alumina powder and cleaned to remove any contamination on the surface. The electrode (3 mm diameter) was loaded with 0.71 mg/cm^2 by drop-casting the above-prepared ink and dried under vacuum. All the measurements were conducted in Ar purged 0.5 M H_2SO_4 solution by sweeping the potential between 0 to -0.5 V (vs. RHE) with a potential sweep rate 2 mV/sec, unless otherwise mentioned. The Tafel slopes were calculated by replotting the polarisation curve, and linear region of Tafel plots was fitted to Tafel equation $\eta = a + b \log j$, where η is the overpotential, j is the current density, a is the intercept relative to the current exchange density. The long-term durability tests were performed by recording the polarization curve at a scan rate of 7 mV/sec for 3500 cycles. The overpotential of all catalytic materials was displayed with respect to reversible hydrogen electrode (RHE) following the equation "E (RHE) = E (Ag/AgCl) + 0.059 *p*H + 0.197 V" and a correction factor for the solution resistance was incorporated to the equation $\eta_{corrected} = \eta\text{-}iR_s$ whereas R_s is solution resistance. For comparative study, commercially available 20 wt% Pt/C catalyst-modified electrode has also been used under the same condition.

5.2.2.4. X-ray Absorption Spectroscopy

The XAFS measurements of the Mo based catalysts along with the Mo standards have been carried out at the Energy Scanning EXAFS beamline (BL-9) at the Indus-2 Synchrotron Source (2.5 GeV, 100 mA), Raja Ramanna Centre for Advanced Technology (RRCAT), Indore, India[21-22] on Mo K-edges. This beamline operates in the energy range of 4 KeV to 25 KeV. The beamline optics consists of a Rh/Pt coated collimating meridional cylindrical mirror and the collimated beam reflected by the mirror is monochromatized by a Si (111) (2d=6.2709 Å) based

double crystal monochromator (DCM). The second crystal of DCM is a sagittal cylinder used for horizontal focusing while Rh/Pt coated bendable post mirror facing down is used for vertical focusing of the beam at the sample position. Rejection of the higher harmonics content in the X-ray beam is performed by detuning the second crystal of DCM. In the present case, XAS measurements have been performed in both transmission and fluorescent modes. For the transmission mode measurement, three ionization chambers (300 mm length each) have been used for data collection, one ionization chamber for measuring incident flux (I_0), the second one for measuring transmitted flux (I_t) and the third ionization chamber for measuring XAS spectrum of a reference metal foil for energy calibration. "The atmospheric gas pressure and a gas mixtures of noble gases have been chosen to achieve 10 -20% absorption in the first ionization chamber and 70 - 90% absorption in the second ionization chamber to improve the signal to noise ratio. The absorption coefficient μ is obtained using the relation $I_t = I_o\, e^{-\mu x}$ where x is the thickness of the absorber. For measurements in the fluorescence mode, the sample is placed at 45° to the incident X-ray beam and a fluorescence detector is placed at a right angle to the incident X-ray beam to collect the signal. One ionization chamber detector is placed prior to the sample to measure the incident flux (I_0) and fluorescence detector measures the fluorescence intensity (I_f). From these intensities, the absorbance of the sample ($\mu = I_f / I_0$) is found as a function of energy.

Mo edge XANES and EXAFS

The Mo K-edge absorption edges of the samples have been obtained from the 1st inflexion point of the μ vs. E curves. The K-edge energy in XANES and Fourier transformed EXAFS (FT-EXAFS) of Mo precursor, Mo foil along with the references MoO_2 and Mo_2C as reference sample are studied to compare with the SiMoCat catalyst. From the XANES spectrum, it can be seen that the oxidation state of the sample is less than +6. The absorption edges of Mo in the samples SiMoCat lies very close to the Mo_2C towards to low energy side of MoO_2, which shows that Mo in SiMoCat having oxidation in between 2 and 3 with little energy difference form the Mo_2C energy edge value. The XANES spectrum of AMH ($(NH_4)_6Mo_7O_{24}$) shows pre-edge at 20007 eV which is due to 1s-4d dipole forbidden transition. AMH has tetrahedral symmetry, which has mixed Mo-d and O-p bond characters.

To obtain the qualitative information about the local structure, oscillations in the absorption spectra $\mu(E)$ have been converted to absorption function $\chi(E)$ defined as follows:

$$\chi(E) = (\mu(E) - \mu_\circ(E))/\Delta\mu_\circ(E_\circ) \quad (5.1)$$

where E_0 is the absorption edge energy, $\mu_\circ(E_\circ)$ is the bare atom background and $\Delta\mu_\circ(E_\circ)$ is the step in $\mu(E)$ value at the absorption edge. The energy-dependent absorption coefficient $\chi(E)$ has been converted to the wave-number dependent absorption coefficient $\chi(k)$ using the relation,

$$k = \sqrt{2m(E - E_\circ)/h^2} \quad (5.2)$$

where m is the electron mass. $\chi(k)$ is weighted by k^2 to amplify the oscillation at high $\chi(k)$ and the $\chi(k)k^2$ functions are Fourier transformed in R space to generate the $\chi(R)$ versus R spectra in terms of the real distances from the centre of the absorbing atom. The set of EXAFS data analysis programme available within Demeter[23] software package has been used for EXAFS data analysis. This includes background reduction and Fourier transforms to derive the $\chi(R)$ versus R spectra from the absorption spectra (using ATHENA[23] software), generation of the theoretical EXAFS spectra starting from an assumed crystallographic structure and finally fitting of experimental data with the theoretical spectra using ARTEMIS[23] software. The data of samples have been fitted by taking Mo_2C and MoO_2 crystal structure. In the fitting process the co-ordination number (C.N), atom to atom bond distance R between the respective atomic pairs and the disorder factor (Debye-Waller factor) (σ^2) which gives the mean square fluctuation in the atomic bond lengths and the thermal disorder in the system, have been used as fitting parameters. The goodness of fit has been determined by the value of the R_{factor} defined by:

$$R_{factor} = \sum \frac{[\mathrm{Im}(\chi_{dat}(r_i) - \chi_{th}(r_i)]^2 + [\mathrm{Re}(\chi_{dat}(r_i) - \chi_{th}(r_i)]^2}{[\mathrm{Im}(\chi_{dat}(r_i)]^2 + [\mathrm{Re}(\chi_{dat}(r_i)]^2} \quad (5.3)$$

where, χ_{dat} and χ_{th} refer to the experimental and theoretical $\chi(r)$values respectively and Im and Re refer to the imaginary and real parts of the respective quantities.

5.3. Result and discussion

In a solid-solid interface, heteroatoms play a significant role in determining the catalytic activity of the material.[7, 24] By using state-of-the-art density functional calculations, Gao et al., have demonstrated that 2D MXenes (new family of two-dimensional (2D) transition metal carbides), which are terminated by a mixture of oxygen atoms and hydroxyl moieties, should exhibit high HER activity.[25] Similar interaction might exist in SiMoCat catalyst which contains two phases,

Mo_2C and MoO_2, creating several interfaces on Silica platform. The SiMoCat catalyst was synthesised following a two-step temperature-programmed calcination method, as mentioned in the experimental section. The high-temperature reaction involving MoO_3 in hydrolysed TEOS reacts with a carbon source (GO-melamine), where MoO_3 is reduced to MoO_2 and Mo_2C in-situ and the extent of reduction depends on the amount of carbon source present in the system. So, the final composition of the catalyst can be controlled by the amount of carbon source added in the high-temperature solid-state reaction. Initially, the metal precursors have been studied and the XRD patterns of MoO_3, melamine-GO, silica assisted Mo_2C and MoO_2 are shown in figure 5.1a, figure 5.2 and figure 5.3 (a and b) respectively. Figure 5.1a confirms that the catalyst having a pure phase of MoO_3 nanoparticles and the corresponding average size of these particles is about 290 nm as described in figure 5.1b.

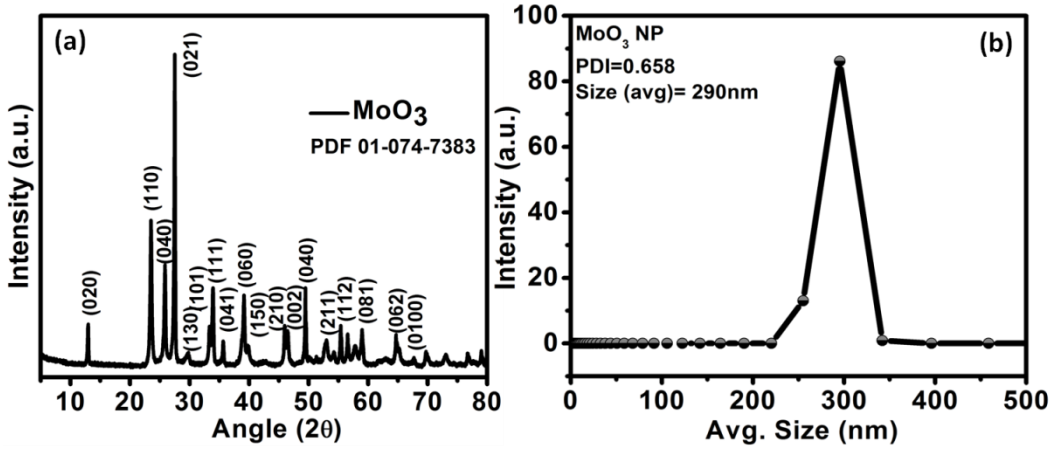

Figure 5.1. *PXRD (a) and DLS (b) pattern of Si-MoO_3 nanoparticles*

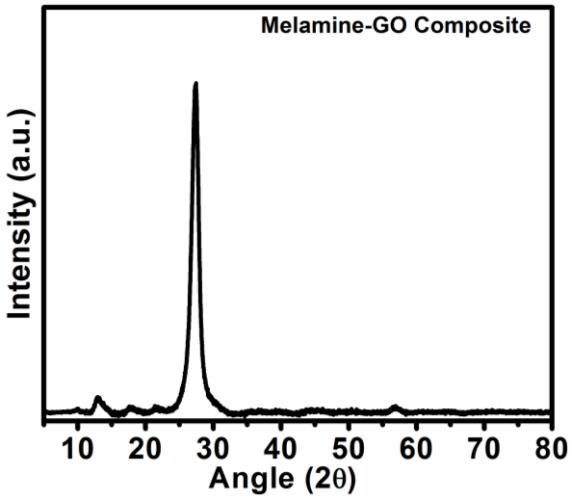

Figure 5.2. *PXRD pattern of Melamine-GO Composite*

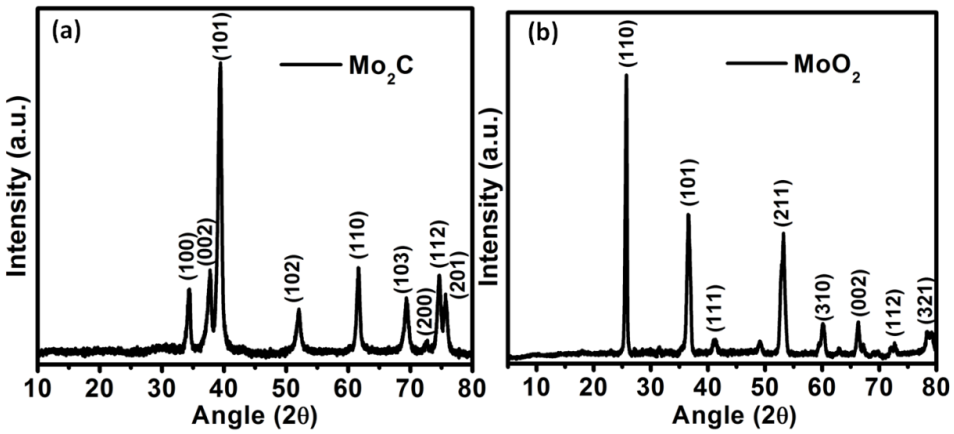

Figure 5.3. *PXRD of (a) Si-Mo_2C and (b) Si-MoO_2*

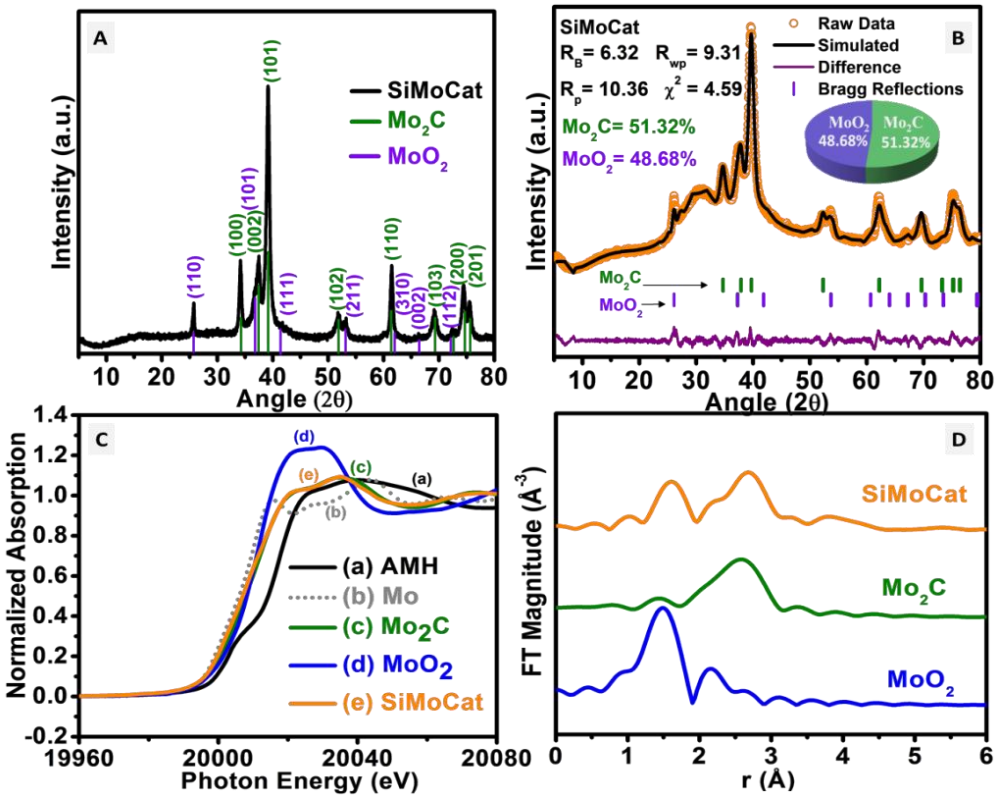

Figure 5.4. *(A) PXRD pattern and (B) Rietveld measurements of SiMoCat containing Mo_2C and MoO_2 phases with a contribution of 51% and 49% respectively (C) Mo K-edge XANES spectra of SiMoCat catalyst compared to standard samples Mo foil and $(NH4)_6.Mo_7O_{24}.4H_2O$ along with references Mo_2C and MoO_2 catalyst (D) The curve corresponding (downside up) k^3 weighted FT of EXAFS spectra of MoO_2, Mo_2C and SiMoCat catalyst further reveal the*

existence of Mo_2C and MoO_2 phases with a structural contribution of 53% and 47%

Temperature programmed reduction (TPR) of the sample was carried out in a stream of argon with a flowing rate of 30 mL/min. The catalyst was heated linearly at 400 °C/h from room temperature to 800 ^{0}C and held for 3 hours at this temperature. Two more catalysts (SiMoCat1 and SiMoCat2) were also synthesised with varying the initial carbon precursor to study the effects of initial stoichiometry on the activity of the catalyst. Hence, an optimum amount of carbon source will only result in the formation of the desired catalyst. The crystal structure and the electrochemical measurements of these catalysts have been describing in the coming sections. The powder X-ray diffraction pattern of SiMoCat (Figure 5.4A) exhibit a series of peaks located at approximately 34.3° (100), 37.9° (002), 39.4° (101), 52.1° (102), 61.5° (110), 69.5° (103), 72.4 (200), 74.5° (112) and 75.4° (201) which attributes to the hexagonal Mo_2C system (PDF 35-0787).[12] The peaks located at approx. 26.02° (110), 37.04° (101), 41.92° (111), 53.54° (211), 61.91° (310), 66.83° (002) and 72.31° (112) corresponds to tetragonal MoO_2 structure (JCPDS: 01-074-4517).[26] Hence it confirms the co-existence of both hexagonal β-Mo_2C and tetragonal MoO_2 phases in the catalyst. A broad hump at around 25° to 35° could be related to the mixed amorphous component of carbon and silica, which appears only in the slow scan. The Rietveld refinement of SiMoCat revealed the composition to be 51.32 % of Mo_2C and 48.68 % of MoO_2 respectively as shown in figure 5.4B. The obtained Rietveld parameters for SiMoCat are described in table 5.1.

Table 5.1. *Rietveld refinement parameters of SiMoCat*

		SiMoCat			
Sr. No.	*Parameters*	*Mo_2C*		*MoO_2*	
1	*Symmetry*	*Hexagonal*		*Tetragonal*	
2	*Space group*	*194*		*136*	
		Input	*Output*	*Input*	*Output*
3	*a*	*2.99091 Å*	*2.98920 Å*	*4.82993 Å*	*4.83969 Å*
4	*b*	*2.99091 Å*	*2.98920 Å*	*4.82993 Å*	*4.83969 Å*
5	*c*	*4.71022 Å*	*4.75052 Å*	*2.81968 Å*	*2.78542 Å*
6	*α*	*90^0*	*90^0*	*90^0*	*90^0*
7	*β*	*90^0*	*90^0*	*90^0*	*90^0*
8	*γ*	*120^0*	*120^0*	*90^0*	*90^0*
9	*R_p %*	*10.36*			
10	*R_{wp} %*	*9.31*			
11	*χ^2*	*4.59*			

The local structure and the valence state of the composites (SiMoCat and other standards) were further studied by the XANES and EXAFS spectroscopy.[27] The K-edge energy in XANES and Fourier transformed EXAFS (FT-EXAFS) of Mo precursor, Mo foil, MoO_2, Mo_2C as reference sample were studied. The introduction of a new phase leads to the change in the electronic environment of an atom which results in the shifting of Mo K-absorption edge photon energy.[28] So this correlation between oxidation state and absorption edge value along with the standard Mo species was applied here to describe the trend of the charge state of the Mo species. The XANES spectra in figure 5.4C display different Mo species having a specific pre-edge position depending upon the oxidation state. The Mo K-edge XANES spectra from the ammonium molybdate precursor (black curve) having a high oxidation state of (VI))[29] shows pre-edge at 20007 eV, where as, the same for Mo foil having "0" oxidation state lies at a photon energy 20000 eV and hence present in the lower region of the photon energy axis of the XANES plot. The K-edge energy of Mo_2C and MoO_2 as obvious towards low energy confirms the less oxidation state than Mo precursor ammonium molybdate. Mo_2C and MoO_2 as corresponds to the oxidation state Mo (II) and Mo (IV) with a close edge position around 20003 and 20004 eV, so the edge energy lies in between Mo foil and Mo precursor ammonium molybdate. However, the position of SiMoCat edge is almost coinciding Mo_2C and MoO_2 towards low energy edge position. The Mo binding environment of SiMoCat catalyst in r-space is described by the k^3-weighted EXAFS analysis as shown in figure 5.4D. The figure shows the Fourier transforms Mo K-edge EXAFS of the SiMoCat catalysts together with the synthesised MoO_2 and Mo_2C species. The theoretically fitted EXAFS spectrum for SiMoCat also supports the composition obtained in Rietveld refinement and found that the structural composition of Mo_2C and MoO_2 is 53% and 47% respectively. From figure 5.4D it can be seen that SiMoCat have a radial distribution which is a linear combination of MoO_2 and Mo_2C radial distribution. The first and second peak has the contribution of Mo-O and Mo-C coordination shell, while the third peak has the contribution of Mo-Mo coordination shell. The EXAFS measurements of Mo_2C and MoO_2 are shown in figure 5.5 and figure 5.6 respectively. The obtained bond length, coordination number and disorder factors of Mo_2C, MoO_2 and SiMoCat are described in table 5.2, table 5.3 and table 5.4 respectively.

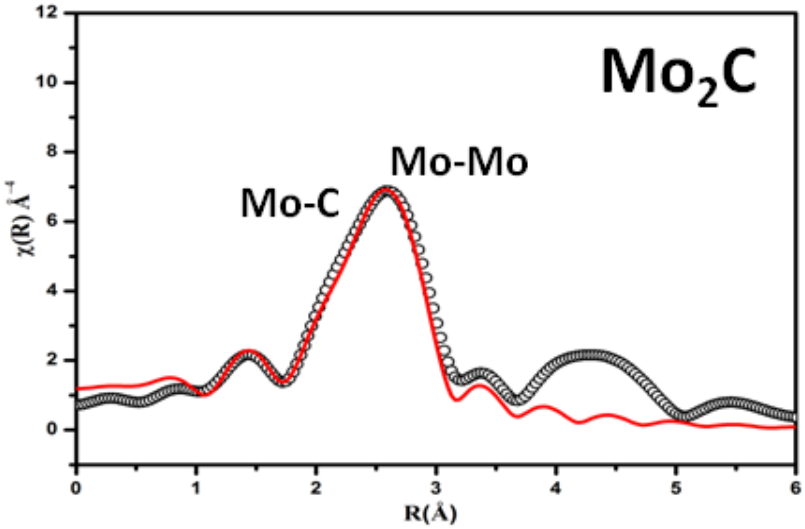

Figure 5.5. *Fourier transformed the EXAFS spectrum of Mo_2C sample measured at Mo K-edge along with best-fit theoretical spectrum. The experimental spectrum is represented by scatter points and the theoretical fit is represented by a solid line*

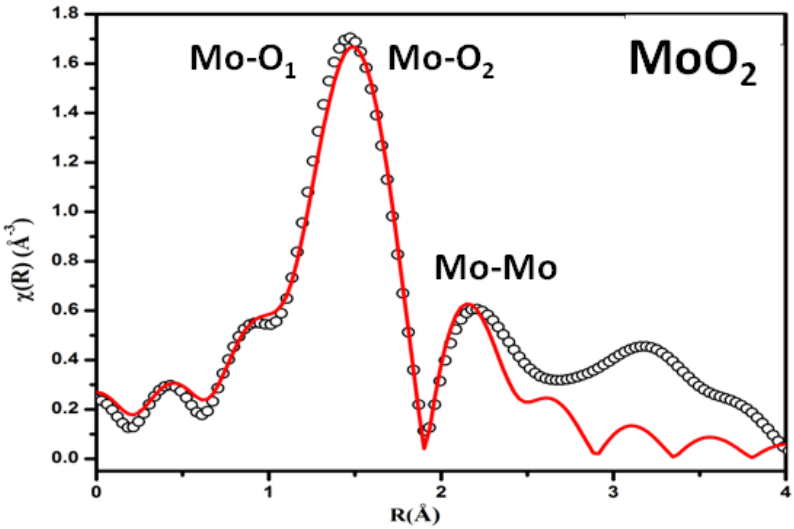

Figure 5.6. *Fourier transformed EXAFS spectrum of MoO_2 sample measured at Mo K-edge along with best-fit theoretical spectrum. The experimental spectrum is represented by scatter points and the theoretical fit is represented by a solid line.*

Table 5.2. *Bond length, coordination number and disorder factor obtained from EXAFS fitting for the standard samples Mo_2C at Mo K-edge*

Path	*Parameters*	*Mo_2C*
	Mo edge	
Mo-C	*R (Å) (2.09)*	*2.14±0.04*
	N(6)	*5.53±1.26*
	σ^2	*0.024±0.009*
Mo-Mo	*R (Å) (2.99)*	*2.93±0.01*
	N(12)	*11.46±1.68*
	σ^2	*0.011±0.001*
R_{factor}		*0.001*

Table 5.3. *Bond length, coordination number and disorder factor obtained from EXAFS fitting for the standard samples MoO_2 at Mo K-edge*

Path	*Parameters*	*MoO_2*
	Mo edge	
Mo-O_1	*R (Å) (1.98)*	*1.98 ± 0.002*
	N(4)	*4.0 ± 0.05*
	σ^2	*0.015 ± 0.0004*
Mo-O_2	*R (Å) (2.07)*	*2.07 ± 0.003*
	N(2)	*2.0 ± 0.03*
	σ^2	*0.015 ± 0.0004*
Mo-Mo	*R (Å) (2.51)*	*2.59 ± 0.006*
	N(1)	*1.0 ± 0.01*
	σ^2	*0.0013 ± 0.0003*
R_{factor}		*0.02*

Table 5.4. *Bond length, coordination number and disorder factor obtained from EXAFS fitting for the standard samples SiMoCat at Mo K-edge*

Path	*Parameters*	*SiMoCat*
	Mo edge	
Mo-C	*R (Å) (2.09)*	*2.14 ± 0.01*
From Mo_2C	*N(6)*	*6.0 ± 0.12*
	σ^2	*0.001*
Mo-Mo	*R (Å) (2.99)*	*2.96 ± 0.003*
From Mo_2C	*N(6)*	*6.0 ± 0.12*
	σ^2	*0.002 ± 0.0006*
Mo-O_1	*R (Å) (1.98)*	*1.83 ± 0.002*
From MoO_2	*N(4)*	*4.0 ± 0.07*
	σ^2	*0.0045 ± 0.0007*
Mo-O_2	*R (Å) (2.07)*	*1.91 ± 0.003*
From MoO_2	*N(2)*	*2.0 ± 0.05*
	σ^2	*0.0045 ± 0.007*
R_{factor}		*0.01*

Two other compositions of Mo_2C and MoO_2 (SiMoCat1 and SiMoCat2) have also been synthesized and the composition analysis of the catalyst has been done by Rietveld refinement.

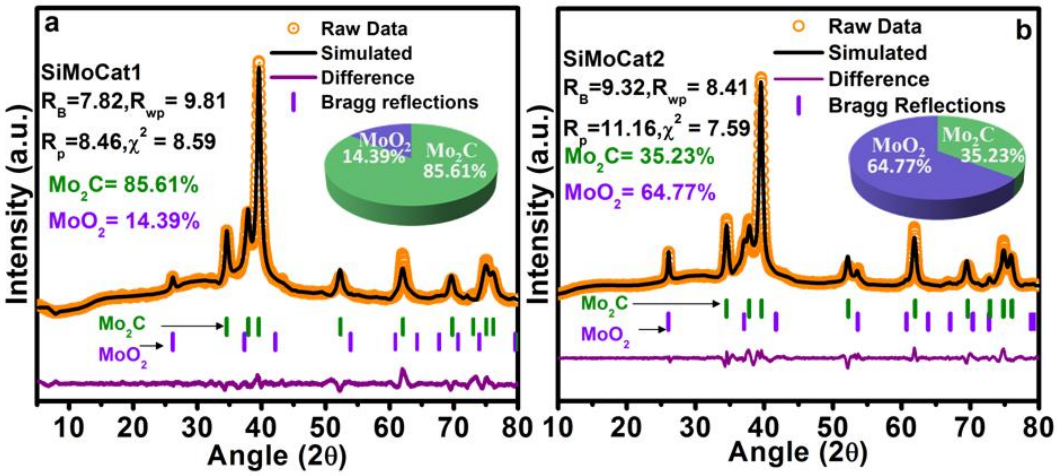

Figure 5.7. *Rietveld refinement of (a) SiMoCat1 and (b) SiMoCat2: The figure typically shows the formation of both Mo_2C and MoO_2 phases and Rietveld analysis of catalyst shows a composition 85.61 % and 14.39 % of Mo_2C and MoO_2 in SiMoCat1 and composition of 35.23 %*

and 64.77 % of Mo_2C and MoO_2 in SiMoCat2.

Table 5.5. *Rietveld refinement parameters of SiMoCat1*

SiMoCat1					
Sr. No.	*Parameters*	*Mo_2C*		*MoO_2*	
1	*Symmetry*	*Hexagonal*		*Tetragonal*	
2	*Space group*	*194*		*136*	
		Input	*Output*	*Input*	*Output*
3	*a*	*2.99091 Å*	*2.99376 Å*	*4.82993 Å*	*4.81431 Å*
4	*b*	*2.99091 Å*	*2.99376 Å*	*4.82993 Å*	*4.81431 Å*
5	*c*	*4.71022 Å*	*4.74662 Å*	*2.81968 Å*	*2.76749 Å*
6	*α*	*90^0*	*90^0*	*90^0*	*90^0*
7	*β*	*90^0*	*90^0*	*90^0*	*90^0*
8	*γ*	*120^0*	*120^0*	*90^0*	*90^0*
9	*R_p %*	*8.46*			
10	*R_{wp} %*	*9.81*			
11	*χ^2*	*8.59*			

The Rietveld refinement of the SiMoCat1 and SiMoCat2 is shown in figure 5.7a and figure 5.7b respectively and corresponding refined parameters are described in table 5.5 and table 5.6 respectively.

Table 5.6. *Rietveld refinement parameters of SiMoCat2*

SiMoCat2					
Sr. No.	*Parameters*	*Mo_2C*		*MoO_2*	
1	*Symmetry*	*Hexagonal*		*Tetragonal*	
2	*Space group*	*194*		*136*	
		Input	*Output*	*Input*	*Output*
3	*a*	*2.99091 Å*	*2.99696 Å*	*4.82993 Å*	*4.83366 Å*
4	*b*	*2.99091 Å*	*2.99696 Å*	*4.82993 Å*	*4.83666 Å*
5	*c*	*4.71022 Å*	*4.75537 Å*	*2.81968 Å*	*2.80616 Å*
6	*a*	*90^0*	*90^0*	*90^0*	*90^0*
7	*b*	*90^0*	*90^0*	*90^0*	*90^0*
8	*g*	*120^0*	*120^0*	*90^0*	*90^0*
9	*R_p %*	*11.16*			
10	*R_{wp} %*	*8.41*			
11	*χ^2*	*7.59*			

The morphological information was obtained from the SEM and TEM micrographs as shown in figure 5.8 (A-H). SEM images of catalyst precursor (MoO_3) before and after annealing were displayed in figure 5.8A & 5.8B. SiMoCat is shown at two different magnifications in figure 5.8C & 5.8D. TEM image reveals that the size of the majority of nanoparticles lies within 30 nm (Figure 5.8E & 5.8F). High-resolution (HR) TEM image (Figure 5.8G and 5.8G-inset) displays the lattice fringe interplanar distance of 0.26 nm and 0.34 nm, corresponds to (100) and (110) crystallographic plane of Mo_2C and MoO_2 respectively.[12, 26]

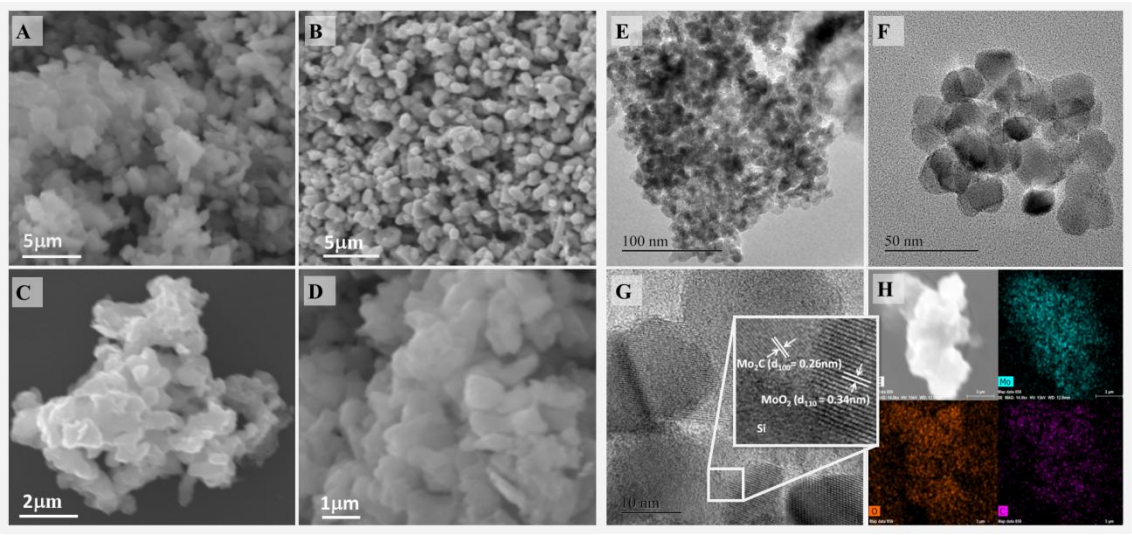

Figure 5.8. *SEM images of (A) MoO_3 on silica platform before annealing (B) MoO_3 on silica platform after annealing (C) and (D) SEM image of SiMoCat catalyst; images in (E), (F) and (G) shows TEM micrographs of SiMoCat nanocomposite at different resolution (Inset: HRTEM images of Mo_2C and MoO_2 fringes) (H) elemental mapping confirms the presence of Mo, C and O in SiMoCat catalyst.*

In addition, the HRTEM image also shows an interface created by the adjoining phases of nanoparticles. The multiple interfaces can be observed in the micrograph featuring the *in-situ* formation of intermingled Mo_2C and MoO_2 nanocrystals. The elemental mapping of SiMoCat on a silicon wafer is shown in figure 5.8H. The mixed distribution of Mo, C, O and Si further confirm the presence of Mo_2C and MoO_2 nanocrystallites on the silica platform. Apart from SiMoCat, two other compositions, SiMoCat1 (Mo_2C, 85.61% and MoO_2,14.39%) and SiMoCat2 (Mo_2C, 35% and MoO_2, 64%) were synthesized. In both these catalysts, we could detect the individual Mo_2C/MoO_2 NPs. The formation of the interfaces could not be detected

possibly because a change in the composition and reaction parameters leads to the variation of the local ingredients responsible for the formation of the Mo_2C/MoO_2 interfaces. STEM images shown in figure 5.9 depicts that Mo, Si and O were homogeneously distributed over the entire structure.

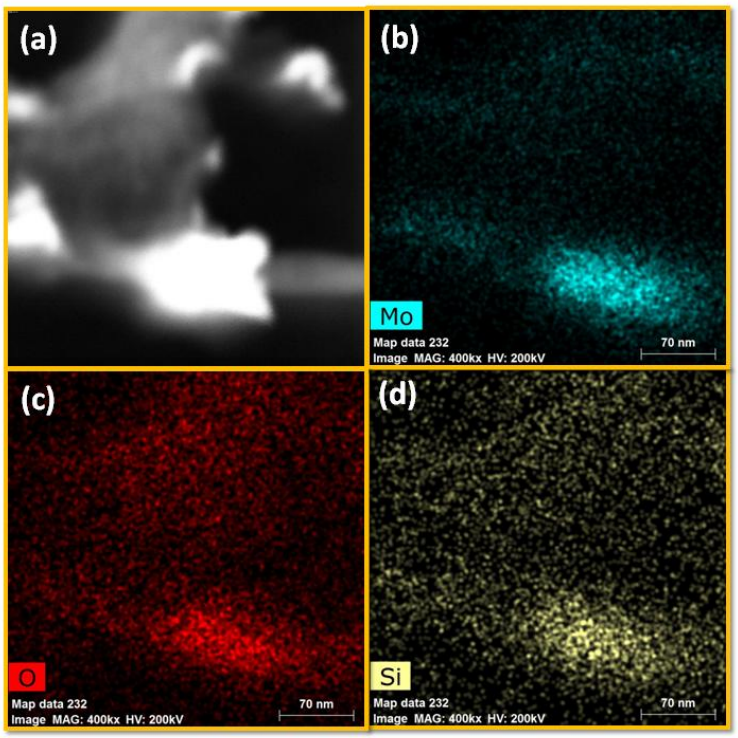

Figure 5.9. *STEM images of SiMoCat Catalyst: The images confirm the presence of Mo (figure b), O (figure c) and Si (figure d) in the SiMoCat*

The surface area and pore size distribution were studied by N_2 adsorption/desorption measurements typically exhibit the type-IV BET isotherm displaying the weak hysteresis, shown at a p/p_0 in the range 0.6–1.0, reveals that the catalyst is mesoporous in nature. The BJH analysis shows the maximum number of the pores in the catalyst is mainly distributed within the range of 19-28 nm in size. The main objective of using silica was to increase the porosity of the catalyst. Such a mesoporous catalyst with uniformity might be inherited from the ordered porous silica platform. The surface area obtained for the silica assisted MoO_3 (Si-MoO_3) nanoparticles is 25 m^2/g as shown in figure 5.10a. But on carburisation of the oxide precursor in the inert atmosphere, the surface area gets enhanced. The surface area of the SiMoCat was found to be 151 $m^2 g^{-1}$ and is shown in figure 5.10b. These spongy structures with a high surface area not only favours high mass transports and better adsorption but also enhances the

interfacial interaction of phases by providing active sites for an easy charge transfer[30] thereby favouring the HER activity.[31] Moreover, the porous silica structure around Mo_2C-MoO_2 edges can efficiently alleviate the composite without blocking their exposure during the HER process.[32-34]

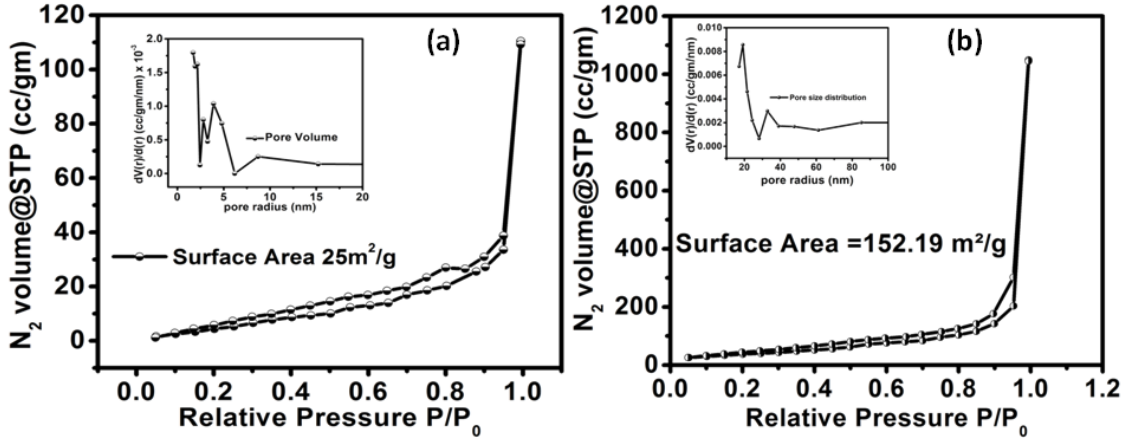

Figure 5.10. *Nitrogen adsorption BET isotherms and inset showing BJH pore distribution of the catalyst (a) Si-MoO_3 (b) SiMoCat: The catalyst was degassed at temperature 200 ^{0}C for 6 h before BET analysis*

The polarization curves of all the catalysts and relevant standards (Figure 5.11) reveals the superior activity of SiMoCat over the other molybdenum catalysts. It exhibits an onset potential of 31 mV, which is very much proximate with the commercially available Pt/C catalyst (onset potential close to zero). Usually, a planar electrode surface in a solar cell produces a charge-carrier flux of 10 mA/cm^2 to from 1 Sun of AM 1.5 illumination.[35] Henceforth, a current density of 10 mA/cm^2 was chosen as the reference for determining the overpotential. SiMoCat exhibits an overpotential of 71 mV in driving a current density of 10 mA/cm^2 (Figure 6.11a). At 20 and 30 mA/cm^2 current densities SiMoCat exhibits an overpotential of 86 mV and 90 mV respectively. The experimentally calculated overpotential (η_{10}) of Pt/C, $SiMo_2C$, SiMoCat-m (a physical mixture of 51% of $SiMo_2C$ and 49% of $SiMoO_2$) were found to be 60 mV, 244 mV and 285 mV respectively. Tafel slope value is an important parameter which can predict the reaction pathways and the adsorption behaviour quantitatively and can determine the kinetics of HER. The linear portion of the Tafel plots of SiMoCat catalyst displays a slope very close to the Pt/C when fitted to Tafel equation ($\eta = b \log j + a$, where j is the current density and b is the Tafel slope, indicating the electrode interface is capable of performing fast electron transfer.

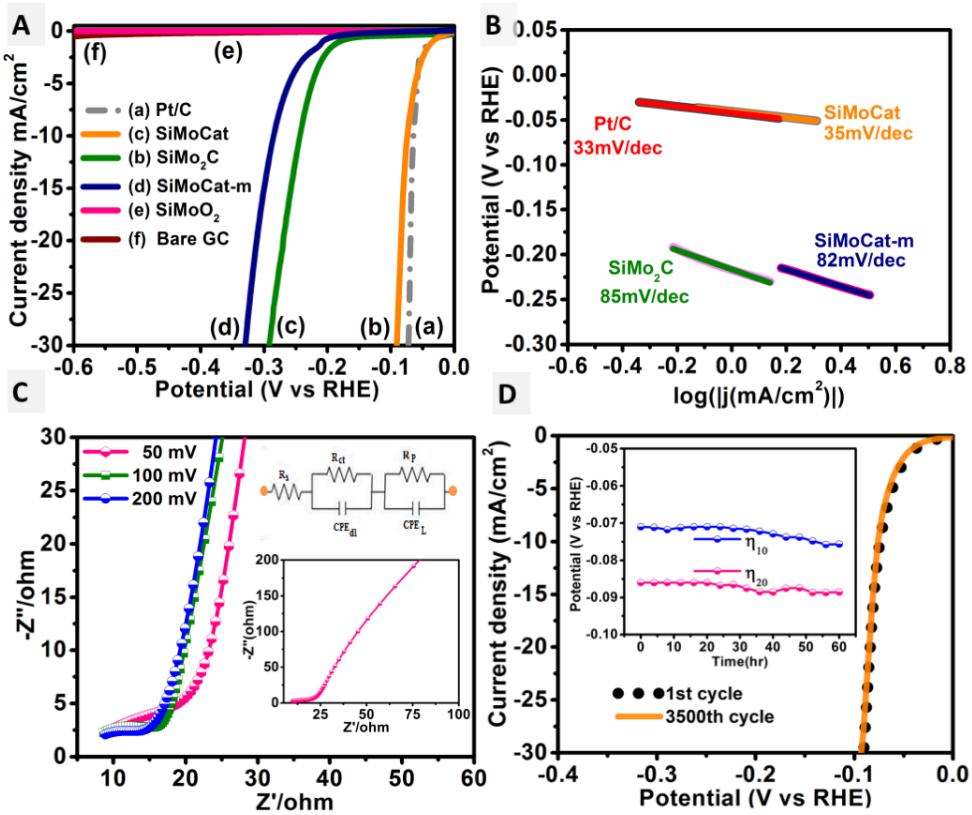

Figure 5.11. *Polarisation curves of SiMoCat catalyst compared with other catalysts in 0.5 M H_2SO_4 (B) the corresponding Tafel plots of Pt catalyst, Si-Mo_2C, SiMoCat-m and SiMoCat (C) Nyquist Plot of the SiMoCat at different values of overpotential (inset- Zoomed Nyquist plot of SiMoCat catalyst @50 mV) (D) Durability test of SiMoCat (inset- A comparative stability curve of SiMoCat at 10 mA/cm^2 and 20 mA/cm^2)*

Three possible reaction steps have been proposed for the HER in acidic media.[36] First step: Volmer reaction (Primary discharge step):

$$H_3O^+ + e^- \rightarrow H_{ads} + H_2O \qquad b = 2.3RT/\alpha F \approx 120mV/dec \qquad (5.4)$$

Where R, T, F corresponds to the ideal gas constant, absolute temperature, Faraday constant respectively and α ≈ 0.5 is the symmetry coefficient. This step is followed by either Heyrovsky reaction (an electrochemical desorption step),

$$H_{ads} + H_3O^+ + e^- \rightarrow H_2 + H_2O \qquad b = 2.3RT/(1+\alpha F) \approx 40mV \qquad (5.5)$$

Or Tafel reaction (a recombination step),

$H_{ads} + H_{ads} \rightarrow H_2$ $\qquad b = 2.3RT/2\alpha F) \approx 30mV$ (5.6)

The Tafel slope value is characteristics of an electrocatalyst and can be evaluated by the rate-determining step of the hydrogen evolution reaction. The Tafel slope is very crucial for the analysis of the primary steps involved in the reaction. For Pt/C catalyst, the H_{ads} coverage ($\theta_H \approx 1$) is very high on the Pt surface, and the mechanism of the reaction proceeds through Volmer-Tafel steps, (i.e., equations 1 and 3). Tafel slope was measured from the corresponding polarisation curve and shown in figure 5.11B. SiMoCat displays a Tafel slope value of 35 mV/dec, which indicates that the reaction mechanism proceeds through mixed Volmer-Heyrovsky process and, the recombination step is the rate-determining step at low overpotentials. The electrochemical impedance spectroscopy (EIS) technique was used to determine the charge-transfer resistance (R_{ct}). EIS was performed at different overpotential value 50, 100 and 200 mV in 0.5 M H_2SO_4 aqueous solution, as shown in figure 5.11C. Simulating and fitting of the experimental curve with the corresponding circuit provides information about the contribution of each component as shown in figure 5.11C-inset. The Nyquist plot reveals the effective resistance exhibited by the electrocatalyst resulting from the collective outcomes of reactance and Ohmic resistance. Studies conducted utilizing DFT calculations on the energetics of HER, the cathodic potential region may be classified into two overpotential regions. The low potential region indicates the formation of a minute amount of molecular hydrogen, lesser H coverage, and stronger M-H bonds. The adsorption of protons in this region is thermodynamically favoured and displays relatively larger semicircles. With the increasing overpotential, the H coverage on the active sites also increases, resulting in the formation of molecular hydrogen. H coverage on active sites decreases as a result of the formation of more and more molecular hydrogen, which lead to the adsorption of more protons from the solution on the unoccupied active sites. This sequence of adsorption and desorption remains active during the increasing overpotential, resulting in relatively smaller semicircles in the Nyquist plot. The equivalent circuit was generated from the simulated pattern, which shows two-time constant model R_{ct}-CPE_d and R_p-CPE_L together with R_s (in series), where R_s symbolises the inherent solution resistance arises during the HER of the concerned catalyst. The constant phase angle element (CPE) can be correlated with the surface properties of the catalyst. R_{ct}-CPE_{dl} is associated with the charge-transfer mechanism at the interface and R_p-CPE_L is arising because of the porosity of the catalyst surface.[37] [38] Generally, the value of R_{ct} is a

function of potential and vary inversely to electrocatalytic performance.[39] As shown in figure 5.11C, the catalyst SiMoCat generates a tiny semicircle in the high-frequency region at 50 mV, exhibiting the charge transfer resistance with an impedance of 12 ohms. This indicates that SiMoCat is very efficient in the charge transfer during the electrochemical HER process, whereas SiMoCat-m (a physical mixture of $SiMoO_2$ and $SiMo_2C$) shows large charge transfer resistance as shown in figure 5.12.

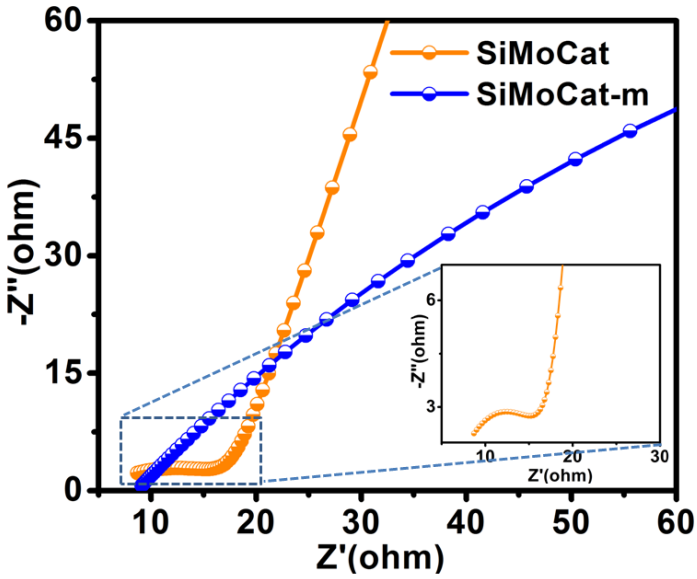

Figure 5.12. *Nyquist plot of SiMoCat and SiMoCat-m; Inset: a magnified image of SiMoCat catalyst at 50 mV applied potential*

The long term durability is one of the most crucial parameters which determines the commercial viability and wide-scale application of HER catalyst. Figure 5.11D and inset demonstrates the stability performance of the catalyst. With a minor increase in the potential from 71 mV to 76 mV @10 mA/cm^2, does not show any notable change in the overpotential even after 3500 cycles (Figure 5.11D inset). The HER activity of the SiMoCat catalyst indicates the existence of a synergistic effect between Mo_2C and MoO_2 when synthesised *in-situ* on silica platform. The major factors which might be responsible for such synergistic effect are: (1) the interaction of the heteroatoms at the interface which forms only when the catalyst is synthesised *in-situ* and (2) Appropriate nanostructuring of the catalyst under the porous platform.

The other catalyst with having the different composition of Mo_2C and MoO_2 also has been synthesized and their catalytic activity has also been studied. The catalyst SiMoCat1 and SiMoCat2 with the extreme composition of Mo_2C and MoO_2 that shows catalytic activity near to SiMoCat studied in acidic medium. The obtained polarization curve and overpotential are shown in figure 5.13 along with the other standard Mo_2C and MoO_2 catalyst that synthesized with the same method except for the inclusion of hydrolysed TEOS in the synthesis method. A comparative description of all the catalyst has been given in table 5.7.

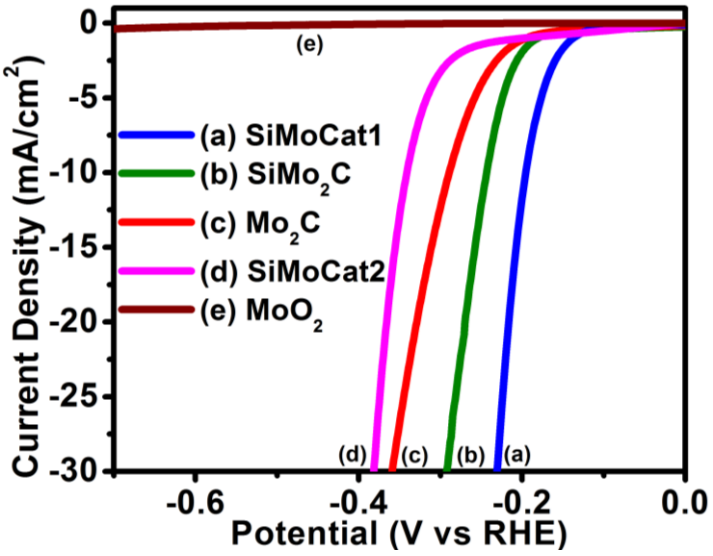

***Figure 5.13**. Polarisation curve of catalyst (a) SiMoCat1 (b) Si-Mo_2C (c) Mo_2C (d) SiMoCat2 (e) MoO_2 in 0.5 M acidic media*

***Table 5.7.** Calculated kinetic parameters of different catalyst in 0.5 M H_2SO_4 solution*

Catalyst	*Onset (vs RHE)*	*η_{10} (vs RHE)*	*η_{20} (vs RHE)*	*η_{30} (vs RHE)*	*Tafel Slope (mV/dec)*	*Exchange Current Density (mA/cm^2)*
SiMoCat	*31 mV*	*71 mV*	*86 mV*	*90 mV*	*35*	*2.33×10^{-2}*
Mo_2C	*204 mV*	*290 mV*	*328 mV*	*359 mV*	*97*	*5.71×10^{-3}*
SiMo_2C	*187 mV*	*244 mV*	*271 mV*	*293 mV*	*85*	*6.32×10^{-3}*
SiMoCat1	*137 mV*	*195 mV*	*216 mV*	*229 mV*	*62*	*8.16×10^{-3}*
SiMoCat2	*218 mV*	*342 mV*	*349 mV*	*380 mV*	*112*	*1.39×10^{-4}*
SiMoCat-m	*209 mV*	*285 mV*	*311 mV*	*329 mV*	*82*	*4.17×10^{-3}*

5.4. Conclusions

Herein, a mesoporous composite of molybdenum carbide and oxide on silica platform (SiMoCat) has been developed by judiciously varying the catalyst precursors and the reaction conditions during the annealing process. The obtained SiMoCat catalyst containing 51.3% and 48.7% of Mo_2C and MoO_2 respectively, exhibits superior HER activity in acid media with low overpotential of 71 mV for driving a current density of 10 mA/cm^2 and a lower Tafel slope value of 35 mV/dec which approaches very close to the Pt/C catalyst (commercially available, η_{10}= 60 mV). The SiMoCat shows high durability and demonstrated up to 3500 catalytic cycles without any significant change in the HER performance. The silica introduces more porosity and supports the appropriate distribution of the active sites. This work elucidates the importance of a solid-solid interface where heteroatoms play a crucial role in enhancing the HER activity of the catalyst. Such systems can be studied further to develop highly efficient non-noble metal-based electrocatalysts.

Note:

- The permission has been granted by the author and corresponding author of the published paper prior to adopting in the present thesis. The associated relevant publication is:

Rajinder Kumar, Zubair Ahmed, Ravi Kumar, Shambhu Nath Jha, Dibyendu Bhattacharyya, Chandan Bera and Vivek Bagchi*; In-situ modulation of silica supported MoO_2/Mo_2C heterojunction for enhanced hydrogen evolution reaction, ***Catal. Sci. Technol.,*** *2020, Accepted Manuscript, https://doi.org/10.1039/D0CY00890G*

References

1. Maggio, G.; Nicita, A.; Squadrito, G., How the hydrogen production from RES could change energy and fuel markets: A review of recent literature. *International Journal of Hydrogen Energy* **2019,** *44* (23), 11371-11384.

2. al Irsyad, M. I.; Halog, A.; Nepal, R., Renewable energy projections for climate change mitigation: An analysis of uncertainty and errors. *Renewable Energy* **2019,** *130*, 536-546.

3. Wang, D. D.; Sueyoshi, T., Climate change mitigation targets set by global firms: Overview and implications for renewable energy. *Renewable and Sustainable Energy Reviews* **2018,** *94*, 386-398.

4. Sharma, T.; Balachandra, P., Model based approach for planning dynamic integration of renewable energy in a transitioning electricity system. *International Journal of Electrical Power & Energy Systems* **2019,** *105*, 642-659.

5. Glenk, G.; Reichelstein, S., Economics of converting renewable power to hydrogen. *Nature Energy* **2019,** *4* (3), 216-222.

6. Wang, Y.; Zhang, J., Structural engineering of transition metal-based nanostructured electrocatalysts for efficient water splitting. *Frontiers of Chemical Science and Engineering* **2018,** *12* (4), 838-854.

7. Ozden, S.; Bawari, S.; Vinod, S.; Martinez, U.; Susarla, S.; Narvaez, C.; Joyner, J.; Tiwary, C. S.; Narayanan, T. N.; Ajayan, P. M., Interface and defect engineering of hybrid nanostructures toward an efficient HER catalyst. *Nanoscale* **2019,** *11* (26), 12489-12496.

8. Peng Xing, D.; Zhong Zeng, H.; Xu Zhang, W.; Li Zhang, W., XPS studies of charging effect induced by X-ray irradiation on amorphous SiO_2 thin films. *IOP Conference Series: Materials Science and Engineering* **2019,** *490*, 022079.

9. Chen, W.-F.; Sasaki, K.; Ma, C.; Frenkel, A. I.; Marinkovic, N.; Muckerman, J. T.; Zhu, Y.; Adzic, R. R., Hydrogen-Evolution Catalysts Based on Non-Noble Metal Nickel–Molybdenum Nitride Nanosheets. *Angewandte Chemie International Edition* **2012,** *51* (25), 6131-6135.

10. Yu, F.; Zhou, H.; Huang, Y.; Sun, J.; Qin, F.; Bao, J.; Goddard, W. A.; Chen, S.; Ren, Z., High-performance bifunctional porous non-noble metal phosphide catalyst for overall water splitting. *Nature Communications* **2018,** *9* (1), 2551.

11. Miao, M.; Pan, J.; He, T.; Yan, Y.; Xia, B. Y.; Wang, X., Molybdenum Carbide-Based Electrocatalysts for Hydrogen Evolution Reaction. *Chemistry – A European Journal* **2017,** *23* (46), 10947-10961.

12. Kumar, R.; Rai, R.; Gautam, S.; De Sarkar, A.; Tiwari, N.; Jha, S. N.; Bhattacharyya, D.; Ganguli, A. K.; Bagchi, V., Nano-structured hybrid molybdenum carbides/nitrides generated in situ for HER applications. *Journal of Materials Chemistry A* **2017,** *5* (17), 7764-7768.

13. Zhao, Z.; Qin, F.; Kasiraju, S.; Xie, L.; Alam, M. K.; Chen, S.; Wang, D.; Ren, Z.; Wang, Z.; Grabow, L. C.; Bao, J., Vertically Aligned MoS_2/Mo_2C hybrid Nanosheets Grown on Carbon Paper for Efficient Electrocatalytic Hydrogen Evolution. *ACS Catalysis* **2017,** *7* (10), 7312-7318.

14. Yan, H.; Xie, Y.; Jiao, Y.; Wu, A.; Tian, C.; Zhang, X.; Wang, L.; Fu, H., Holey Reduced Graphene Oxide Coupled with an Mo_2N–Mo_2C Heterojunction for Efficient Hydrogen Evolution. *Advanced Materials* **2018,** *30* (2), 1704156.

15. Chen, Z.; Duan, X.; Wei, W.; Wang, S.; Ni, B.-J., Recent advances in transition metal-based electrocatalysts for alkaline hydrogen evolution. *Journal of Materials Chemistry A* **2019,** *7* (25), 14971-15005.

16. Li, D.; Shi, J.; Li, C., Transition-Metal-Based Electrocatalysts as Cocatalysts for Photoelectrochemical Water Splitting: A Mini Review. *Small* **2018,** *14* (23), 1704179.

17. Lee, G. H.; Lee, M. H.; Kim, Y.; Lim, H.-K.; Youn, D. H., Facile synthesis of nanostructured molybdenum carbide/nitrogen-doped CNT-RGO composite via a modified urea glass route for efficient hydrogen evolution. *Journal of Alloys and Compounds* **2019,** *805*, 113-119.

18. Li, J.-S.; Wang, Y.; Liu, C.-H.; Li, S.-L.; Wang, Y.-G.; Dong, L.-Z.; Dai, Z.-H.; Li, Y.-F.; Lan, Y.-Q., Coupled molybdenum carbide and reduced graphene oxide electrocatalysts for efficient hydrogen evolution. *Nature Communications* **2016,** *7*, 11204.

19. Li, A.; Sun, Y.; Yao, T.; Han, H., Earth-Abundant Transition-Metal-Based Electrocatalysts for Water Electrolysis to Produce Renewable Hydrogen. *Chemistry – A European Journal* **2018,** *24* (69), 18334-18355.

20. Rao, K. S.; El-Hami, K.; Kodaki, T.; Matsushige, K.; Makino, K., A novel method for synthesis of silica nanoparticles. *Journal of Colloid and Interface Science* **2005,** *289* (1), 125-131.

21. Poswal, A. K.; Agrawal, A.; Yadav, A. K.; Nayak, C.; Basu, S.; Kane, S. R.; Garg, C. K.; Bhattachryya, D.; Jha, S. N.; Sahoo, N. K., Commissioning and first results of scanning type EXAFS beamline (BL-09) at INDUS-2 synchrotron source. *AIP Conference Proceedings* **2014,** *1591* (1), 649-651.

22. Basu, S.; Nayak, C.; Yadav, A. K.; Agrawal, A.; Poswal, A. K.; Bhattacharyya, D.; Jha,

S. N.; Sahoo, N. K., A comprehensive facility for EXAFS measurements at the INDUS-2 synchrotron source at RRCAT, Indore, India. *Journal of Physics: Conference Series* **2014,** *493* (1), 012032.

23. Newville, M.; Ravel, B.; Haskel, D.; Rehr, J. J.; Stern, E. A.; Yacoby, Y., Analysis of multiple-scattering XAFS data using theoretical standards. *Physica B: Condensed Matter* **1995,** *208-209*, 154-156.

24. Ge, R.; Huo, J.; Sun, M.; Zhu, M.; Li, Y.; Chou, S.; Li, W., Surface and Interface Engineering: Molybdenum Carbide–Based Nanomaterials for Electrochemical Energy Conversion. *Small* **2019,** *n/a* (n/a), 1903380.

25. Gao, G.; O'Mullane, A. P.; Du, A., 2D MXenes: A New Family of Promising Catalysts for the Hydrogen Evolution Reaction. *ACS Catalysis* **2017,** *7* (1), 494-500.

26. Nishanthi, S. T.; Baruah, A.; Yadav, K. K.; Sarker, D.; Ghosh, S.; Ganguli, A. K.; Jha, M., New low temperature environmental friendly process for the synthesis of tetragonal MoO2 and its field emission properties. *Applied Surface Science* **2019,** *467-468*, 1148-1156.

27. Timoshenko, J.; Duan, Z.; Henkelman, G.; Crooks, R. M.; Frenkel, A. I., Solving the Structure and Dynamics of Metal Nanoparticles by Combining X-Ray Absorption Fine Structure Spectroscopy and Atomistic Structure Simulations. *Annual Review of Analytical Chemistry* **2019,** *12* (1), 501-522.

28. Penner-Hahn, J. E., 2.13 - X-ray Absorption Spectroscopy. In *Comprehensive Coordination Chemistry II*, McCleverty, J. A.; Meyer, T. J., Eds. Pergamon: Oxford, 2003; pp 159-186.

29. Chen, W. F.; Wang, C. H.; Sasaki, K.; Marinkovic, N.; Xu, W.; Muckerman, J. T.; Zhu, Y.; Adzic, R. R., Highly active and durable nanostructured molybdenum carbide electrocatalysts for hydrogen production. *Energy & Environmental Science* **2013,** *6* (3), 943-951.

30. Dutta, S.; Bhaumik, A.; Wu, K. C. W., Hierarchically porous carbon derived from polymers and biomass: effect of interconnected pores on energy applications. *Energy & Environmental Science* **2014,** *7* (11), 3574-3592.

31. Yang, L.; Zhou, W.; Hou, D.; Zhou, K.; Li, G.; Tang, Z.; Li, L.; Chen, S., Porous metallic MoO_2-supported MoS_2 nanosheets for enhanced electrocatalytic activity in the hydrogen evolution reaction. *Nanoscale* **2015,** *7* (12), 5203-5208.

32. Liang, H.-W.; Brüller, S.; Dong, R.; Zhang, J.; Feng, X.; Müllen, K., Molecular metal–Nx centres in porous carbon for electrocatalytic hydrogen evolution. *Nature Communications* **2015,** *6*, 7992.

33. Zhang, B.; Xue, Y.; Jiang, A.; Xue, Z.; Li, Z.; Hao, J., Ionic Liquid as Reaction Medium for Synthesis of Hierarchically Structured One-Dimensional MoO_2 for Efficient Hydrogen Evolution. *ACS Applied Materials & Interfaces* **2017,** *9* (8), 7217-7223.

34. Xie, X.; Lin, L.; Liu, R.-Y.; Jiang, Y.-F.; Zhu, Q.; Xu, A.-W., The synergistic effect of metallic molybdenum dioxide nanoparticle decorated graphene as an active electrocatalyst for an enhanced hydrogen evolution reaction. *Journal of Materials Chemistry A* **2015,** *3* (15), 8055-8061.

35. Walter, M. G.; Warren, E. L.; McKone, J. R.; Boettcher, S. W.; Mi, Q.; Santori, E. A.; Lewis, N. S., Solar Water Splitting Cells. *Chemical Reviews* **2010,** *110* (11), 6446-6473.

36. Conway, B.; Tilak, B., Interfacial processes involving electrocatalytic evolution and oxidation of H_2, and the role of chemisorbed H. *Electrochimica Acta* **2002,** *47* (22-23), 3571-3594.

37. Alexander, C. L.; Tribollet, B.; Vivier, V.; Orazem, M. E., Contribution of Surface Distributions to Constant-Phase-Element (CPE) Behavior: 3. Adsorbed Intermediates. *Electrochimica Acta* **2017,** *251*, 99-108.

38. Mei, B.-A.; Munteshari, O.; Lau, J.; Dunn, B.; Pilon, L., Physical Interpretations of Nyquist Plots for EDLC Electrodes and Devices. *The Journal of Physical Chemistry C* **2018,** *122* (1), 194-206.

39. Qamar, M.; Adam, A.; Merzougui, B.; Helal, A.; Abdulhamid, O.; Siddiqui, M. N., Metal–organic framework-guided growth of Mo_2C embedded in mesoporous carbon as a high-performance and stable electrocatalyst for the hydrogen evolution reaction. *Journal of Materials Chemistry A* **2016,** *4* (41), 16225-16232.

Chapter 6

Copper doped Mo_2C/Mo_2N hetero-structures showing enhanced hydrogen evolution in acidic medium

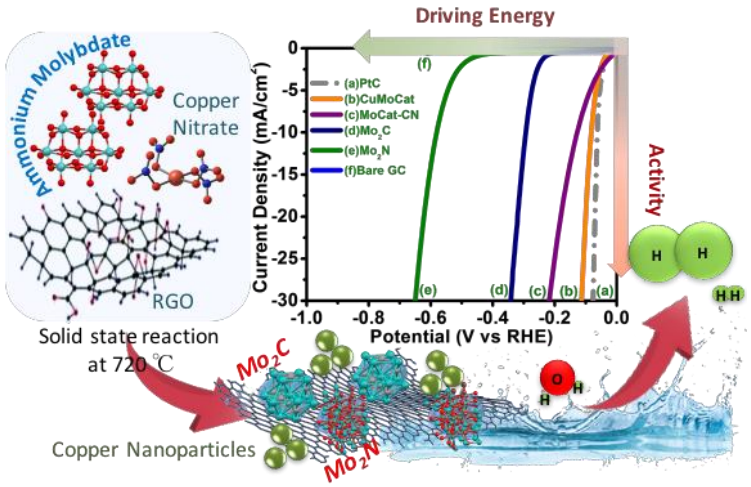

Abstract: *Hydrogen is one of the cleanest forms of energy which can solve several issues, including environmental pollution and depletion of fossils fuels. Hydrogen evolution reaction (HER), being a carbon-neutral process can reduce the carbon footprint in the earth's atmosphere. Molybdenum based solids are among the most popular electrocatalysts, which have been explored extensively for HER processes as an alternative to Platinum. Herein, we report a nanostructured electrocatalyst (CuMoCat) consist of molybdenum carbide, molybdenum nitride, and elemental copper, forming a heterojunction within the composite. Copper doping in molybdenum carbide/nitride composite not only facilitates the lowering of the overpotential but also improves the catalyst to perform at high current density. CuMoCat exhibits an overpotential of 82 mV for attaining a current density of 10 $mAcm^{-2}$ with a Tafel slope value of 33 mV/dec and shows excellent stability of 3000 cycles in acidic media. The theoretical study reveals that Cu doping brings a change in the electronic properties of the catalyst, which improves the overall adsorption and desorption of hydrogen on the catalyst surface during the hydrogen evolution reaction. The Free Energy diagram for 'Mo' and 'N' hydrogen adsorptions sites of CuMoCat displays, a shift of free energy making these more favourable for HER with respect to Mo/N sites of the undoped catalyst.*

Brief Outcome: Molybdenum based solids such as carbide, nitride, sulfide, oxide, phosphide, etc. are among the most popular electrocatalysts, which have been explored extensively for HER processes as an alternative to Platinum. Compositions involving two or more phases may enhance the catalytic activity of the material. For such compositions, heterojunctions play an important role in improving HER activity. Multiple phases manifest interesting properties due to the formation of solid-solid interfaces which behaves differently than the bulk material. The consequently formed interface mutually modifies the structural and electronic environment of the contrasting phase in materials. These modifications sometimes favour the reaction kinetics and improve the catalytic activity of the material. Furthermore, the incorporation of promoter elements like Fe, Co, Mn, Ni, Cu, etc. are known to boost HER activity and are reported in recent literature. However, to the best of our knowledge, copper doping into a biphasic system prepared in-situ using a solid-state reaction is not known. Herein, we report a nanostructured electrocatalyst (CuMoCat) consist of molybdenum carbide, molybdenum nitride, and elemental copper, forming a heterojunction within the composite, serving as a highly active, and durable nonprecious metal electrocatalyst for Hydrogen Evolution Reaction (HER) in acidic medium. Rietveld analysis reveals that 1.14 % of copper is incorporated in the CuMoCat catalyst. The catalyst shows superior HER activity, exhibiting an overpotential of 82 mV at 10 $mAcm^{-2}$ with a Tafel slope value of 33 mV/dec and displays excellent stability of 3000 cycles in acidic medium. The high catalytic activity of CuMoCat catalyst is attributed to the synergy attained between the Mo_2C, Mo_2N, and Cu heterojunctions, and facilitates the kinetics of the reaction operating through the Cu modified Mo_2N/Mo_2C interfaces. The density functional theory calculations reveal Cu doping brings a change in the electronic structure at Mo and N sites in the CuMoCat catalyst, which improves the overall adsorption and desorption process of hydrogen on its surface. The Free Energy diagram of hydrogen adsorptions for Mo and N sites of CuMoCat displays a shift of free energy making them more favourable for HER with respect to Mo/N sites of the un-doped catalyst.

6.1. Introduction

The massive consumption of fossil fuels leading to extensive carbon emission has a far-reaching consequence on our atmosphere.[1] The concentration of CO_2 in Earth's atmosphere has touched a record high and increasing steadily according to a report released by the World Meteorological Organization. In 2017, global average concentrations of CO_2, which is a by-product of burning fossil fuels, has reached 400.0 parts per million permanently. This phenomenon indicates that even if the world stops releasing CO_2 tomorrow, what has already put in the atmosphere will linger for many decades to come. Therefore, the exploration of carbon-neutral energy resources is of prime importance. The elimination or minimization of the hazardous greenhouse gases and introduction of new renewable energy sources are principal objectives towards the green future. The identification and adoption of environmentally friendly energy sources could be a significant step towards addressing the global energy crisis.[2-3] The renewable energy resources with zero carbon emission could be an excellent back-up for a sustainable society.[4] The solar, wind, hydropower, geothermal etc. are some of the known clean energy sources, if used judiciously, can fulfil future energy demands without deteriorating the environment caused by carbon emission.[5] The geographical and environmental uncertainties limit the efficacy of such carbon-free renewable energy resources to a large extent.[6] However, if the energy is converted into hydrogen, which is having the highest gravimetric energy density, can act as a sustainable pollution-free energy carrier.[7] Hydrogen has a prospective to accumulate electric or solar energy in the form of chemical bonds and can be transported and used at will with negligible impact on the environment.[8] Nevertheless, the production, transport and storage of hydrogen is yet another obstacle to be acknowledged as the universal fuel for future energy needs.[9] There is a variety of processes used for hydrogen production such as cracking of petroleum, hydrocarbon reforming, steam reforming of natural gases, coal gasification, etc. but these techniques are either costly or dependent on fossil fuels with the emission of hazardous by-products.[10-11] Hence, the possibility of hydrogen production through water splitting makes it a potential carbon-neutral process for fulfilling energy needs. To date, platinum supported materials are mostly found efficient and resourceful electrocatalysts towards hydrogen production. However, the large scale use of such catalysts is restricted by their scarcity and high cost of the material. In order to accomplish an industrial scale hydrogen production with minimizing the cost, extensive research has been devoted to discovering materials which have similar or better activity than platinum.[12-13]

Several transition metal derivatives are considered to be potential catalysts for hydrogen generation. Molybdenum derivatives such as molybdenum carbides,[14-15] nitrides,[16] sulfides,[17] oxides,[18] phosphides,[19] etc. have been explored extensively for hydrogen evolution reaction.

Compositions involving two or more phases may enhance the catalytic activity of the material.[20] For such compositions, heterojunctions play an important role in improving HER activity.[21-22] Multiple phases manifest interesting properties due to the formation of solid-solid interfaces which behaves differently than the bulk material. The consequently formed interface mutually modifies the structural and electronic environment of different materials in the composite. These modifications might favour the reaction kinetics and improve the catalytic activity of the material.[23-24] The heteroatom incorporation in the lattice could further improve the reaction kinetics of these materials. This incorporation of elements in the structure by re-establishing the bonds between different atoms mutates the hydrogen adsorption energy at different active sites. Furthermore, the incorporation of promoter elements like Fe, Co, Mn, Ni, Cu, etc. are known to boost HER activity and are reported in recent literature. [25, 26] However, to the best of our knowledge, copper doping into a biphasic system during an *in-situ* solid-state reaction is not known. [25-26]

Since the structural modification due to heteroatom inclusion in the crystal lattice provides a more feasible way to improve catalytic activity towards HER,[21] herein, in this chapter we report a nanostructured electrocatalyst (CuMoCat) consist of molybdenum carbide, molybdenum nitride and copper, forming a heterojunction within the composite. CuMoCat exhibits an overpotential of 82 mV to attain a current density of 10 $mAcm^{-2}$ with a Tafel slope value of 33 mV/dec and shows excellent stability of 3000 cycles in acidic media. The theoretical study reveals that Cu doping brings a change in the electronic properties of the catalyst, which improves the overall adsorption and desorption of hydrogen on the catalyst surface during the hydrogen evolution process. The Free Energy diagram for hydrogen evolution reaction on active sites of CuMoCat displays, a shift in free energy making these more catalytically favourable compared to the un-doped catalyst.

6.2. Experimental section

6.2.1. Materials

Chemicals used in the synthesis are ammonium molybdate tetrahydrate ($(NH_4)_6.Mo_7O_{24}.4H_2O$) 99.0%; Copper Nitrate tri-hydrate ($Cu(NO_3)_2 \cdot 3H_2O$) 99.0%; Nafion® perfluorinated resin solution (5 wt. %); N, N-Dimethylformamide anhydrous (99.8%), Melamine ($C_3H_6N_3$) 99%, purchased from Sigma Aldrich chemicals Pvt. Ltd. Other chemicals like Acetic acid $C)_2H_4O_2$) 99.9%; Ammonium Hydroxide $NH_3.H_2O$ (25%) were procured from Merck chemicals; All the chemical were used as obtained. Deionized water was used in all preparations.

6.2.2. Methodology

6.2.2.1. Catalyst Synthesis: It involves two major steps.

Step 1. Synthesis of precursors

(a). Synthesis of RGO. Graphite flakes have been used to synthesize GO by modified Hummer method. The obtained GO was further thermally exfoliated at 900 °C for 15 minutes in an Argon environment with a flow rate of 30 mL/min. [27] This thermally exfoliated RGO was further used as a carbon source in the synthesis of catalyst.

(b). Preparation of Mo precursor. The Mo precursors have been synthesized with 0.025 mol (1.5 gm) of Urea $(NH_2)_2CO$ and 1 mmol (12.358 gm) of ammonium molybdate tetrahydrate ($(NH_4)_6Mo_7O_{24}.4H_2O$) dissolved into 20 mL ammonia solution (25%) and stirred till it becomes transparent. The pH of the solution has been optimised to 1-2 by addition of acetic acid. This solution mixture (Mo-X) was further used for the synthesis of CuMoCat1, CuMoCat2 and CuMoCat3.

While for synthesis Mo_2C and Mo_2N, this solution mixture has been hydrothermally heated at 180 °C for 24 hr and dried (Mo-Y).

(c). Synthesis of Mo-Cu-rGO precursor. The molybdenum precursor solution was mixed with 50 ml ethanolic copper nitrate solution (0.1 mmol, 0.0241 gm) and 200 mg of thermally exfoliated rGO and sonicated for 2 hours. The amount of copper used here corresponds to the synthesis of CuMoCat. For CuMoCat1, CuMoCat2 and CuMoCat3, the amount of copper nitrate taken is 0.05 mmol, 0.3 mmol, and 0.5 mmol respectively, to study the effect of copper concentration in the molybdenum carbide and nitride composite. The obtained dispersion was sonicated for one hour and transferred into a hydrothermal bomb and heated at 180 °C for 24 hr. The synthesis of all the other composites of Cu-doped Mo_2C/Mo_2N composites was done following a similar process.

Step 2. The high-temperature reaction of the Mo-Cu-rGO precursors:

(d). Synthesis of Mo_2C. The 200 mg of Mo precursor (Mo-Y) with 300 mg of rGO was mixed with mortar pestle and kept in the quartz tube of the tubular furnace. The precursor was heated for 2 h at 720 ºC temperature in an argon atmosphere with a flow rate of 30 mL/min.

(e). Synthesis of Mo_2N. The Mo_2N is obtained by annealing the mixture of 200 mg of Mo precursor (Mo-Y) and 100 mg of rGO by crushing it in a mortar pestle and kept it in furnace tube in ammonia atmosphere for 2 h at 600 ºC with a flow rate of 20 mL/min.

(f). Synthesis of MoCat-CN. The 200 mg of Mo precursor (Mo-Y) with 300 mg of rGO was mixed with mortar pestle and kept in the sealed quartz tube of the tubular furnace. The precursor was heated for 1 h at 600 ºC temperature in ammonia environment with a flow rate of 20 mL/min and 2 h at 720 ºC temperatures in an argon atmosphere with a flow rate of 30 mL/min.

(g). Synthesis of CuMoCat. This step involves the mixing of Mo-Cu-rGO (200 mg) and rGO (500 mg), in a mortar pestle and heating the resulting mass into a temperature-programmed furnace. Initially, the tube was purged with argon gas to get rid of unwanted gases for 30 minutes. The catalyst precursor was calcined under ammonia gas at 600 °C with a heating rate of 5 °C/min. The reaction was kept for one hour under a constant flow of ammonia gas at a rate of 20 mL/min; later, the gas was changed to argon. The temperature further increased to 720 °C and held for another two hours in an argon atmosphere with a flow rate of 30 mL/min and cooling was followed under argon atmosphere. The synthesis of *in-situ* phases is highly sensitive to the initial stoichiometry and the heating conditions. Based on these observations, the methodology was prudently optimized to yield copper incorporated molybdenum carbide and molybdenum nitride nanocomposite

(h). Synthesis of CuMoCat1, CuMoCat2 and CuMoCat3. The CuMoCat1, CuMoCat2 and CuMoCat3 catalyst has been synthesized by mixing of 200 mg of respective Mo-Cu-rGO precursor as mentioned in section ‘c’ above with 500 mg of rGO in a mortar pestle and kept in the quartz tube of the tubular furnace. The precursor was heated for 1 h at 600 ºC temperature in ammonia environment with a flow rate of 20 mL/min and 2 h at 720 ºC temperatures in an argon atmosphere with a flow rate of 30 mL/min.

6.2.2.2. Physical characterization

The crystal diffraction pattern of all the materials was obtained using Bruker Eco D8 advance X Powder X-ray diffractometer between 2θ angular region 5º to 80º. The diffraction pattern was obtained by exposing a powder sample with Cu-Kα radiation with wavelength (λ) 1.54056 Å through Ni filter operated at 40 kV and 25 mA current with an incremental step 0.00190º/step. The surface properties were evaluated by Autosorb IQ Quantachrome instrument by conducting

nitrogen adsorption-desorption isotherm at 77 K. The samples were outgassed before measurements at 200 °C for 6 h under vacuum in the degassing port of the adsorption analyser. The pore analysis and surface area were calculated by Barrett-Joyner-Halenda (BJH) and Brunauer-Emmett-Teller (BET) equations respectively. The surface morphology and composition were examined by JEOL (JSM IT-300) scanning electron microscope equipped with the energy-dispersive X-ray spectroscopy (Bruker). The transmission electron microscopy and STEM images were recorded at an accelerated voltage of 200 kV with JEOL-2100. The copper grids with carbon coating were used as sample holders for TEM analysis. X-ray photoelectron spectroscopy (XPS) analysis was carried out in PHI 5000 Versa Probe II, FEI Inc. scanning XPS microprobe. The binding energies were referenced to the C1s peak at 284.6 eV adventitious carbon to correct the shift caused by the charge effect.

6.2.2.3. Electrochemical measurements

The electrochemical HER studies of the catalyst were performed in argon saturated 0.5 M H_2SO_4 with CHI 760E electrochemical workstation connected with a three-electrode system. The glassy carbon electrode (GCE, 3 mm in diameter) was used as a working electrode. Standard Ag/AgCl electrode and carbon-based electrode served as a reference and counter electrode, respectively. Initially, 500µL homogeneous catalyst ink was prepared by taking 5µL of Nafion (5 wt %) in 495µL of DMF and mixed with 5 mg of catalyst followed by 2-hour sonication using a Bath sonicator. An appropriate amount of the catalyst suspension (5 µL) was drop-coated onto the glassy carbon electrode and dried under vacuum. Before accomplishing the measurements, the glassy carbon electrode was cleaned with alumina powder and sonicated for 5 minutes to remove all the contamination present onto the electrode surface. All the measured potential was referenced with reversible hydrogen electrode with $E_{(RHE)} = E_{(Ag/AgCl)} + 0.197 + 0.059*pH$. In all the studies, the polarization curves were measured under argon at a scan rate of 5 mVs^{-1} having 0.5 M H_2SO_4 solution unless otherwise mentioned. The overpotential was further modified to exclude the ohmic-drop as per equation $\eta_{corrected} = \eta - iR_s$ whereas R_s is the solution resistance. The electrochemical impedance spectroscopic (EIS) measurements were done at particular values of the applied potential, i.e. η =50, 100 and 150 mV under a frequency range of 100000 Hz to 0.1 Hz.

6.2.2.4. Theoretical calculations

The adsorption of H-atom on the Cu-doped Mo_2N/Mo_2C (CuMoCat) composite has been analyzed by using density functional theory (DFT). The adsorption energy of Hydrogen atom on various sites of CuMoCat is calculated as[28-29]

$$\Delta E_{ads} = E_{surface+H} - E_{surface} - {}^{1}/_{2}\, E_{H_2} \qquad (6.1)$$

where $E_{surface+H}$ is the total energy of the adsorbate and adsorbent, $E_{surface}$ is the total energy of the clean surface and $E_{(H2)}$ is the energy of H_2 gas. Further, the Gibbs free energy of hydrogen evolution reaction is considered as an essential parameter to describe the overall performance of the catalyst, suggests that only those catalysts are found to be an ideal catalyst for which ΔG is nearly equal to zero and can be written as.[28-29]

$$\Delta G = \Delta E_{ads} + 0.24\ eV \qquad (6.2)$$

All the energy calculations of the supercell having dimensions a = 8.50 Å, b = 24.58 Å, and c = 16.17 Å, are performed using the Vienna Ab-initio Simulation Package (VASP)[30] with projector-augmented wave (PAW) method. The exchange-correlation functional is treated with the Perdew, Burke, and Ernzerhof (PBE) version of the generalized gradient approximation (GGA).[31] A vacuum space of approximately 10 Å is added along the c-axis to avoid the interaction between the adjacent layers. For geometry optimization, the plane wave energy cutoff is set to 520 eV, and the Brillouin-zone is sampled using a 5×5×1 Γ-centred k-point mesh.

6.3. Results and discussion

The synthesis of CuMoCat was carried out in two steps, as illustrated in the experimental section. Molybdenum-copper precursor supported on reduced graphene oxide (rGO) was prepared hydrothermally. An appropriate portion of ammonium molybdate, copper nitrate and rGO were mixed in water at acidic pH and kept for 24 hrs at 180 °C in a hydrothermal bomb. After the synthesis of the precursor, a solid-state reaction in the presence of ammonia and argon at suitable temperature was carried out in a tubular furnace. This resulted in the *in-situ* formation of nanostructured Cu-Mo_2C-Mo_2N heterojunctions supported on carbon. The *in-situ* synthesis of the catalyst depends upon several factors, for example, initial stoichiometry, nature of gas, time and temperature conditions used in the reaction. Usually, in the synthesis of transition metal carbides and nitrides, temperature conditions play an important role which controls the final product. The molybdenum nitride formation takes place at a relatively lower

temperature as compared to the molybdenum carbide. Therefore, an *in-situ* synthesis was judiciously planned, to obtain copper doped molybdenum carbide/molybdenum nitride nanocomposite. Here, the precursor was heated for 1 h at 600 ºC and for 2 h at 720 ºC in ammonia and argon atmosphere respectively. Ammonia gas provides nitrogen source required for the formation of nitrides and also act as a reducing agent resulting in the simultaneous synthesis of nitride and carbide. To study the effect of copper on HER performance, a series of catalysts have been synthesized by varying the amount of Cu dopant and keeping other parameters identical. Rietveld analysis reveals 1.14 % of copper doping in CuMoCat catalyst, which outperforms other three catalysts i.e. CuMoCat1(0.58% of Cu), CuMoCat2 (1.86% of Cu) and CuMoCat3 (2.63% of Cu). The detailed synthesis of the catalyst is described in the experimental section of this chapter.

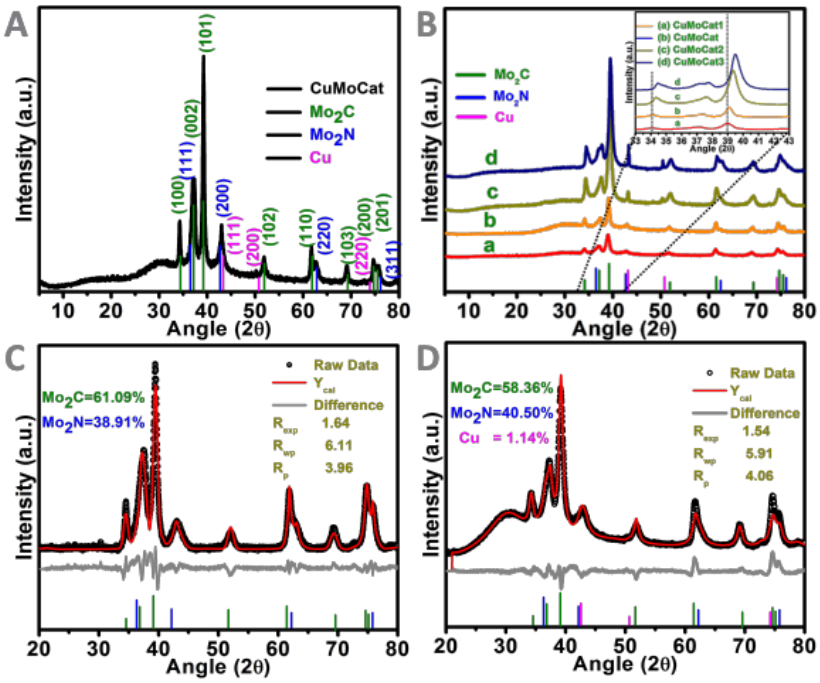

Figure 6.1. *Structural characterization. (A) Powder X-ray diffraction typically shows the formation of both Mo_2C-Mo_2N phases with copper doping and (B) The comparative XRD pattern of CuMoCat1 (a) CuMoCat (b) CuMoCat2 (c) CuMoCat3 (d) and (Figure inset) shows the peak shifting on an increasing amount of copper in Mo_2C/Mo_2N composite. Rietveld Study. (C) MoCat-CN having a phase contribution of 61.09 % and 38.91 % of Mo_2C and Mo_2N respectively and (D) CuMoCat having a contribution of 58.36 %, 40.50 % and 1.14% of Mo_2C, Mo_2N and Copper respectively.*

The PXRD measurements describe the structural details of the material. The PXRD pattern of the material shown in figure 6.1A consist of the characteristics peaks located at 34.3° (100), 37.9° (002), 39.4° (101), 52.1° (102), 61.5° (110), 69.5° (103), 72.4 (200), 74.5° (112) and 75.4° (201) which feature the hexagonal Mo_2C system (PDF 35-0787).[32] The peaks at 37.3° (111), 43.4° (200), 63.1° (220) and 75.7° (311) are characteristics of cubic γ-Mo_2N (PDF 25-1366).[33] Absence of peaks for the impurities such as metallic molybdenum, molybdenum oxide or molybdenum alloy with copper, indicates the formation of the pure phase of Mo_2N/Mo_2C in the nanocomposite. A comparative study is shown in figure 6.1B indicates the increased peak intensity on increasing the doping amount. The catalysts with higher copper concentration, namely, CuMoCat2 and CuMoCat3 displays new peaks. The trend showing an increase in the peak intensity at 43.5° (111), 51.7° (200), and 63.1° (220) are aligned with the predicted amount of copper in the composite.[34] The zoomed 2θ area from 33° to 43° shows shifting of peaks towards the higher diffraction angle in plane 100 (34.3°) and 101 (39.4°) as shown in figure 6.1B (inset). A similar kind of shifting pattern in all the peaks suggests the change in crystal parameters on the incorporation of copper. The shifting in the diffraction angle attributes the shrinkage of molybdenum unit cell and illustrates the structural changes in the unit cell with the incorporation of copper.

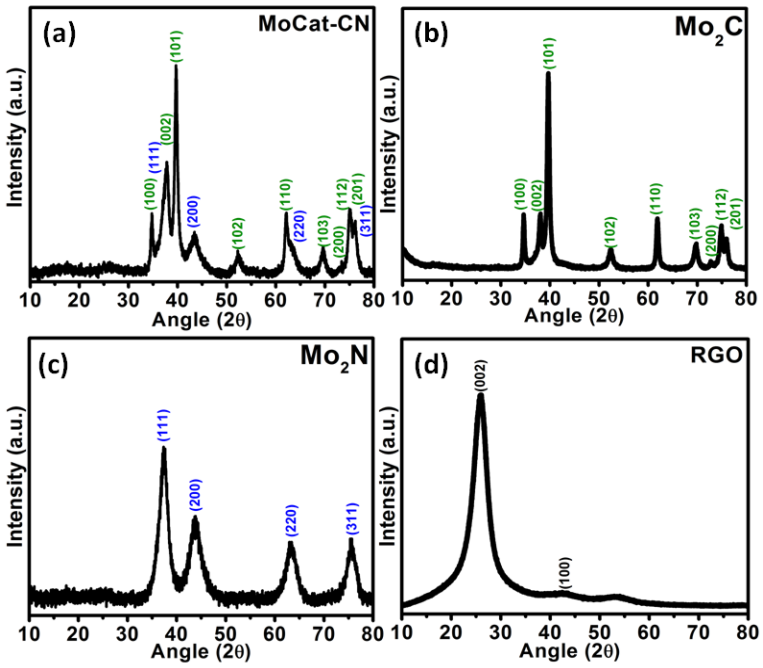

Figure 6.2. *PXRD of (a) MoCat-CN consist of Mo_2C and Mo_2N phases (b) Mo_2C (c) Mo_2N and (d) rGO*

The PXRD pattern of individually synthesized Mo_2C/Mo_2N composite (MoCat-CN), Mo_2C, Mo_2N and carbon source rGO is shown in figure 6.2a, 6.2b, 6.2c and 6.2d respectively. All the above-mentioned catalysts except MoCat-CN as shown in figure 6.1A, 6.1B and 6.2a divulge the co-existence of molybdenum carbide and molybdenum nitride along with the Cu in the nanocomposite. MoCat-CN was synthesized using similar reaction conditions but in the absence of copper precursor. A Rietveld analysis showing the composition of MoCat-CN and

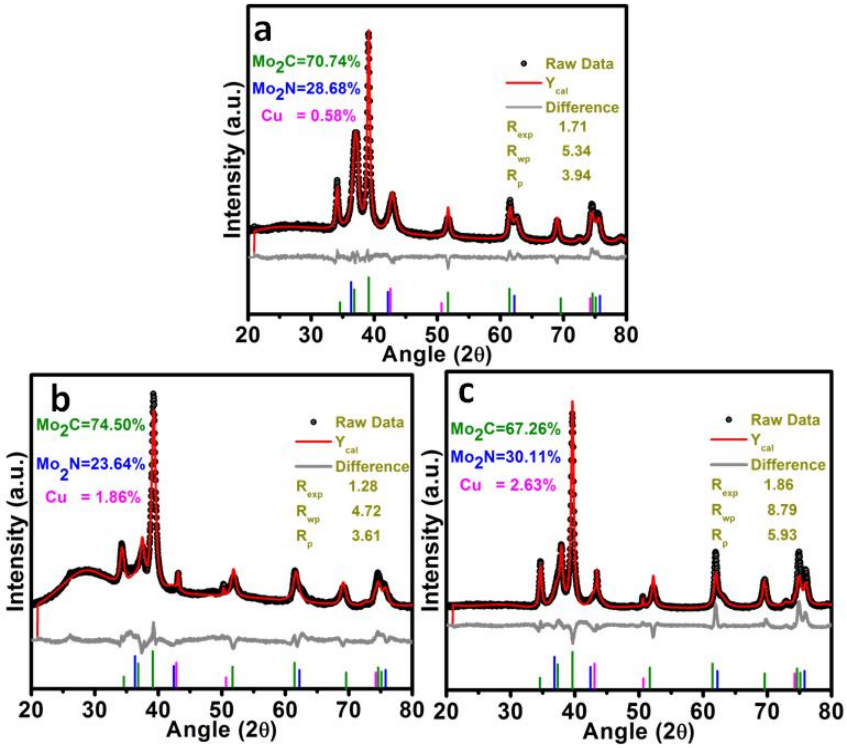

Figure 6.3. *Rietveld refinement of (a) CuMoCat1, (b) CuMoCat2 and (c) CuMoCat3 catalyst. Rietveld analysis of catalyst shows a composition 0.58 %, 1.86 % and 2.63 % of Cu in the CuMoCat1, CuMoCat2 and CuMoCat3 catalyst respectively. The figure typically shows the existence of all three Mo_2C, Mo_2N and Cu phases.*

CuMoCat is displayed in figure 6.1C and 6.1D respectively and the same for CuMoCat1, CuMoCat2 and CuMoCat3 are displayed in figure 6.3(a, b and c respectively).

figure 6.4A-H displays SEM, TEM, HRTEM micrographs and elemental mapping of the CuMoCat catalyst. The SEM micrograph (Figure 6.4A) reveals the heterogeneous morphology consists of feathery structures and nucleated particles that are accumulated in large irregular shaped porous structures. The TEM images uncover detailed structural information about the CuMoCat catalyst, which can be further described by the high-resolution TEM, (Figure 6.4B,

and 6.4C) showing nanoparticles with the diameter 15-25 nm. A zoomed version of the high-resolution TEM image (Figure C') shows the fringes consistent with (100) and (111) planes of hexagonal Mo_2C and cubic Mo_2N with an interplanar spacing of 0.26 nm and 0.24 nm respectively.[32-33]

The molybdenum carbide and nitride nanoparticles interfacially align along with the copper nanoparticles. Such multiple interfaces enhance the mass and charge transfer within the hybrid structure and favour the efficient hydrogen evolution process.[32] The elemental mapping (Figure 6.4D-H) reflects the co-existence of Mo_2C, Mo_2N and Cu nanoparticles on the carbon support in CuMoCat catalyst.

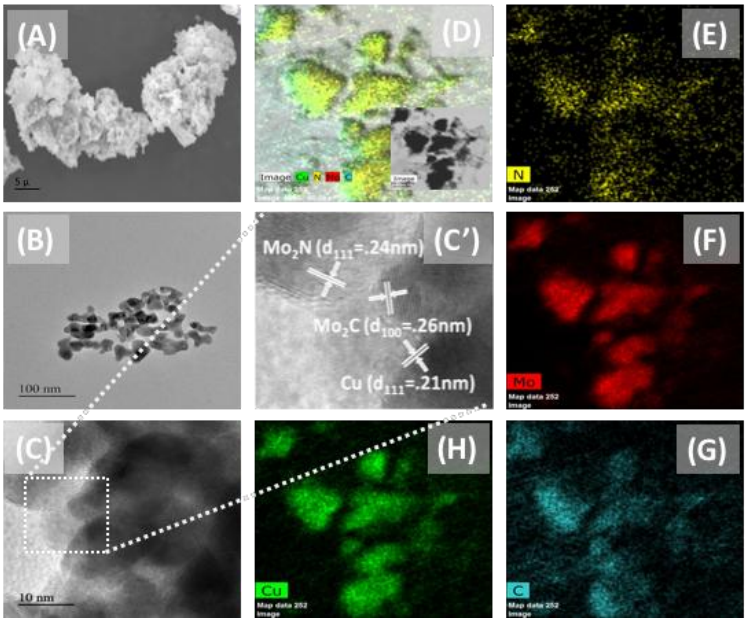

Figure 6.4. *Morphology characterization: SEM image (A) of as obtained CuMoCat catalyst. TEM Image (B) and (C), HRTEM image (C') of catalyst. STEM image (D) and corresponding elemental mapping (E), (F), (G) and (H) of the nanostructure with Nitrogen, Molybdenum, Carbon and Copper elements respectively that illustrate the uniform distribution of these elements within the catalyst.*

The surface area and pore size distribution of nanocomposite were calculated by N_2 adsorption/desorption measurements (Figure 6.5) using BET (Brunauer-Emmett-Teller) and BJH (Barrett–Joyner–Halenda) models. The BET specific surface area calculated for CuMoCat nanocomposite was found to be 113.71 m^2/g. The acquired isotherm displays a classical type-IV

isotherm curve as per IUPAC classification, with weak hysteresis shown at a p/p_0 in the range 0.6–1.0, reveals the mesoporous character of the catalyst. Further, the pore size distribution curve centred at 3.8 nm shows that the maximum pore size lies within the range of 2 to 8 nm (Figure 6.5 inset). Such a porous nature of the catalyst also increases the mass transport and enhances the accessibility of active sites of the catalyst.[35]

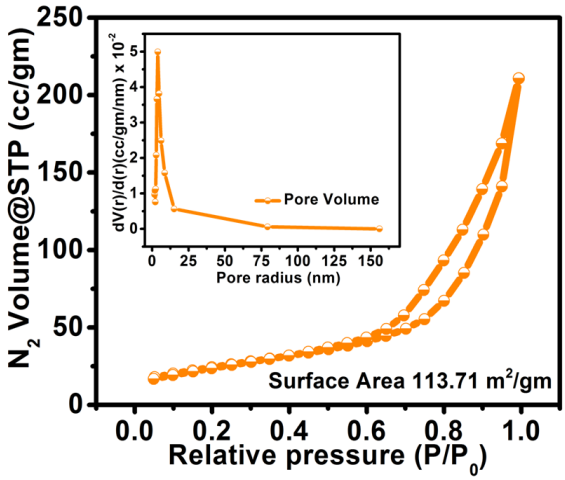

Figure 6.5. *Nitrogen adsorption-desorption BET isotherms and inset showing BJH pore size distribution. The curve represents the mesoporous structure of the catalyst.*

The CuMoCat catalyst was further characterized using X-ray photoelectron spectroscopy, and the corresponding results are displayed in figure 6.6.

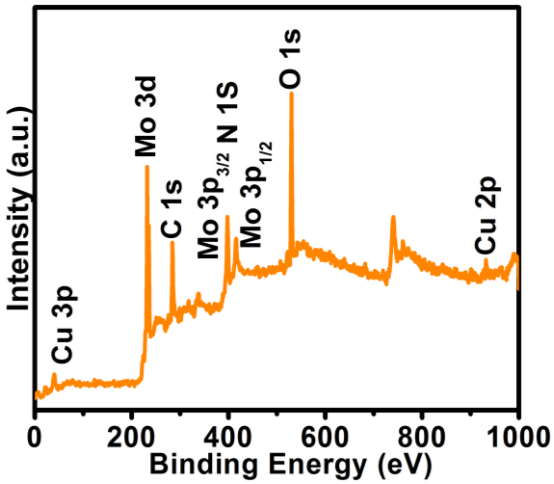

Figure 6.6. *XPS wide angle spectrum of CuMoCat catalyst. The spectrum consists of peaks at binding energy corresponds to Mo, C, N and Cu elements present in the CuMoCat catalyst.*

figure 6.6 shows the survey spectrum with intense signals at 233.6 eV, 285.2 eV, 397.9 eV, 416.5 eV, 532.1 eV and 934.7 eV assigned to Mo 3d, C 1s, Mo 3p, N 1s, O 1s, and Cu 2p respectively present in the catalyst. The high-resolution XPS spectra of Mo 3d (Figure 6.7A) as a result of core level spin-orbit coupling, splits up into Mo $3d_{5/2}$ and Mo $3d_{3/2}$ peaks centred at binding energy values 228.5 eV and 231.6 eV respectively.[36] These peaks indicate the presence of Mo_2C and belong to Mo^{2+} spectral lines. The peaks positioned at 232.4 eV and 235.5 eV confirms the existence of MoO_3 and are belong to Mo^{6+} species.[36] These peaks originate because of surface oxidation of Mo_2C (during the XPS measurements) and show the existence of higher oxidation states of molybdenum oxides. Figure 6.7B displays high-resolution spectra of C 1s that have been deconvoluted into two peaks centred at 284.2 eV and 285.3 eV characteristics to Mo_2C and C—N bond respectively.[37-38]

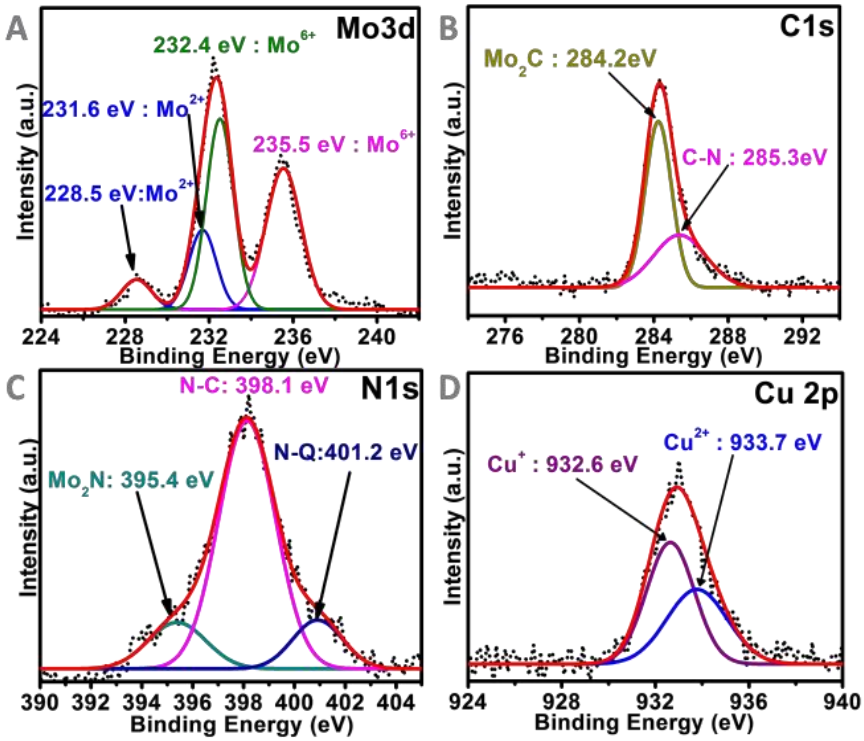

Figure 6.7. *X-ray photoelectron spectroscopy (XPS) of CuMoCat catalyst: High-resolution spectra of Mo3d (A), C1s (B), N1s (C) and Cu2p (D) electron: Experimental data (dotted curve) and fitting results (solid curve). The peaks are assigned by oxidation states of different elements with their corresponding binding energy.*

The asymmetric signal from N 1s spectra shown in figure 6.7C can be deconvoluted into three different peaks with binding energy 395.4 eV, 398.1 eV, and 401.2 eV. The peak appearing at 395.4 eV resulted from Mo $3p_{3/2}$ of Mo_2N and the value of 398.1 eV is aligned with the N 1s peak in N–C bond.[39-40] The peak centred at 401.2 eV assign to the quaternary types N (N-Q) in the material.[41] The binding energy region of copper Cu 2p (Figure 6.7D) can be deconvoluted into two peaks centred at 932.6 eV and 933.7 eV which corresponds to the Cu^+ and Cu^{2+} oxidation state respectively and confirms the presence of copper in the catalyst.[42] Detailed XPS peak parameters are displayed in table 6.1.

Table 6.1. *Table showing the existing elements with corresponding deconvoluted peaks positions and FWHM values*

Element	*Peak*	*BE (eV)*	*FWHM*	*Area (%)*
Mo 3d	*Mo^{2+}*	*228.5 and 231.6*	*1.613 and 1.613*	*6.82 and 16.43*
	Mo^{6+}	*232.4 and 235.5*	*1.734 and 1.734*	*37.68 and 39.05*
C 1s	*Mo_2C*	*284.2*	*1.671*	*61.55*
	C-N	*285.3*	*3.317*	*38.44*
N 1s	*Mo_2N*	*395.4*	*2.674*	*23.65*
	N-C	*398.1*	*2.638*	*51.32*
	N-Q	*401.2*	*2.312*	*25.03*
Cu 2p	*Cu^+*	*932.6*	*2.391*	*56.26*
	Cu^{2+}	*933.7*	*3.034*	*43.73*

The HER performance of CuMoCat catalyst was preliminarily evaluated using a standard three-electrode setup, consisting of a carbon-based electrode, glassy carbon electrode and Ag/AgCl as a counter, working and reference electrodes respectively. Commercially available platinum (Pt/C), CuMoCat, MoCat-CN, CuMoCat1 and CuMoCat2 were coated on working electrode (3 mm in diameter) have been investigated under the same measurement condition (see Experimental section). figure 6.8A displays the HER polarization curves acquired with a sweep rate of 5 mV s^{-1}.

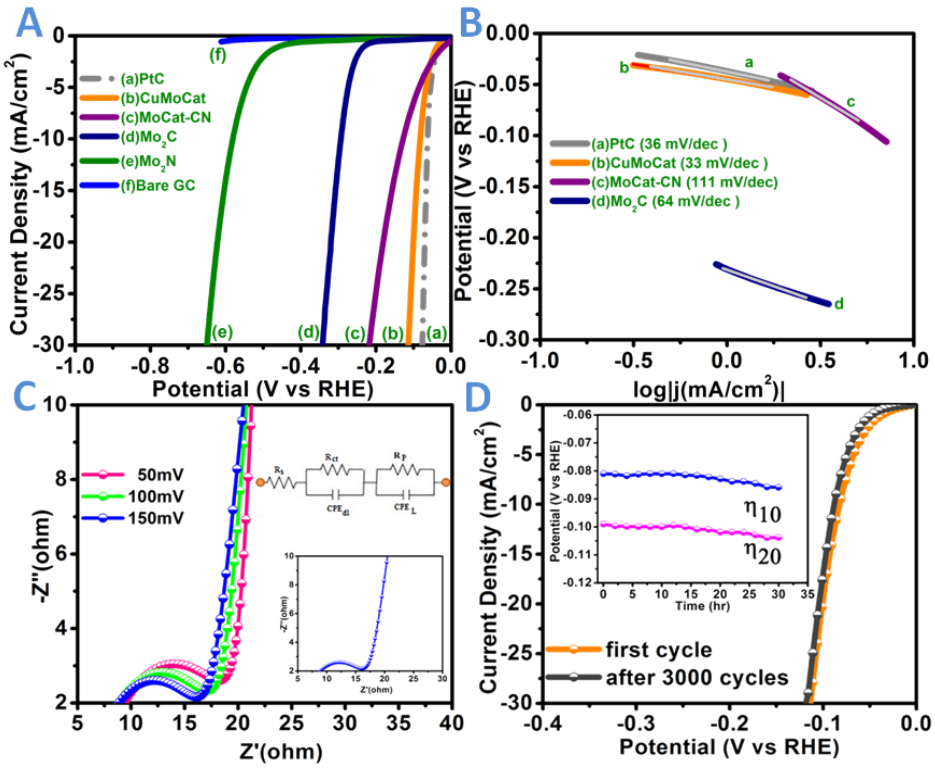

Figure 6.8. *Electrochemical Study for HER in 0.5 M H_2SO_4 acidic medium. (A) Polarization curves (iR-corrected) of CuMoCat and other electrodes with (B) the corresponding Tafel plots (C) EIS Nyquist Plot (equivalent circuit inset) of the electrode @50 mV, @100 mV and @150 mV (inset shows zoomed Nyquist plot of electrode @150 mV) (D) Repetitive LSV durability curve at 1st and 3000th cycle (inset t-V he plot at constant current density 10 $mAcm^{-2}$ and 20 $mAcm^{-2}$.*

The catalytic activity of the material follows the trends Pt/C > CuMoCat > MoCat-CN and the corresponding overpotential at a current density of 10 $mAcm^{-2}$ are 62, 82 and 127 mV, respectively. For a comparative study, Mo_2C and Mo_2N catalysts were studied with the same mass loading, which displayed an overpotential of 294 and 588 mV respectively. Moreover, a steady-state condition has been achieved through cyclic voltammetry (CV) by 20 repetitive cycle tests with a scan rate of 50 mV s^{-1} before data measurement. The polarisation curves for other catalysts CuMoCat1, CuMoCat2 and CuMoCat3 are shown in figure 6.9. The polarization curve shows that the other composition of Mo_2C and Mo_2N along with the copper doping does not give such catalytic activity as shown by the CuMoCat catalyst. The overpotential obtained for CuMoCat1, CuMoCat2 and CuMoCat3 is 112 mV, 147 mV and 163 mV respectively which is far above the CuMoCat Catalyst.

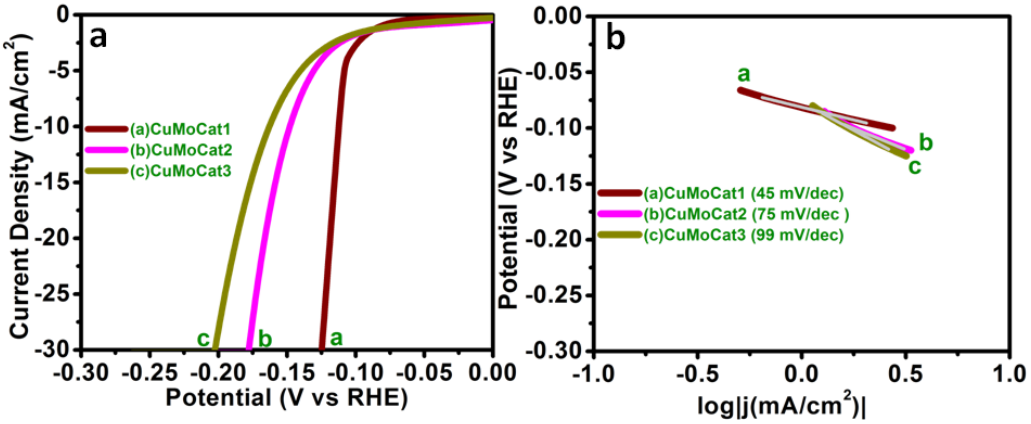

Figure 6.9. *(a) Polarization curves and corresponding (b) Tafel slope of CuMoCat1, CuMoCat2 and CuMoCat3 catalysts in 0.5 M H_2SO_4 solution.*

The possible mechanistic insights of the hydrogen evolution reaction of the materials may be manifested through the values of onset potential, overpotential (η_{10}), Tafel slope values, EIS studies etc. One of the most important parameters is the Tafel slope value, which can be used to interpret the reaction pathways and kinetics involved in HER process. The Tafel slope value can be determined by fitting the linear portions of the Tafel plots with equation $\eta = b \log j + a$, where j is the current density and b is the Tafel slope. The Tafel slope value indicates how much amount of overpotential needs to be increased in order to increase the reaction rate by a factor of ten.

For the Hydrogen Evolution Reaction in acidic media, three possible reaction steps are accepted widely for explaining the mechanism. The first step (1) proceeds through a Volmer reaction (Primary discharge step):

$$H_3O^+ + e^- \rightarrow H_{ads} + H_2O \qquad b = 2.3RT/\alpha F \approx 120mV/dec \qquad (6.3)$$

Where R denotes ideal gas constant, T is the absolute temperature, $\alpha \approx 0.5$ is the symmetry coefficient, and F is the Faraday constant. The value greater than or equal to 40 mV dec^{-1} indicates the Volmer–Heyrovsky mechanism which corresponds to the electrochemical desorption step 2 (Equation 6.4) as rate-limiting.[43-44]

$$H_{ads} + H_3O^+ + e^- \rightarrow H_2 + H_2O \qquad b = 2.3RT/(1+\alpha F) \approx 40mV \qquad (6.4)$$

$$H_{ads} + H_{ads} \rightarrow H_2 \qquad b = 2.3RT/2\alpha F) \approx 30mV \qquad (6.5)$$

A Tafel slope value less than or equal to 30 mV dec^{-1} corresponds to the Volmer–Tafel mechanism where recombination step 3 (Equation 6.5) is the rate-determining step. Commercially available Pt/C catalyst yields a Tafel slope value of 36 mV dec^{-1} while CuMoCat has exhibited a better Tafel slope value of 33 mVdec^{-1} (Figure 6.8B). These results indicate that the electron transfer is a fast process and the reaction proceeds through Volmer-Heyrovsky (electrochemical desorption) mechanism. Similarly, CuMoCat1 and Mo_2C have displayed a Tafel slope value 45 mV dec^{-1} and 64 mV dec^{-1} respectively and show less activity towards the hydrogen evolution reaction. Exchange current density (j_0) obtained from the Tafel plot is another important factor which describes the inherent activity of electrocatalysts. The exchange current density (j_0) obtained for CuMoCat was calculated to be 3.12 x 10^{-2} mA cm^{-2} and the details are presented in table 6.2.

***Table 6.2**. Table showing all electrochemical kinetic parameters of all the electrocatalysts*

Catalyst	*Onset (vs RHE)*	*η_{10} (vs RHE)*	*η_{20} (vs RHE)*	*η_{30} (vs RHE)*	*Tafel Slope (mV/dec)*	*Exchange Current Density (mA/cm^2)*
CuMoCat	*40 mV*	*82 mV*	*101 mV*	*112 mV*	*33*	*3.12×10^{-2}*
CuMoCat1	*77 mV*	*112 mV*	*119 mV*	*125 mV*	*45*	*2.97×10^{-2}*
MoCat-CN	*26 mV*	*127 mV*	*182 mV*	*217 mV*	*111*	*2.43×10^{-3}*
CuMoCat2	*78 mV*	*147 mV*	*166 mV*	*178 mV*	*75*	*1.96×10^{-3}*
CuMoCat3	*75 mV*	*163 mV*	*186 mV*	*202 mV*	*99*	*1.09×10^{-3}*
Mo_2C	*233 mV*	*294 mV*	*320 mV*	*340 mV*	*64*	*1.17×10^{-4}*

Electrochemical impedance spectroscopy (EIS) was carried out to explore the electrode kinetics.[45] EIS measurements were conducted within a frequency range of 0.1 Hz to 100 kHz. The Nyquist plot with an equivalent circuit provides the ionic and charge transfer resistances of catalysts in a 0.5 M H_2SO_4. The curve was fitted with the simulated one following an equivalent circuit consists of classical two-time constants R_p-CPE_L and R_{ct}-CPE_{dl}, displayed in figure 6.8C. The term R_s corresponds to the uncompensated electrolyte solution resistance and the frequency-dependent component, R_p-CPE_L (constant phase element) can be correlated with the surface porosity of the catalyst while R_{ct}-CPE_{dl} indicates the charge transfer resistance of the catalyst in the electrolyte.[46-47] The resistance R_{ct} at the low-frequency region (charge-transfer

resistance) was calculated from the equivalent circuit obtained from the fitted plot. CuMoCat exhibits a charge transfer resistance of 14 ohms at an applied potential of 50 mV.

The CuMoCat is highly stable in the acidic medium during the operation of the reaction and does not show a significant change in the overpotential even after 3000 catalytic cycles as shown in the linear sweep voltammograms in figure 6.8D. The applied potential vs time plot shown in the inset of figure 6.8D, reveals that the overpotential is quite steady at higher current densities even after 3000 catalytic cycles. The overpotential at 10 $mAcm^{-2}$ current density, increased by 5 mV at the end of the catalytic cycle. All these results indicate that CuMoCat nanocomposite is a highly durable HER catalyst.

Theoretical studies demonstrate how Cu affects the electronic properties of Mo_2N/Mo_2C hybrid composite. In the present work, specific adsorption sites on Cu-doped Mo_2N/Mo_2C (CuMoCat) and un-doped Mo_2N/Mo_2C (MoCat-CN) have been explored for the adsorption of single H-atom. To describe the electrocatalytic properties of CuMoCat, 'Mo' site, 'N' site and 'Cu' site near the interface of Mo_2N and Mo_2C, have been considered: The carbon atoms of Mo_2C are not exposed to the surface of the catalyst; hence, adsorption studies are not carried out at these sites.

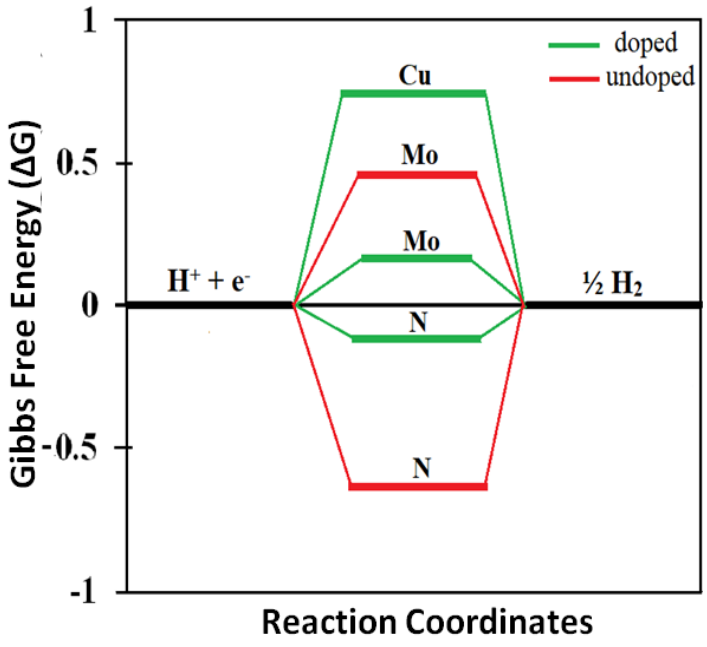

Figure 6.10. *The Free Energy diagram for 'Mo' and 'N' hydrogen adsorptions sites of CuMoCat (depicted by green lines) displays, a shift of free energy making these more favourable for HER with respect to Mo/N sites of the un-doped catalyst (depicted by red lines).*

Gibbs free energy is one of the most significant parameters used to examine the catalytic activity of material for hydrogen evolution. On a different ground, recalling the above-mentioned mechanism, hydrogen evolution reaction can also be described as (1): $H^+ + e^- + $ '*' → H*, revealing H^+ binding to the catalyst surface, where "*" indicates the binding sites; The next step involved the desorption of H_2 molecule from the surface (2): 2H* → H_2 + 2'*' or H^+ + e- → H_2 + '*'. The theoretical calculations of thermochemistry revealed here, do not reflect a precise mechanism involved in the 2nd step. However, an essential criterion for a catalyst to behave ideally, is that Gibb's free energy of adsorbed hydrogen must be proximate to that of the reactant or product (i.e., $\Delta G_H \approx 0$). By carefully looking at the adsorption data, it has been observed that Cu site itself shows the positive value for free energy change; however, it enhances the catalytic activity for HER on the remaining possible adsorption sites of the catalyst. For instance, Mo atom possesses high positive ΔG value without any dopant and in the presence of Cu dopant, the value reduced approximately by 4 times enhancing the catalytic performance for Mo site. Similarly, for N-atom near the interface, the study reflects very high negative value which is reduced by ~ 6 times for the Cu doped catalyst as compared to un-doped one. In other words, in the presence of Cu atom as dopant ΔG value tends to approach 0 for both Mo and N sites, as shown in figure 6.10. It has also been noticed that there is no significant change in bond length between the adsorption site and H-atom for all the cases. The calculated results reveal that Cu-doped Mo_2N/Mo_2C (CuMoCat) has excellent adsorption properties for H-atom than the undoped Mo_2N/Mo_2C. Calculated adsorption energy, Gibbs free energy and bond length are listed in table 6.3.

Table 6.3. *Theoretically calculated values of Bond length, Adsorption Energy and Gibbs free energy in the catalyst*

Adsorption site	*Bond length (Å)*		*ΔE_{ads} (eV)*		*ΔG (eV)*	
	doped	*undoped*	*doped*	*undoped*	*doped*	*undoped*
Mo	*1.731*	*1.695*	*-0.0745*	*-0.2119*	*+0.1655*	*-0.452*
N	*1.026*	*1.025*	*-0.346*	*-0.9330*	*-0.106*	*-0.693*
Cu	*1.534*	-	*0.463*	-	*+0.7034*	-

6.4. Conclusion

Copper doped Mo_2C/Mo_2N nanocomposite (CuMoCat catalyst) has been synthesized *in-situ* via a temperature-programmed solid-state reaction under ammonia and argon atmosphere. The catalyst exhibits high HER performance with an overpotential of 82 mV to achieve a cathodic current density of 10 $mAcm^{-2}$, a Tafel slope of 33 $mVdec^{-1}$, and also displays excellent long term durability up to 3000 HER cycles. A series of catalysts starting with CuMoCat, CuMoCat1, CuMoCat2 and CuMoCat3 were synthesized by varying the amount of copper dopant in the nanocomposite while keeping all other parameters unchanged. Rietveld analysis reveals that 1.14 % of copper incorporation results in the formation of CuMoCat catalyst, which outperforms other three catalysts i.e. CuMoCat1(0.58% of Cu), CuMoCat2 (1.86% of Cu) and CuMoCat3 (2.63% of Cu). The catalytic activity indicates that an optimized amount of copper incorporated into the nanocomposite can only result in the enhancement of hydrogen adsorption and desorption process onto the catalyst surface. The theoretical studies are also in-line with the experimental findings and supporting the above statement. The Cu doping brings a change in the electronic structure at 'Mo' and 'N' sites in the CuMoCat catalyst, which improves the overall adsorption and desorption process of hydrogen on its surface. The Free Energy diagram for hydrogen evolution reaction on specific active sites of CuMoCat displays, a shift in free energy making these more catalytically favourable compared to the un-doped catalyst. With High HER performance and excellent long term durability, CuMoCat shows a promising possibility towards using non-noble, HER electrocatalyst in acidic conditions. This work illustrates how the promoter elements can be used in a multiphasic nanocomposite to enhance the overall catalytic activity.

Note:

- The permission has been granted by the author and corresponding author of the published paper prior to adopting in the present thesis. The associated relevant publication is:

Rajinder Kumar, Zubair Ahmed, Harwinder Kaur, Chandan Bera and Vivek Bagchi "Probing into the effect of heterojunctions between $Cu/Mo_2C/Mo_2N$ on HER performance" ***Catal. Sci. Technol., 2020,10, 2213-2220, https://doi.org/10.1039/C9CY02526J***

References

1. Attari, S. Z.; Krantz, D. H.; Weber, E. U., Climate change communicators' carbon footprints affect their audience's policy support. *Climatic Change* **2019,** *154* (3), 529-545.

2. Hosseini, S. E.; Wahid, M. A., Hydrogen production from renewable and sustainable energy resources: Promising green energy carrier for clean development. *Renewable and Sustainable Energy Reviews* **2016,** *57*, 850-866.

3. Althor, G.; Watson, J. E. M.; Fuller, R. A., Global mismatch between greenhouse gas emissions and the burden of climate change. *Scientific Reports* **2016,** *6* (1), 20281.

4. Erickson, L. E., Reducing greenhouse gas emissions and improving air quality: Two global challenges. *Environmental progress & sustainable energy* **2017,** *36* (4), 982-988.

5. Badal, F. R.; Das, P.; Sarker, S. K.; Das, S. K., A survey on control issues in renewable energy integration and microgrid. *Protection and Control of Modern Power Systems* **2019,** *4* (1), 8.

6. Leitner, W.; Quadrelli, E. A.; Schlögl, R., Harvesting renewable energy with chemistry. *Green Chemistry* **2017,** *19* (10), 2307-2308.

7. Staffell, I.; Scamman, D.; Velazquez Abad, A.; Balcombe, P.; Dodds, P. E.; Ekins, P.; Shah, N.; Ward, K. R., The role of hydrogen and fuel cells in the global energy system. *Energy & Environmental Science* **2019,** *12* (2), 463-491.

8. Roger, I.; Shipman, M. A.; Symes, M. D., Earth-abundant catalysts for electrochemical and photoelectrochemical water splitting. *Nature Reviews Chemistry* **2017,** *1*, 0003.

9. Abdalla, A. M.; Hossain, S.; Nisfindy, O. B.; Azad, A. T.; Dawood, M.; Azad, A. K., Hydrogen production, storage, transportation and key challenges with applications: A review. *Energy Conversion and Management* **2018,** *165*, 602-627.

10. Rosen, M. A.; Koohi-Fayegh, S., The prospects for hydrogen as an energy carrier: an overview of hydrogen energy and hydrogen energy systems. *Energy, Ecology and Environment* **2016,** *1* (1), 10-29.

11. Nikolaidis, P.; Poullikkas, A., A comparative overview of hydrogen production processes. *Renewable and Sustainable Energy Reviews* **2017,** *67*, 597-611.

12. Chen, Y.; Yu, G.; Chen, W.; Liu, Y.; Li, G.-D.; Zhu, P.; Tao, Q.; Li, Q.; Liu, J.; Shen, X., Highly active, nonprecious electrocatalyst comprising borophene subunits for the hydrogen evolution reaction. *Journal of the American Chemical Society* **2017,** *139* (36), 12370-12373.

13. Safizadeh, F.; Ghali, E.; Houlachi, G., Electrocatalysis developments for hydrogen evolution reaction in alkaline solutions–a review. *international journal of hydrogen energy* **2015,** *40* (1), 256-274.

14. Miao, M.; Pan, J.; He, T.; Yan, Y.; Xia, B. Y.; Wang, X., Molybdenum Carbide-Based Electrocatalysts for Hydrogen Evolution Reaction. *Chemistry–A European Journal* **2017,** *23* (46), 10947-10961.

15. Ma, Y.; Guan, G.; Hao, X.; Cao, J.; Abudula, A., Molybdenum carbide as alternative catalyst for hydrogen production–A review. *Renewable and Sustainable Energy Reviews* **2017,** *75*, 1101-1129.

16. Zhu, Y.; Chen, G.; Xu, X.; Yang, G.; Liu, M.; Shao, Z., Enhancing electrocatalytic activity for hydrogen evolution by strongly coupled molybdenum nitride@ nitrogen-doped carbon porous nano-octahedrons. *ACS Catalysis* **2017,** *7* (5), 3540-3547.

17. Li, D. J.; Maiti, U. N.; Lim, J.; Choi, D. S.; Lee, W. J.; Oh, Y.; Lee, G. Y.; Kim, S. O., Molybdenum sulfide/N-doped CNT forest hybrid catalysts for high-performance hydrogen evolution reaction. *Nano letters* **2014,** *14* (3), 1228-1233.

18. Ren, H.; Sun, S.; Cui, J.; Li, X., Synthesis, functional modifications, and diversified applications of molybdenum oxides micro-/nanocrystals: a review. *Crystal Growth & Design* **2018,** *18* (10), 6326-6369.

19. Xiao, P.; Chen, W.; Wang, X., A Review of Phosphide-Based Materials for Electrocatalytic Hydrogen Evolution. *Advanced Energy Materials* **2015,** *5* (24), 1500985.

20. Wang, Y.; Kong, B.; Zhao, D.; Wang, H.; Selomulya, C., Strategies for developing transition metal phosphides as heterogeneous electrocatalysts for water splitting. *Nano Today* **2017,** *15*, 26-55.

21. Zhang, J.; Wang, T.; Pohl, D.; Rellinghaus, B.; Dong, R.; Liu, S.; Zhuang, X.; Feng, X., Interface Engineering of MoS_2/Ni_3S_2 Heterostructures for Highly Enhanced Electrochemical Overall-Water-Splitting Activity. *Angewandte Chemie International Edition* **2016,** *55* (23), 6702-6707.

22. Wang, J.; Cui, W.; Liu, Q.; Xing, Z.; Asiri, A. M.; Sun, X., Recent Progress in Cobalt-Based Heterogeneous Catalysts for Electrochemical Water Splitting. *Advanced Materials* **2016,** *28* (2), 215-230.

23. Gao, Q.; Zhang, W.; Shi, Z.; Yang, L.; Tang, Y., Structural Design and Electronic Modulation of Transition-Metal-Carbide Electrocatalysts toward Efficient Hydrogen Evolution. *Advanced Materials* **2019,** *31* (2), 1802880.

24. Wei, J.; Zhou, M.; Long, A.; Xue, Y.; Liao, H.; Wei, C.; Xu, Z. J., Heterostructured Electrocatalysts for Hydrogen Evolution Reaction Under Alkaline Conditions. *Nano-Micro Letters* **2018,** *10* (4), 75.

25. Lau, T. H.; Lu, X.; Kulhavý, J.; Wu, S.; Lu, L.; Wu, T.-S.; Kato, R.; Foord, J. S.; Soo, Y.-L.; Suenaga, K., Transition metal atom doping of the basal plane of MoS_2 monolayer nanosheets for electrochemical hydrogen evolution. *Chemical science* **2018,** *9* (21), 4769-4776.

26. Pan, Y.; Liu, Y.; Lin, Y.; Liu, C., Metal doping effect of the M–Co_2P/Nitrogen-Doped carbon nanotubes (M= Fe, Ni, Cu) hydrogen evolution hybrid catalysts. *ACS applied materials & interfaces* **2016,** *8* (22), 13890-13901.

27. Song, L.; Khoerunnisa, F.; Gao, W.; Dou, W.; Hayashi, T.; Kaneko, K.; Endo, M.; Ajayan, P. M., Effect of high-temperature thermal treatment on the structure and adsorption properties of reduced graphene oxide. *Carbon* **2013,** *52*, 608-612.

28. Jiao, Y.; Ma, F.; Zhou, L.; Ng, Y. H.; Bell, J.; Tretiak, S.; Du, A., Ab initio study of two-dimensional PdPS as an ideal light harvester and promising catalyst for hydrogen evolution reaction. *Materials Today Energy* **2018,** *7*, 136-140.

29. J. K. Nørskov, T. B., A. Logadottir, J. R. Kitchin, J. G. Chen, S. Pandelov,; Stimming, U., Trends in the exchange current for hydrogen evolution. *Journal of The Electrochemical Society* **2005,** *152*, J23–J26.

30. Kresse, G.; Furthmüller, J., Efficiency of ab-initio total energy calculations for metals and semiconductors using a plane-wave basis set. *Computational Materials Science* **1996,** *6* (1), 15-50.

31. Perdew, J. P.; Burke, K.; Ernzerhof, M., Generalized Gradient Approximation Made Simple. *Physical Review Letters* **1996,** *77* (18), 3865-3868.

32. Liang, P.; Gao, H.; Yao, Z.; Jia, R.; Shi, Y.; Sun, Y.; Fan, Q.; Wang, H., Simple synthesis of ultrasmall β-Mo_2C and α-MoC_{1-x} nanoparticles and new insights into their catalytic mechanisms for dry reforming of methane. *Catalysis Science & Technology* **2017,** *7* (15), 3312-3324.

33. Song, Y.-J.; Yuan, Z.-Y., One-pot Synthesis of Mo_2N/NC Catalysts with Enhanced Electrocatalytic Activity for Hydrogen Evolution Reaction. *Electrochimica Acta* **2017,** *246*, 536-543.

34. Yin, Z.; Lee, C.; Cho, S.; Yoo, J.; Piao, Y.; Kim, Y. S., Facile Synthesis of Oxidation-Resistant Copper Nanowires toward Solution-Processable, Flexible, Foldable, and Free-Standing Electrodes. *Small* **2014,** *10* (24), 5047-5052.

35. Zhang, J.-W.; Gong, S.; Mahmood, N.; Pan, L.; Zhang, X.; Zou, J.-J., Oxygen-doped nanoporous carbon nitride via water-based homogeneous supramolecular assembly for photocatalytic hydrogen evolution. *Applied Catalysis B: Environmental* **2018,** *221*, 9-16.

36. Zhang, K.; Li, C.; Zhao, Y.; Yu, X.; Chen, Y., Porous one-dimensional Mo_2C–amorphous carbon composites: high-efficient and durable electrocatalysts for hydrogen generation. *Physical Chemistry Chemical Physics* **2015,** *17* (25), 16609-16614.

37. Zhao, J.; Wang, B.; Yu, W.; Li, Z.; Xu, Y.; Ma, X., Carbon-Limited Conversion of Molybdenum Carbide into Curved Ultrasmall Monolayer Molybdenum Disulfide under Effects of ZrO_2 Crystal Phases for Efficient Sulfur-Resistant Methanation. *ChemCatChem* **2019,** *11* (13), 3046-3053.

38. Tang, Y.-J.; Liu, C.-H.; Huang, W.; Wang, X.-L.; Dong, L.-Z.; Li, S.-L.; Lan, Y.-Q., Bimetallic Carbides-Based Nanocomposite as Superior Electrocatalyst for Oxygen Evolution Reaction. *ACS Applied Materials & Interfaces* **2017,** *9* (20), 16977-16985.

39. Ojha, K.; Saha, S.; Banerjee, S.; Ganguli, A. K., Efficient Electrocatalytic Hydrogen Evolution from MoS_2-Functionalized Mo_2N Nanostructures. *ACS Applied Materials & Interfaces* **2017,** *9* (23), 19455-19461.

40. Liu, Q.; Liu, T.; Fang, Q. F.; Liang, F. J.; Wang, J. X., Preparation and characterization of nanocrystalline composites Mo–C–N hard films. *Thin Solid Films* **2006,** *503* (1), 79-84.

41. Pels, J. R.; Kapteijn, F.; Moulijn, J. A.; Zhu, Q.; Thomas, K. M., Evolution of nitrogen functionalities in carbonaceous materials during pyrolysis. *Carbon* **1995,** *33* (11), 1641-1653.

42. Platzman, I.; Brener, R.; Haick, H.; Tannenbaum, R., Oxidation of Polycrystalline Copper Thin Films at Ambient Conditions. *The Journal of Physical Chemistry C* **2008,** *112* (4), 1101-1108.

43. Zeng, M.; Li, Y., Recent advances in heterogeneous electrocatalysts for the hydrogen evolution reaction. *Journal of Materials Chemistry A* **2015,** *3* (29), 14942-14962.

44. Shinagawa, T.; Garcia-Esparza, A. T.; Takanabe, K., Insight on Tafel slopes from a microkinetic analysis of aqueous electrocatalysis for energy conversion. *Scientific reports* **2015,** *5*, 13801-13801.

45. Anantharaj, S.; Ede, S. R.; Karthick, K.; Sam Sankar, S.; Sangeetha, K.; Karthik, P. E.; Kundu, S., Precision and correctness in the evaluation of electrocatalytic water splitting: revisiting activity parameters with a critical assessment. *Energy & Environmental Science* **2018,** *11* (4), 744-771.

46. Mei, B.-A.; Munteshari, O.; Lau, J.; Dunn, B.; Pilon, L., Physical Interpretations of Nyquist Plots for EDLC Electrodes and Devices. *The Journal of Physical Chemistry C* **2018,** *122* (1), 194-206.

47. Dhillon, S.; Kant, R., Theory for electrochemical impedance spectroscopy of heterogeneous electrode with distributed capacitance and charge transfer resistance. *Journal of Chemical Sciences* **2017,** *129* (8), 1277-1292.

Chapter 7

Molybdenum carbide and molybdenum phosphide based hybrid materials for mutually enhanced hydrogen evolution reaction

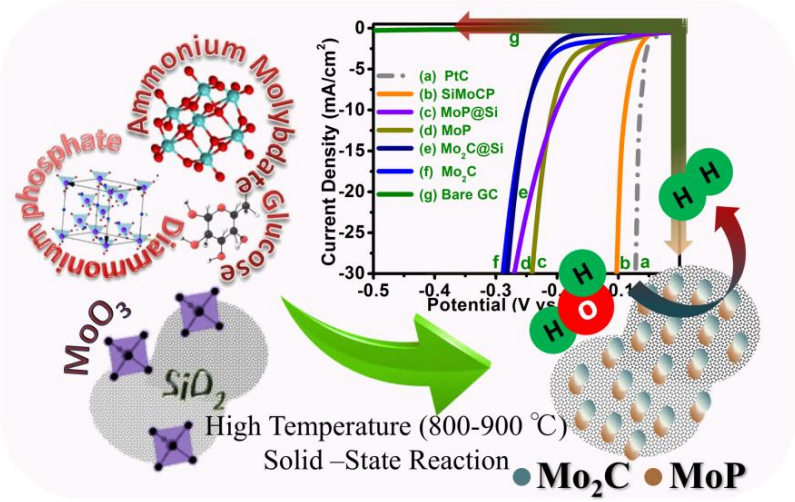

Abstract: *The increase of greenhouse gases which majorly consists of carbon dioxide have been showing devastating effects on the environment and causing a huge climate change. The exploration of low cost and earth-abundant electrocatalysts for hydrogen generation process is an emerging area of research. Profound catalyst tailoring with different composition of Mo_2C and MoP phases on porous support for crafting large HER active sites increases the catalytic activity in many folds. Herein, a porous silica-supported molybdenum phosphide and molybdenum carbide nanoparticles (SiMoCP) has been synthesized. The intermingled porous molybdenum carbide and molybdenum phosphide nanohybrid shows excellent catalytic activity towards hydrogen evolution. Such modified nanostructured electrocatalyst enhances the electrode-electrolyte interaction and suppresses the charge transfer resistance. As a result, electrocatalyst (SiMoCP) accomplished very high HER activity with an onset potential of 53 mV and an overpotential of 88 mV at a current density of 10 $mAcm^{-2}$ in the acidic medium. Furthermore, the SiMoCP catalyst showed a Tafel slope value of 37 $mVdec^{-1}$ with long term durability of 5000 cycles.*

Brief Outcome: The molybdenum carbide and molybdenum phosphide have been known as HER active catalyst. In this chapter, a composite of molybdenum carbide and molybdenum phosphide has been synthesized with the partial carburisation and phosphorization of the oxide material at high temperature. The major challenge in electrochemistry of HER electrocatalyst is durability. The synthesis of highly durable hydrogen evolution electrocatalyst from the non-noble metal group like is a major challenge. Herein, a biphasic composite of molybdenum derivatives in assistance with the silica shows excellent durability in the acidic medium for hydrogen evolution reaction. The in-situ synthesis of the molybdenum carbide and molybdenum phosphide synergistically enhances the catalytic activity of the material. The synthesis involves the establishment of the mutual synergy between the two phases along with the incorporation of silica. The inherent property of silica provides a high surface area material with a large number of active sites. The synergistic enhancement of activity gives excellent durability of 5000 cycles to the molybdenum carbide and molybdenum phosphide (SiMoCP) catalyst. The catalyst achieves a current density of 3.56×10^{-2} *mA/cm*^{2} *in acidic media. The characterisation of the material indicates that superior catalytic activity that attributed form the electrode conductivity improvement for charge transfer. This study shows that molybdenum carbide is potentially a highly active non-noble metal electrocatalyst for hydrogen production if it combines with the other synergic phase that enhances the charge transfer through the interface.*

7.1. Introduction

The consequences of global warming have been showing its grievous picture in the form of extreme floods, rising temperature and other catastrophes. It is a high time that people should swap conventional energy resources with the new renewable energy source. Hydrogen emerges out to be one of the best alternatives to meet future energy needs. Electrocatalytic hydrogen production could be a mercantile method to globally persuade a clean and carbon-free energy demand.[1-2] Noble metals like Pt and Pt-based materials are the best known HER electrocatalysts which exhibit low overpotential and high current densities but are restricted by the extremely high cost and low abundance that weigh down the industrial production.[3-4] Finding earth-abundant alternatives to these noble metals which have similar or better activity could be used to scale up the hydrogen production.[5] These challenges have motivated people to make huge efforts in the exploration of low cost and earth-abundant transition metals compounds including molybdenum sulphide,[6-8] molybdenum carbide,[9-11] molybdenum phosphide and molybdenum nitride etc. for HER process.[12-15] The inadequacies based on the overall performance of these materials towards HER, confine the viability of taking a laboratory-scale hydrogen evolution with ideal experimental conditions to a large scale industrial production. The enormous efforts have been put forward focusing the activity-enhancement through designing new catalysts. A synergic approach among specific solids have been explored to exploit the mutual coactions of these materials.[16] These strategies based on synergistic effects due to the combination of different phases further excavate the potential of Mo-based electrocatalysts.[17-18] The Mo_2C/MoP binary phase composites show encouraging results in the process by the significant decrease in the overpotential value.[19] The combination of electron-rich phosphorous with carbon remarkably enhances the overall HER activity.[20] However, the concomitant carbonization, nitridation and phosphorization is a challenging task. The molybdenum phosphide and molybdenum carbide derivatives are foremost in molybdenum family which were used for HER applications.[9, 13, 21-22]A long series of carbon-based materials such as reduced graphene oxide, carbon nanotubes (CNTs), carbon black have been used for supporting molybdenum based compounds because of their high electron conductivity, large surface area and extremely high stability.[17, 23] However, the strategically enhanced active sites and surface area by using mesoporous silica with Mo_2C/MoP nanoparticles is quite inspiring. The catalyst with evenly distributed nanoparticles provides the maximum probability of H^+ interaction between the catalyst surface and the electrolyte. The overall feature of such porous electrocatalyst contributes to the excellent HER activity in the acidic medium.[24-25] Herein, we report a composite (SiMoCP) synthesized from molybdenum phosphide and molybdenum carbide grown over the mesoporous silica. The

catalyst exhibits an excellent HER performance with an overpotential of 88 mV achieved at a current density of 10 $mAcm^{-2}$ in acidic medium. There is no significant change in overpotential even after 5000 repetitive catalytic cycles which be a shred of evidence for the excellent durability of the catalyst towards HER process. Theoretical studies are also carried out to support the activity of the HER catalyst. A DFT calculation along the interface of the Mo_2C–MoP nanoparticles exhibits free energy which is much more favourable than the individual phases.

7.2. Experimental Section

7.2.1. Materials

All the chemicals were of analytical grade and used without any further purification. For the synthesis of the catalyst and electrode fabrication, the following chemicals were used. Ammonium molybdenum tetrahydrate ($(NH_4)_6.Mo_7O_{24}.4H_2O$, 99.98%); Tetraethyl orthosilicate ($(C_2H_5O)_4Si$, 98%); Diammonium hydrogen phosphate ($(NH_4)_2HPO_4$, 98%); Ammonium Hydroxide ($NH_3.H_2O$, 25%); N, N Dimethylformamide ($HCON(CH_3)_2$, 98%); Glucose ($C_6H_{12}O_6$); Nafion perfluorinated resin solution, were purchased from Sigma Aldrich. Other chemicals namely, Citric acid ($C_6H_8O_7$, 99.9%); Ammonium Hydroxide ($NH_3.H_2O$, 25%), Ethanol (C_2H_5OH), Hydrochloric Acid (HCl) were procured from Merck chemicals; Deionised water was used in all the synthesis process.

7.2.2. Methodology

7.2.2.1. Synthesis of Catalyst

The synthesis involves the two major steps. First, the preparation of metal precursor and then the calcination of the molybdenum precursor by temperatures controlled annealing in an argon atmosphere at different time periods.

7.2.2.2. Synthesis of catalyst precursor (First Step)

(a). Synthesis of hydrolysed TEOS: The hydrolysed TEOS has been synthesized through Stöber-Fink-Bohn method with slight modification.[26] A solution of 25 ml ethanol with 0.022 moles of TEOS has been prepared and 15 ml of ammonium hydroxide (12%) was gently added into it. The solution was sonicated and kept for overnight stirring. The turbid solution as obtained used as a precursor for the preparation of mesoporous silica-supported MoO_3 nanoparticles.

(b). Synthesis of molybdenum precursor

(i) Synthesis of silica assisted molybdenum oxide (MoO_3@Si): A hydrothermal reaction was carried out using ammonium molybdenum tetrahydrate $(NH_4)_6.Mo_7O_{24}.4H_2O$ (0.001 moles, 1.2358 g) and citric acid (0.03 moles, 5.8 g)in 20 ml distilled water and stirred for two hours until the formation of a transparent solution. The solution was sonicated for one hour followed by addition of 20 ml of already prepared hydrolysed TEOS solution and stirred for 60 min. The solution was maintained at a pH between 1 and 2 by adding few drops of 12 M HCl solution. The resulting solution was heated into a 50 ml autoclaved at 180 °C for 24 h. The hydrothermal product was filtered and the residue was dried under vacuum oven at 40 °C. The obtained powder was annealed at 500 °C for 2 h with a ramp rate of 6 °C per minutes under argon.

(ii) Synthesis of molybdenum oxide (MoO_3): The molybdenum oxide has been prepared with the same method as described in the above section (i). The only difference is that in this case the hydrolysed TEOS has not been used in this synthesis.

Step 2. High-temperature calcination of the molybdenum precursor

(c). Synthesis of SiMoCP catalyst

The catalyst SiMoCP was synthesized by annealing a mixture of as-prepared silica-supported MoO_3 (MoO_3@Si) nanoparticles (25 mg), diammonium hydrogen phosphate (0.001 moles, 0.132 g) and glucose (0.005 moles, 0.9 g) in a tube furnace. A streamlined flow of argon gas was made through the tube for half-an-hour to replace all the air present inside the tube. The mixture was annealed for 3 hours at temperature 800 °C with a heating rate of 6 °C/min in an argon atmosphere with the flow rate of 30 mL/min, after that, the temperature was raised to 900 °C and halted for one hour and then cooled under inert environment. The synthesized product and its composition highly influenced by temperature manipulation, the stoichiometry of precursors, and the flow rate used in the solid-state reaction.

(d). MoP: The catalyst has been synthesized by annealing 25 mg of MoO_3 with glucose (0.001 moles, 0. 018 g) and diammonium hydrogen phosphate (0.001 moles, 0.132 g) at 900 °C for 2 h in an argon atmosphere.

(e). Mo_2C: For Mo_2C catalyst has been synthesized with 25 mg MoO_3 nanoparticles and glucose (0.005 moles, 0.9 g) as carbon source, mixed in a mortar pestle. The mixture was heated at 800 °C for 3 h in an argon atmosphere.

(f). Silica-based MoP (MoP@Si): MoP@Si was synthesized by annealing 25 mg of MoO_3@Si with glucose (0.001 moles, 0. 018 g) and diammonium hydrogen phosphate (0.001 moles, 0.132 g) annealed at 900 °C for 2 h in an argon atmosphere.

(g). Silica-based Mo_2C (Mo_2C@Si): Mo_2C@Si catalyst was synthesized annealing 25 mg MoO_3@Si nanoparticles and glucose (0.005 moles, 0.9 g) was mixed in a mortar pestle. The mixture was heated at 800 °C for 3 h in an argon atmosphere.

(h). SiMoCP1: SiMoCP1 was synthesized by annealing a mixture of 25 mg MoO_3@Si precursor with glucose (0.005 moles, 0.9 g) and diammonium hydrogen phosphate (0.001 moles, 0.132 g) at 800 °C for 3 h and at 900 °C for a half-hour in an argon atmosphere.

(i). SiMoCP2: SiMoCP2 was synthesized by annealing a mixture of 25 mg MoO_3@Si precursor with diammonium hydrogen phosphate (0.001 moles, 0.132 g) and glucose (0.005 moles, 0.9 g) at 800 °C for 1 h and at 900 °C for 2 h in an argon atmosphere.

Note: The heating rate in all the synthesis process was 6 °C/min, and the post-reaction cooling was done in an argon environment with a gas flow of 30 mL/min.

7.2.2.3. Physical characterization of the catalyst

The characterization of the catalyst was done by several instrumental and spectroscopic techniques. The crystallographic information was acquired by powder X-ray diffraction analysis executed through Bruker Eco D8 advance diffractometer with Ni filter utilizing Cu Kα radiation (λ=1.54056 Å, 40 kV and 25 mA) in the 2θ range of 5° to 80° with an increment of 0.00190/Step. Phase distribution was determined by the Rietveld refinement method. The morphological analysis of the catalyst and precursors were shown using images produced by scanning electron microscope (SEM-JEOL, ZSM IT-300) equipped with energy-dispersive X-ray spectroscopy. High-resolution transmission electron microscopy (HRTEM) was acquired by TEM-JEOL 2100 operated at 200 kV along with the STEM analysis. BET surface area analysis was performed by Autosorb IQ Quantachrome instrument. The N_2 adsorption-desorption analysis was executed using the Brunauer-Emmett-Teller (BET) and the Barrett-Joyner-Halenda (BJH) models to get a clear picture of the porosity and surface area of the material. Before performing the adsorption-desorption study the sample was degassed at 200 °C for 6 h under vacuum. The X-ray photoelectron spectroscopy was carried out by Esca Lab: 220-IXL with Mg-Kα non-monochromated X-ray beam having photon energy 1253.6 eV. The charge effect that results in a shift of binding energy was corrected by referencing the binding energies of C1s peak at 284.6 eV.

7.2.2.4. Electrochemical measurement

Electrochemical measurement was performed in argon purged 0.5 M H_2SO_4 solution using a three-electrode setup on CHI 760E electrochemical workstation at 25 °C. A glassy carbon electrode (3 mm diameter) used as a working electrode while the graphite rod and Ag/AgCl electrode used as a counter and reference electrode respectively. The electrode surface contamination was cleaned by sonicating in alcoholic solution and cleaning it with alumina powder. The homogeneous catalytic dispersion of the catalyst was prepared by sonicating 5 mg of catalyst in 495 µL of DMF. The catalyst ink dispersion contained 5 µL of Nafion binder (5%), which was sonicated for 2 h in Labsonic bath sonicator (LBS2-10) and then drop cast on GCE. The polarization curves were collected at a scan rate of 5 mVs^{-1} unless otherwise mentioned. All the potential data were collected with respect to the Ag/AgCl electrode and converted as potential versus reversible hydrogen electrode (RHE) by using the expression, "$E_{(RHE)} = E_{(Ag/AgCl)} + 0.197 + 0.059*pH$". The ohmic drop modification was done by correcting the overpotential as per equation, $\eta_{corrected} = \eta - iR_s$ whereas R_s is the solution resistance. The durability of the catalyst was measured by running continuous 5000 LSV cycles at a scan rate of 5 mVs^{-1}. The electrochemical impedance spectroscopy was carried out at the selected overpotential between a frequency range 1 MHz to 0.1 Hz. The Tafel slopes were obtained by fitting the linear region of the Tafel plot using equation $\eta = a + b \log j$, where "η" is the overpotential, j is the current density, "a" is the intercept relative to the current exchange density and b is the Tafel slope.

7.3. Results and discussion

The SiMoCP catalyst was synthesized by reducing molybdenum oxide (MoO_3) with carbon and phosphorus source which resulted in the formation of molybdenum carbide and molybdenum phosphide (MoP) nanoparticles, grown over mesoporous silica present as support. The whole synthesis of SiMoCP was carried out in a temperature-programmed two-step process, which involves the synthesis of the metal precursor followed by carburization and phosphorization of the as-obtained mixture. Glucose and diammonium hydrogen phosphate were used as a carbon and phosphorus source respectively. To optimize the composition, two more catalysts were also synthesized from molybdenum carbide and molybdenum phosphide (SiMoCP1 and SiMoCP2) with a variation in the composition. Silica-supported molybdenum carbide (Mo_2C@Si) and molybdenum phosphide (MoP@Si) were synthesized individually along with Mo_2C and MoP by tuning the amount of carbon and phosphorous source using similar procedures mentioned in the experimental section. The scheme initiated by the synthesis of silica-supported MoO_3 by hydrolysed TEOS and molybdenum precursor. The glucose and diammonium phosphate serve as carbon and

phosphorus source in the overall reaction. The complete process proceeds through the reduction of silica-supported MoO_3 nanoparticles followed by simultaneous carburization and phosphorization. The reduction led to the *in-situ* formation of molybdenum carbide (Mo_2C) and molybdenum phosphide (MoP) nanoparticles. The extent of carburization and phosphorization depends on the amount of carbon and phosphorus source taken as precursors during the reaction. Hence, by judicious manipulation of the stoichiometry of the precursors and the reaction conditions, the final composition of the catalyst can be tuned for a better catalytic activity. The powder X-ray diffraction (PXRD) patterns (shown in Figure 7.1a) consist of peaks attribute to a mixture consists of Mo_2C and MoP phases. The peaks indexed at 34.4° (100), 37.9° (002), 39.5° (101), 52.2° (102), 61.4° (110), 69.5° (103), 72.3° (200), 74.6° (112) and 75.4° (201) corresponds to the hexagonal Mo_2C system (PDF 35-0787).[27] The other peaks indexing to 27.9° (001), 31.9° (100), 42.8° (101), 56.7° (110), 57.5° (002), 64.8° (111), 67.2° (200) and 73.3° (201) confirms the existence of hexagonal MoP phase (PDF 24-0771).[12] The initial precursor i.e. MoO_3@Si used for the synthesis of the catalyst has also been characterized by the powder X-ray diffraction (Figure 7.2a). The MoO_3 particles are having an average size of 265 nm (Figure 7.2b) as obtained by the DLS measurements. The PXRD measurements of as-synthesized Mo_2C@Si and MoP@Si also confirm the existence of a pure phase of individual material along with silica (Figure 7.3 (a&b)).

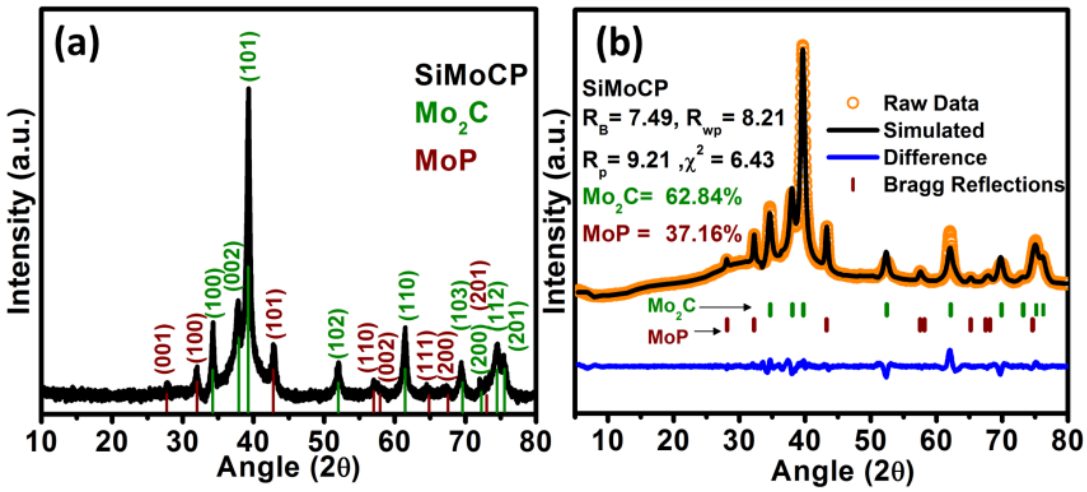

Figure 7.1. *Structural characterization (a) powder X-ray diffraction typically shows the formation of both Mo_2C-MoP phases and (b) Compositional measurements: Rietveld analysis of catalyst shows a composition 62.84 % and 37.16 % of Mo_2C and MoP respectively.*

Rietveld refinement of the PXRD measurements has revealed the compositions of all the catalysts. The SiMoCP catalyst was analysed, which shows 62.84% of Mo_2C and 37.16% of MoP (Figure 7.1b).

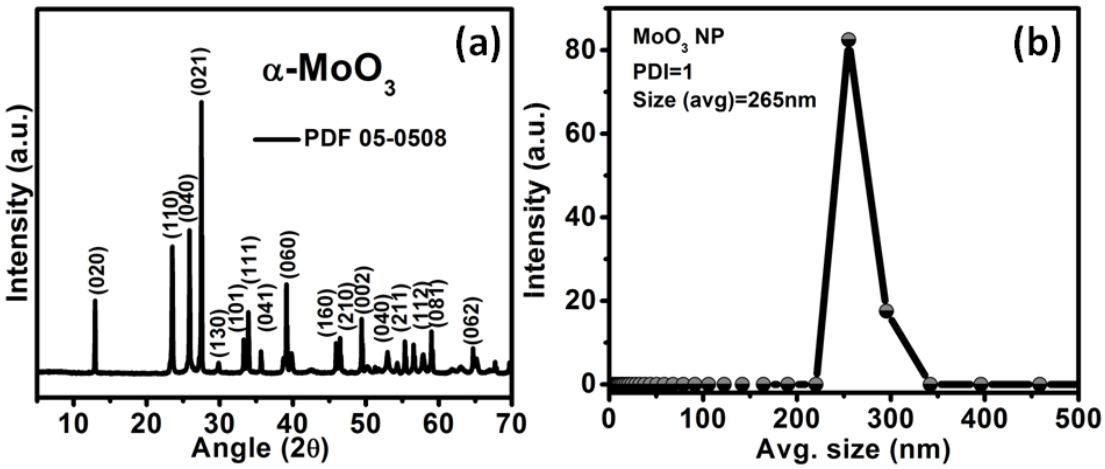

Figure 7.2. *PXRD (a) and DLS (b) pattern of MoO_3@Si nanoparticles*

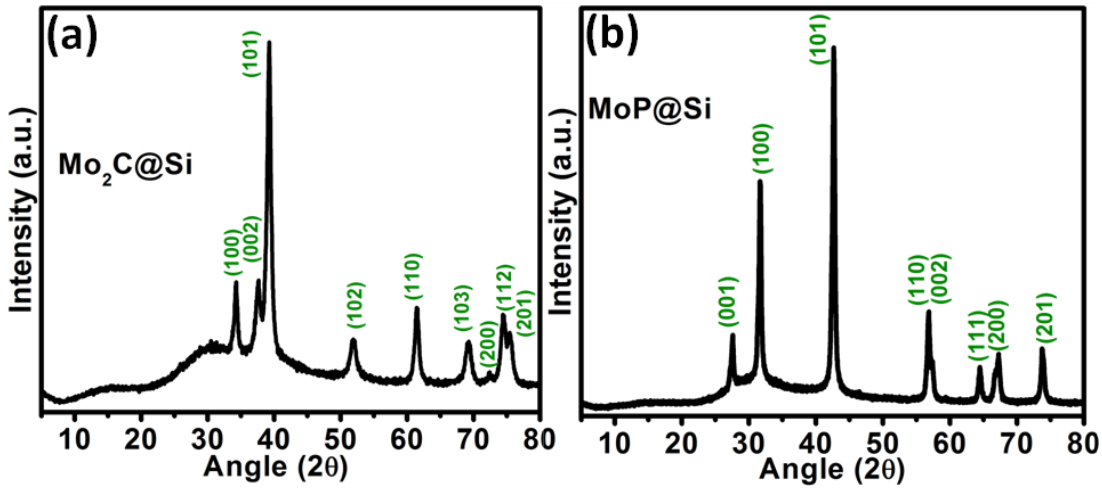

Figure 7.3*. PXRD of (a) Mo_2C@Si and (b) MoP@Si*

The other two catalysts, SiMoCP1 (81.35% of Mo_2C, and 19.65% of MoP)and SiMoCP2 (21.27% of Mo_2C, and 78.73% of MoP), also displays the existence of both Mo_2C and MoP (Figure 7.4).

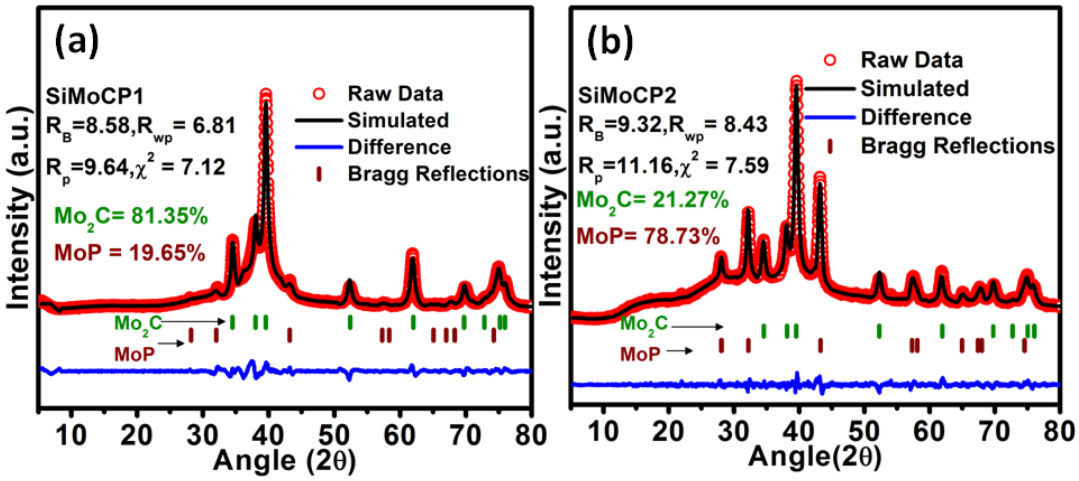

Figure 7.4. *Rietveld refinement of (a) SiMoCP1 and (b) SiMoCP2: The figure typically shows the formation of both Mo_2C and MoP phases and Rietveld analysis of catalyst shows a composition 81.35 % and 19.65 % of Mo_2C and MoP respectively in SiMoCP1 and composition of 21.27 % and 78.73 % of Mo_2C and MoP in SiMoCP2.*

All the parameters obtained from Rietveld refinement of the catalysts SiMoCP, SiMoCP1 and SiMoCP2 are given below (Table 7.1., Table 7.2 and Table 7.3 respectively).

Table 7.1. *Refinement parameters of SiMoCP*

		SiMoCP			
Sr. No.	*Parameters*	*Mo_2C*		*MoP*	
1	*Symmetry*	*Hexagonal*		*Hexagonal*	
2	*Space group*	*194*		*187*	
		Input	*Output*	*Input*	*Output*
3	*a*	*2.99400 Å*	*2.991048 Å*	*3.22300 Å*	*3.203092 Å*
4	*b*	*2.99400 Å*	*2.991048 Å*	*3.22300 Å*	*3.203092 Å*
5	*c*	*4.72200 Å*	*4.731474 Å*	*3.19100 Å*	*3.176890 Å*
6	*α*	*90^0*	*90^0*	*90^0*	*90^0*
7	*β*	*90^0*	*90^0*	*90^0*	*90^0*
8	*γ*	*120^0*	*120^0*	*120^0*	*120^0*
9	*R_p %*		*9.49*		
10	*R_{wp} %*		*8.21*		
11	*χ^2*		*6.43*		

Table 7.2. *Refinement parameters of SiMoCP1*

SiMoCP1					
Sr. No.	*Parameters*	*Mo_2C*		*MoP*	
1	*Symmetry*	*Hexagonal*		*Hexagonal*	
2	*Space group*	*194*		*187*	
		Input	*Output*	*Input*	*Output*
3	*a*	*2.99400 Å*	*2.99811 Å*	*3.22300 Å*	*3.22317 Å*
4	*b*	*2.99400 Å*	*2.99811 Å*	*3.22300 Å*	*3.22317 Å*
5	*c*	*4.72200 Å*	*4.73147 Å*	*3.19100 Å*	*3.16174 Å*
6	*α*	*90^0*	*90^0*	*90^0*	*90^0*
7	*β*	*90^0*	*90^0*	*90^0*	*90^0*
8	*γ*	*120^0*	*120^0*	*120^0*	*120^0*
9	*R_p %*	*9.64*			
10	*R_{wp} %*	*6.81*			
11	*χ^2*	*7.12*			

Table 7.3. *Refinement parameters of SiMoCP2*

SiMoCP2					
Sr. No.	*Parameters*	*Mo_2C*		*MoP*	
1	*Symmetry*	*Hexagonal*		*Hexagonal*	
2	*Space group*	*194*		*187*	
		Input	*Output*	*Input*	*Output*
3	*a*	*2.99400 Å*	*3.001609 Å*	*3.22300 Å*	*3.213830 Å*
4	*b*	*2.99400 Å*	*3.001609 Å*	*3.22300 Å*	*3.213830 Å*
5	*c*	*4.72200 Å*	*4.729463 Å*	*3.19100 Å*	*3.180524 Å*
6	*α*	*90^0*	*90^0*	*90^0*	*90^0*
7	*β*	*90^0*	*90^0*	*90^0*	*90^0*
8	*γ*	*120^0*	*120^0*	*120^0*	*120^0*
9	*R_p %*	*11.16*			
10	*R_{wp} %*	*8.43*			
11	*χ^2*	*7.59*			

In order to probe the surface properties, the metal oxide precursor and the catalyst were subjected to N_2 adsorption/desorption measurements (Figure 7.5a). The Brunauer−Emmett−Teller (BET) isotherm

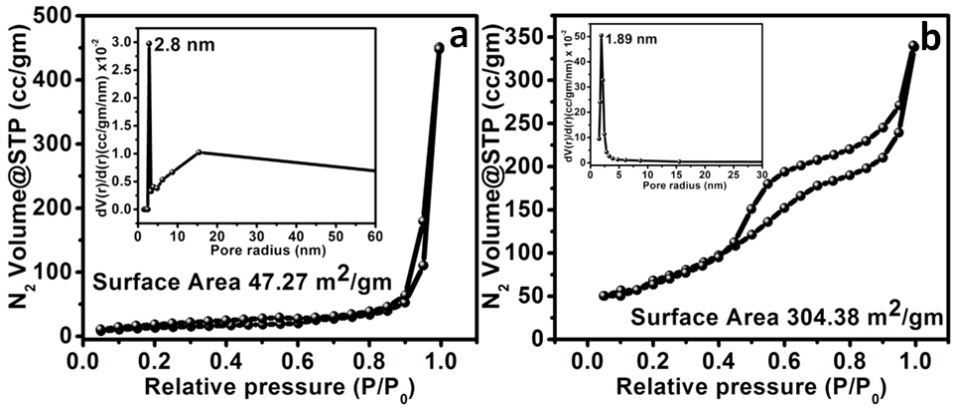

Figure 7.5. *Nitrogen adsorption BET isotherms and inset showing BJH pore distribution of the catalyst (a) Si-MoO_3 (b) SiMoCP; The catalyst was degassed at temperature 200 °C for 6 h before BET analysis*

of SiMoCP catalyst characteristically exhibits a type-IV curve (Figure 7.5b), which, according to IUPAC standards, reveals that the material to be highly mesoporous in nature and exhibits a surface area of 304.38 m^2g^{-1}. The pore size distribution plot of the catalyst reveals numerous pores primarily spotted within a range of 5 nm (Figure7.5b inset) and centred at a pore size of 2.8 nm. The presence of a mesoporous silica platform provides better distribution of the active sites which are more accessible for hydrogen adsorption/desorption in the HER process.[28] This is highly favourable for the high mass transport and adsorption creating a smooth interaction between electroactive species present in the electrolyte and the catalyst surface.[29] The morphological study of the catalyst was performed under scanning electron microscopy (SEM). Figure 7.6a depicts the SEM image of SiMoCP catalyst showing porous silica-supported agglomerated entities. Figure 7.6b corresponds to the STEM images of the catalyst and confirms the presence of Mo, C P and Si which are uniformly distributed in the catalyst. Figure 7.6c and 7.6d show TEM images of SiMoCP nanoparticles at different magnifications. The zoomed version of a high-resolution TEM image of figure 7.6d, shows an interplanar spacing of 0.26 nm and 0.21 nm corresponds to the (100) plane of Mo_2C and (101) plane of MoP respectively.[12, 27]

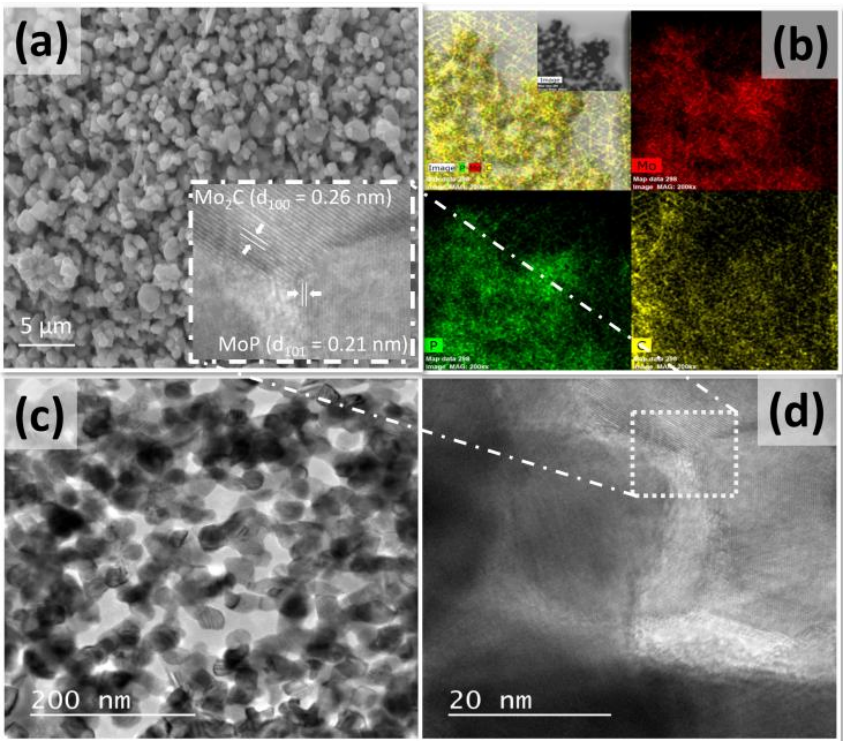

Figure 7.6. *(a) Scanning electron microscopy images of silica-supported SiMoCP catalyst. (b) The elemental mapping image of the SiMoCP nanostructures shows a uniform existence of Carbon, Molybdenum and Phosphorus elements in these nanostructures. (c)Tem image of the catalyst displays uniformly distributed 20-25 nm nanostructures. (d) The HRTEM image shows a selected area between 2-3 nanoparticles is shown. A zoomed version of the image shows an interplanar spacing of 0.26 nm and 0.21 nm corresponds to 100 and 101 planes of Mo_2C and MoP respectively.*

The SiMoCP catalyst was further characterized by X-ray photoelectron spectroscopy as depicted in figure 7.7. XPS affirms that the catalyst is constitutive of Mo, C, P, O and Si elements (Figure 7.7a) as observed in the survey spectrum. The Mo 3d spectrum (Figure 7.7b) shows six pronounced peaks centred at 228.1, 230.0, 231.2, 232.7, 234.3 and 235.7. The peaks at 228.1 and 231.2 eV can be attributed to $Mo^{\delta+}$ ($0 \leq \delta \leq 4$) species, confirming the presence of Mo_2C and MoP. The oxidation state of Mo^{+4} (230.0 and 232.7 eV), Mo^{+5} (234.3 eV) and Mo^{+6} (235.7 eV) may arise due to oxidation of surface in the presence of air during analysis.[30-32] The high-resolution C1s peaks of SiMoCP (Figure 7.7c) sample can be deconvoluted using four peaks at 283.7, 284.6, 285.6 and 289.6 eV corresponding to the C-P, C=C, C-O and O-C=O respectively.[12, 33-34] Furthermore, the P 2p peaks of SiMoCP (Figure 7.7d) can be deconvoluted into three peaks centred at 129.6, 133.5 and 134.5 eV corresponding to the Mo-P, P-C and P-O.[6, 22] The deconvoluted parameters for different peaks are shown in Table 7.4

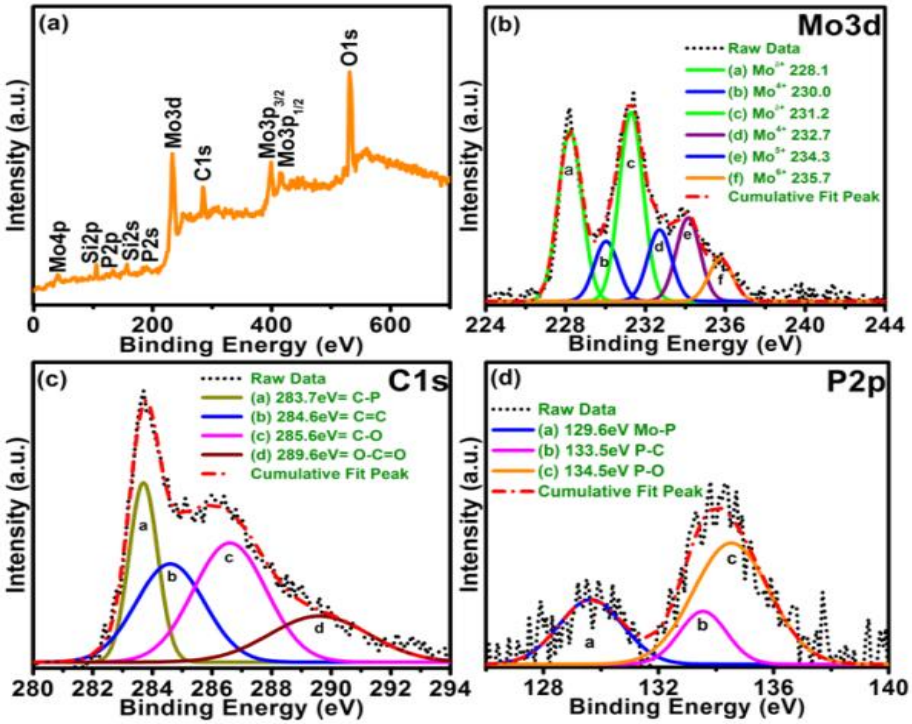

Figure 7.7. *XPS of the SiMoCP catalyst: wide-scan survey spectra (a) and HR spectra of Mo 3d (b), C 1s (c), and N 1s (d) electron: experimental data (dotted curve) and fitting results (solid curve). The peaks are assigned by oxidation states of different elements with their corresponding binding energy*

Table 7.4*. Deconvoluted parameters in XPS measurements*

Element	*Peak*	*BE (eV)*	*FWHM*	*Area (%)*
Mo 3d	*Mo^{d+} (Mo_2C)*	*228.1 and 231.2*	*1.032 and 1.032*	*27.60 and 30.66*
	Mo^{4+} (MoO_2)	*230.0 and 232.7*	*1.048 and 1.048*	*9.71 and 11.61*
	Mo^{5+} (Mo_4O_{11})	*234.3*	*1.062*	*13.50*
	Mo^{6+} (MoO_3)	*235.7*	*1.067*	*6.87*
C1s	*C-P*	*283.7*	*1.13*	*20.46*
	C=C	*284.6*	*2.70*	*26.74*
	C-O	*285.6*	*2.88*	*34.56*
	O-C=O	*289.6*	*3.92*	*18.22*
P 2p	*Mo-P*	*129.6*	*2.62005*	*26.18*
	P-C	*133.5*	*1.92866*	*15.76*
	P-O	*134.5*	*3.09477*	*58.04*

The electrocatalytic activity of SiMoCP towards HER was assessed in argon purged 0.5 M H_2SO_4 solution via a three-electrode setup. A glassy carbon electrode (3 mm diameter) used as a working electrode while the graphite rod and Ag/AgCl electrode used as a counter and reference electrode respectively. The iR corrected polarization curves obtained by linear sweep voltammetry (LSV) with a sweep rate of 5 mVs^{-1}. Figure 7.8a shows the comparative polarization curve of SiMoCP along with Mo_2C, MoP and commercially available 20% Pt/C catalyst in 0.5 M H_2SO_4.

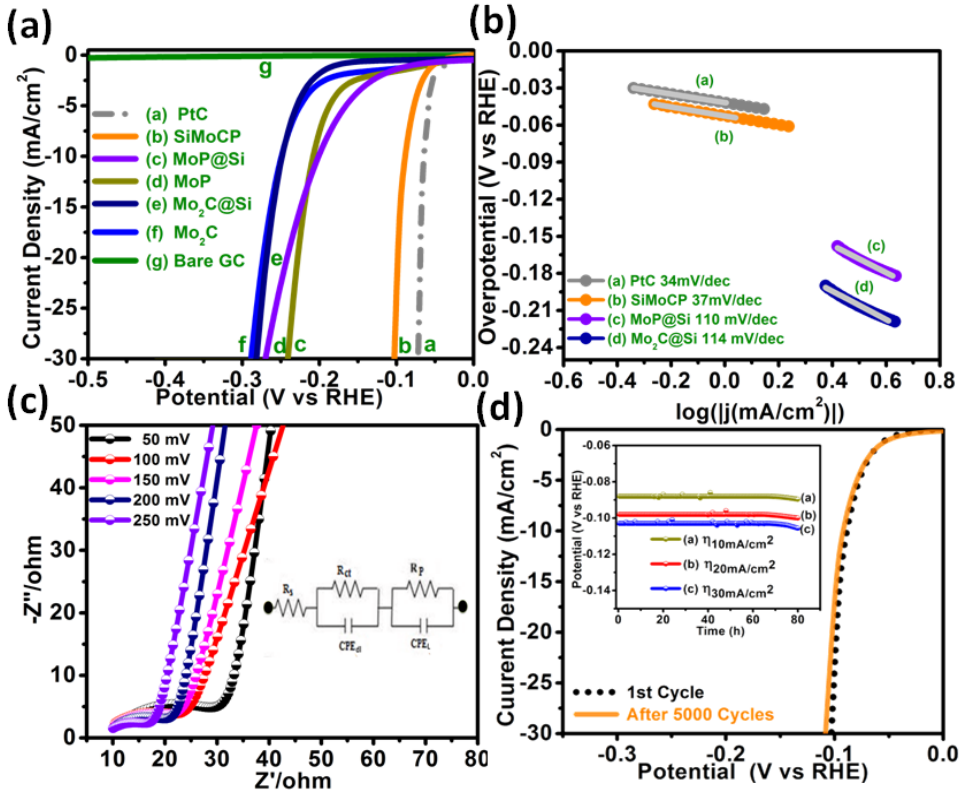

Figure 7.8. *(a) Polarization curves of SiMoCP catalyst with a comparison of other catalysts in 0.5 M H_2SO_4 (b) the corresponding Tafel plot of PtC, SiMoCP, MoP@Si and Mo_2C@Si catalyst (c) Nyquist Plot of the SiMoCP at different values of overpotential (inset- Zoomed Nyquist plot of SiMoCP catalyst @50 mV) (d) Durability test of SiMoCP (inset- the potentiostat study of SiMoCP at different current density i.e. 10 mA/cm^2, 20 mA/cm^2 and 30 mA/cm^2)*

Before LSV measurements repetitive cycles of cyclic voltammetry (CV) has been carried out to establish a steady-state condition. The measurements show that SiMoCP exhibit slightly higher onset potential 53 mV as compared to the commercial Pt/C (20 wt %) at the same time the onset potential of MoP@Si is 90 mV and Mo_2C@Si is 173 mV, which is much higher than SiMoCP. The overpotential (η_{10}) obtained for commercial Pt/C, SiMoCP, MoP@Si and Mo_2C@Si catalyst at a current density of 10 $mAcm^{-2}$ is 59 mV, 88 mV, 202

mV and 251 mV respectively (Figure 7.8a). These results substantiate that the SiMoCP shows much superior electrocatalytic performance compared to the Mo_2C and MoP phases supported on mesoporous silica. The overpotential obtained for MoP and Mo_2C is 208 mV and 248 mV respectively. The electrochemical behaviour of other compositional variants, as well as the physical mixture of MoP@Si (62%) and Mo_2C@Si (38%), were also examined. The overpotential of SiMoCP1, SiMoCP2 and SiMoCP-m were found to be 199, 176 and 241 mV respectively at 10 mA cm^{-2} current density (Figure 7.9a). This result concludes that the electrochemical behaviour of catalyst unambiguously reliant on the composition of MoP and Mo_2C in SiMoCP catalyst. It also indicates that the physical mixture of MoP@Si (62%) and Mo_2C@Si (38%) did not match the performance of SiMoCP catalyst synthesized *in-situ*. Thus, *in-situ* synthesis of the catalyst with an appropriate composition of MoP and Mo_2C supported on silica can lead to an excellent HER activity as evidenced by the electrochemical study of the compositional variant given in Figure 7.9a. Tafel slope value is also very significant in order to understand the quality of the HER catalyst. The Tafel slopes value obtained for Pt/C, SiMoCP, MoP@Si and Mo_2C@Si catalysts are 34 mV dec^{-1}, 37 mV dec^{-1}, 106 mV dec^{-1} and 113 mV dec^{-1} respectively (Figure 7.8b). Tafel plots were determined by using Tafel equation, $\eta = a + b \log j$, where, η, j, a & b are the overpotential, current density, Tafel slope, and intercept, respectively. Among these as-synthesized electrocatalysts, the SiMoCP shows the smallest Tafel slope, indicating faster reaction kinetics than those of Mo_2C@Si, MoP@Si and physical mixture of molybdenum carbide and molybdenum phosphide SiMoCP-m (Figure 7.8b and 7.9b).

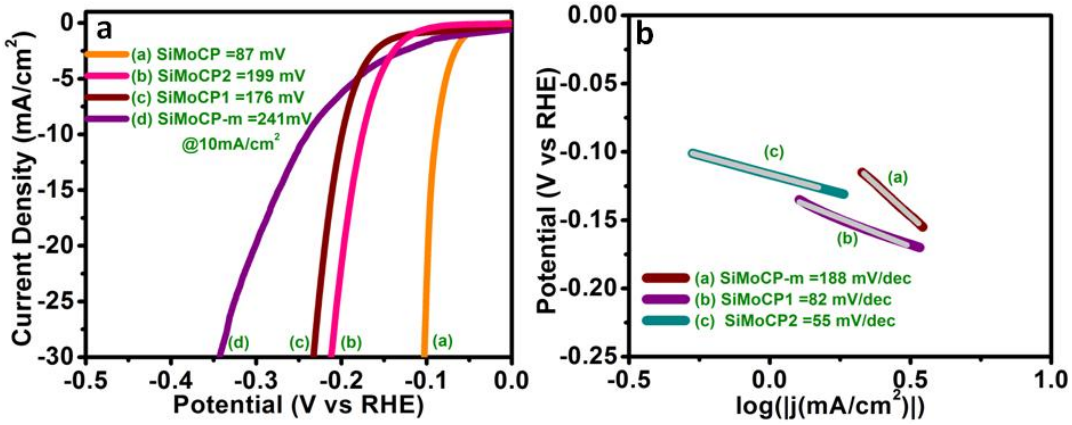

Figure 7.9. *Polarisation curve of (a) SiMoCP, SiMoCP1, SiMoCP2 and SiMoCP-m catalyst and corresponding (b) Tafel slope in 0.5 M* H_2SO_4

Among these as-synthesized electrocatalysts, the SiMoCP shows the smallest Tafel slope, indicating faster reaction kinetics than those of Mo_2C@Si, MoP@Si and physical mixture of molybdenum carbide and molybdenum phosphide SiMoCP-m. These results imply that the

electron transport in SiMoCP ensues through Volmer-Heyrovsky (electrochemical desorption) mechanism.[35] An exchange current density (j_0) of 3.56 x 10^{-2} mA $cm^{-2}$was acquired by extrapolation of Tafel plot portray the innate activity of electrocatalysts. The HER kinetics proceeding through the electrode/electrolyte interface of SiMoCP catalyst can be further scrutinized using electrochemical impedance spectroscopy (EIS). The EIS measurements were obtained at an applied potential of 50, 100, 150, 200 and 250 mV in 0.5 M H_2SO_4 aqueous solution (Figure 7.8c). The studies were conducted in the frequency range of 0.1 Hz to 100 kHz and obtained values were simulated using the equivalent circuit to evaluate the contribution of each component of electrochemical impedance. The ionic and charge transfer behaviour of the catalyst described by the Nyquist plot shown in Figure 7.8(c) and the resolved components present in the equivalent circuit are shown in the inset of figure 7.8c.The equivalent circuit can be expressed with two time-constant components R_{ct}—CPE_{dL} and R_p—CPE_L along with an uncompensated solution resistance R_s (connected in series). The equivalent circuit enumerates the electron transfer processes occurring during the HER and also describes the nature of the surface of the catalyst used in the process. The constant phase element (CPE) models the behaviour of a double layer, which deviates from an ideal capacitor. The component R_{ct}—CPE_{dL} signify the charge-transfer dynamics and R_p—CPE_L can be correlated with surface porosity.[36-37] The low-frequency region reveals the potential-dependent R_{ct} (charge-transfer resistance) component having a value of 19 ohms at 50 mV applied potential and 8 ohms at 250 mV potential (inset Figure 7.8c). A comparative impedance plot of the SiMoCP catalyst and SiMoCP-m, (a physical mixture of silica-supported molybdenum carbide and molybdenum phosphide) resembling the composition of SiMoCP is displayed in figure 7.10. The charge transfer resistance, R_{ct} of the SiMoCP was found to be much smaller than SiMoCP-m catalyst.

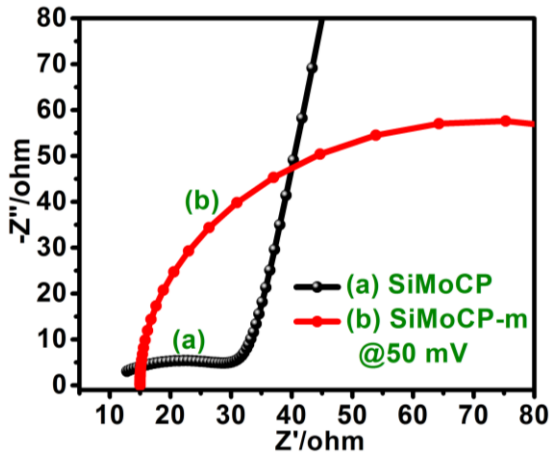

Figure 7.10. *Nyquist plot of SiMoCP and SiMoCP-m at 50 mV applied potential*

The plot and the simulated values obtained from the data fitting signifies that the reaction kinetics at the electrode-electrolyte interface is very fast. The durability test of the catalyst SiMoCP inspected through the repetitive catalytic cycles were displayed in figure 7.8d. The study shows that there is no significant change in the overpotential of catalyst even after 5000 cycles. The overpotential value of the catalyst changes from 88 mV to 94 mV. The 'V vs t' plot demonstrates that the potential at higher current density 20 mA cm^{-2} and 30 mA cm^{-2} follow a similar trend, indicating long term stability even under high current densities. The comparison of kinetic parameters of all the catalyst is given in table 7.5

Table 7.5. *Calculated kinetic parameters of different catalyst in 0.5 M H_2SO_4 solution*

Catalyst	*Onset (vs RHE)*	*η_{10} (vs RHE)*	*η_{20} (vs RHE)*	*η_{30} (vs RHE)*	*Tafel Slope (mV/dec)*	*Exchange Current Density (mA/cm^2)*
SiMoCP	*53 mV*	*88 mV*	*99 mV*	*102 mV*	*37*	*3.56×10^{-2}*
SiMoCP1	*136 mV*	*199 mV*	*219 mV*	*234 mV*	*82*	*1.89×10^{-3}*
SiMoCP2	*122 mV*	*176 mV*	*196 mV*	*213 mV*	*55*	*2.52×10^{-3}*
MoP@Si	*90 mV*	*202 mV*	*242 mV*	*270 mV*	*106*	*5.72×10^{-4}*
Mo_2C@Si	*173 mV*	*251 mV*	*274 mV*	*291 mV*	*113*	*3.06×10^{-4}*
SiMoCP-m	*87 mV*	*241 mV*	*301 mV*	*345 mV*	*188*	*0.17×10^{-4}*
Mo_2C	*104 mV*	*248 mV*	*274 mV*	*288 mV*	*71*	*2.34×10^{-3}*
MoP	*61 mV*	*208 mV*	*227 mV*	*240 mV*	*115*	*1.89×10^{-4}*

The adsorption of H-atom on the MoP/Mo_2C composite has been studied by using density functional theory (DFT). The adsorption energy of Hydrogen atom on various sites of the heterostructure is calculated as[38-39]

$$\Delta E_{ads} = E_{surface+H} - E_{surface} - {}^{1}/_{2}\, E_{H_2} \qquad (7.1)$$

where "$E_{surface}$+ H" is the total energy of the adsorbate and adsorbent, $E_{surface}$ is the total energy of the clean surface and $E(H_2)$ is the energy of H_2 gas. Further, the Gibbs free energy of hydrogen evolution reaction is considered as an essential parameter to describe the overall performance of the catalyst, means only those catalysts are found to be an ideal catalyst for which ΔG is nearly equalled to zero. It can be written as

$$\Delta G = \Delta E_{ads} + 0.24\ eV \qquad (7.2)$$

All the energy calculations of the supercell having dimensions a = 36.46 Å, b = 13.62 Å and c = 13.67 Å, α = 69.14°, β = 90.78° and γ = 110.85° are performed using Vienna Ab-initio

Simulation Package (VASP)[40] with projector-augmented wave (PAW) method. The exchange-correlation functional is treated with the Perdew, Burke, and Ernzerhof (PBE) version of the generalized gradient approximation (GGA)[41]. A vacuum space of approximately 10 Å is added along the c-axis to avoid the interaction between the adjacent layers. For geometry optimization, the plane wave energy cutoff is set to 520 eV and the Brillouin-zone is sampled using a Γ-centered k-point mesh.

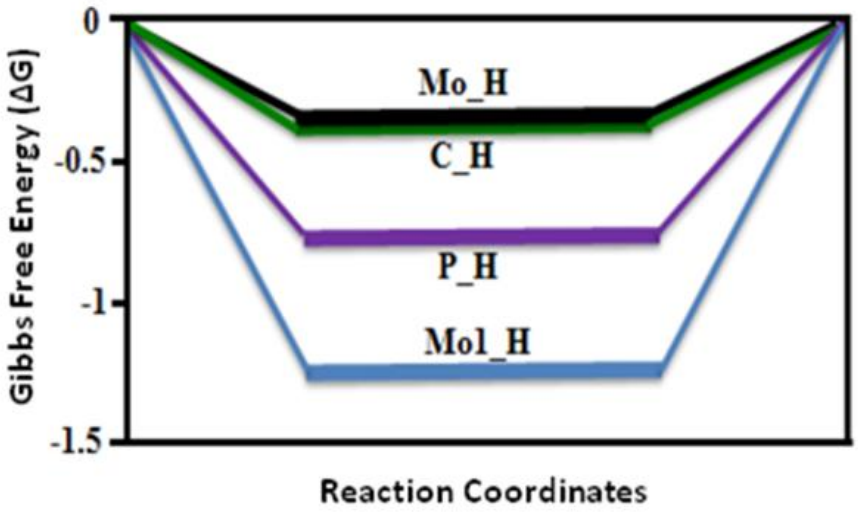

Figure 7.11. *The Free Energy diagram for 'Mo', 'C' and 'P' hydrogen adsorptions sites of SiMoCP (depicted by green/black lines) displays, a shift of free energy making these more favourable for HER with respect to Mo_2C sites of the catalyst (depicted by blue lines).*

7.4. Conclusion

SiMoCP catalyst synthesized using a temperature-controlled *in-situ* solid-state reaction resulting in a silica-supported molybdenum carbide and molybdenum phosphide nanostructures show excellent hydrogen evolution reaction in acidic medium. The catalyst exhibits onset potential of 53 mV and a low overpotential of 88 mV at a current density of 10 mA cm^{-2}. The SiMoCP exhibits a Tafel slope value of 37 $mVdec^{-1}$ also shows high stability of withstanding more than 5000 cycles in acidic medium with significant retention of the current density. Silica support offers enhanced porosity, high surface area and provides a uniform distribution of Mo_2C and MoP nanoparticles on spongy silica. The *in-situ* grown phases within the composite catalyst express a synergistic effect through the interface. Thus *in-situ* synthesis of the catalyst with an appropriate composition of MoP and Mo_2C supported on silica can lead to the formation of SiMoCP catalyst which excels HER activity. It was also evidenced by the catalysts of other composition namely SiMoCP1 and SiMoCP2 which underperforms than SiMoCP.

References

1. Chu, S.; Majumdar, A., Opportunities and challenges for a sustainable energy future. *Nature* **2012,** *488* (7411), 294-303.

2. Li, X.; Hao, X.; Abudula, A.; Guan, G., Nanostructured catalysts for electrochemical water splitting: current state and prospects. *Journal of Materials Chemistry A* **2016,** *4* (31), 11973-12000.

3. Cheng, N.; Stambula, S.; Wang, D.; Banis, M. N.; Liu, J.; Riese, A.; Xiao, B.; Li, R.; Sham, T.-K.; Liu, L.-M.; Botton, G. A.; Sun, X., Platinum single-atom and cluster catalysis of the hydrogen evolution reaction. *Nature Communications* **2016,** *7* (1), 13638.

4. Wei, J.; Zhou, M.; Long, A.; Xue, Y.; Liao, H.; Wei, C.; Xu, Z. J., Heterostructured Electrocatalysts for Hydrogen Evolution Reaction Under Alkaline Conditions. *Nano-micro letters* **2018,** *10* (4), 75-75.

5. Yu, L.; Zhu, Q.; Song, S.; McElhenny, B.; Wang, D.; Wu, C.; Qin, Z.; Bao, J.; Yu, Y.; Chen, S.; Ren, Z., Non-noble metal-nitride based electrocatalysts for high-performance alkaline seawater electrolysis. *Nature Communications* **2019,** *10* (1), 5106.

6. Huang, Y.; Ge, J.; Hu, J.; Zhang, J.; Hao, J.; Wei, Y., Nitrogen-Doped Porous Molybdenum Carbide and Phosphide Hybrids on a Carbon Matrix as Highly Effective Electrocatalysts for the Hydrogen Evolution Reaction. *Advanced Energy Materials* **2018,** *8* (6), 1701601.

7. Seo, B.; Joo, S. H., Recent advances in unveiling active sites in molybdenum sulfide-based electrocatalysts for the hydrogen evolution reaction. *Nano Convergence* **2017,** *4* (1), 19.

8. Wang, Z.; Li, Q.; Xu, H.; Dahl-Petersen, C.; Yang, Q.; Cheng, D.; Cao, D.; Besenbacher, F.; Lauritsen, J. V.; Helveg, S.; Dong, M., Controllable etching of MoS_2 basal planes for enhanced hydrogen evolution through the formation of active edge sites. *Nano Energy* **2018,** *49*, 634-643.

9. Miao, M.; Pan, J.; He, T.; Yan, Y.; Xia, B. Y.; Wang, X., Molybdenum Carbide-Based Electrocatalysts for Hydrogen Evolution Reaction. *Chemistry – A European Journal* **2017,** *23* (46), 10947-10961.

10. Dong, J.; Wu, Q.; Huang, C.; Yao, W.; Xu, Q., Cost effective Mo rich Mo_2C electrocatalysts for the hydrogen evolution reaction. *Journal of Materials Chemistry A* **2018,** *6* (21), 10028-10035.

11. Chen, Y.-Y.; Zhang, Y.; Jiang, W.-J.; Zhang, X.; Dai, Z.; Wan, L.-J.; Hu, J.-S., Pomegranate-like N,P-Doped Mo_2C@C Nanospheres as Highly Active Electrocatalysts for Alkaline Hydrogen Evolution. *ACS Nano* **2016,** *10* (9), 8851-8860.

12. Zhang, L.-N.; Li, S.-H.; Tan, H.-Q.; Khan, S. U.; Ma, Y.-Y.; Zang, H.-Y.; Wang, Y.-H.; Li, Y.-G., MoP/Mo_2C@C: A New Combination of Electrocatalysts for Highly Efficient Hydrogen Evolution over the Entire pH Range. *ACS Applied Materials & Interfaces* **2017,** *9* (19), 16270-16279.

13. Li, J.-S.; Sha, J.-Q.; Du, B.; Tang, B., Highly efficient hydrogen evolution electrocatalysts based on coupled molybdenum phosphide and reduced graphene oxide derived from MOFs. *Chemical Communications* **2017,** *53* (93), 12576-12579.

14. Song, Y.-J.; Yuan, Z.-Y., One-pot Synthesis of Mo_2N/NC Catalysts with Enhanced Electrocatalytic Activity for Hydrogen Evolution Reaction. *Electrochimica Acta* **2017,** *246*, 536-543.

15. Zhu, Y.; Chen, G.; Xu, X.; Yang, G.; Liu, M.; Shao, Z., Enhancing Electrocatalytic Activity for Hydrogen Evolution by Strongly Coupled Molybdenum Nitride@Nitrogen-Doped Carbon Porous Nano-Octahedrons. *ACS Catalysis* **2017,** *7* (5), 3540-3547.

16. Zeng, F.; Broicher, C.; Palkovits, S.; Simeonov, K.; Palkovits, R., Synergy between active sites and electric conductivity of molybdenum sulfide for efficient electrochemical hydrogen production. *Catalysis Science & Technology* **2018,** *8* (1), 367-375.

17. Zhou, W.; Jia, J.; Lu, J.; Yang, L.; Hou, D.; Li, G.; Chen, S., Recent developments of carbon-based electrocatalysts for hydrogen evolution reaction. *Nano Energy* **2016,** *28*, 29-43.

18. Ito, Y.; Cong, W.; Fujita, T.; Tang, Z.; Chen, M., High Catalytic Activity of Nitrogen and Sulfur Co-Doped Nanoporous Graphene in the Hydrogen Evolution Reaction. *Angewandte Chemie International Edition* **2015,** *54* (7), 2131-2136.

19. Ledendecker, M.; Schlott, H.; Antonietti, M.; Meyer, B.; Shalom, M., Experimental and Theoretical Assessment of Ni-Based Binary Compounds for the Hydrogen Evolution Reaction. *Advanced Energy Materials* **2017,** *7* (5), 1601735.

20. Shi, Z.; Nie, K.; Shao, Z.-J.; Gao, B.; Lin, H.; Zhang, H.; Liu, B.; Wang, Y.; Zhang, Y.; Sun, X.; Cao, X.-M.; Hu, P.; Gao, Q.; Tang, Y., Phosphorus-Mo_2C@carbon nanowires toward efficient electrochemical hydrogen evolution: composition, structural and electronic regulation. *Energy & Environmental Science* **2017,** *10* (5), 1262-1271.

21. Guo, J.; Wang, J.; Wu, Z.; Lei, W.; Zhu, J.; Xia, K.; Wang, D., Controllable synthesis of molybdenum-based electrocatalysts for a hydrogen evolution reaction. *Journal of Materials Chemistry A* **2017,** *5* (10), 4879-4885.

22. Wang, T.; Du, K.; Liu, W.; Zhu, Z.; Shao, Y.; Li, M., Enhanced electrocatalytic activity of MoP microparticles for hydrogen evolution by grinding and electrochemical activation. *Journal of Materials Chemistry A* **2015,** *3* (8), 4368-4373.

23. Suliman, M. H.; Adam, A.; Siddiqui, M. N.; Yamani, Z. H.; Qamar, M., The impact of microstructural features of carbon supports on the electrocatalytic hydrogen evolution reaction. *Catalysis Science & Technology* **2019,** *9* (6), 1497-1503.

24. Zhang, L.; Jin, L.; Liu, B.; He, J., Templated Growth of Crystalline Mesoporous Materials: From Soft/Hard Templates to Colloidal Templates. *Frontiers in Chemistry* **2019,** *7*, 22.

25. Sudarsanam, P.; Peeters, E.; Makshina, E. V.; Parvulescu, V. I.; Sels, B. F., Advances in porous and nanoscale catalysts for viable biomass conversion. *Chemical Society Reviews* **2019,** *48* (8), 2366-2421.

26. Rao, K. S.; El-Hami, K.; Kodaki, T.; Matsushige, K.; Makino, K., A novel method for synthesis of silica nanoparticles. *Journal of Colloid and Interface Science* **2005,** *289* (1), 125-131.

27. Liang, P.; Gao, H.; Yao, Z.; Jia, R.; Shi, Y.; Sun, Y.; Fan, Q.; Wang, H., Simple synthesis of ultrasmall β-Mo_2C and α-MoC_{1-x} nanoparticles and new insights into their catalytic mechanisms for dry reforming of methane. *Catalysis Science & Technology* **2017,** *7* (15), 3312-3324.

28. Ouyang, C.; Wang, X.; Wang, C.; Zhang, X.; Wu, J.; Ma, Z.; Dou, S.; Wang, S., Hierarchically Porous Ni_3S_2 Nanorod Array Foam as Highly Efficient Electrocatalyst for Hydrogen Evolution Reaction and Oxygen Evolution Reaction. *Electrochimica Acta* **2015,** *174*, 297-301.

29. Zhang, J.-W.; Gong, S.; Mahmood, N.; Pan, L.; Zhang, X.; Zou, J.-J., Oxygen-doped nanoporous carbon nitride via water-based homogeneous supramolecular assembly for photocatalytic hydrogen evolution. *Applied Catalysis B: Environmental* **2018,** *221*, 9-16.

30. Zhang, P.; Zou, L.; Hu, H.; Wang, M.; Fang, J.; Lai, Y.; Li, J., 3D Hierarchical Carbon Microflowers decorated with MoO_2 Nanoparticles for lithium ion batteries. *Electrochimica Acta* **2017,** *250*, 219-227.

31. Yang, X.; Feng, X.; Tan, H.; Zang, H.; Wang, X.; Wang, Y.; Wang, E.; Li, Y., N-Doped graphene-coated molybdenum carbide nanoparticles as highly efficient electrocatalysts for the hydrogen evolution reaction. *Journal of Materials Chemistry A* **2016,** *4* (10), 3947-3954.

32. Qin, P.; Fang, G.; Ke, W.; Cheng, F.; Zheng, Q.; Wan, J.; Lei, H.; Zhao, X., In situ growth of double-layer MoO_3/MoS_2 film from MoS_2 for hole-transport layers in organic solar cell. *Journal of Materials Chemistry A* **2014,** *2* (8), 2742-2756.

33. Ji, L.; Wang, J.; Teng, X.; Dong, H.; He, X.; Chen, Z., N,P-Doped Molybdenum Carbide Nanofibers for Efficient Hydrogen Production. *ACS Applied Materials & Interfaces* **2018,** *10* (17), 14632-14640.

34. Kerber, S. J.; Bruckner, J. J.; Wozniak, K.; Seal, S.; Hardcastle, S.; Barr, T. L., The nature of hydrogen in x-ray photoelectron spectroscopy: General patterns from hydroxides to hydrogen bonding. *Journal of Vacuum Science & Technology A* **1996,** *14* (3), 1314-1320.

35. Conway, B. E.; Tilak, B. V., Interfacial processes involving electrocatalytic evolution and oxidation of H_2, and the role of chemisorbed H. *Electrochimica Acta* **2002,** *47* (22), 3571-3594.

36. Mei, B.-A.; Munteshari, O.; Lau, J.; Dunn, B.; Pilon, L., Physical Interpretations of Nyquist Plots for EDLC Electrodes and Devices. *The Journal of Physical Chemistry C* **2018,** *122* (1), 194-206.

37. Alexander, C. L.; Tribollet, B.; Vivier, V.; Orazem, M. E., Contribution of Surface Distributions to Constant-Phase-Element (CPE) Behavior: 3. Adsorbed Intermediates. *Electrochimica Acta* **2017,** *251*, 99-108.

38. Jiao, Y.; Ma, F.; Zhou, L.; Ng, Y. H.; Bell, J.; Tretiak, S.; Du, A., Ab initio study of two-dimensional PdPS as an ideal light harvester and promising catalyst for hydrogen evolution reaction. *Materials today energy* **2018,** *7*, 136-140.

39. Nørskov, J. K.; Bligaard, T.; Logadottir, A.; Kitchin, J.; Chen, J. G.; Pandelov, S.; Stimming, U., Trends in the exchange current for hydrogen evolution. *Journal of The Electrochemical Society* **2005,** *152* (3), J23-J26.

40. Kresse, G.; Furthmüller, J., Efficiency of ab-initio total energy calculations for metals and semiconductors using a plane-wave basis set. *Computational materials science* **1996,** *6* (1), 15-50.

41. Perdew, J. P.; Burke, K.; Ernzerhof, M., Generalized Gradient Approximation Made Simple. *Physical Review Letters* **1996,** *77* (18), 3865-3868.

Conclusion and Future Perspectives

The thesis consists of the different kind of material synthesized for electrocatalytic hydrogen generation through earth-abundant molybdenum derived electrocatalysts. The first part of the thesis describes how energy is the fundamental requirements of the world and a basic social need that necessary in driving economic growth and civilizing human development. As all knows that the energy services directly affect our social and physical prosperity in terms of health, education, water and communication services. In the modern scenario, the major energy-consuming sectors like electricity, agriculture, modern cooking technologies and transports systems etc. all are running on energy.[1-2] It is a bitter truth that there is a wide gap between developed and developing countries in terms of energy consumption. How it affects and how it could be minimised it's briefly discussed in the initial part of the thesis. Further, the thesis explores other aspects like how the energy distribution, generation and supply to the last users influence the people's livelihoods in local, regional and global human development prospects. It describes how any one of the prime factors influences the overall development of human kinds. Once again if we talk about today, the world is keen to search for a more efficient, environment-friendly and durable energy source. Several different energy sources are available but largely we are dependent on the fossil fuels which have a parallel concern of climate change that originates from the greenhouse gas emission.[3] The effects of these changes and the related solution have been tried to discuss in the first part of the thesis. The different renewable energy sources and their overall energy production is not enough to fulfil today's energy needs. Here, the concept of storing energy in chemical form and distribution it for the various purpose has come into existence for the future clean energy source. So in this way hydrogen marks its presence as a clean and future energy carrier which not only can fulfil the energy needs but also have less negative impacts on our environment. Here, the perspective behind the establishment of a hydrogen economy and how apposite preservation must be is discussed. The various aspects and the usefulness, hurdles and the current scenario of the hydrogen economy have also conversed. The chapter describes the reasons behind the recent energy crisis faced by the world and the various positive step taken to avoid the future energy crisis. The hydrogen economy is mainly based upon the hydrogen production and in this section, the hydrogen production through a carbon-neutral process has been widely explored, discussed and motivates.[4-5] It also describes how hydrogen can be generated through water splitting electrochemical reactions. The fundamental and the mechanism of the water splitting for hydrogen production is understood. The proper selection approach of the material that enhances the hydrogen generating efficiency is primarily concerned and described how it improves the reaction kinetics in the electrocatalytic process by properly selecting the suitable material. There, it has been briefly

described how the catalytic activity of the transition metal could resemble the noble metal electrocatalyst like platinum for the hydrogen production process.[6-7] The motive behind the exploration of the non-noble electrocatalysts for hydrogen production has been discussed and understood how it affects the overall economy of the system. The successful synthesis of the material needs to characterization and all the techniques have been discussed in chapter 2. In chapter 2, the material characterization has been completed through different characterization techniques that describe in the second chapter. First of all the structural characterisation has been performed by PXRD measurements and the details of the powder X-ray diffractometers are given in chapter 2. On the successful structural characterization of the material, the material undergoes electrochemical study in which reaction kinetics, charge transfer process, durability and the various other parameters have been calculated. On measuring different electrochemical parameters the morphological and structural study has been performed in by scanning electron microscopy and the transmission electron microscopy. The other properties like surface area measurements, porosity measurements and size measurements have been executed through BET analysis and the size analyzers respectively. The composition analysis is performed by the Rietveld analysis and the XAS measurements. The elemental states in few catalysts are analysed by the XPS measurements. The comparative analysis of the electronic states also examined by the XANES measurements with the standard material other catalysts. The overall analysis of the catalyst involves the structural, compositional, morphological and electronic state's measurements along with the surface analysis and theoretical measurement of the synergy behind the improved activity measuring through DFT calculations.

The focus on the present thesis is to identify the low cost, an earth-abundant electrocatalyst for hydrogen evolution reaction. The molybdenum derivatives have shown the HER activity in different media for hydrogen generation. Molybdenum carbide (Mo_2C), molybdenum nitride (Mo_2N), molybdenum oxide (MoO_2), molybdenum phosphide (MoP) are among the well known HER active electrocatalysts.[7-8] Although all these catalysts are not the fully efficient catalyst for hydrogen generation, here we planned to make them more efficient for hydrogen generation by combing through an *in-situ* synthesis process. The synthesis and electrochemical activity of the materials are described in the chapters and the main spotlight is the synthesis of biphasic structure which provides the synergistic effect to the catalyst that improves the catalytic activity by enhancing the charge transfer at the interface. The study involves the identification of active sites for suitable adsorption hydrogen and optimizing the total energy required for the overall hydrogen generation process. The study involves the theoretical calculation and the

experimental demonstration of the catalytic activity of particular material. In this context, the effect of surface structure, electrode material, compositional variation in the material and other synthesis methodology has been optimised. Electrocatalysts synthesized during PhD tenure have been described from chapter 3 to chapter 7. The chapters successfully explore the molybdenum derivative synthesis methodology especially the molybdenum carbide and its composites have been widely explored along with their electrochemical study. The *in-situ* synthesis of the molybdenum derivatives provides the synergic improvements in the catalytic behaviour of the material. The integrating template and/or the conductive surface much enhanced the catalytic activity of the molybdenum catalyst. The thesis describes molybdenum has the wide acceptance of being a more efficient electrocatalyst for hydrogen production. The morphology, structure, dimensions and size etc. of the material directly affects the catalytic activity of the material. The thesis effectively elaborates the synthesis methodology of more effective, efficient, low cost and highly abundant molybdenum derived material for hydrogen production. Herein, it investigates that the molybdenum composite catalyst shows much improved electrocatalytic activity in the acidic media. The incorporation of templates, contrast phase and doping heteroatom atom etc. highly affects and improve the catalytic activity of the material. All these modifications favours in making Mo one of the most suitable candidates for enhanced electrochemically activity of the material. Molybdenum carbide is preliminary obtained one of the best and efficient electrocatalysts for hydrogen generation. The molybdenum nitride, molybdenum oxide, molybdenum phosphide and the heteroatom doped molybdenum derivatives are also showing the electrocatalytic activity in the acidic media for hydrogen evolution reaction. The thesis explores that the individual catalyst is less active towards the electrochemical hydrogen evolution reaction as compared to the composites of the molybdenum derivatives. This thesis also shows that the *in-situ* synthesis of the material synergistically enhances the catalytic activity of the material and methodology plays a crucial role in this. The improvement in the catalytic activity has been experimentally and theoretically explored. The experimental work supported by the theoretical study shows that the system undergoes through some electronic changes and modifies the overall electronic conduction which enhances the catalytic activity of the material. The electronic changes mainly occur at the interface of the different phases present in the catalyst that improves the charge transfer through the interface and enhances the catalytic activity of the material. The formation of the interfaces within the crystallites plays the leading role and the theoretical study elaborates the rationale behind how it affects the electronic structure near the interface. From the obtained results its confirm that the synergistic enhancement in catalyst could be achieved only when if it *in-situ*

synthesized. The synthesis of a different phase in the same composite by the judicially optimizing the reaction condition results into the multiphase composite that synergistically modifies the electronic environment near the interface and improves the catalytic activity of the material. This all has been observed in all the catalyst starting from the section of biomass-derived Mo_2C/Mo_2N (Chapter 3) to the end with the porous silica-supported Mo_2C/MoP electrocatalyst (Chapter 7) and regularly observed that the catalytic activity gets improves with the particular change in the composition of materials. The biomass-derived (Cotton) molybdenum carbide and molybdenum nitride (MoCot) having good stability of 2500 cycles in the acidic medium (0.5 M H_2SO_4) along with an overpotential of 167 mV to derive the current density of 10 mA/cm^2. The onset potential obtained for the catalyst is 110 mV. The catalyst having a 59.12% of Mo_2C and 40.88% of Mo_2N in the MoCot catalyst. Different composition of the Mo_2C and Mo_2N has been successfully synthesized by optimizing the reaction condition through high-temperature calcination but the analysis shows that when the composition of the molybdenum carbide and molybdenum nitride when approaching nearly equal to half the catalytic activity of the material is maximum. The individually synthesized Mo_2C and Mo_2N and even the mere mixing of them both with the same composition as obtained in MoCot does not give the same catalytic activity as observed in MoCot. From this, it confirms that the *in-situ* synthesis of molybdenum carbide and molybdenum nitride derived from the biomass material having synergistic effects and improves the catalytic activity of the material. The biomass itself acts as a carbon source as well as carbon support to the molybdenum carbide and molybdenum nitride nanoparticles.[9] But the variation in the carbon content in the biomass material could lead to the different activity of the material synthesized even if using the same reaction conditions. Thus in the second step, in chapter 4 the commercially available carbon and nitrogen sources have been used and a composite of Mo_2C and Mo_2N (MoCat) with using g-C_3N_4 and hexamethylenetetramine (HMT) as carbon and nitrogen sources in the inert atmosphere has been successfully synthesized. The formation of interfaces between Mo_2C and Mo_2N nanoparticles have been observed in different crystallites and the theoretical study explores the reason behind the synergy obtained in the catalyst. The *in-situ* synthesized MoCat catalyst and interface formation highly favours the adsorption process and improves the reaction kinetics. The catalyst requires an overpotential of 96 mV to derive a current density of 10 mA/cm^2 with a composition of 47% of β-Mo_2C and 53% γ-Mo_2N in the MoCat catalyst. Here again, the mere mixing of the same composition of the Mo_2C and Mo_2N nanoparticles also has been studied and found that catalytic behaviour of the mixture does not repeat the same results as obtained in the *in-situ* synthesized Mo_2C and Mo_2N nanoparticles. Here the stability obtained in acidic media

(1M H_2SO_4) is only of 1000 cycles. The catalytic activity of the material get enhances but the stability concern motivates us to further explore the catalytic activity of the material.[10] So, to enhance the catalytic activity of such hybrid nanostructured the effect of other molybdenum phases in composites has been studied in chapter 5. In chapter 5 a different strategy has been adopted and a new phase along with the molybdenum carbide with silica support has been introduced. In this work, a composite of molybdenum carbide and molybdenum oxide within the porous silica structure (SiMoCat) has been successfully synthesized by the high-temperature calcination method. The catalyst has been synthesized by the partial carburization of the oxide material and here different carburization rate leads to the different composition of molybdenum carbide and molybdenum oxide in the composite material. The different carburization rate of the oxide precursor has been achieved by different reaction conditions. In this work, the different composite catalyst with different Mo_2C and MoO_2 contribution with the incorporation of the silica has been synthesized. But the catalyst with a composition of 51.32% and 48.68% of Mo_2C and MoO_2 (SiMoCat) respectively shows very good catalytic activity. The catalyst has an overpotential of 71 mV to derive a current density of 10 mA/cm^2 in 0.5 M H_2SO_4 solution. The catalyst exhibits an onset potential of 31 mV and durability of 3500 cycles in acidic medium. Here again, the *in-situ* synthesis and a composition optimization of Mo_2C and MoO_2 phases leads to the synergistically enhanced catalytic activity of the material. Chapter 5 successfully illustrates that not only the molybdenum nitride but molybdenum oxide along with the molybdenum carbide also shows the same kind of synergy in the *in-situ* synthesized catalytic material. Chapter 6 involves the synthesis of transition metal-doped molybdenum carbide and molybdenum nitride. The promoter elements improve the catalytic activity of the material. The successful synthesis of a different nanostructured hybrid using different transition metals has been achieved but the copper doping in the molybdenum carbide and molybdenum nitride nanostructured hybrid strategically enhances the catalytic activity of the material. The Cu doped Mo_2C/Mo_2N (CuMoCat) nanohybrid has been synthesized by use of copper as doped metal and rGO as a carbon source in the presence of argon and ammonia environment at the desired temperature. The catalyst CuMoCat which shows the higher stability than the previously studied nanohybrid catalyst on copper doping and it has a stability of 3000 cycles. The variation of copper doping in Mo_2C/Mo_2N nanohybrid shows that a particular amount of the copper atoms synergistically improves the catalytic activity of the material. The stability of the material gets enhanced from 1000 cycles to the 3000 cycles and the catalyst have an overpotential of 82 mV at a current density of 10 mA/cm^2. The onset potential of the catalyst obtained is 40 mV in 0.5 M H_2SO_4 solution. As compared to the low overpotentials the catalytic activity of the material

at high current density is really impressive and it requires only an overpotential of 112 mV to reach a current density of 30 mA/cm^2 as compared to the Mo_2C/Mo_2N (MoCat-CN) nanocomposite which requires an overpotential of 217 mV for the same current density. Even though MoCat-CN having an onset potential of 24 mV as compared to the onset of CuMoCat which have an onset potential of 40 mV the catalytic activity at high current density is remarkable. In this case, again, the *in-situ* synthesis plays a crucial role and provides the synergistic enhancement in the catalytic activity of the material. The theoretical study reveals that the adsorption process in the CuMoCat catalyst is highly favourable at the Mo and N sites. The adsorption study with and without copper doping reveals that process gets modifies on copper doping and it makes the Mo and N sites more favourable to the HER activity.[11] Chapter 6 successfully shows that the suitable doping of the transition metal in the molybdenum carbide and molybdenum nitride nanohybrid structure could lead to the more efficient and durable HER electrocatalyst. The study has been further explored to synthesize a composite of molybdenum carbide and molybdenum phosphide and is described in chapter 7. Both molybdenum carbide and molybdenum phosphide are known as good HER active materials. Here in this chapter, a composite of molybdenum carbide and molybdenum phosphide (SiMoCP) has been synthesized through high-temperature calcination method to study the combination of two different HER active material. The molybdenum carbide and molybdenum phosphide nanoparticles have been mutually grown with the incorporation of mesoporous silica. The silica support provides more active sites to the catalyst with an increased surface area of the material as compared to the commonly synthesized molybdenum electrocatalysts. The catalyst shows excellent stability of 5000 cycles with an overpotential of 88 mV at a current density of 10 mA/cm^2. The catalyst exhibits an onset potential of 53 mV having a composition of 62.84% of Mo_2C and 37.16% of MoP in the catalyst. Several other composites of with different compositions of the molybdenum carbide and molybdenum phosphide have also been synthesized and studied their electrochemical activity in same 0.5 M H_2SO_4 solution. Here again, in this, it found that the *in-situ* synthesis and the composition optimization of molybdenum carbide and molybdenum phosphide provide a better HER electrocatalyst. The physical mixing of the molybdenum carbide and molybdenum phosphide does not provide the same catalytic activity even with the same composition as achieved by the SiMoCP catalyst. The theoretical study further reveals that the Mo, C and P adsorption sites in the SiMoCP catalyst are more favourable as compared to the individual molybdenum derivatives. The catalyst shows that the combination of molybdenum carbide and molybdenum phosphide synergistically enhances the catalytic activity when it mutually grew with the silica incorporation.

Thus thesis successfully explains that the *in-situ* synthesis of the molybdenum derivatives that provide the synergy to the catalyst and improves the catalytic activity of the material. Suitable conductive support, proper doping and an optimised composition of the phases present in the composite improve the HER activity. Here, the study involves the use and synthesis of only molybdenum derivatives this could be extended to the other transition metal derivatives like transition metal sulphides (TMSs), transition metal oxides (TMOs), transition metal selenides (TMSes), transition metal phosphides (TMPs), and transition metal borides (TMBs) etc. The different promoter element like Cu, Ni, Co, Mn and Fe etc ould be incorporated along with the other heavy transition metals. The assisting material like graphene oxide, silica or any biomass material could be replaced with highly conductive supports likes carbon nanotubes, carbon nanowires, carbon aerogels, MOFs, Ni foams etc. This work opens up a new area where carbides, nitrides, oxide and phosphides of other metals can also give rise to such effects and a durable and excellent material could be found for hydrogen generation at industrial scale through economically viable and environment-friendly water splitting approach. Hence, it is of great significance to analyse the origins of versatile abilities and offer valuable guidance for the design of future high-performance electrocatalysts through this study. These state of the art strategy aim at the specific goals like improvement of inherent catalytic activity by mutually synthesizing the multiphase material. The hybridization or interface engineering regulates the catalytic activity of the material by providing the improved charge conduction through the interface. The doping enriches the active sites and helps in designing transition metal-doped architectures and this could be extended to the other forms of hierarchical/porous structure etc. The combination of HER active and HER inactive material through *in-situ* or any other means could provide an improved electrochemical activity to the HER electrocatalyst. As seen in the Mo_2C/MoO_2 (SiMoCat) and Mo_2C/MoP (SiMoCP) the combination of HER active and the less active electrocatalyst provides an excellent activity and the durability to the catalyst. This can be extended to the other transition metal or non-transition metal catalyst. Furthermore, the theoretical computation plays a decisive role in exploring such kind of interface that forms due to the simultaneous synthesis of different kind of phases in the same composites. The DFT calculation is the valuable tools that can be applied to the material catalyst and divulge the catalytic routes at the atomic scale. The combination of experimental measurements and computational outcomes will improve the research competence and evade the lingering trial-and-error itinerary for catalyst synthesis. The other important parameters are the catalyst reparation procedures in which the different parameters leads to the different yields of the catalyst. The catalyst synthesis with the desired composition is highly influenced by the

temperature and heating rate, holding time, type of gas for inert atmosphere and its flow rate and its and initial precursors and their composition. Finally, it is astonishing to end that the HER electrocatalysts described above are of great importance and are great candidates for the hydrogen evolution reaction. These catalysts can minimize the total cost and facilitate the experimental setups in water-splitting reactions for hydrogen generations.

References

1. Chu, S.; Majumdar, A., Opportunities and challenges for a sustainable energy future. *Nature* **2012,** *488* (7411), 294-303.

2. al Irsyad, M. I.; Halog, A.; Nepal, R., Renewable energy projections for climate change mitigation: An analysis of uncertainty and errors. *Renewable Energy* **2019,** *130*, 536-546.

3. Owusu, P. A.; Asumadu-Sarkodie, S., A review of renewable energy sources, sustainability issues and climate change mitigation. *Cogent Engineering* **2016,** *3* (1), 1167990.

4. Maggio, G.; Nicita, A.; Squadrito, G., How the hydrogen production from RES could change energy and fuel markets: A review of recent literature. *International Journal of Hydrogen Energy* **2019,** *44* (23), 11371-11384.

5. Dincer, I.; Acar, C., Review and evaluation of hydrogen production methods for better sustainability. *International Journal of Hydrogen Energy* **2015,** *40* (34), 11094-11111.

6. Ashik, U. P. M.; Viswan, A.; Kudo, S.; Hayashi, J.-i., Chapter 3 - Nanomaterials as Catalysts. In *Applications of Nanomaterials*, Mohan Bhagyaraj, S.; Oluwafemi, O. S.; Kalarikkal, N.; Thomas, S., Eds. Woodhead Publishing: 2018; pp 45-82.

7. Chen, Z.; Duan, X.; Wei, W.; Wang, S.; Ni, B.-J., Recent advances in transition metal-based electrocatalysts for alkaline hydrogen evolution. *Journal of Materials Chemistry A* **2019,** *7* (25), 14971-15005.

8. Guo, J.; Wang, J.; Wu, Z.; Lei, W.; Zhu, J.; Xia, K.; Wang, D., Controllable synthesis of molybdenum-based electrocatalysts for a hydrogen evolution reaction. *Journal of Materials Chemistry A* **2017,** *5* (10), 4879-4885.

9. Kumar, R.; Ahmed, Z.; Rai, R.; Gaur, A.; Kumari, S.; Maruyama, T.; Bagchi, V., Uniformly Decorated Molybdenum Carbide/Nitride Nanostructures on Biomass Templates for Hydrogen Evolution Reaction Applications. *ACS Omega* **2019,** *4* (9), 14155-14161.

10. Kumar, R.; Rai, R.; Gautam, S.; De Sarkar, A.; Tiwari, N.; Jha, S. N.; Bhattacharyya, D.; Ganguli, A. K.; Bagchi, V., Nano-structured hybrid molybdenum carbides/nitrides generated in situ for HER applications. *Journal of Materials Chemistry A* **2017,** *5* (17), 7764-7768.

11. Kumar, R.; Ahmed, Z.; Kaur, H.; Bera, C.; Bagchi, V., Probing into the effect of heterojunctions between Cu/Mo_2C/Mo_2N on HER performance. *Catalysis Science & Technology* **2020**., DOI: 10.1039/C9CY02526J

Appendix 1

List of Publication

1. **Rajinder Kumar,** Ritu Rai, Seema Gautam, Abir De Sarkar, Nidhi Tiwari, Shambhu Nath Jha, Dibyendu Bhattacharyya, Ashok K. Ganguli and Vivek Bagchi*; Nano-Structured Hybrid Molybdenum Carbides / Nitrides Generated In-Situ For HER Applications; ***J. Mater. Chem. A,*** 2017, 5, 7764-7768, DOI: 10.1039/C7TA01815K.

2. **Rajinder Kumar**, Zubair Ahmed, Ritu Rai, Takahiro Maruyama and Vivek Bagchi*; Uniformly decorated Mo_2C/Mo_2N nanoparticles on biomass template for HER activity in acidic media, ***ACS Omega,*** 2018, 3 (11), pp 15112–15118

3. **Rajinder Kumar,** Zubair Ahmed, Harwinder Kaur, Chandan Bera and Vivek Bagchi*;* Probing into the effect of heterojunctions between $Cu/Mo_2C/Mo_2N$ on HER performance, ***Catal. Sci. Technol.,*** *2020,10, 2213-2220 https://doi.org/10.1039/C9CY02526J*

4. **Rajinder Kumar**, Zubair Ahmed, Ravi Kumar, Shambhu Nath Jha, Dibyendu Bhattacharyya, Chandan Bera and Vivek Bagchi***;*** In-situ modulation of silica supported MoO_2/Mo_2C heterojunction for enhanced hydrogen evolution reaction, ***Catal. Sci. Technol.,*** *2020, Accepted Manuscript, https://doi.org/10.1039/D0CY00890G*

5. Ritu Rai, Zubair Ahmed, **Rajinder Kumar**, Rameshwar L. Kumawat, Kalyani Chordiya, Takahiro Maruyama, Md. Ehesan Ali, and Vivek Bagchi*; Environmentally Benign Metal-Free Reduction of GO Using Molecular Hydrogen: A Mechanistic Insight, **ACS Omega,** 2018, 3 (11), pp 15112–15118, DOI: 10.1021/acsomega.8b00848

6. Zubair Ahmed, Ritu Rai, **Rajinder Kumar**, Takahiro Maruyama, and Vivek Bagchi*; Hydrated $FePO_4$ nanoparticles supported on P-doped RGO shows enhanced ORR activity compared to its dehydrated form in alkaline medium, ***RSC Advance,*** 2019,9 24654-24658

7. Deepika Rani, **Rajinder Kumar,** Vineet Kumar, Monika Singh; High yield Cycloaddition of Carbon Dioxide to Epoxides Catalysed by Metal-Organic Frameworks; ***Materials Today Sustainability*** 2019, 5, 100021, doi.org/10.1016/j.mtsust.2019.100021

8. Zubair Ahmed, P K. Sachdeva, Ritu Rai, **Rajinder Kumar,** Takahiro Maruyama,b Chandan Bera,a and Vivek Bagchi*, ***ACS Appl. Energy Mater.*** 2020, 3, 4, 3645–3652

Under Revesion:

- **Rajinder Kumar**, Ashish Gaur, Takahiro Maruyama, Chandan Bera and Vivek Bagchi*; Mutually grown molybdenum carbide and phosphide on silica support shows enhanced HER activity

List of Conferences attended

1. Srinagar, India (April 2019), *International Conference on Nanotechnology for Better Living-2019* by NIT Srinagar and IIT Kharagpur**;** **Rajinder Kumar,** Vivek Bagchi

Poster presentation: In-situ synthesis and electrochemical activity of Carbon coupled Mo_2C/Mo_2N nanohybrid as an efficient HER application

2. Mumbai, India (January 2018), *Conference on Advances in Catalysis for Energy and Environment* by TIFR, Mumbai; **Rajinder Kumar**, Vivek Bagchi

Poster presentation: Nanostructured Materials Synthesized from Transition Metal Carbides / Nitrides for Electrocatalytic Applications

3. Mohali, India (November 2016), *1st In-house symposium at INST Mohali;* **Rajinder Kumar**, Vivek Bagchi

Poster presentation: Molybdenum derived HER electrocatalyst for HER applications.

4. Mohali, India (August 2016), 2nd CRICK Nanoscience Day at INST Mohali; **Rajinder Kumar**, Vivek Bagchi

Poster presentation: Molybdenum Carbide and Molybdenum Nitride Nonohybrid for HER applications

5. Chandigarh, India (February 2016), *10th CRSI-RSC organized by INST- Punjab University*; **Rajinder Kumar**, Vivek Bagchi

Poster and Active member of the organizing committee; Transition metal carbide and Nitride for HER applications

6. Mohali, India (November 2015), *6th MRS Trilateral Symposium organized by INST*; **Rajinder Kumar**, Ashok Kumar Ganguli and Vivek Bagchi

Poster presentation: Development of transition metal-based carbide and nitride nanostructured through *in-situ* synthesis

7. Mohali, India (December 2014), *One Day Conclave on Nano-biotechnology organized by INST*; **Rajinder Kumar**, Ashok Kumar Ganguli and Vivek Bagchi

Poster presentation: Understanding the behaviour of *in-situ* synthesized transition metal carbide, nitride and oxide for HER applications

Workshop attended

1. Mohali, India (February 2016), *Workshop on Solid-State Material Chemistry organised by INST;* **Rajinder Kumar,** Vivek Bagchi

Gmail

RAJINDER KUMAR <rajinder4iit@gmail.com>

RE: request for permission

1 message

CONTRACTS-COPYRIGHT (shared) <Contracts-Copyright@rsc.org> 6 March 2020 at 20:20
To: "rajinder4iit@gmail.com" <rajinder4iit@gmail.com>

Dear Rajinder

The Royal Society of Chemistry (RSC) hereby grants permission for the use of your paper(s) specified below in the printed and microfilm version of your thesis. You may also make available the PDF version of your paper(s) that the RSC sent to the corresponding author(s) of your paper(s) upon publication of the paper(s) in the following ways: in your thesis via any website that your university may have for the deposition of theses, via your university's Intranet or via your own personal website. We are however unable to grant you permission to include the PDF version of the paper(s) on its own in your institutional repository. The Royal Society of Chemistry is a signatory to the STM Guidelines on Permissions (available on request).

Please note that if the material specified below or any part of it appears with credit or acknowledgement to a third party then you must also secure permission from that third party before reproducing that material.

Please ensure that the thesis includes the correct acknowledgement (see http://rsc.li/permissions for details) and a link is included to the paper on the Royal Society of Chemistry's website.

Please also ensure that your co-authors are aware that you are including the paper in your thesis.

Regards

Gill Cockhead
Contracts & Copyright Executive

Gill Cockhead
Contracts & Copyright Executive
Royal Society of Chemistry,
Thomas Graham House,
Science Park, Milton Road,
Cambridge, CB4 0WF, UK
Tel +44 (0) 1223 432134

-----Original Message-----
From: rajinder4iit@gmail.com <rajinder4iit@gmail.com>
Sent: 06 March 2020 12:38
To: CONTRACTS-COPYRIGHT (shared) <Contracts-Copyright@rsc.org>
Subject: request for permission

Name: Rajinder Kumar
Message: Dear Sir/Maam,
I want to use the article
"Nano-structured hybrid molybdenum carbides/nitrides generated in situ for HER applications"

https://pubs.rsc.org/en/content/articlelanding/2017/ta/c7ta01815k#!divAbstract

in which I am the first author and I want to use it in my thesis as the whole article.
Please allow me for the same, so that I can make my thesis.
in my thesis.

My mailing address is - rajinder4iit@gmail.com

Rajinder Kumar

Gmail **RAJINDER KUMAR <rajinder4iit@gmail.com>**

RE: request for permission

1 message

CONTRACTS-COPYRIGHT (shared) <Contracts-Copyright@rsc.org> 6 March 2020 at 20:20
To: "rajinder4iit@gmail.com" <rajinder4iit@gmail.com>

Dear Rajinder

The Royal Society of Chemistry (RSC) hereby grants permission for the use of your paper(s) specified below in the printed and microfilm version of your thesis. You may also make available the PDF version of your paper(s) that the RSC sent to the corresponding author(s) of your paper(s) upon publication of the paper(s) in the following ways: in your thesis via any website that your university may have for the deposition of theses, via your university's Intranet or via your own personal website. We are however unable to grant you permission to include the PDF version of the paper(s) on its own in your institutional repository. The Royal Society of Chemistry is a signatory to the STM Guidelines on Permissions (available on request).

Please note that if the material specified below or any part of it appears with credit or acknowledgement to a third party then you must also secure permission from that third party before reproducing that material.

Please ensure that the thesis includes the correct acknowledgement (see http://rsc.li/permissions for details) and a link is included to the paper on the Royal Society of Chemistry's website.

Please also ensure that your co-authors are aware that you are including the paper in your thesis.

Regards

Gill Cockhead
Contracts & Copyright Executive

Gill Cockhead
Contracts & Copyright Executive
Royal Society of Chemistry,
Thomas Graham House,
Science Park, Milton Road,
Cambridge, CB4 0WF, UK
Tel +44 (0) 1223 432134

-----Original Message-----
From: rajinder4iit@gmail.com <rajinder4iit@gmail.com>
Sent: 06 March 2020 12:42
To: CONTRACTS-COPYRIGHT (shared) <Contracts-Copyright@rsc.org>
Subject: request for permission

Name: Rajinder Kumar
Message: Dear Sir/Maam,
I want to use the article
"Probing into the effect of heterojunctions between Cu/Mo2C/Mo2N on HER performance" in Catalysis Science and Technology journal

https://pubs.rsc.org/en/content/articlelanding/2020/cy/c9cy02526j#!divAbstract

in which I am the first author and I want to use it in my thesis as the whole article.
Please allow me for the same, so that I can make my thesis.
in my thesis.

My mailing address is - rajinder4iit@gmail.com

support@services.acs.org <support@services.acs.org> 2 March 2020 at 19:40
To: RAJINDER KUMAR <rajinder4iit@gmail.com>

Dear Dr. Kumar,

Thank you for contacting ACS Publications Support.

Your permission requested is granted and there is no fee for this reuse.

In your planned reuse, you must cite the ACS article as the source, add this direct link https://pubs.acs.org/doi/10.1021/acsomega.9b02321 and include a notice to readers that further permissions related to the material excerpted should be directed to the ACS.

Please do not hesitate to contact us if you need any further assistance.

Kind regards,

Ivan Ostojic

ACS Publications

Customer Services & Information

Website: https://help.acs.org

-----Original Message-----

Priority: None

From: (RAJINDER KUMAR) rajinder4iit@gmail.com

Sent: 3/2/2020

To: support@services.acs.org

Cc:

Subject: request for permission

[Quoted text hidden]

{CMI: MCID874193}

6/18/2020 Gmail - request for permission

CONTRACTS-COPYRIGHT (shared) <Contracts-Copyright@rsc.org> 17 June 2020 at 12:05
To: RAJINDER KUMAR <rajinder4iit@gmail.com>

Dear Rajinder

The Royal Society of Chemistry (RSC) hereby grants permission for the use of your paper(s) specified below in the printed and microfilm version of your thesis. You may also make available the PDF version of your paper(s) that the RSC sent to the corresponding author(s) of your paper(s) upon publication of the paper(s) in the following ways: in your thesis via any website that your university may have for the deposition of theses, via your university's Intranet or via your own personal website. We are however unable to grant you permission to include the PDF version of the paper(s) on its own in your institutional repository. The Royal Society of Chemistry is a signatory to the STM Guidelines on Permissions (available on request).

Please note that if the material specified below or any part of it appears with credit or acknowledgement to a third party then you must also secure permission from that third party before reproducing that material.

Please ensure that the thesis includes the correct acknowledgement (see http://rsc.li/permissions for details) and a link is included to the paper on the Royal Society of Chemistry's website.

Please also ensure that your co-authors are aware that you are including the paper in your thesis.

Regards

Gill Cockhead

Contracts & Copyright Executive

Gill Cockhead

Contracts & Copyright Executive

Royal Society of Chemistry,

In-situ modulation of silica-supported MoO_2/Mo_2C heterojunction for enhanced hydrogen evolution reaction

Vitae

Rajinder Kumar

Ph.D. Research Scholar
Institute of Nanoscience and Technology
&
Indian Institute of Science Education and Research,
Mohali (Punjab), India

Rajinder Kumar completed his bachelor's degree in Science from Dyal Singh College Karnal affiliated to Kurukshetra University, Kurukshetra in 2007 and completed his Master Degree in Physics from Department of Physics, Kurukshetra University, Kurukshetra in 2009. In 2010 he joined Dyal Singh College, Karnal as guest faculty and worked as Physics lecturer from July 2010 to May 2012. From 2012 to 2014 he completed his M. Tech. degree in Nanotechnology from National Institute of Technology, Kurukshetra. In August 2014 he joined Institute of Nanoscience and Technology as a Ph.D. research scholar under the guidance of Dr. Vivek Bagchi. He authored several research articles and presented his research work in several National and International conferences. His research interest includes the synthesis of transition metal carbides, nitride, oxide and phosphides electrocatalyst and their electrochemical study for hydrogen evolution reaction.